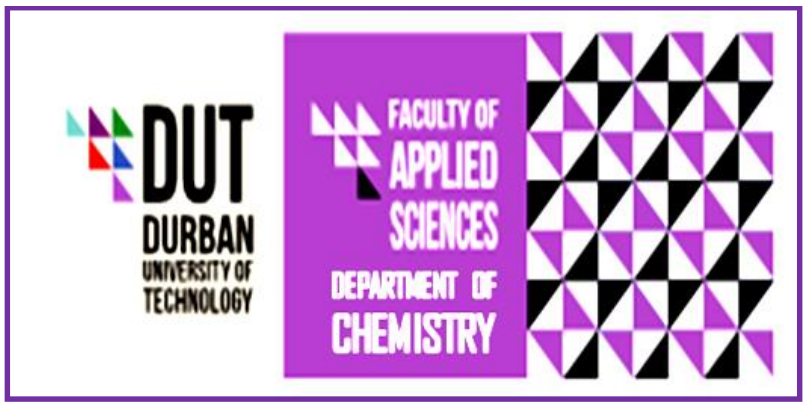

DEVELOPMENT OF ELECTROPHORETIC AND BIOSENSOR METHODS APPLIED TO HIGH INTENSITY SWEETENERS

By

Ayyappa Bathinapatla

(Reg. No: 21243352)

Submitted in fulfillment of the requirements of the degree of Doctor of Philosophy in Chemistry in the Faculty of Applied Sciences at the Durban University of Technology

March 2015

Declaration

I **Ayyappa Bathinapatla** declare that the thesis submitted for the degree of Doctor of Philosophy in Chemistry at the Durban University of Technology has not been submitted to any other university and no portion of this or any other closely related work is under consideration for publication elsewhere in any medium. All the work was done by my self

STUDENT NAME---------- AYYAPPA BATHINAPATLA

SIGNATURE------ [redacted] -------- **DATE** **12-3-2015**

CO-SUPERVISOR NAME---------- DR. M. DOVEY

SIGNATURE---------- [redacted] **DATE** **12-3-2015**

SUPERVISOR NAME---------- PROF. K. BISETTY

SIGNATURE----- [redacted] **DATE** **12-3-2015**

Acknowledgements

First of all I would like to express my sincere thanks to Prof. Krishna Bisetty for his close guidance and encouragement during this entire project. I would like to extend my sincere gratitude to Dr. Martin Dovey from Kerry Ingredients (South Africa) for providing sweetener standards to do this project. I would also like to express my sincere gratitude to Dr. Suvardhan Kanchi for sharing his experience and his moral support throughout this project.

I am grateful of the support received from Dr. Parvesh Singh in the field of computational chemistry to make this project a success. I would also like to extend my acknowledgements to Mr. M. I. Sabela who taught instrumental handling such as CE and voltammetry and very concerned from the preliminary studies of this project up to the last day. I would like to thank Dr. Phumlane Mdluli who helped me to do the XRD analysis. Special thanks to computational modelling and bio analytical chemistry (CMBAC) group members Dr. Deepali Sharma, Mr. Faez Khan, Mr. Shahbaaz, Mr. Mpanza, Mrs. Khulu and lab technician Mrs. M. Xhakaza for their assistance and healthy research environment.

Not forgetting to mention, my sincere thanks to Dr. Natesh Kumar who initially helped and referred me to get this opportunity. Finally, my deepest gratitude goes to my brother and parents, for their benevolent support throughout my studies. This thesis is dedicated to them.

Lastly my sincere thanks to the Department of Chemistry and National Research Foundation for their financial support.

Abstract

Materials which show sweetness are classified as nutritive sweeteners and non-nutritive sweeteners or artificial sweeteners. In the present work, capillary electrophoresis and electrochemical biosensors have been used to analyse and quantify the natural and chemical artificial sweeteners in different food samples. The experimental work was further supported by computational studies. Capillary electrophoresis (CE) is a technique in which charged molecules can efficiently be separated in a buffer solution within a capillary tube under the influence of a strong electric field. While in the case of a biosensor, the analyte interacts with the bioreceptor and the resulting output is measured by a specially designed transducer. Steviol glycosides (rebaudioside A and stevioside) are natural sweeteners, extracted from Stevia rebaudiana Bertoni belonging to the Asteraceae family. On the other hand, neotame and sucralose are chemical sweeteners manufactured from their structural analogues aspartame and sucrose, respectively. Accordingly in this work, two CE modes, namely electro kinetic chromatography–capillary electrophoresis (EKC–CE) and an indirect UV-Capillary zone electrophoresis were used for the evaluation of analytes studied. Steviol glycosides (rebaudioside A and stevioside) and neotame diastereomers (L,L and D,D) were analysed using EKC-CE in the presence of a chiral separating agent β-cyclodextrin (TM-β-CD). However, since sucralose demonstrates chromophore-like properties, an indirect UV-CZE method was therefore developed using simple amines (morpholine, piperidine, ethylamine and triethylamine) as the background electrolytes (BGE).

The optimum separation conditions in EKC-CE were; UV detection at 210 nm, 50 mM phosphate buffer, 30 mM TM-β-CD, 20 kV applied voltage, 5 s hydrodynamic injection and pH of 8.0 and 5.5 (for steviol glycosides and neotame), respectively. On the other hand, optimum separation

conditions for the indirect UV-CZE method were; UV detection at 230 nm, 0.2 M morpholine buffer at pH 12.0, +20 kV applied voltage, 30 ^{0}C cassette temperature and 6 s sample injection.

Furthermore, a highly sensitive and novel electrochemical biosensor was developed using platinum and glassy carbon electrodes fabricated with different nanomaterials. Accordingly, cytochrome c/graphene oxide – gold NPs/multiwalled carbon nanotubes (MWCNTs) modified platinum electrodes were used for the analysis of rebaudioside A. Similarly, copper NPs capped with ammonium piperidine dithiocarbamate-MWCNTs-β-cyclodextrin and laccase/2,2,6,6-tetramethylpiperidine-1-oxyl (TEMPO) immobilized graphene oxide-*p*-aminothiophenol capped ZnO NPs nanocomposites modified with glassy carbon electrodes were developed for the determination of neotame and sucralose, respectively. The electrochemical behaviour of these sweeteners towards the developed sensors was tested by using cyclic voltammetry and differential pulse voltammetry under optimum experimental conditions (pH, scan rate, accumulation time, accumulation potential, pulse amplitude, voltage step and voltage step time). The prepared nanocomposites were characterized using thermogravimetric analysis (TGA), fourier transform infrared spectroscopy (FT-IR), X-ray diffraction (XRD) and transmission electron microscopy (TEM) techniques. It was found that the developed electrochemical biosensors showed excellent catalytic activity towards the determination of natural and chemical sweeteners in commercially available food samples.

Additionally, a comparative study between capillary electrophoresis and biosensor methods revealed that at optimum experimental conditions, typical detection limits ranging from 0.02017 to 0.07386 mM for steviol glycosides, 0.01857 to 0.08214 mM for neotame diastereomers and for sucralose 0.2804 mM were achieved. In contrast to CE methods, biosensor methods attained very low detection limits of 0.264 µM, 0.013 mM and 0.325 µM for rebaudioside A, neotame and

sucralose, respectively. The unique properties of the nanomaterials in combination with electro chemical techniques provided best results with shorter analysis time in contrast to the conventional separation methods.

Finally, the computational molecular modelling tools were used to better understand the results obtained from the separation mechanisms using capillary electrophoresis. The interaction of β-cyclodextrin with steviol glycosides/neotame diastereomers and sucralose with the amine buffers were studied and the computational results were in good agreement with the elution orders observed in capillary electrophoresis. Furthermore, docking studies were performed to predict the binding affinity interactions between the artificial sweeteners and biomolecules (cytochrome c and laccase) to understand a molecular level.

List of Contents

List of Tables

List of Tables

List of Schemes

List of Figures

List of Figures

List of Figures

List of Figures

List of Figures

Acronyms and Symbols

AS	Artificial sweeteners
ADI	Acceptable daily intake
APDC	Ammonium piperidine dithiocarbamate
ATP	*p*-aminothiophenol
AuNPs	Gold nanoparticles
BE	Binding energy
BGE	Back ground electrolyte
CD	Cyclodextrin
CDE	C Docker energy
CDIE	C Docker interaction energy
CE	Capillary electrophoresis
CHAPS	3-[(3-Cholamidopropyl)dimethylammonio]-1-propanesulfonate
CHAPSO	3-([3-Cholamidopropyl]dimethylammonio) -2-hydroxy-1-propanesulfonate
CTAB	Cetyltrimethylammonium bromide
CuNPs	Copper nanoparticles
CV	Cyclic voltammetry
CZE	Capillary zone electrophoresis
CVD	Cardiovascular diseases
Cyt c	Cytochrome c
DAD	Diode array detector
DFT	Density functional theory

DPV	Differential pulse voltammetry
DTAB	Dodecyl trimethylammonium bromide
EA	Ethylamine
EDC	1-Ethyl-3-(3-dimethylaminopropyl) carbodiimide
EKC	Electro kinetic chromatography
EOF	Electro-osmotic flow
EKC	Electrokinetic Chromatography
ESI-MS	Electro spray ionization mass spectrometry
FDA	Food and drug administration
FSANZ	Food Standards Australia and New Zealand
FT-IR	Fourier transforms infrared specroscopy
GB/SA	Generalized-Born/ surface area
GCE	Glassy carbon electrode
GC-MS	Gas chromatography-Mass spectrometry
GO	Graphene oxide
GRAS	Generally recognized as safe
HF	Hartree-Fock
HILIC	Hydrophilic interaction liquid chromatography
HOMO	Highest occupied molecular orbitals
HPLC-ELSD	High performance liquid chromatography-evaporative light scattering detection
HPTLC	High performance thin layer chromatography
ITC	Isothermal titration calorimetry

JECFA	Joint Expert Committee of Food Additions
Lac	Laccase
LC–ESI–MS	Liquid chromatography-electro spray ionization-Mass spectrometry
LC–MS	Liquid chromatography-Mass spectrometry
LC-TOFMS	Liquid chromatography-Time of flight Mass spectrometry
LOD	Limit of detection
LOQ	Limit of quantification
LUMO	Lowest unoccupied molecular orbitals
MEKC	Micellar Electrokinetic Chromatography
MIA	Metal ion affinities
MM	Molecular mechanics
Mor	Morpholine
MWCNTs	Multiwall carbon nanotubes
NTM	Neotame
PB/SA	Poisson–Boltzmann/ surface area
Pip	Piperidine
Pt/Au electrode	Platinum/gold electrodes
RDE	Rotating disc electrode
Reb A	Rebaudioside A
RP-HPLC	Reversed phase-high performance liquid chromatography
RSD	Relative standard deviation
SDS	Sodium dodecyl sulphate
SPE	Solid phase extraction

Stv	Stevioside
SubFE	Subcritical fluid extraction
SUC	Sucralose
SWCNTs	Single wall carbon nanotubes
TGA	Thermogravimetric analysis
TEA	Triethylamine
TEM	Transmission electron microscope
TEMPO	2,2,6,6-tetramethylpiperidine-1-oxyl
TM-β-CD	Heptakis-(2,3,6-tri-O-methyl)-β-cyclodextrin
UNFAO	United Nations Food and Agricultural Organization
WHO	World Health Organization
XRD	X-ray diffraction
ZnO NPs	Zincoxide nanoparticles

Aims

The main focus of this study was to develop novel analytical methodologies for the determination of high intensity artificial sweeteners, steviol glycosides, neotame and sucralose in various food samples using capillary electrophoresis, biosensor based electrochemical methods complimented with computational techniques.

Objectives

1. To develop a new, facile, reliable, reproducible and accurate analytical protocols for the separation and quantification of steviol glycosides, neotame and sucralose with capillary electrophoresis and electrochemical biosensor methods.
2. To select labelling agents to enhance the sensitivity and selectivity of the methods.
3. To select nanomaterials and bio molecules to construct a biosensor to recognize steviol glycosides, neotame and sucralose molecules is a key step because the sensitivity and selectivity mainly depends on this.
4. To evaluate the performance of the developed analytical methods using various food and beverage matrices collected from different industries.
5. To validate the accuracy and precision of the developed methods using the certified reference materials.
6. To utilize molecular modelling approaches for elucidation of the receptor-ligand, metal-ligand and nanomaterial-bio molecule interactions.

Publications arising from this study

1. Ayyappa Bathinapatla, Suvardhan Kanchi, Parvesh Singh, Myalowenkosi I. Sabela and Krishna Bisetty. "Determination of neotame by high-performance capillary electrophoresis using β-Cyclodextrin as a chiral selector." *Analytical Letters*, 47 (17) **(2014)** 2795-2812.
2. Ayyappa Bathinapatla, Suvardhan Kanchi, Parvesh Singh, Myalowenkosi I. Sabela, Martin Dovey and Krishna Bisetty. "Analytical evaluation of steviol glycosides in food samples by capillary electrophoresis supported with molecular docking studies." *Journal of the Iranian Chemical Society*, 12 **(2015)** 127-136.
3. Ayyappa Bathinapatla, Suvardhan Kanchi, Parvesh Singh, Myalowenkosi I. Sabela and Krishna Bisetty. "Fabrication of copper nanoparticles decorated multiwalled carbon nanotubes as a high performance electrochemical sensor for the detection of neotame." *Biosensors and Bioelectronics*, 67 **(2015)** 200-207.
4. Ayyappa Bathinapatla, Suvardhan Kanchi, Parvesh Singh, Myalowenkosi I. Sabela and Krishna Bisetty. "Electrophoretic analysis of sucralose in food samples using amines as background electrolyte." *Analytical Methods,* (communicated).
5. Ayyappa Bathinapatla, Suvardhan Kanchi, Parvesh Singh, Myalowenkosi I. Sabela and Krishna Bisetty. "An electrochemical biosensor based on Cytochrome c/Graphene oxide – Gold NPs/ Multiwalled carbon nanotubes modified Platinum electrode for determination of Rebaudioside A". *Biomaterials,* (communicated).
6. Ayyappa Bathinapatla, Suvardhan Kanchi, Parvesh Singh, Myalowenkosi I. Sabela and Krishna Bisetty. "Laccase based biosensor for the determination of sucralose in different food samples. *RSC Advances,* (communicated).

Presentations

1. **A. Bathinapatla,** S. Kanchi, P. Singh, M. I. Sabela and K. Bisetty. "Method development for chiral separation of neotame by EKC-CE supported with molecular docking studies." SACI, held at Department of chemistry, University of KwaZulu Natal, Westville campus on September 26th, 2013, Durban, South Africa (*Poster*).

2. **A. Bathinapatla,** S. Kanchi, P. Singh, M. I. Sabela and K. Bisetty. "Analytical evaluation of Steviol glycosides in food samples by capillary electrophoresis supported with molecular docking studies, 41st SACI National Convention-Chemistry for Africa: New perspectives in the 21st century held at Walter Sisulu University, 1st -6th December, 2013, East London, South Africa (*Poster*).

3. S. Kanchi, M. I. Sabela, **A. Bathinapatla** and K. Bisetty. "Multivariant optimization and catalytic differential pulse polarographic determination of Cr (VI) in waste water samples." First International conference on Composites, Biocomposites and Nano Composites (ICCBN-2013), held at Department of Mechanical Engineering, Durban University of Technology, 2nd-4th December 2013, Durban, South Africa (*Poster*).
4. S. Kanchi, **A. Bathinapatla,** M. I. Sabela and K. Bisetty. "Nanocomposite Electrochemical sensor for the Detection of Neotame: A Density Functional Theory Approach for Biological Applications". Biosensors 2014 Conference, held at Melbourne, 27-30 May 2014, Australia (*Poster*).
5. K. Bisetty, **A. Bathinapatla,** S. Kanchi, P. Singh, M. I. Sabela. "An electrochemical biosensor based on Cyt c/GO-AuNPs/ MWCNT modified Pt electrode for determination of Rebaudioside A". Smart Materials & Surfaces International Conference; 26-28th August 2014, Bangkok, Thailand (*Oral*).

CHAPTER 1

INTRODUCTION

1.1 Dissertation overview

In nature, a number of food ingredients have sweetening features, a property that mainly varies with the change in food systems, temperature, physical state and the presence of other flavors. These food ingredients stimulate the sweet sensation by interacting with the sweet taste receptors in the mouth and throat. The materials which show sweetness are divided into two types (i) nutritive sweeteners and (ii) non-nutritive sweeteners. Nutritive sweeteners provide a sweet taste with the addition of energy and non-nutritive sweeteners provides a sweet taste without any addition of energy. The main nutritive sweeteners include glucose, crystalline fructose, dextrose, corn sweeteners, honey, lactose, maltose, invert sugars, concentrated fruit juice, refined sugars, high fructose corn syrup and various syrups. Non-nutritive sweeteners are sub-divided into two groups of artificial sweeteners and reduced polyols as shown in Figure 1.1.

On the other hand, based on their generation artificial sweeteners can further be divided into three types as (a) first generation artificial sweeteners which includes saccharin, cyclamate and glycyirizzin (b) second generation artificial sweeteners are aspartame, acesulfame K, thaumatin and neohesperidine dihydrochalcone and (c) neotame, sucralose, alitame and steviol glycosides falls under third generation artificial sweeteners [Bahndorf and Kienle, 2004]. Artifical sweeteners are also classified into three types based on their synthesis and extraction: (i) synthetic (saccharin, cyclamate, aspartame, acesulfame K, neotame, sucralose, alitame) (ii) semi-synthetic (neohesperidine dihydrochalcone) and (iii) natural sweeteners (steviol glycosides, mogrosides and brazzein protein) [Duffy and Anderson, 1998].

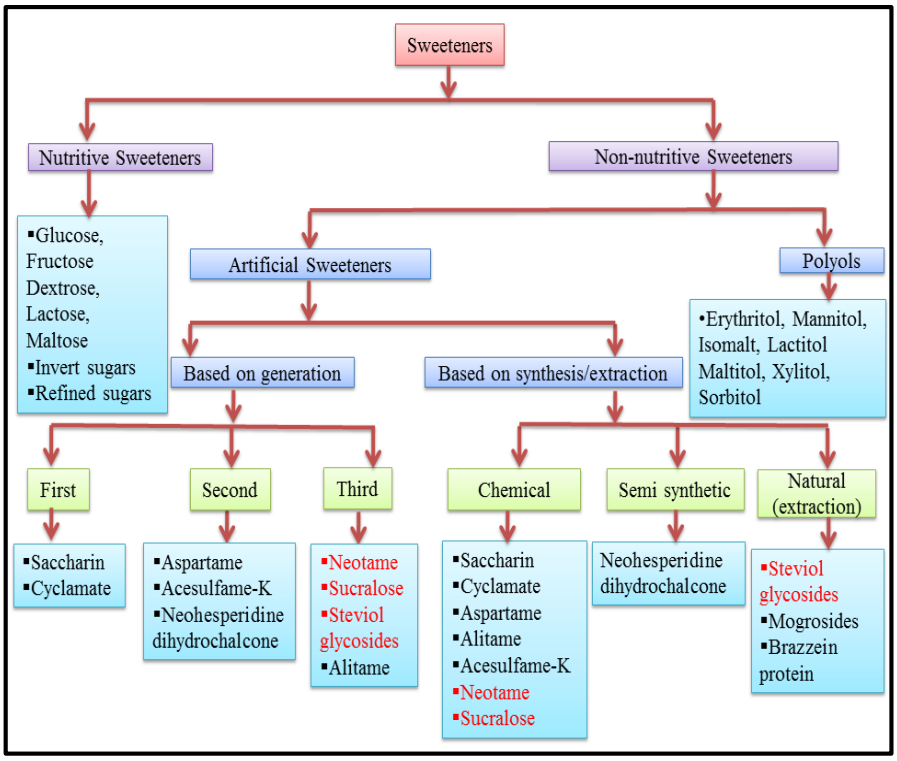

Figure 1.1: Classification of sweeteners

Polyols are other groups of reduced-calorie sweeteners which provide bulk of the sweeteness, but with fewer calories than sugars. Polyols are used in a wide variety of food products, including chewing gums, confections, ice creams, toothpastes, mouth washes, pharmaceuticals and baked goods. The commonly used polyols are: erythritol, mannitol, isomalt, lactitol, maltitol, xylitol, sorbitol and hydrogenated starch hydrolysates (HSH) as shown in Figure 1.1 [Larry and Greenly, 2003].

The high consumption of nutritive sweeteners leads to an increase in some chronic diseases like obesity, cardiovascular diseases (CVD), diabetes mellitus (type-II), dental caries, certain cancers and behavioral disorders [Shankar et al., 2013]. Hence, many of the sweet lover's want the taste of sweetness without any addition of energy. In this regard food industries were introduced to a number of low-calorie artificial sweeteners in the food and beverage sectors. Artificial sweeteners

and polyols can substitute to the nutritive sweeteners and therefore termed as macronutrient substitutes or sugar substitutes.

According to the Food Additives amendment to the Food, Drug and cosmetic Act, some sweeteners were considered as "Generally Recognized As Safe" (GRAS) and others were considered as additives [Fitch and Keim, 2012]. Based on the 1958 amendment, Food and Drug Administration (FDA) states that United States of America must approve the safety of all the additives and sweeteners [Duffy and Anderson, 1998]. The safety limit of sweeteners and food additives are expressed as the acceptable daily intake (ADI) and this concept is used by FDA and Joint Expert Committee of Food Additions (JECFA) of the United Nations Food and Agricultural Organization (UNFAO) and World Health Organization (WHO) [Duffy and Anderson, 1998].

The ultimate goal of this work was to develop simple and accurate analytical methods using capillary electrophoresis and electrochemical biosensors for the detection of "third generation" artificial sweeteners, specifically steviol glycosides, neotame and sucralose. During the past decade, capillary electrophoresis (CE) became a preferred separation method for many analytical problems. The main advantages of CE over high performance liquid chromatography (HPLC) are the shorter separation times, simpler instrumentation, use of inexpensive capillary materials and very low solvent consumption. Literature survey revealed that numerous HPLC methods have been developed for these sweeteners, but very few CE methods were reported. Few disadvantages were identified in the separation of artificial sweeteners with HPLC and HPLC coupled methods as stated: (i) HPLC-RI method was sensitive to temperature fluctuations and inconsistence in retention times withlow compatability andgradient elution (ii) HPTLC methods shows less separation efficiencywhen compared to the CZE method (iii) HPLC-ELSD is an inexpensive mode in liquid chromatography but it is completely applicable for volatile mobile phases to avoid

deposits in the heating chamber or optical cell (iv) HPAEC-PAD and LC-MS methods requires expensive experimental setup and elaborate cleanup procedures.

Considering the drawbacks from HPLC, HPLC coupled methods, in this work an electro kineticchromatography (EKC-CE) and an indirect capillary zone electrophoresis (UV-CZE) method was developed for the determination of steviol glycosides, neotame and sucralose in different food samples. An electrokinetic kinetic chromatography-CE was developed by Bathinapatla et al., for the separation and determination of two major steviol glycosides [Rebaudioside A (Reb A) and Stevioside (Stv)]. At optimum experimental conditions the achieved detection limits ranging from 2.017 X 10^{-5} to 7.386 X 10^{-5} M for Reb A and Stv with fair resolution between peaks [Bathinapatla et al., 2015]. Bathinapatla et al., developed an EKC-CE method in presence of TM-β-CD as a chiral selector for the chiral separation of neotame (L,L and D,D). Under the optimum experimental conditions the obtained recoveries and limits of detection for L,L-neotame and D,D-neotame were 95.66–99.00%, 0.01857 and 0.08214mM respectively [Bathinapatla et al., 2014]. Simple amine buffers (morpholine, piperidine, ethyl amine and triethyl amine) were used as background electrolytes and the separation of sucralose (SUC) were achieved in less than 7.5 min with low detection limits ranging from 0.3804 to 1.5215 mg/ L.

Additionally, nanomaterials and their applications in electrochemistry to enhance the performance of biosensors has gained widespread interest. Currently, there are no reported biosensor methods for the determination of these sweeteners. Accordingly, in this work it was necessary to develop new robust analytical methods for the separation and determination of high intensity artificial sweeteners in various food matrices using CE and biosensor based electrochemical methods. Additionally, this work was also supported by computational modelling experiments.

1.2 Importance of chiral separation

In the early 1980s, there were no preparative analytical chiral separation methods and it was difficult to achieve chiral separation in the field of pharmaceutical and the food industry. From the difficulties observed especially in pharmaceutical industries due to the usage of recemic mixtures, it was clear that chiral drugs be enantio-separated and that each enantiomer be used separately. Currently, enantiomers or diastereomers are considered as different compounds, which shows distinct biological interactions and with different pharmacological, pharmacokinetic or toxicological activities. The body is highly chiral selective; it will interact with each enantiomer or diastereomer differently and metabolize them in separate pathways to produce different pharmacological activities. One isomer may show desired therapeutic activities, while the other may be inactive or produces unwanted side effects. In the case of the latter, the inactive enantiomer must be metabolized and thus represents an unnecessary burden for the organism. Hence, it is important to avoid the impact of one isomer on the significant activities of the other, using chiral separation technique [Li and Haynie, 2006].

Chiral molecules (enantiomers or diastereomers) are mainly differentiated on the basis of their interaction with the chiral selectors. Development of chiral selectors or chiral stationary phases for different analytical techniques such as CE, HPLC and GC attracted increasing interest for the enantioseparation. An appropriate chiral selector plays an important role in the resolution of chiral compounds. Over the past decade CE has become a popular alternative to HPLC for enantiomer separation in the pharmaceutical industry. The list of chiral selectors used in CE for the chiral separation includes copper–amino acid complexes [Gassmann et al., 1985; Cohen et al., 1987], bile salts [Nishi et al., 1990], chiral crown ethers [Kuhn et al., 1992], chiral micelles [Otsuka et al., 1990, 1991; Dobashi et al., 1989], proteins [Barker et al., 1992; Arai et al., 1994] and

cyclodextrins (CDs) or their derivatives [Sepaniak et al., 1992; Soini et al., 1992; Altria et al., 1993]. These CDs and their derivatives are extensively studied and widely used for the enantiomeric resolution of a large number of compounds in the pharmaceutical and food industries. [Godel and Weinberger, 1995; Chankvetadze and Blaschke, 2001; Liau et al., 2003; Min et al., 2006; Giuffrida et al., 2012].

1.2.1 Cyclodextrins (CDs)

Cyclodextrins (CDs) are structurally cyclic and non-reducing oligosaccharides which are obtained from starch and contains six-α-CD, seven-β-CD and eight-γ-CD or more glucopyranose units, reported by Schardinger [Szejtli, 2004] [Figure 1.2].

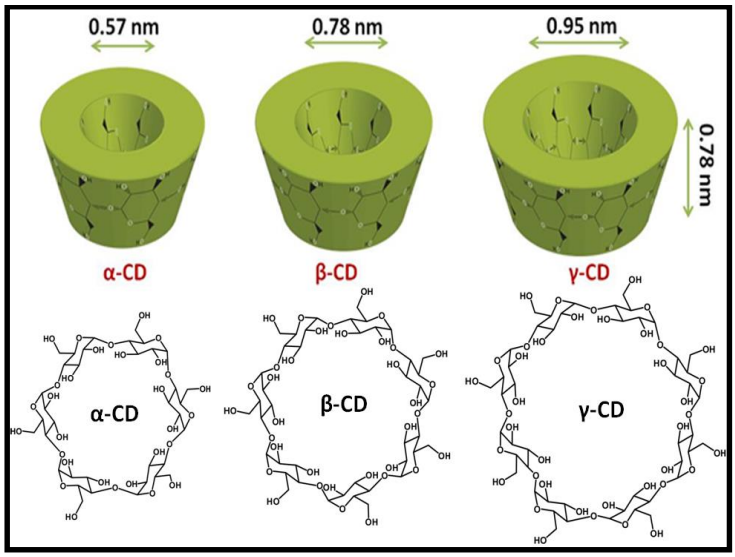

Figure 1.2: Chemical structures of different cyclodextrins

They are also known as cyclohexamylose (α-CD), cycloheptamylose (β-CD), cycloctamaylose (γ -CD), cycloglucans, glucopyranose and schardinger dextrins. The ability of CDs to form complexes with a wide variety of molecules mainly depends on their glucopyranose

structural units with a hollow basket/cavity providing a hydrophobic interior and a hydrophilic exterior (Appendix Table 2.1).

Chiral recognition is based on the inclusion of the bulky hydrophobic group of the analyte into the hydrophobic cavity of the CD and lateral interactions of the hydroxyl groups at the C2 and C3 on the upper rim of the CD, such as hydrogen bonds and dipole-dipole interactions with the analyte. Therefore, CDs and their derivatives have been widely used in separation science since the early 1980s. A number of CDs have been synthesized and utilized, but our main focus will be on the β-cyclodextrins. From the physical properties, β-CDs have less solubility than other CDs, hence the functionalization with hydroxylpropylated, sulphobutylated, methylated branching with glucosyl or maltosyl rings increases the solubility and inclusion capacity of parent CD. Heptakis-(2,3,6-tri-O-methyl)-β-CD [Figure 1.3] falls under neutral CDs with other various CDs including Heptakis-(O-methyl)-β-CD, Heptakis-(2,6-di-O-methyl)-β-CD, hydroxyethyl-β-CD etc.

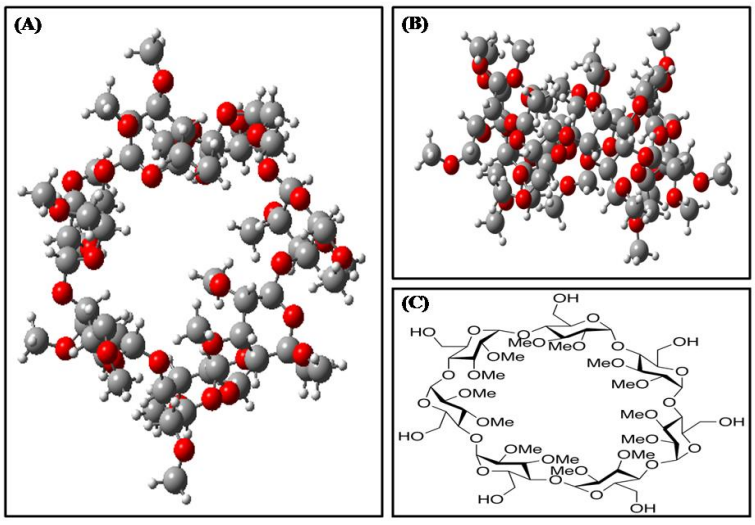

Figure 1.3: Structures of heptakis 2,3,6-tri-o-methyl-β-cyclodextrin: A: 2D image (top), B: side view (ball and stick model carbons are in grey and oxygens are in red colour) C:general structure.

Most of the CD derivatives represent mixtures of different products showing different substitution patterns resulting in difficulties in trying to reproduce separations. Studies have shown that chiral recognition/selectivity of various chiral selectors varies with different analytes depending on their bulkiness and hydrogen bonding ability.

Literature studies have also shown that the β-CD has a cavity that is able to cover a wide range of analytes in particular those of pharmaceutical interest. In the inclusion-complexation process the analytes either fit in completely or with their hydrophobic part interacting with the CD cavity. The analyte's hydrophobic part enters the cavity through either of the two openings, with the 6-hydroxyl and 3-hydroxyl groups. The hydroxyl groups on the CDs can however be easily modified *via* chemical reactions, in order to obtain different derivatives to suite the nature of the analyte. The composition of the derivative however, is highly dependent on the reaction conditions, reagents type, ratio and other parameters [Fanali, 2000]. Hence, based on the solubility and cavity size Heptakis-(2,3,6-tri-O-methyl)-β-CD was used as a chiral selector in this work.

1.3 Electrochemical and biosensor methods

To the best of my knowledge, literature survey revealed that only chromatographic methods are available for these sweeteners with no reported electrochemical work using biosensors. In this regard, our laboratory recently [Bathinapatla et al., 2015] reported an electrochemical sensor based method for the determination of neotame (NTM) in different food samples. The obtained results showed the detection limit of 0.013 mM with a recovery percentage of 98.97%. Further, a novel cytochrome c modified nanocomposite electrochemical biosensor was developed for the electrochemical determination of rebaudioside A (Reb A) in different food

samples. Under the optimized conditions, linear calibration differential pulse voltammetry (DPV) plots for the detection of Reb A ranged from 0.001to 1.25 mM with detection limits ranging from 0.26 to 0.75 µM. Sucralose was determined by the laccase immobilized biosensor and the detection limits were achieved ranging from 0.32 to 1.15 µM at a signal to noise ratio of 3. To construct the different biosensors various nanomaterials and biomolecules such as carbon nanotubes, graphene oxide, nanoparticles, cytochrome c and laccase were used.

1.3.1 Nanomaterials

Nanotechnology plays an increasingly important role in the development of sensors, especially "Electrochemical and biosensors". The sensitivity and detection ranges are vital parameters for the development of biosensors. Hence, the sensitivity of the sensor system mainly depends on the effective surface area of the device, i.e. the area which interacts with the analyte. By increasing the surface area, numerous nanomaterials such as carbon nanotubes, fullerenes, graphene oxide and nanoparticles have been introduced in the field of sensors and among these nanomaterials, nanoparticles has gained widespread recognition. In recent years, a wide variety of nanoparticles with different properties were applied to the biosensors. Nanoparticles exhibits unique chemical, physical and electronic properties that are different from those of bulk materials. Nanoparticles can provide high surface-to-volume ratio due to their small size (normally in the range of 1-100nm) [Buzea et al., 2007] which improves the performance of the biosensors.

Different types of nanoparticles are used in the fabrication of biosensors including metal nanoparticles (Au, Ag, Pd, Pt, Cu and Ru), metal oxide nanoparticles (TiO_2, CeO_2, ZnO and Al_2O_3), semiconductor nanoparticles and even composite nanoparticles. Most recent studies showed that biosensors composed of nanoparticles yielded rapid, simple and accurate measurements, which

offering exciting new opportunities for the development of biosensors. Accordingly, in this work metal nanoparticles (Au and Cu) and metal oxide nanoparticles (ZnO) were used to fabricate the electrodes.

(i) Metallic nanoparticles (MNPs) (Au/Cu NPs)

MNPs have many potential applications in the field of chemical, medical and biological sciences [Murphy et al., 2008]. There are two common approaches used in the preparation of MNPs namely: physical & chemical approaches. In the former, NPs are synthesized directly from the bulk parent metal, where metal salts are used as starting materials followed by the reduction steps which in the case of chemical methods [Biswal et al., 2011; Bajpai et al., 2007], the most important aspect of these NPs are for the stabilization and to avoid aggregation.

Literature reports revealed that in many cases ligands with thiol (-SH) and amine ($-NH_2$) functional groups were used to co-ordinate the NPs strongly to avoid the formation of bulk NPs [Daniel and Astruc, 2004].

The use of gold nanoparticles (AuNPs) in the fabrication of sensors to detect eugenol **[**Lina et al., 2014], dibutyl phthalate [Li et al., 2015], estradiol [Dharuman et al., 2013], nickel and zinc [Azzam et al., 2014], quercetin and rutin [Yola and Atar, 2014] were widely reported. Copper nanoparticles (CuNPs) were used to analyze ascorbic acid [Chauhan et al., 2011], acrylamide [Batra et al., 2013], D-amino acid [Lata et al., 2013], glucose [Lin et al., 2013] and NTM [Bathinapatla et al., 2015].

(ii) Metal oxide NPS (ZnO NPs)

ZnO NPs have attracted the interest of several scientists in recent years due to their remarkable properties, because of their large surface area and high catalytic activity. ZnO NPs is a semi-conductor with a band gap energy of 3.36 eV at ambient temperature. The morphology and size of ZnO NPs depends on the content of the precursors used in the preparation of these NPs [Park et al., 2010].

Regarding the use of ZnO NPs for sensor applications, Baruwati et al., [Baruwati et al., 2006] reported a liquefied petroleum gas (LPG) and ethanol (EtOH) sensor. The ZnO NPs were prepared from zinc nitrate as a precursor and ammonium hydroxide as a base at 120 ^{0}C for 6-24 h. ZnO NPs were prepared by a solid-state chemical reaction between zinc chloride and NaOH under ambient conditions and resulted ZnO NPs were used in sensing of methanal and xylene [Cao et al., 2008]. Li et al., developed a mediator-free phenol biosensor, ZnO NPs were used for the immobilization of tyrosinase via electrostatic interactions and further this material was casted onto a GCE surface via a chitosan film [Li et al., 2006].

(iii) Capping agents

Current modifications of the electrode surface or the nanomaterial surfaces with metal nanopartcles (MNPs) with diameters ranging between 1 and 100 nm included gold, silver, platinum, palladium, nickel, copper and zirconium showed good performances such as high effective surface area, enhancement of mass transport, catalysis and good biocompatibility which led to the development of various electrochemical or biosensors based on MNPs [Turkmen et al., 2014; Liu et al., 2012; Kaur et al., 2013]. These significant properties are mainly dependent on the size and shape; it was found that MNPs in small sizes can facilitate the predominant electron

transfer to the electrode surfaces. However, the size control of MNPs is a challenge, due to their high surface energy which easily undergoes aggregation and precipitation which will greatly reduce the catalytic activity.

Dithiocarbamates (DTCs) on the other hand, belongs to a class of small organic molecules with a strong chelating ability towards inorganic species and NPs are synthesized by the exothermic reaction between either ammonium or a primary/secondary amine and carbon disulfide in the presence of sodium hydroxide or excess amine. *N*-substituted dithiocarbamic acids are generally prepared as their substituted ammonium or sodium salts by the reaction of carbon disulfide (CS_2) with a primary/secondary amine in alcoholic [Hester and Rohm, 1953] or aqueous solution [Martin, 1959]. Due to the exceptional chelating properties of DTCs, they were recently introduced into the field of electrochemical sensors and biosensors. DTCs are used as good capping agents through their thiol functional groups for nanoparticles, such as gold [Mpanza et al., 2014], copper [Bathinapatla et al., 2015], cobalt [Nabipour, 2011] and ruthenium [Chen et al., 2007]. Accordingly, in this study ammonium piperidine dithiocarbamate (APDC) [Figure 1.4] was used for the capping or functionalization of CuNPs to prepare APDC anchored copper nanoparticles on multi-walled carbon nanotubes with assimilated β-cyclodextrin nanocomposite to determine NTM. P-amino thiophenol (ATP) [Figure 1.4] has attracted a great deal of attention for the preparation of 2D/3D assembly for the NPs through covalent or electrostatic interactions.

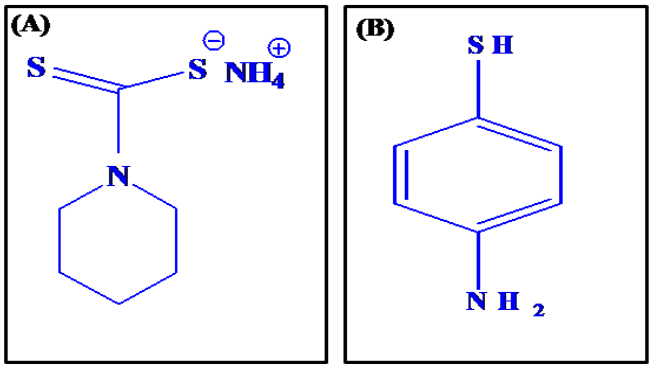

Figure 1.4: Chemical structures of (A) Ammonium piperidine dithiocarbamate (APDC) (B) *p*-amino thio phenol (ATP).

NPs were capped by thiol groups and amino groups useful to make covalent bonds on the functionalized surfaces. In addition, the presence of phenyl groups in ATP enhanced the electrical coupling between the electrode and nanoparticles. ATP extensively used for the capping of nanoparticles such as gold [Gopalan et al., 2006, 2007; Yola et al., 2013, 2014], Palladium [You et al., 2013]. In this work ATP was used as a capping agent for ZnO NPs and also to prepare GO-ATP-ZnO nanocomposite for the determination of SUC.

(iv) Carbon nanotubes

Carbon nanotubes (CNTs) have been a promising novel type of smart material with unique chemical, electrical, mechanical and structural properties and steadily growing interest on this material since their discovery [Rao et al., 2001]. Compared to other smart materials, CNTs shows metallic, semi conducting, super conducting electron transport and have largest elastic modulus with a hollow core. CNTs are made by chemical vapor deposition (CVD), carbon arc or laser evaporation methods and can be divided into two types: single wall carbon nanotubes

(SWCNTs) and multiwall carbon nanotubes (MWCNTs). SWCNT was formed by rolling up a single graphite sheet into a tube which results in a cylindrical nano structure with a high aspect ratio. MWCNTs contains several graphene sheets with inter layer spacing of 3.4 Å, resulting in cylindrical case like structures as shown in Figure 1.5 [Wang, 2005]. Due to their exceptional properties, CNTs are used as nanomaterials in numerous studies.

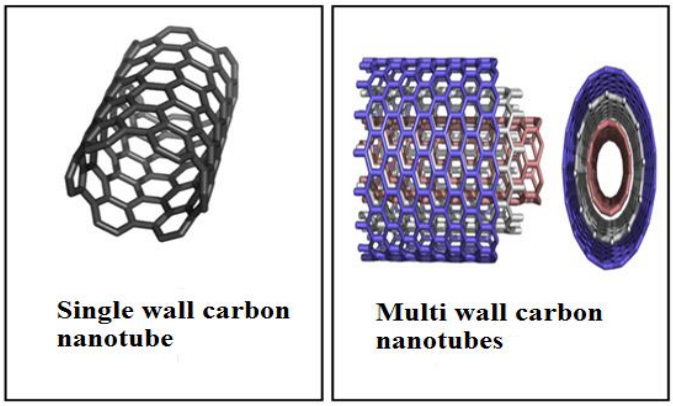

Figure 1.5: Structures of carbon nanotubes

MWCNTs have a high surface area in the 3D arrangements by forming edge-plane-like graphite sites at the ends and possess interesting electrochemical properties which can be used for the construction of electrochemical sensors (CNTs-ECS). CNTs based ECS exhibit low detection limits, high sensitivities and fast responses due to their signal enhancement provided by high surface area, low overvoltage and rapid electrode kinetics. Accordingly, in this work MWCNTs were used for the construction of electrochemical and biosensors for the determination of NTM and Reb A.

(v) Graphene oxide

Graphene oxide (GO) is the product of chemical exfoliation of graphite which has attracted great interest in recent years. Its structure seems like functionalized graphene, carboxylic acid groups at the edges and phenol hydroxyl and epoxide groups mainly on the basal plane as shown in Figure 1.6.

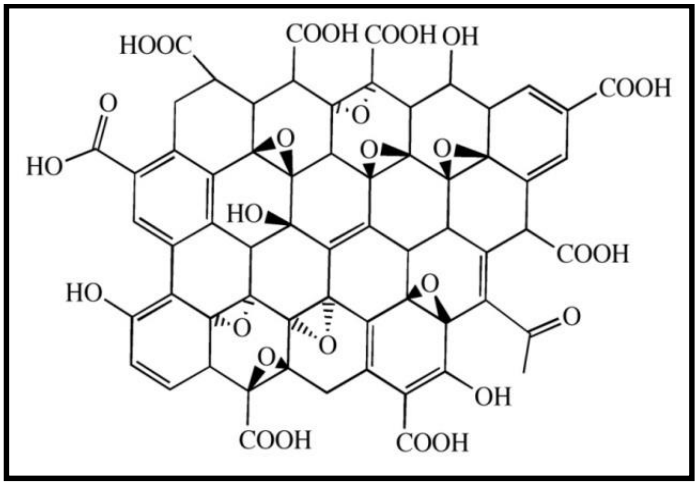

Figure 1.6: Chemical structure of Graphene oxide

These functionalities provide amphiphilic nature with a largely hydrophobic basal plane and hydrophilic edges to disperse in water [Zhoua et al., 2014]. Recently it was reported that some carbon materials including fullerenes, multiwalled and single walled carbon nanotubes which could be dispersed in water with the aid of GO through π-π interactions. [Zhoua et al., 2014]. Additionally, the large surface area (two accessible sides), the abundant oxygen containing surface functionalities such as epoxide, hydroxyl and carboxylic acid groups affords GO sheets to be promising for many more applications [Li et al., 2008; Park and Ruoff, 2009; Tung et al., 2009]. Accordingly, in this work GO was used for the construction of electrochemical biosensors for the determination of Reb A and SUC.

1.4 Cytochrome c

The cytochrome complex or Cyt c is a small metallo-heme protein which is found in the inner membrane of the mitochondrion. It is a highly water soluble protein with a solubility of about 100 g/L and is an essential component of the electron transport chain, where it carries one electron. Cyt c is a highly conserved protein with a molecular weight of 12.7 kDa and consists of 108 amino acids with a single heme group [Volkov et al., 2011; Fuku et al., 2012; Kroemer, 1999]. The protein contains mainly two groups which are Cytochrome c reductase (Complex III) and Cytochrome c oxidase (Complex IV). The mechanism for the electron transportation between Cytochrome c reductase and Cytochrome c oxidase is, Cytochrome c reductase reduces the iron of Cyt c's heme group to Fe^{2+}, while Cytochrome c Oxidase oxidizes it back to Fe^{3+} [Voet and Voet, 2004]. Cyt c reacts with various inorganic and organic radicals [Koppenol and Butler, 1984] and due to the unique electron transfer property of Cyt c, it is using as a novel electrode modification biomaterial to construct an electrochemical biosensor. Accordingly, Cyt c was used for the construction of a biosensor based on Cyt c/AuNPs–GO/ MWCNTs modified platinum electrode for determination of rebaudioside A.

Molecular docking methods were applied to evaluate the interactions between Cyt c with a series of structurally different flavonoid glycosides and flavonoid molecules to characterize the effective binding sites and binding modes of the protein complexes [Wang et al., 2013]. Hence, in this work we studied the interactions of Reb A with Cyt c which acts like a molecular receptor. To create a binding sphere in Cyt c for docking, nearly 22 amino acids in chain "A" were considered [Figure 1.7] and docking results showed that rebaudioside A comfortably fits into the binding pocket of Cyt c through hydrophobic and hydrophilic interactions.

The binding pockets were created by using amino acid lysine at different positions such as: 8, 13, 27, 72, 79, 86 and 87 (thus containing the evolutionary conservative 72-87 loop)

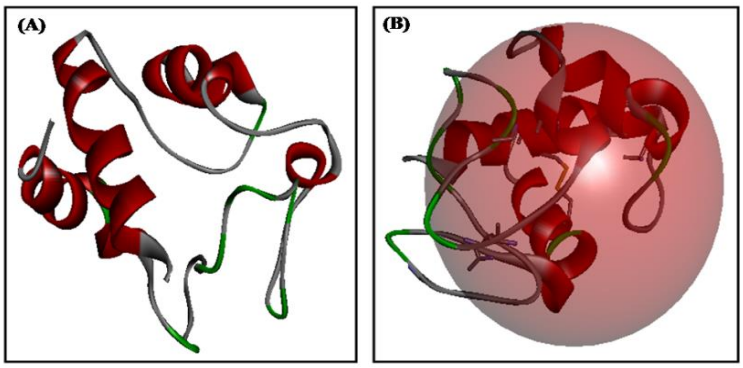

Figure 1.7: (A) Crystallographic structure of Cyt c (Chain A) (B) The binding sphere created using active sites in Cyt c showing in dark red colour

1.5 Laccase

Laccase (Lac) (p-diphenol: oxygen oxidoreductase, (EC 1.10.3.2) [Figure 1.8] is one of the few enzymes investigated from the 19th century. Laccases are either mono or multimeric copper-containing oxidases that catalyses the oxidation of a wide variety of organic and inorganic substrates, including amino phenols, mono-, di-, poly phenols, methoxy phenols, benzenethiols, aromatic amines and ascorbates by the four electron reduction of oxygen to water [Xu et al., 2009]. Laccase can oxidize most of the phenolic compounds alone, but in some cases the reactivity of the Lac is ineffective towards the substrates. In such cases the presence of mediators, which are low molecular weight electron transfer agents can enhances the reactivity of the Lac.

In the past decade, usage of stable nitroxyl radical 2,2,6,6-tetramethylpiperidine-1-oxyl (TEMPO) in the catalytic oxidation of carbohydrates has becoming one of the most promising procedure. Laccases are able to oxidize TEMPO via one electron oxidation to the corresponding oxoammonium cation and this oxoammonium cation can oxidize alcohols, thus allowing regeneration of TEMPO [Arends et al., 2006]. Using laccase/TEMPO system, Baratto et al., studied oxidation of natural glycosides to their carbonyl products [Baratto et al., 2006] and glycerol

oxidation studied by Liebminger et al., [Liebminger et al., 2009]. Recently, Jausovec et al., used this system to introduce aldehyde and carboxylic groups to cellulose nanofibers [Jausovec et al., 2014]. In this work laccase/TEMPO system was used to construct a biosensor in combination of GO-ATP-ZnO NPs based nanocomposite to determine SUC.

To create a binding sphere in Lac for docking, nearly 6 amino acids in chain "A" were considered [Figure 1.8] and docking results showed that sucralose comfortably fits into the binding pocket of Lac through hydrophobic and hydrophilic interactions. The binding pockets were created by using amino acids lysine-261, Ser-255, Asp-242 and Arg-256.

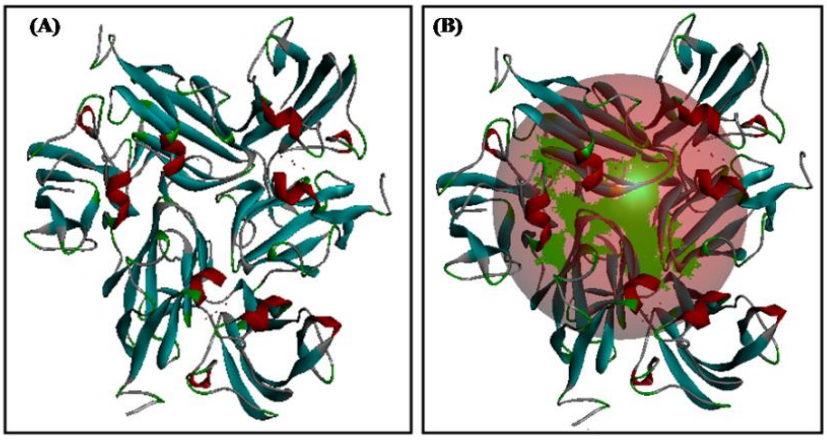

Figure 1.8: (A) Crystallographic structure of Lac (B) The binding sphere created using active sites in Lac showing in dark red colour.

CHAPTER 2

LITERATURE REVIEW

This chapter deals with an in depth literature review of the artificial sweeteners, steviol glycosides, neotame and sucralose investigated in this work, with particular emphasis on the analytical separation mechanism including the background electrolyte (BGE) and the role of chiral selectors for the analysis of sweeteners through capillary electrophoresis.

2.1 High intensity sweeteners

High intensity sweeteners can be used individually or in combination with other sweeteners. Among all the known artificial sweeteners, very few are allowed to be used in the food industries. The use of artificial sweeteners varies from country to country, for example eight authorized artificial sweeteners allowed to use in European Union (EU) (acesulfame K, aspartame, cyclamate, neotame, neohesperidine dihydrochalcone, saccharin, steviol glycosides and sucralose). In terms of the Food and Drug Administration (FDA) in the US and Japan, cyclamate, neohesperidine dihydrochalcone and steviol glycosides were not included in the list [Japan FFCR, 2013]. However, in Food Standards Australia and New Zealand (FSANZ), China and Taiwan all artificial sweeteners, except neohesperidine dihydrochalcone remaining are allowed to be used in their food industries [Chang and Yeh, 2014] [Appendix Table 2.2]. The common trend in the food industry is to use mixed forms of artificial sweeteners, commonly referred to as “Sweetener blends”. The main advantage of sweetener blends is to reduce the side effects of one sweetener in the mixture and to enhance the overall sweetness of the system. A well-known sweetener blend is saccharin-cyclamate (1:10), the bitterness of the saccharin can be masked with cyclamate and the unpleasant taste of the cyclamate can be masked by saccharin, as a result the sweetening capability

of the mixture finally increases [Zygler et al., 2009]. Similarly the bitterness taste of stevioside is masked with the mixture of rebaudioside A and other artificial sweeteners [Midmore, 2002]. The safety of artificial sweeteners is also controversial due to their undesirable health effects which includes dermatological problems, headaches, mood variations, behavior changes, respiratory difficulties, seizures, allergies and cancer [Shankar et al., 2013]. Recently, the sweeteners have been considered as "global emerging pollutants" because the prominent concentration levels in ground water, soil, dust were noticed [Ordonez et al., 2013]. Hence, considering the safety aspect of the consumer it is therefore necessary to control the content of artificial sweeteners in foods and beverages.

Saccharine (2H-1λ6,2-benzothiazol-1,1,3-trione)was first discovered by Remsen and Fahlberg at John Hopkins University in 1879 [Shankar et al., 2013]. Saccharine is marketed under the brand names of Sweet'N Low, Sugar Twin and Necta Sweet. Due to excellent thermal stability and solubility of saccharine, it is used in the wide range of food products like soft drinks, baked goods, jams, canned fruit, candy, salad dressing, dessert toppings, chewing gum and in household products such as toothpaste, lip gloss, mouthwash, vitamins and also in pharmaceuticals. The Adequate Dietary Intake (ADI) for saccharin is set at 5 mg/kg body weight per day for adults and children [Appendix Table 2.3]. Cyclamate (sodium N-cyclohexyl sulfamate) is a first generation artificial sweetener with sweetness being more than 30 times than sugar and approved in nearly 50 countries [Bopp et al., 1986]. In 1966 a first study was conducted on the safety of cyclamate in animals and revealed that some intestinal bacteria can metabolize this sweetener as cyclohexylamine resulting chronic toxicity [Hellsten, 2010]. Acesulfame K (potassium 6-methyl-2,2-dioxo-2H-1,2λ6,3-oxathiazin-4-olate) was discovered by Hoechst company in 1967 [Claub

and Jensen, 1970]. It is well known sweetener under the brand names of Sunette, Sweet One and Swiss Sweet. In 1998, the FDA approved the use of this sweetener in soft drinks and beverages which was previously allowed to be used only in foods such as sugar free baked goods, chewing gum and gelatin desserts. The ADI for acesulfame K is 15 mg/kg body weight [Kroger et al., 2006]. Alitame ((3S)-3-amino-4-[[(1R)-1-methyl-2-oxo-2-[(2,2,4,4-tetramethyl-3-thietanyl) amino]ethyl]amino]-4-oxobutanoic acid) was discovered by chemists at the Pfizer pharmaceutical company in 1979 [Ellis, 1995] [Appendix Table 2.3]. The brand name of alitame is "Aclame" and due to its thermal and acidic stability, it is used in a wide range of food and beverages including bakery wares and water-based flavored drinks [Chattopadhyay et al., 2011]. Neohesperidine dihydrochalcone (NHDC) (1-[4-[[(2S,3R,4S,5S,6R)-4,5-Dihydroxy-6-(hydroxymethyl)-3-[[(2S,3R,4R,5R,6S)-3,4,5trihydroxy-6-methyl-2-tetrahydropyranyl]oxy]-2-tetrahydropyranyl]oxy]-2,6-dihydroxyphenyl]-3-(3-hydroxy-4-methoxyphenyl)propan-1-one), is a semi-synthetic sweetener which was first synthesized by Horowitz and Gentili in 1963 [Amin et al., 2013]. The safety studies of NHDC demonstrates that about 750 mg neohesperidin dihydrochalcone per kg body weight per day do not show any effect in rats [Linaet al., 1990]. Aspartame (methyl ester of L-aspartic acid and L-phenylalanine) was first discovered by James Schalatter, a chemist who was working on anti-ulcer drugs in 1965 [Shankar et al., 2013]. It is nearly 250 times sweeter than sucrose and approved in nearly 90 countries under the commercial name of Equal, Nutra Sweet, and Nutra Taste. According to the FDA, the acceptable daily intake of aspartame for humans is about 50 mg/kg body weight for both adults and children [Learn about cancer, 2012]. The safety studies of aspartame revealed that, enzymes called "peptidases" which is used to break the peptide bond can rupture aspartame into two amino acids resulting in the formation of phenylalanine and aspartic acid. People, who suffer with genetic disorder like

phenylketonuria are to avoid the usage of aspartame because they cannot metabolize phenylalanine to tyrosine and this causes to brain damage [FDA statement on European aspartame study, 2013] [Appendix Table 2.3].

2.1.2 Analytical separation of steviol glycosides (Diterpene glycosides)

Stevia rebaudiana Bertoni, an herbaceous perennial shrub, belonging to the Asteraceae family also known as ‘‘Sweet Leaf’’, “Sweet weed”, “Honey leaf” and “Sweet Herb” has attracted economic and scientific interest due to the non-nutritive sweetness and the therapeutic properties of its leaf [Midmore, 2002]. From hundreds of years in Paraguay and Brazil stevia leaves have been used as “Sweet Treat” to prepare local teas and medicines. Japan and Korea, are the largest consumers of stevia extracts consuming about 200 and 115 tons, respectively. In Japan, stevia replaces the artificial sweeteners like aspartame which were around since 1970s. The stevia sweeteners are approximately 300 times sweeter than sugar [Liu et al., 1997; Geuns, 2010]. Lately, the use of stevia has been approved by the Food and Drug Association in South Africa with the recent promulgation (Foodstuffs, Cosmetics and Disinfectants Act, 1972, 10th September 2012) of the new sweetener regulations [Regulations relating to the use of sweeteners in foodstuffs. Foodstuffs, cosmetics and disinfectants act (1972)]. The regulations made by Joint FAO/WHO Expert Committee on Food Additives (JECFA) for steviol glycosides requiring a purity level of about 95% of the seven well known steviol glycosides [Liu et al., 1997]. The ADI (acceptable daily intake) for steviol glycosides by JECFA expressed from 2 to 4 mg/kg bodyweight [Geuns, 2010]. Stevia leaves were recently reported to contain more than 35 *ent*-kaurene-type diterpene glycosides, the most abundant of which are rebaudioside A (Reb A) and stevioside (Stv) [Zimmermann et al., 2011] [Figure2.1].

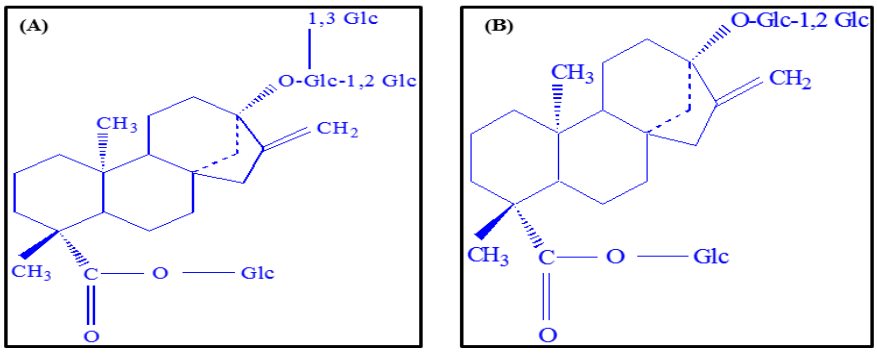

Figure 2.1: Chemical structures of major steviol glycosides rebaudioside A (Reb A) and stevioside (Stv)

Traditionally, the dry weight percentages of glycosides present in the leaves were reported as stevioside (Stv) ranging from 5 to 10 %, rebaudioside a (Reb A) from 2 to 4 % and with a lower percentage reported for rebaudioside C (Reb C). On the other hand, the relative sweetness of the Stv ranges from 60 to 70 % and between 110 to 270 times sweeter than sugar, while Reb A ranged from 30 to 40 % and between 180 to 400 times sweeter than sugar, resulting in these two compounds being the sweetest compounds amongst the remaining glycosides [Midmore, 2002]. The quality of the taste also varies among the compounds; Stv has a slight bitterness and astringency after taste in addition to sweetness, while Reb A has a more pure sweetness than Stv without any bitterness after taste, comparatively similar to those of sucrose [Woelwer-Rieck, 2012; Tadhani et al., 2007]. Hence, in most of the commercially available real stevia samples, Reb A is used as a sweetening component due to its exceptional stability and superior sweetness [Mauri et al., 1996]. Apart from the sweetening properties, other health benefits of steviol glycosides includes anti-hypertensive, anti-hyperglycemic and anti-human rotavirus activities [Tadhani et al., 2007]. On the other hand, the reported drawbacks for the impure stevia glycosides include hypotension, diuresis, natriuresis and kaliuresis [Mauri et al., 1996; Melis,

1992a, 1992b]. The composition of the stevia components in the leaves is highly dependent on the nature of the soil, climate and the methods used for extraction and purification [Kuznesof, 2007].

A survey of the reported literature for the separation and the determination of steviol glycosides in different food samples revealed that most of the analytical work were done with high-performance liquid chromatography (HPLC). Jadhao et al., reported an improved RP-HPLC method for the quantitative estimation of stevioside (Stv) with the average recovery of 97-99 % and detection limits of 0.02 to 0.05 µg/mL [Jadhao et al., 2011]. Samah et al., reported preparative HPLC with soxhlet extraction method for the analysis of Stv and Reb A. In this method, two analytes (Stv and Reb A) were not well separated, a major drawback of this method [Samah et al., 2012]. Sold phase extraction coupled with HPLC method was developed for the determination of Stv in plant material and fruit teas. Experimentally 20 tea bags from 5 tea boxes were randomly selected and analysed for Stv with mean value of 8.14 ± 2.71 mg/mL [Vanek et al., 2001]. A fast isocratic HPLC method was reported by Bergs et al., for the analysis of nine steviol glycosides with a LOD and LOQ of 0.0004 and 0.0038 mg/mL in less than 15 min [Bergs et al., 2012]. Kolb et al., reported HPLC method using an amino column for the analysis of two major steviol glycosides in 30 food samples, and found that Stv and Reb A content ranged from3.78-9.75 to 1.62-7.27% with recoveries ranging from 98.5% and 100.5%, respectively [Kolb et al., 2001]. Improved HPLC method was reported by Woelwer-Rieck et al., by analyzing two major steviol glycosides collected from different places in Germany. In this method authors employed water and a solid-phase extraction (SPE) methodologies using two types of HPLC columns. The results for the real samples with the Luna HILIC columns were in good agreement in terms of concentration and ratios than with the Luna $NH_2$100A [Woelwer-Rieck et al., 2010]. Zimmermann et al., reported HILIC method for the analysis of three steviol glycosides by studying the effect of HILIC column

robustness against the buffer concentration and aqueous percentage. The obtained results showed that the column order in terms of robustness against changes in the buffer concentration were: TSK gel > Luna > Nucleodur > Kinetex [Zimmermann et al., 2011]. Hurum and Robbers compared the charged aerosol detection with UV detection in HPLC method and they found that the charged aerosol detection was better than the UV detection. The LOD values with charged aerosol and UV detection for Reb A and Stv were found to be 0.7, 0.4 and 2.3, 1.2 µg/mL respectively [Hurum and Rohrer, 2011]. Erkucuk et al., reported a HPLC method coupled to super critical fluid extraction (SFE) with yield of 36.66 mg/g for Stv and 17.79 mg/g for Reb A [Erkucuk et al., 2009]. Hutapea et al., developed a HPLC method for the separation and quantification of Stv and its metabolites using reversed-phase C18Nova-Pack column with a gradient elution of acetonitrile/water mixture. The applicability of the method was demonstrated by different real samples like blood, feces and urine of hamsters with detection limits of 0.4 to 0.6 µg/L [Hutapea et al., 2005]. Chang and Yeh developed a liquid chromatography coupled with tandem mass spectrometry LC–MS for the determination of Stv in nine sweeteners with the detection limits of 0.1 µg/g [Chang and Yeh, 2014]. Kakigi et al., reported a LC-TOF-MS method with principle component analysis (PCA) for detection of 30 steviol glycosides from nine stevia sweeteners. The soft drinks analyzed were classified into three groups, and the soft drinks of each group contained high Reb A extract, normal stevia extract or alfa –glucosyltransferase–treated stevia extract [Kakigi et al., 2013].

Shafii et al., described a UHPLC-MS method for the quantification of seven stevia glycosides with a detection limit of < 15ng/mL for all steviol glycosides [Shafii et al., 2012]. Pol et al., developed pressurized fluid extraction followed by LC-UV and LC-MS methods for the determination of Stv with a detection limits of 30 and 2 ng using UV and MS detections, respectively [Pól et al., 2007]. Hearn and Subedi developed two methods, liquid chromatography coupled with electrospray

ionization mass spectrometry (LC–ESI–MS) and near infrared reflectance spectroscopy (NIRS) for the analysis of Stv and Reb A with response factors of 3.5 and 4.5 X 10^{-5} with respect to peak areas [Hearn and Subedi, 2009]. Rajasekaran et al., developed a LC-ESI-MS method for the detection of 8 diterpene glycosides and the highest content of Steviolbioside and Reb A were found to be 6.48 and 0.099% respectively on a dry weight basis in *ex vitro* and *in vitro* leaves [Rajasekaran et al., 2008]. Chung et al., reported a HPLC method using evaporative light scattering detector and UV detector to estimate the daily intakes (EDIs) of Stv in combination of aspartame, saccharine and D-sorbitol. A total of 274 food samples were analyzed and found that the EDIs were 0.008, 0.14, 0.028 and 4.9 mg/kg for stevioside, aspartame, saccharine and D-sorbitol, respectively [Chung et al., 2005]. Recently, Lorenzo et al., developed a solid phase extraction followed by LC–ESI–MS method for the analysis of two major steviol glycosides (Stv and Reb A) with detection limits of 1.07 mg/L [Lorenzo et al., 2014]. Ten stevia compounds were separated by Shah et al., using ESI-LC-MS method with detection limits ranging from 0.01–0.34 mg/g and 34 commercially available food products were tested and the results showed that Reb A and Stv comprised of 52–100% of the total steviol glycosides [Shah et al., 2012]. A validated HPTLC method was reported by Jaitak et al., for the determination of three steviol glycosides. The retention factor values for Reb A and Stv were 0.18-0.20 and 0.30-0.31 respectively. The detection limits were also calculated and found to be 80 to 500 ng for Reb A and 180 to 1000 ng for Stv [Jaitak et al., 2008]. Kedic et al., reported a HPLC method supported with TLC and ^{1}H NMR measurements for the analysis of Stv in food samples with a detection limit of 0.1 g/L [Kedic et al., 2003]. Li et al., reported a separation and purification method for Reb A by macro porous adsorption resin (HPD750–LSA40–LSA30–DS401) mixed bed was selected and furthermore, the optimization of different parameters for the separation of Reb A were studied based on the HPLC technique. Under

the optimal conditions, the separation degree for Reb A was increased from 0.771 to 1.54 when compared to the general HPLC method [Li et al., 2012]. Jackson et al., developed an desorption electrospray ionization (DESI) mass spectrometric technique for the analysis of 10 known steviol glycosides and the concentrations were 4-14 µg/g and 2-4 % for Stv and Reb A respectively and the remaining 8 steviol glycosides were present in less than 2% [Jackson et al., 2009]. Few capillary electrophoresis methods were reported for the separation and determination of steviol glycosides. Micellar electrokineticchromatography (MEKC) technique was reported by Mauri et al., using sodium dodecyl sulfate (SDS) as a charged micelle in the methanol for the separation of steviol glycosides [Mauri et al., 1996]. Liu and Li, developed a subcritical fluid extraction (SubFE) method for the extraction of steviol glycosides from Stevia rebaudiana, which suggests that the CE is an alternative method to HPLC but with longer migration times and poor resolution between the two peaks [Liu and Li, 1995].

2.1.3 Analytical separation of neotame

In 1996 Nofri and Tinti reported neotame (NTM) as a non-nutritive artificial sweetener with an *N*-substituted aspartame derivative, (*N*-[*N*-(3,3-dimethylbutyl)-L-α-aspartyl]-L-phenylalanine-1-methyl ester) and with a dipeptide bond [Kroger et al., 2006] [Figure2.2].

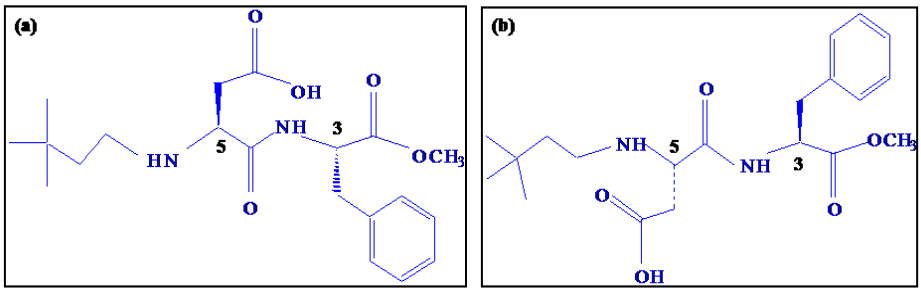

Figure 2.2: Chemical structures of (a) L,L-neotame and (b) D,D-neotame

In 2002 and in 2013 neotame was approved by the United States Food and Drug Administration as an artificial sweetener [USFDA, 2002a; U.S. Food and Drug Administration, news releases, May 19, 2013]. On an industrial scale, neotame (NTM) which contains all the elements of aspartame can be prepared by the reductive alkylation of aspartame with a 3,3-dimethylbutyl group. In contrast to aspartame, NTM has less side effects and the mechanism of NTM safety can be compared with aspartame, generally due to the enzyme "Peptidases" which is used to break the peptide bonds in dipeptides [Fisher, 1989]. In NTM the bonds between aspartic acid and the phenylalanine groups are effectively blocked by the presence of the 3,3-dimethylbutyl moiety, thus reducing the availability of phenylalanine, thereby eliminating concerns for those who suffer from phenylketonuria [Nofre and Tinti, 2000]. The safety of the NTM has been investigated and the results indicated that NTM is not carcinogenic, genotoxic, teratogenic or associated with any reproductive toxicity [Scientific opinion, European Food Safety Authority Journal, 2007]. However 3,3-dimethylbutyraldehyde, a highly flammable component used in the synthesis of NTM, may cause minor side effects like irritation to the skin, eyes, respiratory and reproductive systems after prolonged consumption of the NTM [Mayhew et al., 2003]. Due to the presence of amino acids and organic groups, NTM exhibits high sweetness nearly 10,000 and 40 times sweeter than sugar and aspartame respectively [Prakash et al., 1999]. NTM has two chiral centers at the C3 and C5 positions, hence it can form four diastereomers namely L,L; L,D; D,D and D,L neotame, and their sweetness is attributed to the presence of well-oriented hydrophobic groups in L,L-diastereomer [Prakash et al., 1999]. NTM has been approved in more than 35 countries around the world including USA, Canada, Mexico, Argentina, Brazil, Russia, Australia, China, Philippines, Indonesia, Japan, Nigeria and South Africa [Hu et al., 2013]. The Acceptable Daily Intake for NTM has been set at 0-2 mg kg^{-1} body weight by the Joint Expert Committe for Food Additives in

2003 as well as by the European Food Safety Authority in 2007 [Fitch and Keim, 2012]. The Center for Science in the Public Interest indicates that NTM is still not used as a sweetener throughout the world, yet it has a wide potential as a third generation dipeptide sweetener [Hu et al., 2013; Tomasik, 2004]. Owing to its low cost, safety and high intensity sweetness the demand and importance of NTM as a sweetener in foods has gained widespread recognition by the food industries. Accordingly, the growing interest on the use of NTM in food and beverages has prompted the need to develop a simple, accurate and reliable method for the determination of NTM. However, some natural food components in complicated food matrices will interfere with the determination of the analyte [Alghamdi et al., 2005; He et al., 2012; Vianna-Soares et al., 2002]. Therefore the highly sensitive and specific determination of the sweetener in foods is analytical challenge.

A literature survey revealed that HPLC methods are only employed for the determination of NTM in various foodstuffs. Jizhi et al., developed a HPLC method for the determination of NTM using Agilent TC C18 column and an acetonitrile buffer with recoveries of 90 to 99% [Jizhi et al., 2009]. Ji et al., reported a UPLC method for simultaneous determination of the NTM using ACQUITY UPLC BEH C18 column and the recoveries were in the range of 80.5 to 95.2 % [Ji et al., 2009]. Min and Dong reported a RP-HPLC method for the determination of NTM in combination with 4 sweeteners and the recoveries ranged from 89 to 107% [Min and Dong, 2008]. Matsumoto et al., determined NTM in a mixture of sweeteners using HPLC-Cosmosil 5C18-AR column with recoveries ranging from 86 to 104% [Matsumoto et al., 2008]. The RP-HPLC technique was used by Yang and Chen [National Standard Method of China 2009; Yang and Chen, 2010] for the NTM determination with a limit of quantification (LOQ) of 0.5 mg/kg. The percentage recovery of NTM from the spiked food samples were >92% with a

coefficient of variation of <3.2%. Zhao et al., analyzed 9 food additives using ion-suppression RP-HPLC with recoveries from 80 to 99.5% and further used magnetic iron nanoparticles with a dispersive solid phase extraction in combination of RP-HPLC and achieved low detection limits [Zhao et al., 2011, 2012 and 2013]. Hyphenated techniques with HPLC included evaporative light scattering detection such as, Buchgraber and Wasik who analyzed NTM in a mixture of sweeteners using solid phase extraction followed by HPLC-ELSD with recoveries from 93 to 109 % [Buchgraber and Wasik, 2009; Wasik et al., 2007]. Gan et al., developed a solid phase extraction method followed by ion pair high performance liquid chromatography-triple quadrupole mass spectrometer with an electro spray ionization source (ESI-MS) in a negative multiple ion monitoring mode and obtained detection limits ranging from 25.4 to 36.6 ng/L [Gan et al., 2013]. Lim et al., developed a HPLC-MS/MS method for the determination of 9 artificial sweeteners and detection limits for NTM ranged from 0.001 to 0.003 µg/mL with recoveries of 99% [Lim et al., 2013]. Berset and Ochsenbein reported a HPLC-MS/MS method for the simultaneous determination of 8 artificial sweeteners and achieved a LOQ of 10 ng/L for NTM [Berset and Ochsenbein, 2012]. Scheurer et al., proposed a LC-MS/MS method for the determination of 7 artificial sweeteners in German wastewaters and NTM was not detected [Scheurer et al., 2009]. Wu et al., developed a UHPLC-MS method for the simultaneous determination of 6 micro sweeteners in distilled spirit with detection limits of 0.1 mg/L for NTM [Wu et al., 2010]. Zygler et al., determined 9 high intensity sweeteners in various foods by HPLC-MS detection with detection limits of 0.1 to 8 µg/mL and the recoveries ranging from 48 to 100% for NTM [Zygler et al., 2011]. HPLC coupled to ESI/MS method for the quantification of NTM in a mixture of sweeteners were reported by Yang and Chen [Yang and Chen, 2009] with a recovery of 103.5% and the detection limit of 0.2 µg/mL. However, these analytical methods are more expensive in

contrast to capillary electrophoresis (CE). CE is a powerful alternative to HPLC, due to its high separation efficiency, high versatility, speed of analysis, low consumption of samples and reagents resulting in a lower environmental impact [Chankvetadze and Blaschke, 2001]. Several papers have demonstrated the applications of CE for the separation and quantification of many artificial sweeteners. However, there is only one reported study thus far on the separation of NTM in food samples using CE. Recently, Hu et al., reported on a CZE method for the analysis of NTM in the presence of 3 sweeteners with detection limit of 0.118 μg/mL in less than 5min [Hu et al., 2013].

2.1.4 Analytical separation of sucralose

The high intensity artificial sweetener sucralose (SUC) [1,6-dichloro-1,6-dideoxy-β-D-fructofuranosyl-4-chloro-4-deoxy-α-D-galactopyranoside] also known as splenda or sucraplus is generally used as a sweetener and flavor enhancer in foods and beverages. Industrially sucralose can be made from the chlorination of sucrose, and it is a process where the selective replacement of three hydroxyl groups with three chlorin atoms [Knight, 1994] [Figure 2.3].

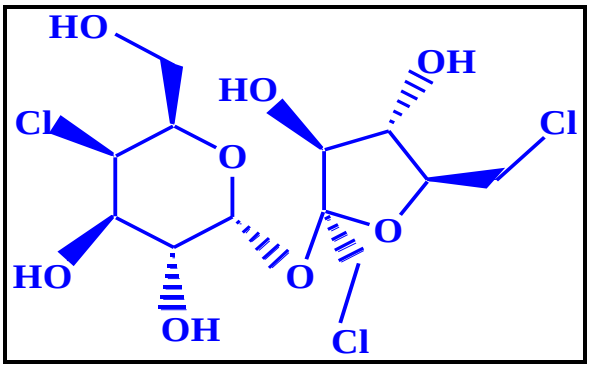

Figure 2.3: Chemical structure of sucralose (SUC)

The presence of two chlorine atoms on the five membered (fructose portion) enhances the hydrophobic nature of the six membered ring (galactose portion) which is present on the opposite side of the sucralose molecule. Due to this orientation, the sweeting strength of SUC increased to 650 times when compared to the sucrose [Jenner and Smithson, 1989]. SUC is exceptionally stable over wider temperature and pH ranges and has been introduced into the food market over 3500 different food products throughout the world. SUC was first approved in Canada in 1991 followed by Australia in 1993, New Zealand in 1996, the United States in 1998 and the European Union in 2004 [Schiffman and Rother, 2013]. By 2008, it had been approved in over 80 countries, including Mexico, Brazil, China, India, Japan and Turkey [McNeil, 2009]. In 2006, the Food and Drug Administration (FAD) amended the regulations for foods to include SUC as a non-nutritive sweetener in food products [EU, 2004]. The acceptable daily intake (ADI) of SUC is 0-15 mg/kg body weight by the Joint FAO/WHO Expert Group on Food Additives (JECFA) in 1990 [Schiffman and Rother, 2013]. The European Parliament and Council Directive in 2003 proposed the maximum usable doses of SUC in different food products as: beverages-300 mg/L, yoghurts-350 mg/kg, candy-200 mg/kg, energy reduced beer-10 mg/L and in breath freshening microsweets-2400 mg/kg [European parliament and council Directive, 2003]. SUC has been discussed as a possible human health hazard mostly in public media because of its chlorinated structure. In a sub-chronic toxicity test, with 2.8-6.4 g/kg body weight per day of SUC administered to rats in the diet, showed several ill-effects [Motwani et al., 2011; Roderoet al., 2009] such as increasing in blindness, mineralization of pelvic area and epithelial hyperplasia in rates [Calza et al., 2013]. In human body, SUC is hardly absorbed and almost 85% excreted after metabolism and studies in human beings have shown that this sweetener did not pose carcinogenic, reproductive or neurological risk [Roberts et al., 2000]. The growing interest on the use of SUC in

the foods, makes it necessary in developing a fast, reliable, cost effective and reproducible analytical method to determine SUC in food samples. The detection of SUC and other carbohydrates like fructose, glucose and sucrose is a challenging task owing to its: (i) unavailability of the charged functions and (ii) lack of absorption of strong chromophoric nature in the UV region. Therefore, separation of non-absorbing neutral molecules need a careful procedure with the suitable electrolyte systems.

A literature survey revealed that different methods were developed for the separation and determination of SUC. Among them, chromatogarphic techniques were the most reported experiments using HPLC coupled with UV detector. Johns and Dowlati developed a gradient reversed phase liqud chromatography method for the simultaneous determination of acesulfame K and SUC in oral electrolyte maintainence solution with recoveries ranging from 97.9 to 102.3 % for SUC [Johns and Dowlati, 2003]. Nojiri et al., reported a pre-column derivatization method using HPLC and the recoveries of SUC from 8 kinds of foods were found to be more than 76.2 % with quantitative limit of 0.005 g/kg [Nojiri et al., 2002]. Anderson et al., reported an RI-HPLC method for the determination of SUC with a LOD of 11 mg/L and recoveries ranging from 101.5 to 105% [Anderson et al., 2005]. Kobayashi et al., reported a RI-HPLC and ion chromatographic technique coupled with a pulsed amperometric detector (PAD-IC) developed for the detection of SUC. The percentage recoveries obtained with this method ranged from 88-105% and detection limit found to be 10 µg/g for RI-HPLC and 1 µg/g for PAD-IC [Kobayashi et al., 2001]. Na and Ken, reported an HPLC method using C18 column with the RI detector for the separation and determination of SUC with average recoveries and precision of 91.5-101.8% and 3.0%-3.2% respectively [Na and Ken, 2009]. Refractive index methods were developed by Yi and Juan to determine the SUC and the method was linear ranging from 1.5 to 2000 mg/L with recovery

percentages of 99.65% [Yi and Juan, 2007]. Two solvent systems [chloroform: methanol: toluene (v/v 5:3.5:1.5) and chloroform: ethanol: benzene (v/v 5:3:2)] were developed for the high performance thin layer chromatography method (HPTLC) to determine the SUC in different food samples. The retention factor and detection limits were 0.62, 0.45 and 40-250 ng respectively [Idris et al., 2010]. Spangenberg et al., reported HPTLC method for the separation and quantification of SUC usingamino-TLC-plates with the detection limits of 30 mg/L [Spangenberg et al., 2003]. Stroka et al., reported an inter laboratory comparison based on HPTLC and UV/fluorescence detection for the determination of SUC resulting recoveries with the UV detection ranging from 104.3 to 124.6 mg/L with an average of 112 mg/L than the fluorescence detection recoveries ranging from 98.4 to 101.3 mg/L [Stroka et al., 2009]. Bei et al., reported a HPLC-ELSD to separate SUC from other matrices. The average recovery rate was 94.3% with a relative standard deviation of 2.40% [Bei et al., 2005]. Guijuan et al., reported an HPLC-ELSD method for the separation and determination of SUC with recoveries above 90% and the RSD lower than 5%. The detection limits achieved with this method was 0.5 mg/kg [Guijuan et al., 2012]. Liu et al., developed SPE-HPLC-ELSD method for the simultaneous determination of 5 synthetic sweeteners in foods with LOD of 2.5 mg/L for SUC [Liu et al., 2012]. Batchu et al., developed an online solid phase extraction liquid chromatography coupled to the tandem mass spectrometry (SPE-LC-MS/MS) for the determination of SUC in reclaimed and drinking waters applied for the photo degradation in natural waters from South Florida. The detection limits were found to be 4.5, 8.5 and 45 ng/L for deionized water, drinking and reclaimed waters (1:10 diluted with deionized water) respectively [Batchu et al., 2013]. Berset and Ochsenbein analyzed 8 artificial sweeteners in water samples and their results suggested that SUC was present in the surface waters with concentration of 10 ng/L [Berset and Ochsenbein, 2012]. Gan et al., developed SPE-LC-ESI-MS for the

quantification of 7 artificial sweeteners in different water samples. The method of detection and quantification limits for SUC were in the range of 1.6 to 7.5 ng/L [Gan et al., 2013]. Hua and Dan developed a LC-MS/MS method for the analysis of SUC in drinks with LOD of 0.001 mg/kg and recoveries ranged from 82.3 to 100.5% [Hua and Dan, 2011]. The 8 artificial sweeteners were determined in the waste water by hydrophilic interaction liquid chromatography-tandem mass spectrometry which was reported by Kokotou and Thomaidis with a LOD of 4.4 ng/ L [Kokotou and Thomaidis, 2013]. Zygler et al., proposed a method for the determination of 9 high-intensity sweeteners in various food samples by using HPLC-MS technique. SUC was one of the eight high intensity sweeteners found in the food samples with a concentration ranging from 0.001 to 0.01 µg/mL [Zyglar et al., 2011]. In the later stages the authors also carried out with the solid phase extraction followed by LC-MS to analyze over 170 samples of different brands of beverages, yoghurts, fruit preparations and vegetable preserves and fish products available in a polish market. The detection limits achieved using this method ranged from 0.069 to 0.207 µg/mL [Zyglar et al., 2012]. A UPLC-MS/MS method was developed for the determination of SUC by Li et al., from Chinese spirit, modified milk and fried peanut kernels at three spiked levels with average recoveries of 85 to 98%. The detection limits achieved were 0.4, 4, 10 mg/kg with a relative standard deviation (n=6) of 1.7-5.0% [Li et al., 2011]. Lim et al., developed a HPLC-MS/MS method with the selective reaction monitoring (SRM) mode for the analysis of 9 artificial sweeteners in imported foods for SUC. The limit of detection ranged from 0.375 to 1.125 µg/mL [Lim et al., 2013]. Analysis of polar organic contaminants like SUC in surface water of the northern Adriatic Sea by solid-phase extraction followed by UHPLC–QTRAP® MS using a hybrid triple-quadrupole linear ion trap instruments were reported by Loos et al., with a detection limit of 11 ng/L [Loos et al., 2009]. Minten et al., reported a method for the analysis of SUC with

electrospray LC/MS in recipient waters and in sewage effluent. The limit of quantification (LOQ) for sewage and recipient waters were found to be 0.2 and 0.02 mg/L [Minten et al., 2011]. Ordonez et al., compared RPLC-MS and HILIC methods in the analysis of 4 artificial sweeteners in the different water samples and confirmed that the RPLC-MS method (LOQ = 25 µg/L) was superior to the HILIC (LOQ = 10 µg/L) method in terms of detection limits [Ordonez et al., 2012]. The same authors extended the method to analyze 6 more artificial sweeteners based on the pressurised liquid extraction (PLE) with water followed by solid-phase extraction (SPE) and subsequent liquid chromatography–tandem mass spectrometry. Using these methods low detection limits were achieved (3 ng/g) for SUC [Ordonez et al., 2013]. SUC in combination with other sweeteners in water and beverage samples were analysed by Ferrer and Thurman using liquid chromatography/time of flight mass spectometric method. The detection limits and recoveries were 0.05 to 0.5 µg/L and 73 % respectively [Ferrer and Thurman, 2010]. Perkola and Sainio analysed 4 artificial sweeteners in Finnish surface waters with isotope dilution mass spectrometry with a detection limits ranging from 20 to 200 ng/L [Perkola and Sainio, 2014]. Stander et al., surveyed nutritive and non-nutritive sweeteners in 46 South African fruit juices using HILIC-ESI-MS method and quantified the concentration of SUC. The results suggests that the detection limits ranges from 0.1 to 0.5 mg/L [Stander et al., 2013]. Five artificial sweeteners in surface and background surface water samples were analyzed using a single-step solid phase extraction (SPE) coupled with HPLC-MS/MS and isotope dilution by Tran et al., and the results showed SUC was present in high concentrations in surface waters than background surface water [Tran et al., 2013]. Motwani et al., studied the interaction of SUC with cyanocobalamine and quantified the SUC in different food samples by LC-MS/MS method with a LOQ of 40 µg/L [Motwani et al., 2011]. HPLC coupled to ESI/MS for the quantification of SUC in a mixture of 8 sweeteners was reported

by Yang and Chen [Yang and Chen, 2009] for the determination of SUC with the detection limit of 0.03 to 30.0 µg/mL. Ohashi et al., developed LC/MS/MS methods for the analysis of SUC in food materials with a detection limit of 0.01 g/mL [Ohashi et al., 2004]. Recently, Wu et al., developed a direct large volume injection UHPLC-MS method for the determination of SUC in eight wells water in combination of acesulfame K. The method was found to be sensitive with a detection limits ranging from of 65–541 ng/L for SUC [Wu et al., 2014]. Mead et al., studied the presence of SUC in different waters collected from the costal and marine waters of United States using GC-MS and found that the concentration levels of 0.37and 0.99 nM [Mead et al., 2009]. Qiu et al., reported a qualitative and quantitative analysis of SUC by GC-MS and GC-FID by converting into its trimethylsilyl (TMS) ether with detection limit of 0.25ng [Qiu et al., 2007]. A simple and time-efficient UV spectrophotometric method was developed for the determination of SUC based on the UV spectrophotometric photo degrade procedure with a LOD value of 0.02 g/L [Idris et al., 2013]. Youssef et al., developed two kinetic spectrometry methods based on (i) oxidation reaction of the drug with alkaline potassium permanganate and (ii) reaction of SUC with cerium (IV) ammonium sulfate in the presence of perchloric acid [Youssef et al., 2011]. Stroka et al., developed an indirect UV-Capillary zone electrophoretic method for the analysis of SUC in the food samples, without any sample clean-up. The limits of detection were found to be 28 and 42 mg/L [Stroka et al., 2003]. McCourt et al., developed a CZE-indirect UV method for determination of SUC in different food samples and the method allows the detection of SUC at >30 mg/kg, with a linearity range of 50–500 mg/kg in less than 8.5 minutes [McCourt et al., 2005]. Zhao and Jhonson, studied the effect of mobile phase composition on the separation of SUC and related compounds in a capillary electrochromatographic analysis and observed that the good peak

separation was achieved within a shorter time than HPLC (8.3 min) at low concentration of (25-30%) acetonitrile as a mobile phase at 15 kV voltage [Zhao and Johnson, 2000].

A great variety of methods based on different principles have been applied to the analysis of the aforementioned compounds in food, drinks and dietary products. Of the great variety of methods used for the determination of sweeteners in different food matrices, chromatographic methods have received widespread recognition. Currently, HPLC and RPLC are the most popular, well-known, mature techniques, perfectly suited for the separation of sweeteners. Capillary electrophoresis (CE) on the other hand, is another attractive separation technique, useful for the simultaneous determination of multiple sweeteners. In some situations, CE is superior to HPLC in terms of separation power, analysis time or low solvent consumption. Accordingly, a description of the separation mechanism and background electrolytes used for the separation of studied sweeteners using CE methods is presented below.

2.1.5 Discription of BGE and separation mechanism for steviol glycosides

The determination of diterpene glycosides from Stevia rebaudiana leaves using MEKC was described by Mauri et al., [Mauri et al., 1996]. Analyses were performed on fused silica capillaries with 20 mM sodium tetraborate buffer and 30 mM sodium dodecyl sulfate at pH 8.3. The effect of injection amount of methanol was studied on peak resolution and observed that resolution was sharply improved by decreasing the injection of lower percentage methanol and an absolute amount of 1.6 nL per injected sample was optimal. At pH 8.3, 20 mM borate buffer and 30 mM SDS permitted the complexation of sugar moieties and hydrophobic interaction with the terpene skeleton results in satisfactory baseline.

The extraction of steviol glycosides in Stevia rebaudiana, including stevioside, rebaudioside A, rebaudioside C, and dulcoside A by subcritical fluid extraction [SubFE (CO_2+polar modifier)] was investigated by Liu et al., [Liu et al., 1997]. This method was evaluated by optimizing the extraction conditions (extraction phase composition, extraction time, etc.) on the rate of recoveries. An extraction efficiency of more than 88% was obtained using methanol as a modifier. Determination of stevioside from the stevia extraction performed using CE, at a wavelength of 210 nm, applied voltage 16.5 kV, 50 mM borate buffer at pH 9.3 and 55% of acetonitrile to buffer ratio were injected using 30 mbar for 20 s. The obtained results from SubFE (13.7 ± 5.8 %) were compared with other liquid extraction methods (13.1 ± 9.3 %) and concluded that SubFE in conjunction with CE were very attractive methods for the separation and analysis of steviol glycosides.

The separation of steviol glycosides in stevia sweeteners including stevioside, rebaudioside A, rebaudioside C and dulcoside A by capillary electrophoresis and high performance liquid chromatography was investigated. A simple and efficient capillary electrophoretic method was developed. The results were compared with those obtained by HPLC. The individual steviol glycosides were obtained by HPLC fraction collection, and peaks in the electropherograms of the sweetener samples from Chinese refining factories were identified by comparing with those of individual steviol glycosides. The method was applied to the determination of real samples [Liu and Li, 1995].

2.1.6 Discription of BGE and separation mechanism for neotame

A CZE method combined with solid phase extraction was developed by Hu et al., [Hu et al., 2013] for the determination of neotame in the presence of aspartame, cyclamate, acesulfame

K and saccharine in non-alcoholic beverages. The optimum separation conditions obtained were 20 mmol L^{-1} sodium borate buffer, pH 8, 25 kV applied voltage, 5 s hydrodynamic injection at 30 mbar and ultraviolet detection at 191 nm. The calibration curve showed good linearity (R^2 = 1.000) in the range 0.5–100 µg mL^{-1}, and the limit of detection was 0.118 µg mL^{-1} for neotame. The method was successfully applied to the determination of neotame in two kinds of beverage with migration time less than 5 min, relative standard deviation (n = 3) less than 2% and recoveries ranging from 90 to 95%.

2.1.7 Discription of BGE and separation mechanism for sucralose

A capillary electrophoresis with indirect ultraviolet absorption in a 3,5-dinitrobenzoic acid buffer at pH 12.1 was reported by Stroka et al., [Stroka et al., 2003]. The indirect ultraviolet detection was suitable for the sensitive determination of chromophore lacking compounds such as sucralose. The optimum conditions were pH 12.1, applied voltage 20 kV, absorption maxima 238 nm, sample injection time 4 sec at 50 mbar and DNBA concentration 3$mmol^{-1}$. The method allowed for the determination of sucralose in low-calorie soft drinks, without any sample clean-up over a linear range of 42–1000 mg l^{-1} (r=0.9991). The limits of detection and quantification were 28 and 42 mg l^{-1}, respectively, and the repeatability for a mean concentration of 100 mg l^{-1} was 4.2% for the signal area and 3.6% for the migration time, which were deemed satisfactory for the use in food control.

A capillary zone electrophoresis (CZE) with indirect UV method was optimised chemometrically with a complete validation for the quantification of sucralose in various foodstuffs. The optimized experimental conditions were: a dinitrobenzoic acid (3 mM)/sodium hydroxide (20 mM) background electrolyte with a pH of 12.1, a potential of 0.11 kV cm^{-1} and a temperature of 22 ^{0}C,

detection wavelength 238 nm and sample injection 4s at 5.52 kPa. This method allowed for the detection of sucralose at >30 mg kg^{-1}, with a linearity range of 50–500 mg kg^{-1}, making it suitable for the quantification of sucralose in many foodstuffs [McCourt et al., 2005]. The principle behind the separation of sucralose is that when the sucralose ion past the UV detection window displays the DNBA molecule resulting in a reduction of the continuously high background electrolyte gives negative peaks.

A capillary electrochromatography method was developed for the determination of sucralose and several similar compounds using C18 silica packing column by Zhao and Johnson [Zhao and Johnson, 2000]. The experimental conditions were optimized as voltage 5 kV, mobile phase was acetonitrile mixing with 4 mM borate buffer, temperature 20 ^{0}C and all injections were made by a 10 kV voltage for 2 s. Different concentrations of mobile phase mixtures at voltage 10 and 15 kV were tested for the complete separation of sucralose and found that 25-30% of acetonitrile with 4 mM borate buffer at 15 kV was giving better base line separation than other combinations.

2.1.8 Capillary electrophoresis studies on older generation sweeteners related to studied sweeteners

The studied sweeteners have structural relations with their older generation sweeteners. Of these, neotame is structurally closer to the popular sweetener aspartame while some of the plant glycosides are structurally similar to the studied steviol glycosides and sucralose is chemical product of sucrose. For this purpose, an in depth study on the separation of aspartame, some plant glycosides and sucrose using capillary electrophoresis reported in literature is presented below.

Table: 2.1: Showing the separation conditions and analytical precisions of older generation sweeteners using capillary electrophoresis

Analyte	Method	Optimum conditions	Detection limits	Reference
Aspartame	CZE	λ_{max}= 211 pH = 2.14 Buffer= 30mM phosphate/19mM Tris Voltage= 30 kV Injection time= 3s at 12.5 cm Hg vaccum	Correlation coefficient= 0.99 Detection limits= 143-507 mg/L	Pesek and Matyska, 1997
Aspartame	CZE	λ_{max}= 214 pH = 9.0 Buffer= 25mM phosphate/25mM borate Voltage= 15 kV Injection time= 20s	Correlation coefficient= 0.99 Recovery= 99.6 ±1.2	Aboul-Enein and Bakr, 1997
Flavone-7-O-glycosides form citrus	EKC-CE	pH = 10.0 Buffer= 0.20M borate Voltage= 15 to 25 kV Injection time= 2s at 20psi Temperature= 20^0C Chiral selector= 10mM DM-β-CD and 0.5 mM SBE-β-CD	-------	Moreto et al., 2003
Flavone-7-O-glycosides form citrus	EKC-CE	λ_{max}= 205 pH = 7.0 Buffer= 0.20M borate/10% methanol Voltage= 20 kV Injection time= 5s Temperature= 20^0C Chiral selector= 5mg/mL SBE-β-CD	--------	Aturki and Sinibaldi, 2003
Flavone and Xanthane glycosides form SwertiaMussotii	MEKC	pH = 9.0 Buffer= 30 mM borate/ 1.0 % acetonitrile Voltage= 24 kV Injection time= 5s Temperature= 25^0C Micelles= 28 mM SDS	Correlation coefficient= 0.9980 Recovery= 98.5 to 102. 4 mg/L	Li et al., 2008
Phenyl propanoid glycosides form T. Chamaedrys	CZE	pH = 8.9 Buffer= 65 mM phosphate/ 10 mMborate/ 15% isopropanol Voltage= 25 kV	Correlation coefficient= 0.9999 Detection limits= 50-70 mg/mL	Avula et al., 2003

		Injection time= 3s at 50mbar		
Iridoid glycosides form PicrorhizaKurroa	MEKC	λ_{max}= 205 pH = 8.60 Buffer= 100 mM borate/ 1% acetonitrile Voltage= 25 kV Injection time= 2s Temperature= 30^0C Micelles= 30 mM SDS	Correlation coefficient= 0.9992 Recovery= 0.338±0.014 to 9.580±0.267 g/100g	Sturm and Stuppner, 2001
Flavanoid glycosides form Scorzoneraaustriaca	CZE	λ_{max}= 254 pH = 10.0 Buffer= 20 mM borate/ 10% methanol Voltage= 25 kV Injection time= 2s Temperature= 25^0C	Correlation coefficient= 0.9990 Detection limits= 5-10 µg/mL	Jiang et al., 2007
Cyanogenic glycosides	MEKC	λ_{max}= 214 pH = 11.0 Buffer= 100 mM acetate buffer Voltage= 25 kV Injection time= 1 to 20 sec Temperature= 30 ^{0}C Micelles= 200 mM SDS	Detection limits= 50-90 µg/g	Campa et al., 2000
Iridoid glycosides	MEKC	λ_{max}= 197, 235, 239, and 283 nm pH = 9.5 Buffer= 20 mM ammonium acetate Voltage= 20 kV Injection time= 5 sec at 50mbar Temperature= 20 ^{0}C Micelles= 100 mM SDS	---------	Suomi et al., 2002
Sucrose	Indirect UV-CZE	λ_{max}= 254 nm pH = 12.2 Buffer= 20 mmol L^{-1} sorbic acid, 0.2 mmol L^{-1} CTAB and 40 mmol L^{-1} NaOH Voltage= 25 kV Injection time= 3 sec at 50mbar Temperature= 20 ^{0}C	Detection limits =0.022 to 0.074 g/L	Rizelio et al., 2012
Sucrose	CZE-Borate complexation	λ_{max}= 195 nm pH = 12.0	Detection limits= 0.25 mg/mL	Anastos et al., 2005

		Buffer= 65 mM borate Voltage= 8 kV Injection time= 1 sec at 50mbar Temperature= 60 ^{0}C		
Sucrose	CZE-indirect UV method	λ_{max}= 207 nm pH = 12.4 Buffer= 10-50 mM ionic liquids Voltage= +20 to -20kV Injection time= 5 sec at 50mbar Temperature= 17 ^{0}C	Detection limits= 0.06-0.20 g/L	Vaher et al., 2011
Sucrose	CZE	λ_{max}= 22 nm pH = 12.0 Buffer= 10 mM benzoate/0.5 mM MTAB Voltage= -20kV Injection time= 5 sec at 50mbar Temperature= 22^{0}C	Detection limits=0.088 mM	Warren and Adams, 2000

*CZE= Capillary zone electrophoresis, MEKC= Micellar electrokinetic chromatography, EKC-CE= Electrokinetic chromatography, SDS= Sodium dodecyl sulphate, SBE-β-CD= Sulfobutyl ether beta cyclodextrin, DM-β-CD= Dimethylated beta cyclodextrin, MTAB= Myrisityletrimethylammonium bromide.

CHAPTER 3

THEORETICAL PRINCIPLES OF CAPILLARY ELECTROPHEROSIS, BIOSENSORS AND MOLECULAR MODELLING

3.1 Capillary electrophoresis

Electrophoresis is a technique in which solutes are separated by their movement with different rates of migration in an electric field. Depending on the type of electrophoresis the separation can be achieved by gel electrophoresis and capillary electrophoresis.

Capillary electrophoresis (CE) emerged by the combination of the separation mechanism of electrophoresis and instrumental automation concepts of chromatography. CE is a very powerful analytical technique with a major and outstanding importance in separations of compounds such as amino acids, chiral drugs, vitamins, pesticides, inorganic ions, organic acids, dyes, surfactants, peptides and proteins, carbohydrates, oligonucleotides, DNA restriction fragments, whole cells and even virus particles because of simpler method development, minimal sample volume requirements and lack of organic waste. Its separations depend on the difference in the solutes migration in an electric field caused by the application of relatively high voltages, thus generating an electro-osmotic flow (EOF) within the narrow-bore capillaries filled with BGE [Henk and Gerard, 2010]

3.1.1 Instrumentation

One key feature of CE is the overall simplicity of the instrumentation. The basic scheme of CE instrumentation consists of an auto sampler, two electrodes (the anode and a cathode), fused-silica capillary (20–100 mm I.D., 20–100 cm length) placed in buffer reservoirs.

The electrodes used to make electrical contact at high voltage power supply (up to 30 kV) operated in either positive or negative polarity. The sample is loaded into the capillary by replacing one of the reservoirs (usually at the anode) with a sample reservoir and applies either an electric field or an external pressure and then separation is performed as shown in Figure 3.1. Generally, the internal and external detectors such as UV/diode-array or fluorometric or electrochemical detector and mass spectrometer (MS) are coupled to the CE system which is present at the cahodic end [Henk and Gerard, 2010; McLaughlin et al., 1991].

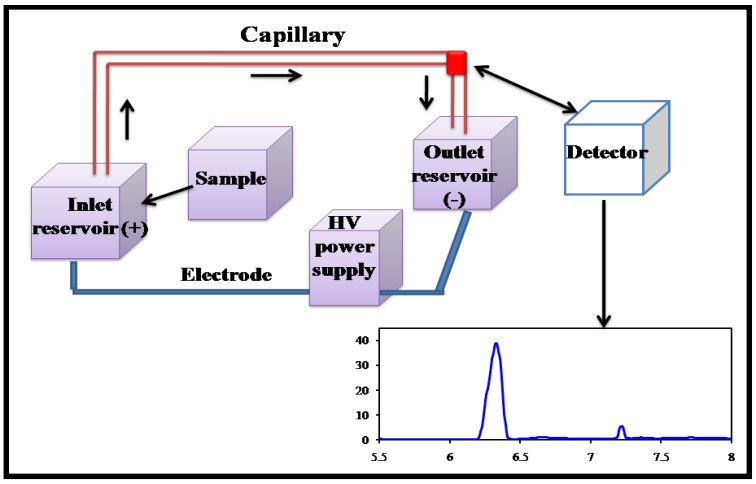

Figure 3.1: Basic components of capillary electrophoresis instrumentation

3.1.2 Principle of operation

The sample is introduced into the capillary from the anodic end by applying either hydrodynamic (external pressure) or electrokinetic (voltage) injection modes. With the buffer reservoir on each end, an electric field is applied through the capillary and separation is depends on the migration of solutes against the field between anode and cathode. The solute migrations depend mainly on their sizes, degree of ionization, their charges as well as dielectric constant of the BGE. As soon as the analytes are introduced to the capillary, voltage is applied and it makes

the analyte molecules to move inside the capillary by the known phenomenon electrophoretic mobility and electro-osmotic flow (EOF). Finally, optical detection is done at the opposite end of the capillary which has an optical window aligned with the detector [Heiger, 2000].

3.1.3 Electro-osmotic flow

EOF is one of the fundamental processes based on electro-osmosis. This phenomenon is mainly generated from the surface charge of the capillary walls. Electro-osmotic flow is the bulk flow of the solute in the capillary and is consequence of the surface charge on the interior capillary wall. Cations migrate towards the negatively charged electrode (cathode), anions attracted by the positively charged electrode (anode) and neutrals not attracted by either of the electrodes. Controlling the EOF can achieve considerably the efficiency and selectivity of a separation. The factors affect the EOF are as follows: concentration/ionic strength of the BGE, electric field, pH, temperature and capillary coatings (e.g. silanol groups). The EOF enables the simultaneous analysis of cations, anions and neutral species in the same analysis.

Based on the pH of the BGE, change in the ionization capacity of silanol groups is observed in the inner walls of the capillary. The silanol groups (SiOH) produce hydrogen cations (H^+) into the BGE leaving the negative (SiO^-) groups on the inner walls of capillary. Even at low pH the positive ions in the electrolyte, thus get attracted to the walls causes double ionization and forming a double layer which is known as zeta potential as shown in Figure 3.2. The ionization increases with increase in pH and same goes for the EOF. When the voltage is applied across the capillary the cations forming the diffuse double layer are attracted towards the cathode. Because they are solvated their movement drags the bulk solution in the capillary towards the cathode [Lukacs and Jorgenson, 1985].

The magnitude of EOF can be defined by [Eqn 3.1]:

$$\mu_{EOF} = (\varepsilon\zeta / \eta) \qquad \text{[Eqn 3.1]}$$

Where ε is the solution dielectric constant, ζ zeta potential and μ_{EOF} is EOF mobility.

The impact of pH on the analyte can also be substantial, particularly for complex zwitterionic compounds such as peptides. The charge on these compound is pH dependent and the selectivity of separation is affected substantially by pH. As a rule of thumb, select a pH that is at least two units above or below the pKa of the analyte to ensure complete ionization. At highly alkaline pH the EOF may be so rapid that incomplete separation may occur [Introduction to capillary electrophoresis, Beckman coulter].

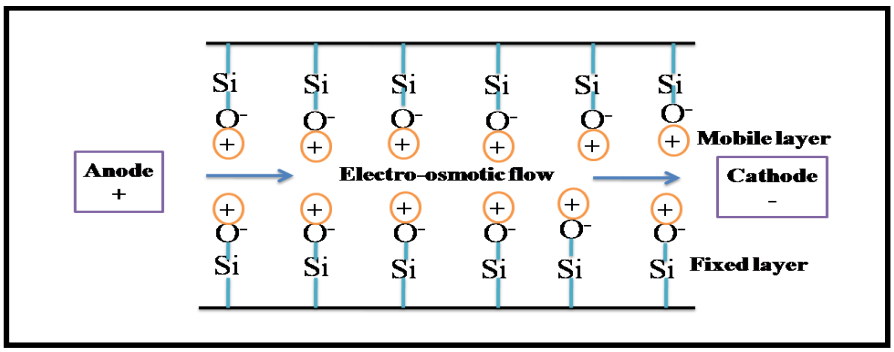

Figure 3.2: Development of electro-osmotic flow: Formation of negatively charged fused silica surfaces (SiO^-) and hydrated cations accumulating on surface

3.1.4 Electrophoretic mobility

The CE efficiency, especially CZE mainly depends on the following fundamental principles of electrophoresis and electro-osmosis:

The electrophoretic mobility is determined by the electric force that the molecule experiences, balanced by its frictional drag through the medium. This phenomenon can be described according to the Eqn. 3.3-3.6 shown below.

The electric force: $\mathbf{F_E = q\,E}$ [Eqn 3.3]

From Stoke's law frictional force for spherical ion is: $\mathbf{F_F = -\,6\,\pi\,\eta\,r\,v}$ [Eqn 3.4]

Where q= Ion charge
η = Solution viscosity
r = Ion radius
v = Ion velocity

At trancient point both electrical and frictional forces are equal

Hence, $\mathbf{q\,E = 6\,\pi\,\eta\,r\,v}$ [Eqn 3.5]

and the ion **velocity (v) = μ_e E**

where μ_e = Electrophoretic mobility
E = Applied electric field

Finally, $q\,E = 6\,\pi\,\eta\,r\,v$
$q\,E = 6\,\pi\,\eta\,r.\,\mu_e\,E$

Electrophoretic mobility $(\mu_e) = \frac{q}{6\pi\eta r}$ [Eqn 3.6]

From this equation it is evident that small, highly charged species have high mobilities whereas large, minimally charged species have low mobilities, as shown in Figure 3.3 [Bird et al., 2001; Landers, 2008].

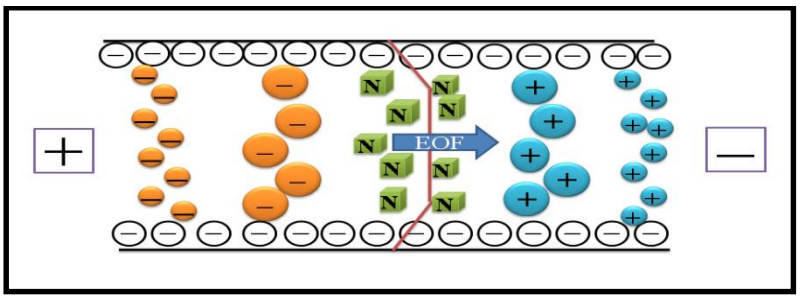

Figure 3.3: Differential solute migration superimposed on electro-osmotic flow in capillary zone electrophoresis

3.1.5 Analytical parameters

(i) Migration time

The time required for a solute to reach the detection point is called the "migration time", and is given by thequotient of migration distance and velocity. The apparent solute mobility can be calculated using Eqn 3.7 shown below.

$$\mu_a = \frac{l}{tE} = \frac{lL}{tV} \qquad \text{[Eqn 3.7]}$$

where

$\mu_a = \mu_e + \mu_{EOF}$
V = Applied voltage
l = Effective capillary length
L = Total capillary length
t = Migration time
E = Electric field

(ii) Dispersion

Peak dispersion σ^2, which result from molecular diffusion, which takes placeas the solute migrate through the capillary, is calculated as using Eqn 3.8:

$$\sigma^2 = 2\,Dm = \frac{2DlL}{\mu_{eV}} \qquad \text{[Eqn 3.8]}$$

Where Dm = the solute's diffusion coefficient cm^2/s.

(iii) Efficiency

The separation efficiency in capillary electrophoresis can be calculated in terms of the number of theoretical plates and it is given by Eqn 3.9:

$$N = \frac{\mu V}{2 D_m} \qquad \text{[Eqn 3.9]}$$

Where: N = Number of theoretical plates
μ = Apparent mobility
D_m = Diffusion coefficient of the analyte

According to this equation, the efficiency of separation is only limited by diffusion and is proportional to the strength of the electric field. In contrast to other separation techniques like HPLC the efficiency of capillary electrophoresis is typically much higher because of the absence of mass transfer between phases. In addition, the flat EOF driven system in CE does not significantly contribute to the band broadening than the characteristic of pressure driven flow in chromatography columns results in much efficiency and a number of theoretical plates.

(iv) Resolution

Achieving fair resolution among sample components is the ultimate goal in separation science. Resolution is defined as the balancing of differential migration and the dispersive processes of sample components. CE yields good separation of small molecules and resolution between two species can be calculated using Eqn 3.10.

$$\mathbf{R = \frac{1}{4} N^{1/2} \left(\frac{\Delta \mu}{\mu *} \right)} \qquad \text{[Eqn 3.10]}$$

$$\mathbf{\Delta \mu = \mu_2 - \mu_1}$$

$$\mathbf{\mu^* = \mu_2 + \mu_1 / 2}$$

With the substitution of the number of theoretical plates (N) in the above Eqn 3.10 gives:

$$\mathbf{R = \left(\frac{1}{4\sqrt{2}}\right) (\Delta \mu) \left(\frac{V}{D\,(\mu * + \mu_{EOF}}\right)^{1/2}}$$

(v) Solute-wall interactions

Interaction between the solute and the capillary wall is unfavorable to CE. The peak tailing and total adsorption of the solute mainly depends on the level of interaction. The adsorption mainly caused by ionic interactions between negatively charged capillary walls and cationic solutes. In case of large peptides and proteins adsorption can occur due to the presence of numerous charges and hydrophobic moieties [Henk and Gerard, 2010; Heiger, 2000]. The variance due to adsorption can be given by Eqn 3.11.

$$\sigma^2 = \frac{k' V_{EOF}\, l}{(l+k')^2}\left(\frac{r^2 k'}{4D} + \frac{2}{K_d}\right) \qquad \text{[Eqn 3.11]}$$

k' = Capacity factor
V_{EOF} = Electro-osmotic flow velocity
D = Solute diffusion coefficient
l = Capillary effective length
K_d= First order dissociation constant

The variance is strongly dependent on the magnitude ofthe capacity factor.

For CZE method capacity factor is like in liquid chromatography $\mathbf{K'} = \frac{t_r - t_0}{t_0}$

Where t_r= Elution time of retained solute

t_0= Elution time of an unretained solute

For EKC or MEKC method capacity factor is

$$\mathbf{K'} = \frac{t_r - t_0}{t_0\left(1 - \frac{t_r}{t_m}\right)}$$

Where t_r= Elution time of retained solute

t_0= Elution time of an unretained solute

t_m= Elution time of pseudostationary phase

3.2 Modes of operation

CE comprises of a family of techniques with different operating and separation characteristics, making it a more versatile technique being able to analyse a wide range of analytes. The techniques are:

(i) Capillary zone electrophoresis (CZE)

CZE is the simplest mode in CE, where the capillary is filled with an electrolyte followed by injection of the sample at the inlet and electric field is applied. The basic principle of this mode is, analytes will migrate at different velocities (apparent mobility) due to their charges and sizes by applying an electric field. Hence, CZE separation is mainly governed by charge/size ratio with electrophoretic mobility which results in small and highly charged molecules migrate faster than larger and less charged. Neutral molecules cannot be separated because they migrate at the velocity of the EOF. CZE is widely employed in the separation of proteins and peptides but one problem with this mode is electrostatic binding of cationic substances to the walls of the capillary. This effect is observed in the case of proteins operating in a buffer that has a pH below the pKa of the analyte. The problem could be overcome by operating at least two pH units above the pKa of the protein. The use of treated capillaries is one of the several ways to reduce the wall binding [Introduction to capillary electrophoresis, Beckman coulter]. Other applications for the CZE mode include the separation of inorganic anions and cations such as those normally separated by ion chromatography [Lauer and McManigill, 1986].

(ii) Micellar electrokinetic capillary chromatography (MEKC)

MEKC is a hybrid form of electrophoresis and chromatography in which surfactants are added to the running buffer at concentrations that form micelles. It is now a widely used mode

for industries including (bio) pharmaceutical, food, environmental and clinical industries. The main strength of the MEKC is, it is the only electrophoretic technique that can be used for the separation of neutral solutes as well as charged once [Henk and Gerard, 2010]. MEKC principle of operation is based on addition of a surfactant to the background electrolyte example being SDS (anionic), CTAB and DTAB (cationic), CHAPS and CHAPSO (zwitterionic). At a concentration above the critical micelle concentration of a surfactant micelles are formed which are contained hydrophobic tails oriented towards the center and the charged heads oriented outside facing towards the buffer. Depending on their charge, micelles will travel either with the EOF or against the EOF and acts like a pseudo-stationary phase in chromatography as shown in Figure 3.4.

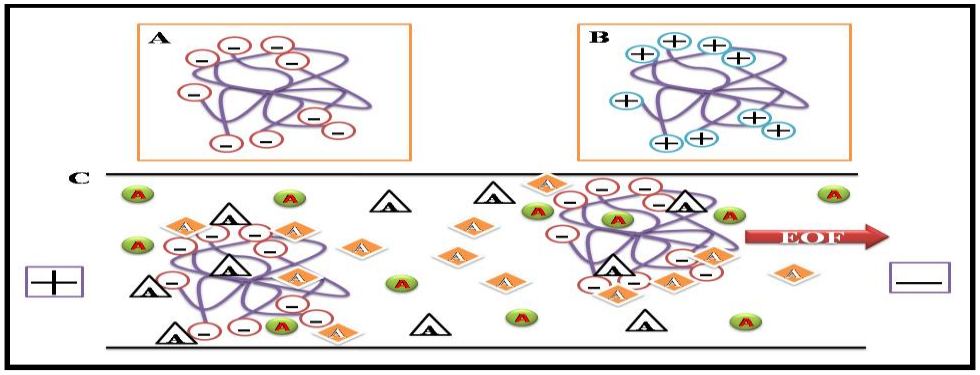

Figure 3.4: A- negatively charged micelles (SDS), B- Positively charged micelles (CTAB) and C- Separation in MEKC (A=analyte)

Those with a negative charge such as SDS travel against the EOF towards the anode. However, at neutral pH or basic pH the migration of micelles is slower than the EOF therefore resulting in the net migration being towards the cathode favouring the direction of the EOF. As the solutes migrate through the column they partition between the micelles and the running buffer in a chromatographic manner through hydrophobic and electrostatic interactions [Terabe et al., 1984; Vindevogel and Sandra, 1992].

(iii) Capillary gel electrophoresis (CGE)

The principle of the CGE is identical to traditional slab or tube gel electrophoresis. It is mostly used for the separation of molecules such as protein and nucleic acids based on their size. In order for the separation to be feasible the molecules have to be denatured using sodium dodecyl sulfate (SDS) and passed through a suitable polymer which acts as a molecular sieve making it easier for smaller molecules to migrate through the polymer as opposed to larger ones as shown in Figure 3.5. CGE is a very useful technique for separations of large biological molecules which have similar electrophoretic migration due to their similar charge-to-mass ratios which could not be varied and be resolved according to size without denaturing. This mode greatly applies to proteins and DNA analysis [Henk and Gerard, 2010; Lux et al., 1990]

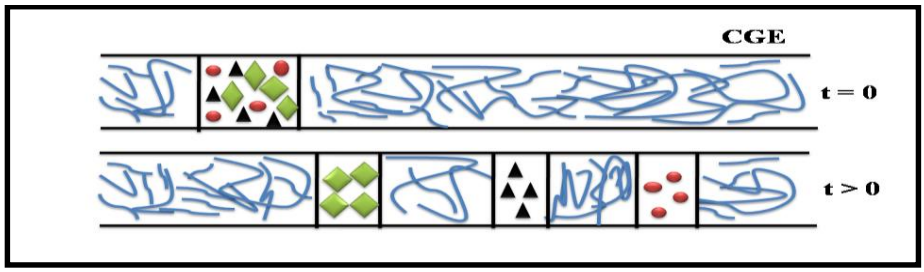

Figure 3.5: Size separation in CGE

(iv) Capillary isoelectric focusing (CIEF)

CIEF is referred to as a high resolution technique for the separation of ampholytes which are zwitterionic substances such as proteins, peptides and amino acids based on their isoelectric points (pI) rather than their apparent mobilities as shown in Figure 3.6. CIEF employs ampholytes with both basic and acidic nature being able to have pI values that last the desired pH range between the anode and the cathode for the analysis. Its principle is based on the "focusing" method which is filled of the capillary with a mixture of ampholytes and solutes forming a pH

gradient where the acidic and basic solutions are at the anode and cathode. When the electric field is applied the ampholytes and solutes are migrating through the capillary to the point where they reach their isoelectric points. Simply put if the analyte has a net charge that is positive it is mostly likely to migrate towards the cathode. At their isoelectric point (pI) migration stops and solute focused into a tight zone and that zone is moved to pass through the detection point by means of pressure or chemical means [Xu, 1996].

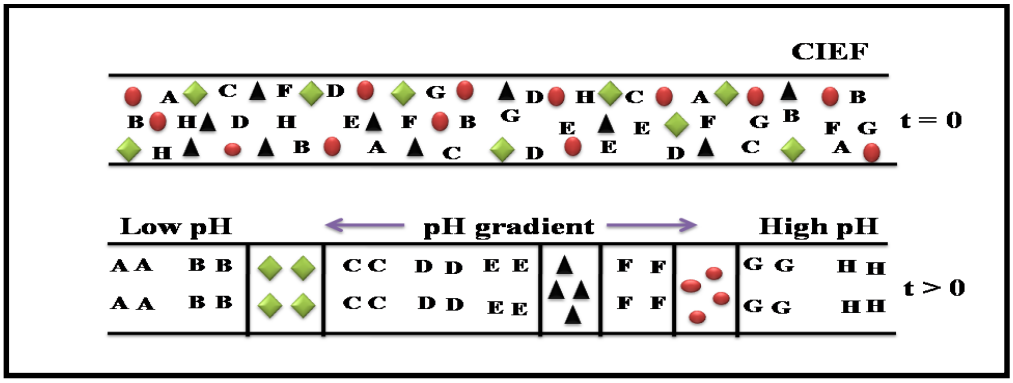

Figure 3.6: Separation in CIEF. A, B, C, D, E, F, G, H represent ampholyte molecules. Symbols ◆, ▲ and ● represent solute molecules for example peptides and proteins.

(v) Electrokinetic chromatography (EKC)

EKC is best described by the cyclodextrin (CD) mediated mode, where enantiomers and diastereomers interacts differently with the CD and allowing for their separation as shown in Figure 3.7. This approach has made a major impact in pharmaceutical industries for analysis of chiral drugs. Godel and Weinberger [Godel and Weinberger, 1995] explain this mode as a hybrid method of MEKC and CZE since it employs not only chiral micelles but non-micellar chiral selectors such as CDs. This method is, however the preferred method in the pharmaceutical industry as it is versatile compared to HPLC in enantio-separation since it's very difficult to

separate enantiomers under normal CE and LC techniques. CDs are however the most widely used chiral selectors and are simply added to the background electrolyte [Terabe, 1989].

Native CDs are macrocyclic oligosaccharides formed from the enzymatic digestion of starch by bacteria. These compounds are formed with 6, 7 or 8 glucopyranose units and are referred to as α-, β- or γ-CD respectively. The shape and size of the CDs are very important factor in chiral separation; generally CDs are torus-shaped and have a relatively hydrophobic internal cavity. The physical properties of the CDs are discussed in introduction section and briefly the formation of inclusion complexes with analytes is mainly depends on the size dimensions of interior hydrophobic cavity. It is also depends on the analyte size, if the analyte is too large, no complex is formed and if it is too small the molecular contact with the CD may not be strong enough to impact the separations and this is the major limitation of CDs for chiral recognition.

The mechanism for chiral separation by CDs, which are mobility modifying BGE additive is quite simple to understand. When a charged solute complexes with a neutral CD, its charge/mass ratio and thus its mobility decreases. Hence, the movement of free analytes will differ from the complexed species and the elution order of analytes depends on the degree of complexation. Differences in the equilibrium constants determine the ratio of free/complexed material. If the equilibrium constants are sufficiently different among enantiomers, separation will occur. Starting with the general resolution for CE is shown in Eqn 3.12.

$$\mathbf{R_s = 0.177\ \Delta\ \mu_{ep}} \sqrt{\frac{EL}{\left(\mu_{ep} + \mu_{eo}\right) Dm}} \qquad \text{[Eqn 3.12]}$$

R_s = resolution
$\Delta\mu$ = difference in mobility between theenantiomers

E = field strength
L = capillary length to detector
μ_{ep} = average mobility
μ_{eo} = electro-osmotic mobility
D_m = diffusion coefficient

Wren and later, Wren and Row derived equations to calculate Δμ and ultimately Rs.

The mobility of the first enantiomer is

$$\boldsymbol{\mu_a = \frac{\mu_1 + \mu_2 K_1[C]}{1 + K_1[C]}}$$

For the second enantiomer the mobility is

$$\boldsymbol{\mu_b = \frac{\mu_1 + \mu_2 K_2[C]}{1 + K_2[C]}}$$

Where:

μ_1 = the mobility of the uncomplexed solute
μ_2 = the mobility of the complexed solute
C = concentration of the chiral selector
K_1 and K_2 = the equilibrium constants

This shows that a solute's apparent mobility is influenced by the proportion of time spent as complexed material. The difference in the apparent electrophoretic mobility of the two enantiomers Δμ is $\mu_a - \mu_b$ and can calculate using Eqn 3.13.

$$\boldsymbol{\Delta \mu = \frac{[C](\mu_1 - \mu_2)(K_1 - K_2)}{1 + [C](K_1 + K_2) + K_1 K_2 [C^2]}} \qquad \text{[Eqn 3.13]}$$

From the above equation, we can see that if $\mu_1 = \mu_2$ or $K_1 = K_2$, then $\Delta\mu = 0$. If [C] approaches zero or is very large, Δμ approaches zero as well. The greater affinity of the solute to the selector (large

K), lower the optimal select or concentration. Therefore, both the solute and the type of cyclodextrin selected impact the final result.

The optimal concentration can be calculated from

$$[C]_{opt} = \frac{1}{\sqrt{K_1 K_2}}$$

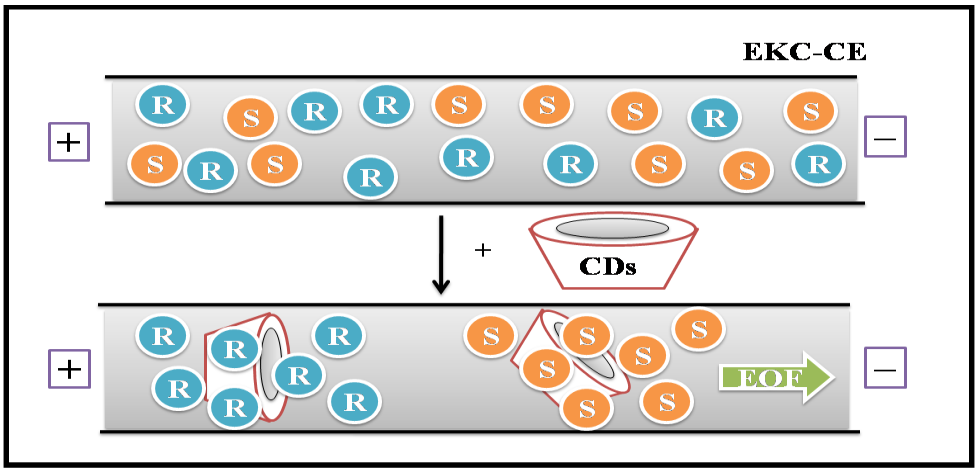

Figure 3.7: Separation mechanism for chiral compounds with cyclodextrin using EKC-CE method

(vi) Capillary electro chromatography (CEC)

Electrochromatography is a term used to describe narrow bore packed column separations where the liquid mobile phase is driven not by hydraulic pressure as in HPLC but by electroosmosis. An additional benefit of CEC compared to HPLC is the fact that the flow profile in a pressure driven system is parabolic, whereas in an electrically driven system it is plug-like and therefore much more efficient. Although Lecoq and Strain discussed the use of electroosmotic flow in chromatography, Pretorius [Pretorius et al., 1974] first demonstrated the ability to use electroosmotic flow in order to drive a mobile phase through a chromatography column. The advantages of using electroosmosis to propel liquids through a packed bed are the same as for in

open capillaries i.e. reduced plate heights as a result of the plug flow profile and the ability to use smaller particles leading to higher peak efficiency than is possible in pressure driven systems (HPLC). The driving force in CEC is the electroosmotic flow and this is highly dependent on pH, the buffer concentration, the organic modifier and the type of stationary phase. The chemistry used to prepare the stationary phase can have a dramatic effect not only on the separation but also the speed of analysis, since the concentration of silanol groups present under the operating conditions largely determine the EOF. For conventional silica based stationary phases, the electroosmotic flow drops off almost linearly between pH 10.0 and pH 2.0 often by as much as a factor of 3, and therefore most CEC is performed above pH 8.0. The following figure illustrates the contribution to the total EOF in a capillary packed with typical silica based 3mm C18 or C8 stationary phases. The vast majority of examples of capillary electrochromatography to date have been performed on either C8 or C18 stationary phases. Non aqueous mobile phases in capillary electrochromatography was employed by Jorgenson and Lukacs [Jorgenson and Lukacs, 1981] where a mobile phase consisting of 100% acetonitrile electrically pumped through a capillary packed with 10 mm Partisil ODS-2 using a voltage of 30kV for high efficiency separation of 9-anthracene. Chiral CEC is a method where immobilizing the chiral cyclodextrin onto the surface of a fused silica capillary and then driving the mobile phase through the capillary at applied voltage.

3.3 Instrumental aspects

(i) Sample injection

To maintain the high efficiency in CE only minute volumes (range up to nanoliters) of samples are loaded into the capillary. The two most commonly used injection methods are electrokinetic and hydrodynamic.

Electrokinetic injection is done by replacing the buffer vial at the injection end of the capillary with a sample vial by applying voltage for a certain period. In this type of injection the sample enters into the capillary through the pumping action and migration of the EOF. Electrokinetic injection is an important aspect in capillary gel electrophoresis, in the use of polymers when the polymer becomes very viscous to be introduced via hydrodynamic injection, thus require voltage in order to be migrated though the capillary. Hydrodynamic injection is a normally used mode for sample introduction into the capillary. It could be performed in three ways, either by applying pressure at the injection point of the capillary, applying vacuum at the exit end of the separation capillary or by doing the siphoning action which is described as the elevation of the sample vial relative to the exit vial. The quantity of sample loaded is nearly independent of the sample matrix with hydrodynamic injection [Huang et al., 1988].

(ii) Capillary

The materials used for manufacturing the capillaries are Teflon and fused silica, at present the fused silica capillaries are widely were for separations. The disadvantage of Teflon is difficult to obtain with homogeneous inner diameters, exhibits sample adsorption problems and has poor heat transfer properties. Compared to Teflon, the fused silica has intrinsic properties, these include high temperature conductance and transparency over a wide range of an

electromagnetic spectrum. Another advantage of using fused silica is that it is easy to use it for the manufacture of capillaries with small diameters of about a few micro metres as shown in Figure 3.8.

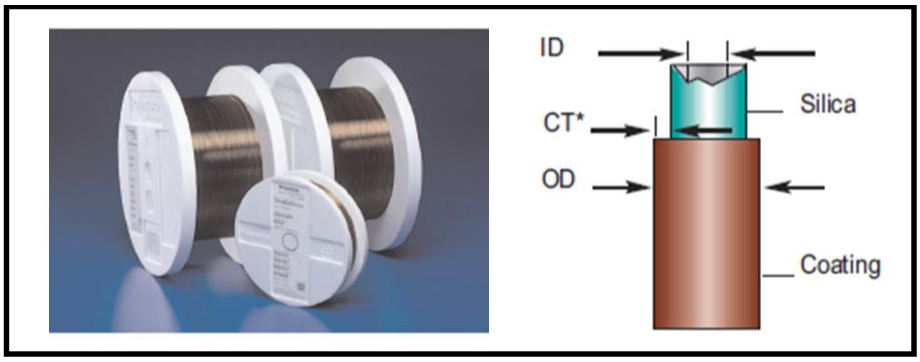

Figure 3.8: Showing fused silica capillaries

From an analysis time perspective, capillaries with short effective lengths should be used. In CGE, 10 cm gel-filled capillaries and 50 to70 cm effective length capillaries are used in CZE. In most cases it is essential to regenerate the surface by preconditioning the capillary before analysis. Recently, wall coated capillaries gained much interest in CE analysis, because they provide good results in terms of analysis time and detection limits than conventional capillaries [Kok, 2000].

(iii) Capillary conditioning

Maintaining a reproducible capillary surface is one of the most challenging aspects in CE. To achieve a good reproducibility, capillary conditioning is the important factor. The most commonly employed approach for reproducibility is to refresh the surface of capillary by deprotonation of the silanol groups and removal of the adsorbents and impurities. A typical wash

method includes flushing a new capillary at 60 ^{0}C using the following sequence: first rinse with 20% methanol, then with1.0M NaOH, then with deionized water, and finally with the running buffer. At the beginning of each working day, the capillaries were conditioned by flushing for 10 min with 1.0M NaOH, 5 min with deionized water and thereafter treated for 10 min with buffer solution. Other washing procedures can employ strong acids, organics such as methanol or DMSO or detergents [Introduction to capillary electrophoresis, Beckman Coulter].

(iv) High voltage power supply

In CE a DC power supply is used to apply up to about 30 kV and current levels of 200 to 300 mA. Stable regulation of the voltage (± 0.1 %) is required to maintain high migration time reproducibility. The current power supply is able to reverse the polarity that can switch from the cathode to anode. Hence, there is no need to introduce the analyte in the cathodic end and also not necessary to move an on-line detector to the other end. It can provide high voltages up to 30 kV, which generate electro-osmosis and electrophoretic flow of the charged species and electrolytes through the capillary. For a good reproducibility of migration time the same voltage are to be applied for the entire analysis [Introduction to capillary electrophoresis, Beckman Coulter].

(vii) Detector

A UV detector or photodiode array detector (DAD) is applicable in CE similar to HPLC. CE also provides an indirect UV detection for analytes that do not absorb in the UV region, in such cases a UV absorbing species (chromophore) is added to the buffer. Generally, in the analysis of peptides and carbohydrates (weak chromophores in UV range) an indirect UV method can be applied successfully. UV detection is widely used as a universal detector due to its collective

detection nature. Besides the UV detection, CE provides nearly five types of detection modes with special instrumental fittings such as Fluorescence, Laser-induced Fluorescence, Amperometry, Conductivity and Mass spectrometry. The limitations of each detection mode are presented in Table 3.1 [Ewing et al., 1989; Lauer and Rozing, 2010].

Table 3.1: Showing limitations of different detection modes in CE

Method	Mass detection	Concentration detection limit (moles) (molar)/ 10 nL injection volume	Advantages/ disadvantages
UV-Vis absorption	10^{-13}-10^{-15}	10^{-5}-10^{-8}	• Universal • Diode array offers spectral
Fluorescence	10^{-15}-10^{-11}	10^{-7}-10^{-9}	• Sensitive • Usually requires sample derivatization
Laser-induced	10^{-18}-10^{-20}	10^{-14}-10^{-16}	• Extremely sensitive fluorescence • Usually requires sample derivatization • Expensive
Amperometry	10^{-l8}-10^{-19}	10^{-10}-10^{-11}	• Sensitive • Selective but useful only for electroactive analyses • Requires special electronics and capillary modification
Conductivity	10^{-15}-10^{-16}	10^{-7}-10^{-8}	• Universal • Requires special electronics and capillary modification
Mass spectrometry	10^{-16}-10^{-17}	10^{-8}-10^{-9}	• Sensitive and offers structural information • Interface between CE and MS complicated
Indirect UV, fluorescence amperometry	10-100, times less than direct methods	–	• Universal • lower sensitivity than direct method

3.4 Electrochemistry in combination with complementary biosensor techniques

A biosensor is a device that consists of a biological recognition system, often called a bioreceptor and a transducer. The basic principle of a biosensor involves the analyte interacting with the bioreceptor and the resulting information measured by a specially designed transducer which converts the information into a measurable electrical signal. Figure 3.9 illustrates the conceptual principle of the biosensing process. The development of biosensors was first reported in the early 1960s [Clark and Lions, 1962]. Biosensors have been extensively used in two major areas such as biological sensing and environmental monitoring with a wide variety of applications.

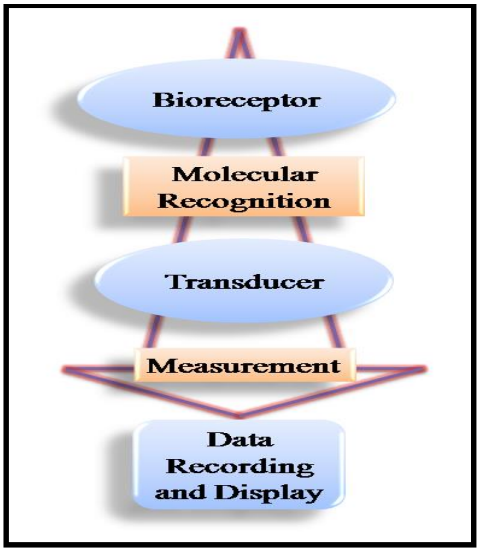

Figure 3.9: Conceptual diagram of the biosensing principle

A bioreceptor utilizes molecular recognition of biological molecular species (e.g., an antibody, an enzyme, a protein, or a nucleic acid) or a living biological system (e.g., cells, tissue, or whole organisms). For a transducer classification, conventional techniques include: (1) optical measurements (2) electrochemical and (3) mass-sensitive measurements.

3.5 Bioreceptors

Bioreceptors are the key element for biosensor technologies because they are responsible for binding the analyte of interest to the sensor for the measurement. However, of the five types of bioreceptors, the two major categories includes enzymes and cellular bioreceptors were used.

(i) Enzyme bioreceptors

Enzymes are macromolecular biological catalysts commonly used as bioreceptors based on their specific binding capabilities as well as their catalytic activity. Most of the enzymes show activity with the building blocks of amino acid residues. Some enzymes require an additional chemical component called a cofactor, which are either inorganic ions (Fe^{2+}, Mg^{2+}, Mn^{2+}, or Zn^{2+}) or organic compounds (flavin and heme) and a coenzyme (NADH, NADPH and ATP). The catalytic activity provided by enzymes allows for much lower limits of detection than would be obtained with common binding techniques [Diamond, 1998]. In this work laccase was used as an enzyme bioreceptor to construct the laccase based biosensor for the determination of SUC.

(ii) Cellular bioreceptors

Cellular structures and cells have been used in the development of biosensors and biochips [Gooding and Hibbert, 1999]. These bioreceptors are either based on bio-recognitionby an entire cell/microorganism or a specific cellular component that is capable of specific binding to certain species. These are presently categorized into three major subclasses: 1) cellular systems, 2) enzymes and 3) non-enzymatic proteins. The major advantage is to provide low detection limits by signal amplification. Microorganisms offer a form of bioreceptor that often allows a whole class

of compounds to be monitored. Microorganisms such as bacteria and fungi have been used as indicators of toxicity or for the measurement of specific substances. For example, cell metabolism, cell respiration or bacterial bioluminescence has been used to evaluate the effects of toxic heavy metals. In this work Cyt c is used as a cellular bioreceptor to construct the Cyt c based biosensor for the determination of Reb A.

3.6 Electrochemical detection

Electrochemical detection is another widely used transduction method in biosensors [Rudel, 1996; Tobalina et al., 1999]. Compared to optical techniques it is very sensitive and easy to operate. By combining the sensitivity of the electrochemical measurements with the selectivity provided by the bioreceptors and nanomaterials, low detection limits are often achievable.

In this work, amperometric devices were used to measure the current-voltage relation and outlined below:

3.6.1 Amperometric devices

Amperometry is a group of techniques in voltammetry, in which the information about an analyte is obtained by varying a potential and then measuring the resulting current. Since there are many ways to vary a potential, there are also many forms of voltammetry, such as: polarography (DC Voltage), linear sweep, differential staircase, normal pulse, reverse pulse, differential pulse and more [Eggins, 2002; Heyrovsky, 1956]. The electrochemical sensors use amperometric measurements for the current resulting from the oxidation or reduction of an electroactive species in a biochemical reaction.

(I) Cyclic voltammetry (CV)

Cyclic voltammetry is a very important amperometry type of electrochemical method in which a redox behaviour of compounds can be calculated to determine mechanisms and rates of oxidation/reduction reactions. Cyclic voltammetry is a simple extension of the linear sweep technique and especially informative about the qualitative aspects of an electrode process.

Cyclic voltammetry was first reported in 1938 and described theoretically by Randles and since it has been established for the evaluation of the charge transfer mechanisms. During these years a number of methods have been developed for the measurement of electrode reaction kinetics.

Advantages of this method include the following:

(a) The wide availability of low cost instrumentation.

(b) Extensive theory available to guide the experimentalist in the interpretation of the empirical results.

(c)A direct estimate of electrode reversibility is provided, because the potentials at which oxidation and reduction occur are observed directly within range.

Cyclic voltammetry reactions can be studied in three ways depending on the analyte behavior of such reversible, irreversible and quasi reversible reaction.

(i) Cyclic voltammetry with reversible systems

The system is described as "*reversible"* when the electrode kinetics is much faster than the rate of diffusion. The Nernst equation [Eqn 3.14] is the final boundary condition for a reversible system.

$$\frac{[Ox]_{x=0}}{[Red]_{x=0}} = \exp\left[\frac{nF}{RT}(E - E^0)\right]$$

The equation is rewritten as:

$$E = E^0 + \frac{RT}{nF} \ln \frac{[Ox]_{x=0}}{[Red]_{x=0}} \quad \text{[Eqn 3.14]}$$

Where $[X]_{x=0}$ is the concentration of analyte at the electrode surface

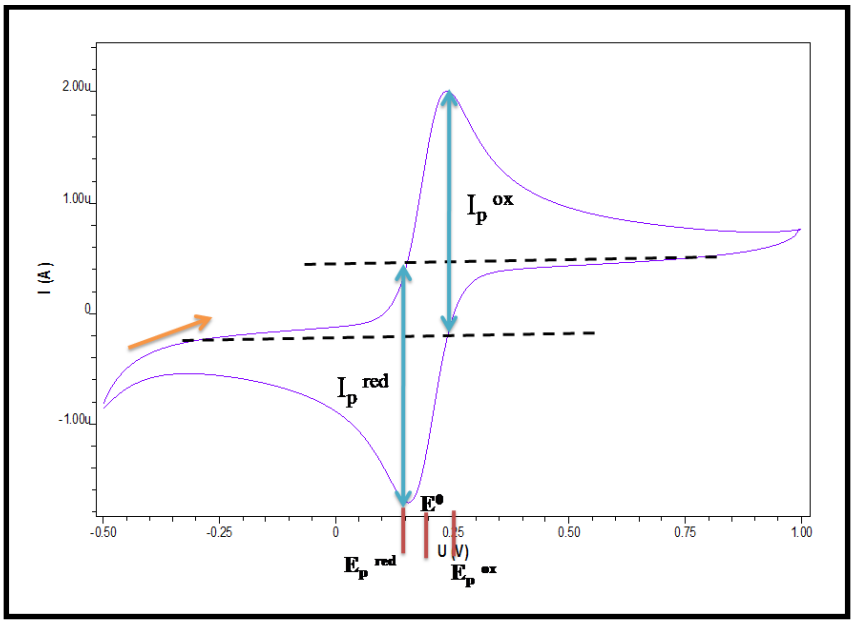

Figure 3.10: Illustrates a reversible system. The arrow shows the direction of the initial scan.

The above voltammogram [Figure 3.10] demonstrate that the electron transfer mechanism is reversible i.e the system initially undergoes oxidation followed by reduction reaction.

The equation for peak current in linear sweep voltammetry at 298 K is [Eqn 3.15]

$$ip = (2.69 \text{ X } 10^5)\, n^{3/2} A D_0^{1/2} C_0 v^{1/2} \quad \text{[Eqn 3.15]}$$

Where A is the area in cm^2, D_0 is the diffusion coefficient in $cm^2\ s^{-1}$, C_0 is the concentration in mol cm^{-3}, v is the scan rate in Vs^{-1} and *ip*is peak current in amperes.

The peak potential E_p is given by Eqn 3.16,

$$E_p = E^0 - 1.109\,\frac{RT}{nF} \qquad \text{[Eqn 3.16]}$$

As the peak is broad, the peak potential may be difficult to analyse, therefore sometimes it is easier to calculate the potential at $i_{p/2}$, named *half-peak potential*, $E_{p/2}$ can calculate using Eqn 3.17,

$$E_{p/2} = E^0 + 1.09\,\frac{RT}{nF}$$

Therefore,

$$E_p - E_{p/2} = 2.20\,\frac{RT}{nF} \qquad \text{[Eqn 3.17]}$$

Hence, the peak potential (Ep) is independent of scan rate (*v*) and the peak current (*ip*) is proportional to $v^{1/2}$.

(ii) Cyclic voltammetry with irreversible systems

The system is described as "*irreversible"* when the electrode kinetics are slower than the rate of diffusion. For an irreversible reaction of the type one-electron, one-step reaction (*Ox* + *e*- →*Red*),linear sweep and cyclic voltammetry give the same voltammetric profile, since no inverse peak emerges on changing the scan direction as shown in Figure 3.11. The Nernstian boundary condition is substituted by a kinetic boundary condition when equilibrium is not retained at the electrode surface as shown in Eqn 3.18

$$\frac{i}{FA} = D_0\left[\frac{\partial C_0\,(x,t)}{\partial x}\right]_{x=0} = k_f\,(t)\,C_0\,(0,t) \qquad \text{[Eqn 3.18]}$$

Where k_f is the rate constant for reduction

In irreversible systems the peak potential appears at higher potentials, exactly beyond E^0 value, due to the small amount or no current flows. Therefore, a bigger over potential is being requested to lead the reduction.

The peak current for irreversible systems (at 298 K) is given by Eqn 3.19,

$$ip = (2.99 \text{ X } 10^5)\,\alpha^{1/2} A D_0^{1/2} C_0 v^{1/2} \qquad \text{[Eqn 3.19]}$$

where A is the area in cm^2, D_0 is the diffusion coefficient in $cm^2\ s^{-1}$, C_0 is the concentration in mol cm^{-3}, v is the scan rate in Vs^{-1} and *ip*is peak current in amperes.

The peak potential for irreversible system is given by [Eqn 3.20-3.21],

$$Ep = E^0 - \frac{RT}{\propto F}\left[0.780 + \ln\frac{D_0^{\frac{1}{2}}}{k_0} + \ln\left(\frac{\propto F v}{RT}\right)^{1/2}\right] \qquad \text{[Eqn 3.20]}$$

$$E_p - E_{p/2} = \frac{1.857\,RT}{\alpha F} \text{[Eqn 3.21]}$$

Consequently, for a totally irreversible system, Ep depends on the scan rate, variably (for reduction) in a negative direction by 30 mV at 298 K (or 1.15RT/αF) for each tenfold increase in the scan rate (*v*).

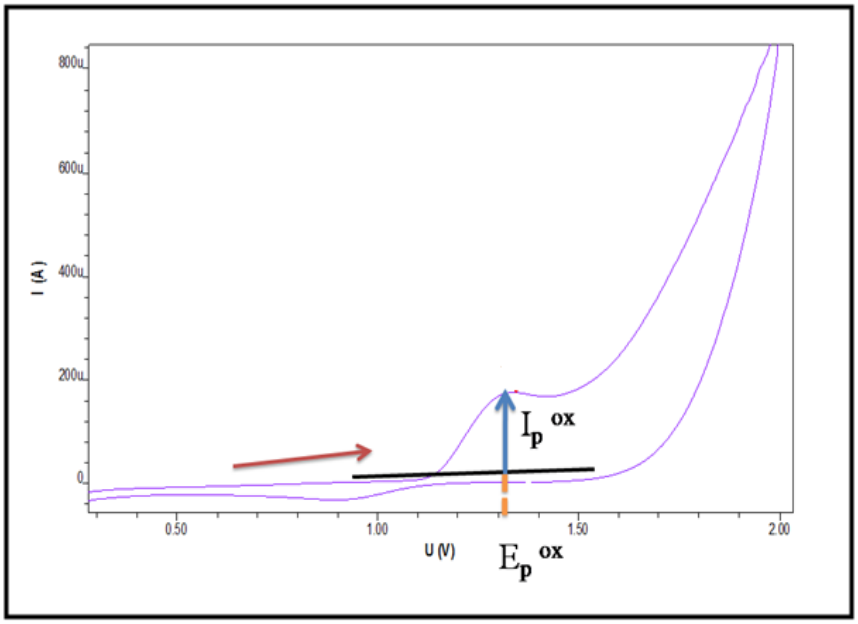

Figure 3.11: Showing an electrochemically-irreversible voltammogram. The numerical values illustrated are dimensionless values of current and potential. The arrow shows the direction of the initial scan.

(iii) Cyclic voltammetry with quasi-reversible systems

The term *quasi-reversible* was introduced by Matsuda and Aybe for reactions that show electron-transfer kinetic limitations. These systems are intermediate between reversible and irreversible systems as shown in Figure 3.12.

For the one-step, one electron case,

$$Ox + e^{-} \underset{K_b}{\overset{K_f}{\rightleftharpoons}} Red$$

The resultant boundary condition is given by Eqn 3.22,

$$D_0 \left\langle \frac{\partial C_0(x,t)}{\partial x} \right\rangle_{x=0} = k^0 e^{-af[E(t) - E0]} \left\{ C_0(0,t) - C_R(0,t) e^{f[E(t) - E0]} \right\} \quad \text{[Eqn 3.22]}$$

The current is given by Eqn 3.23,

$$i = FAD_0^{1/2} C_0 f^{1/2} v^{1/2} \Psi(E) \quad \text{[Eqn 3.23]}$$

where, $f = F/RT$, $\Psi(E)$ is a function of quasi-reversible system, A is the area in cm^2, $D_0$is the diffusion coefficient in cm^2s^{-1}, C_0 is the concentration in $molcm^{-3}$and v is thescan rate in Vs^{-1}.

$$\Delta = \frac{k_0}{D_0^{1/2} \left(\frac{F}{RT}^{1/2} \right) v^{1/2}}$$

When $\Delta > 10$, the behaviour approaches of a reversible system.

The values of i_p, E_p *and* $E_{p/2}$depends on Δ and α. The peak current is given by,

$$i_p = i_p(rev)\, K(\Delta, \alpha)$$

Where, i_p *(rev)*: is the reversible i_p value. For a quasi-reversible reaction, i_p is not proportional to $v^{1/2}$. The peak potential is given by an integral equation which is solved using numerical methods.

A Nernstian, quasi-reversible, or totally irreversible behavior depends on the Δ and on the scan rate employed.

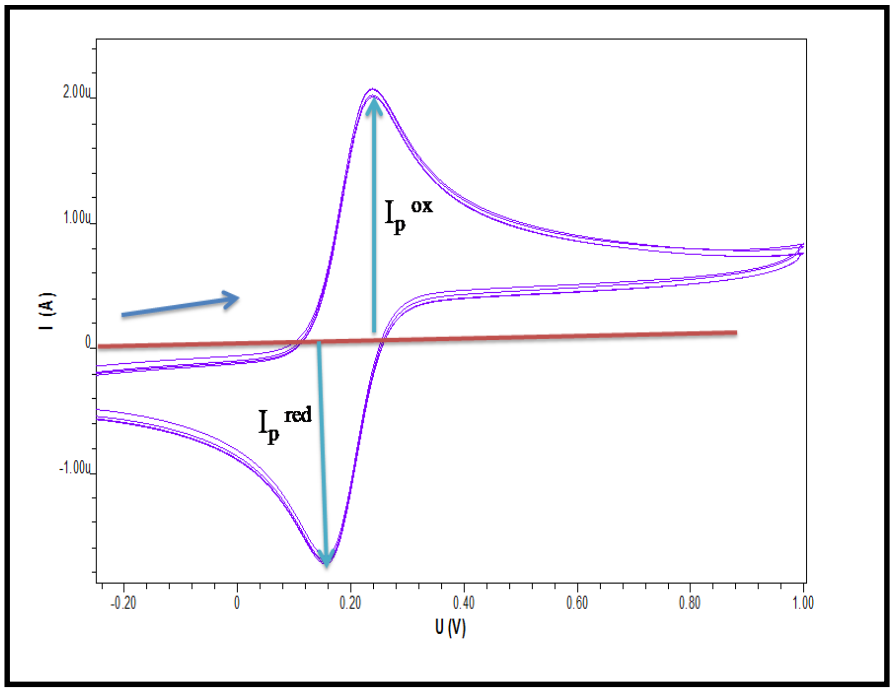

Figure 3.12: Cyclic Voltammogram of a quasi-reversible system. The numerical values illustrated are dimensionless values of current and potential. The arrow shows the direction of the initial scan.

The working principle of cyclic voltammetry is that a, voltage is measured between the reference electrode and the working electrode, while the current is measured between the working electrode and the counter electrode. The obtained measurements are plotted as current *vs* voltage, also known as a voltammogram. To get a meaningful chemical reaction, the critical factor scan rate is very important because the duration of a scan must provide sufficient timefor a particular reaction. By varying the scan rate, the corresponding results also varies for example with an increase in the scan rate the oxidation and reduction peak potentials gradually moves to the right and left sides with a gradual increase and decrease in the oxidation and reduction peak currents. Especially, in the

development of biosensors, the shape of the voltammogram for a given compound depends not only on the scan rate and the electrode surface, but also depends on the catalyst (biomolecules or nano materials) concentration.

(II) Differential pulse voltammetry/polarography

Differential Pulse Voltammetry (DPV) is the most universal and frequently used voltammetric measurement mode. It is equally well suited for irreversible and reversible systems and offers a high sensitivity. In digital instruments the excitation signal consists of a staircase-shaped increasing direct potential, to which small square wave pulses with a constant potential (pulse amplitude) are applied in periodic succession. In the pulse mode the current is measured twice at each mercury drop, before each pulse and at the end of the pulse time. The difference between the measurements is plotted against the direct potential and produces peak-shaped polarograms, as the change in current is the largest for the potential alterations in the region of the half-wave potential as shown in Figure 3.13. The formation of this difference also leads to a further reduction of the capacitive current contribution and therefore to an increase in sensitivity, even when compared with determinations by normal pulse polarography.

According to the Ilkovich equation [Eqn 3.24],

$$i_p = \frac{n^2F^2}{4RT} A C_a \Delta \, E_A \sqrt{\frac{D}{\pi t_p}} \qquad \text{[Eqn 3.24]}$$

for reversible electrode processes the peak height i_p in the DP polarograms is proportional to the analyte concentration C_a and is determined by the amplitude ΔE_A of the square wave pulses as well as by the pulse time t_p among other factors [Gumede, 2008].

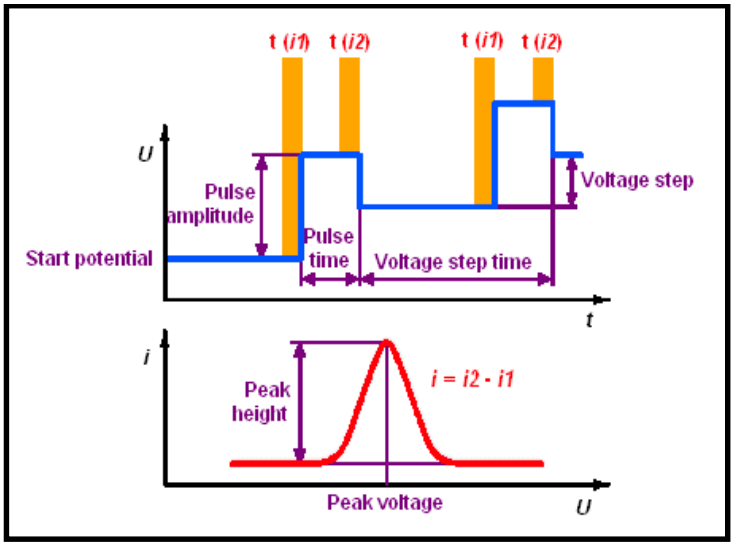

Figure 3.13: A typical DPV measurement process whereby the current is measured twice at each mercury drop, before each pulse and at the end of the pulse time. The difference between the measurements is plotted against the direct potential and produces peak-shaped polarograms, as the change in current is the largest for the potential alterations in the region of the half-wave potential. Typical current-potential curve expected for a DPV measurement

The detection limit for determinations by differential pulse voltmmetry is similar to that for square wave polarography at about 10^{-7}-10^{-8} mol/L; however, the decrease in sensitivity resulting from irreversibility is lower.

3.7 The three electrode system

In the three electrode system [Figure 3.14], the *working or test* electrode is used to investigate the redox reactions. The second functional electrode is the *reference electrode*, whose potential is constant enough that it can be taken as the reference standard against which the potentials of the other electrodes present in the cell can be measured. Commonly used reference electrodes are the silver-silver chloride electrode (Ag/AgCl/4M KCl, e=0.222 V) or the calomel

electrode (Hg/HgCl/KCl). The third functional electrode is the *counter or auxiliary electrode,* which serves as a source or sink for electrons so that current can be passed from the external circuit through the cell. In general, neither its true potential nor current is ever measured or known. The normal material for cell construction is Pyrex glass for reasons both of visibility and general chemical inertness.

Based on the chosen function of a specific electrode, the electrode material, its surface modification or its dimensions greatly influence its detection ability. Electrochemical sensing usually requires a reference electrode, a counter or auxiliary electrode and a working electrode, also known as the sensing or redox electrode.

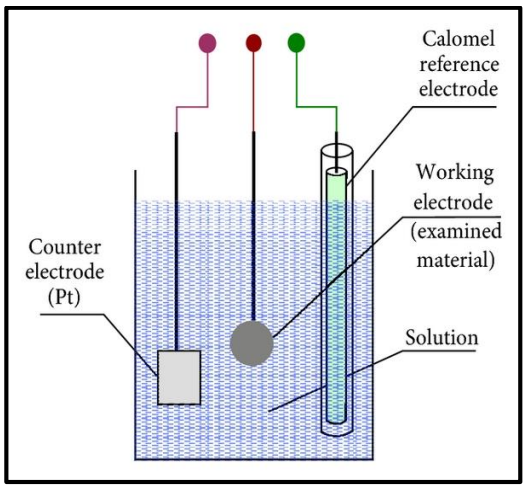

Figure 3.14: A typical electrochemical cell consists of three electrode system

The reference electrode commonly made from Ag/AgCl, is kept at a distance from the reaction site in order to maintain a known and stable potential. The working electrode serves as the transduction element in the biochemical reaction, while the counter electrode establishes a connection to the electrolytic solution so that a current can be applied to the working electrode.

These electrodes should be both conductive and chemically stable. Therefore, platinum, gold, carbon (*e.g.* graphite) and silicon compounds are commonly used, depending on the analyte.

(i) Metal electrodes (Pt and Au)

Platinum and gold have proven to be the most widely used metallic electrodes. Such electrodes offer very favorable electron-transfer kinetics and a large anodic potential range. By contrast, the low hydrogen overvoltage at these electrodes limits the cathodic potential window (from -0.2 to -0.5 regions, depending upon the pH). The high background currents associated with the formation of surface-oxide or adsorbed hydrogen layers are more problematic. Such films can also strongly alter the kinetics of the electrode reaction, leading to irreproducible data [Wang, 2004]. Compared to platinum electrodes, gold electrodes are more inert, and hence are less prone to formation of stable oxide films or surface contamination. Gold electrodes are also widely used as substrates for self-assembled organosulfur monolayers or for stripping measurements of trace metals. Other metals, such as copper, nickel, or silver have been used as electrode materials in connection specific applications, such as the detection of amino acids or carbohydrates in alkaline medium (copper and nickel) and of cyanide or sulphur compounds (silver). Unlike platinum or gold electrodes, the copper electrode offers a stable response for carbohydrates at constant potential. Figure 3.15A shows the different types of commercially available working electrodes.

(ii) Glassy carbon electrodes

Glassy (or "vitreous") carbon (GC) has been very popular because of its excellent mechanical and electrical properties, wide potential window, chemical inertness (solvent resistance), and relatively reproducible performance. The material is prepared by means of a

carefully controlled heating program of a pre-modeled polymeric (phenol-formaldehyde) resin body in an inert atmosphere. The carbonization process is carried out very slowly over the 300-1200^{0}C temperature range to insure the elimination of oxygen, nitrogen and hydrogen. The structure of glassy carbon involves thin, tangled ribbons of cross-linked graphite-like sheets. Because of its high density and small pore size, no impregnated procedure is required. However, a surface pre-treatment is usually employed to create active and reproducible glassy-carbon electrodes and to enhance their analytical performance. Such pre-treatment is usually achieved by polishing (to a shiny "mirror-like" appearance) with successively smaller alumina particles (< 0.05μm) on a polishing cloth. The electrode should then be rinsed with deionised water before use. Additional activation step, such as electrochemical, chemical, heat, or laser treatments, have also been used to enhance performance. The improved electron-transfer reactivity has been attributed to the removal of surface contaminants, exposure of fresh carbon edges, and an increase in the density of surface oxygen groups (which act as interfacial surface mediators). Several reviews provide more information on the physical and electrochemical properties of glassy carbon electrodes (Figure 3.15) [Henze, 2007; Achterberg et al., 2000].

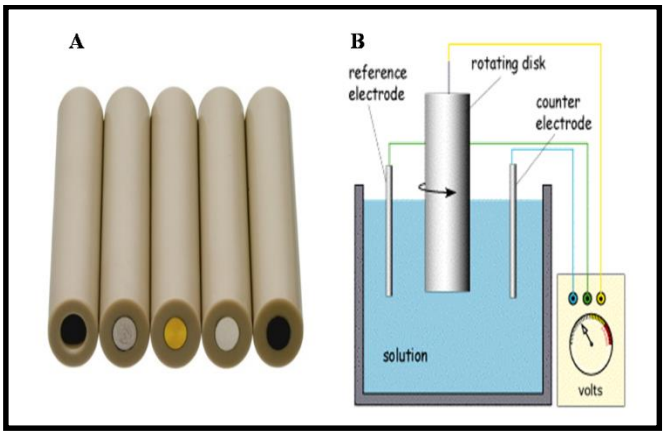

Figure 3.15: (A) Different types of working electrodes (Glassy carbon, platinum and gold electrodes (B) Illustrating mechanism of rotating disc electrode

(iii) Rotating disc electrode (RDE)

The limited anodic potential of mercury electrodes has precluded their utility for monitoring oxidizable compounds. Accordingly, solid electrodes with extended anodic potential windows have attracted considerable analytical interest. Of the many different solid materials that can be used as working electrodes, the most often used is carbon, platinum and gold. Silver, nickel and copper can also be used for specific applications. An important factor in using solid electrodes is the dependence of the response on the surface state of the electrode. Accordingly, the use of such electrodes require precise electrode pre-treatment and polishing to obtain reproducible results. The nature of these pre-treatment steps depends on the materials involved. Mechanical polishing (to a smooth finish) and potential cycling are commonly used for metal electrodes, while various chemical, electrochemical or thermal surface procedures are added for activating carbon-based electrodes. Unlike mercury electrodes, solid electrodes present a heterogeneous surface with respect to the electrochemical activity. Such surface heterogeneity leads to deviations from the behavior expected for homogenous surfaces [Figure 3.15B]. Solid electrodes can be stationary or rotating, usually in a planar disk configuration. Such electrodes consists of a short cylindrical rod of the electrode material embedded in a tightly fitting tube of an insulating material (Teflon, Kel-F etc.). It is essential to avoid crevices between the sleeve and the electrode materials, and thus to prevent solution creeping (and an increase in background response). Electrical contact is made at the rear face. The RDE provides an efficient and reproducible mass transport and hence the analytical measurement can be made with high sensitivity and precision. Such well-defined behavior greatly simplifies the interpretation of the measurement. The convective nature of the electrode also results also in very short response times. The detection limits can be lowered via periodic changes in the rotation speed and isolation of small mass transport-dependent currents

from simultaneously flowing surface-controlled background currents [Achterberg et al., 2000; Mello et al., 2005].

(iv) Chemically modified electrodes

Chemically modified electrodes (CMCs) represent a modern approach to electrode systems. These rely on the placement of a reagent onto a surface to impart the behavior of reagent to the modified surface. Such deliberate alteration of electrode surfaces can thus meet the needs of many electro-analytical problems, and may form the basis for new analytical application and different sensing devices [Msangati et al., 2002, 2003]. There are various ways in which CMEs can benefit analytical applications. These include acceleration of electron-transfer reactions, preferential accumulation, or selective membrane permeation. Such steps can impart higher selectivity, sensitivity, or stability to electrochemical devices. Many important applications, such as electrochromic devices, controlled release of drugs, electro synthesis, and corrosion protection, should also benefit from the rational design of electrode surfaces. One of the most common approaches for incorporating a modifier onto the surface has been the covered with an appropriate polymer film. Polymer modified electrodes are often prepared by casting a solution containing the dissolved polymer onto the surface and allowing the solvent to evaporate or via electro-polymerization in the presence of the dissolved monomer. The latter offers precise control of the film thickness and is particularly attractive in connection with miniaturized sensor surfaces.

3.8 Principles of computational modelling

Molecular modelling is the general term used to describe the use of computers to construct macro and micro molecules and perform a broad range of calculations in order to predict their chemical characteristics and behavior. Protein modelling is one of the interesting areas, which

uses quantum mechanical methods to evaluate the possibility of interactions between the micro molecules with proteins. The latest improvements in the protein modelling is to understand the ligand-protein or protein-protein and host-guest interactions by calculating the free energies [Ballester and Mitchell, 2010]. Most commonly used methodologies for the evaluation of protein-ligand or host-guest interactions are molecular docking approaches which are based on the molecular dynamics, robotics or rotamer libraries [Čučković et al., 2002]. There is still a need for a better understanding of host-guest interactions or chiral mechanism in chromatographic, electrophoretic and other separations techniques, thus adding demand for molecular modelling of enantio-separations. In this work, molecular docking was used to study the interaction of two major steviol glycosides and neotame diastereomers with cyclodextrin receptor and the obtained results were used to explain elution order of analytes in capillary electrophoresis [Bathinapatla et al., 2014]. On the other hand molecular dynamics (MD) was used to predict binding affinities and host-guest relation of Reb A with Cyt c and SUC with laccase.

3.8.1 Molecular docking

Docking is a computational method to study the formation of intermolecular complexes former uses smaller molecule interacts with a larger molecule. Different types of interactions between the molecules can be distinguished, protein-protein, protein-DNA, DNA-ligand, protein-ligand or any receptor-ligand interactions. The involvement of biologically active molecules such as proteins, nucleic acids, carbohydrates and lipids plays an important role in the signal transduction. The type of signals produced by the two interacting partners mainly depends on the relative orientation. Therefore, docking is a useful tool to predict both the strength and type of signals produced. The aim of docking is to achieve an optimized conformation for both the

receptor and ligand with a relative orientation between the receptor and ligands such that the free energy of the overall system is minimized.

3.8.2 Docking tools

In docking mainly two aspects are important: viz., the prediction of the affinity between the ligand and the protein along with the prediction of correct poses of the ligands in the active site of the protein. Molecular docking consists of two steps: (i) searching and (ii) scoring functions as outlined in Table 3.2.

Table 3.2: Types of scoring functions

Type	Scoring function
Force field-type	DOCK, DOCK 3.5 (PB/SA), DOCK/GBSA (SDOCK), AutoDock, GOLD, SYBYL/D-Score, SYBYL/G-Score
Empirical	FlexX, Glide, ICM, LUDI, PLP, ChemScore, SCORE, X-Score, Surflex, SYBYL/F-Score, LigScore, MedusaScore, AIScore, SFCscore
Knowledge based	ITScore, PMF, DrugScore, DFIRE, SMoG, BLEEP, MScore, GOLD/ASP, KScore

3.8.3 Scoring functions

The scoring function is an important aspect for protein-ligand docking algorithm and speed, accuracy are the two important aspects of a scoring function. Mainly scoring functions have three important applications in molecular docking (i) includes determination of the binding mode and binding site of ligand on a protein [Rajamani and Good, 2007] (ii) to predict the absolute

binding affinity between protein and ligand [Shoichet et al., 2002] (iii) virtual database screening which is to identify the potential drug hits/leads for a given protein target by searching a large ligand database [Seifert et al., 2006]. The three main categories of scoring functions are described below.

(i) Force field scoring function

Force field (FF) scoring functions are based on the physical atomic interactions [Huang et al., 2006] including electrostatic interactions, van der Waals (VDW) interactions and bond stretching/bending/torsional forces. Force field functions and parameters are usually derived from both experimental data and *ab* initio quantum mechanical calculations according to the principles of physics. But the major challenge in the force field scoring functions is the consideration of the solvent in ligand binding. For this reason implicit solvent models includes the Poisson–Boltzmann/ Surface Area (PB/SA) model [Rocchia et al., 2002; Grant et al., 2001] and the generalized-Born/ Surface Area (GB/SA) model [Qiu et al., 1997] that are often used in post-scoring of docking programs.

One typical force field scoring function in molecular docking is the scoring function of DOCK whose energy parameters are taken from the amber force field [Eqn 3.25].

$$E = \sum_i \sum_j \left(\frac{A_{ij}}{r_{ij}^{12}} - \frac{B_{ij}}{r_{ij}^{6}} + \frac{q_i q_j}{\varepsilon(r_{ij}) r_{ij}} \right) \qquad \text{[Eqn 3.25]}$$

Where r_{ij} stands for the distance between protein atom i and ligand atom j, A_{ij} and B_{ij} are the VDW parameters, and q_i and q_j are the atomic charges. Here, the effect of solvent is implicitly considered by introducing a simple distance dependent dielectric constant $e(r_{ij})$ in the coulombic term.

(ii) Empirical scoring functions

Empirical scoring functions work on the basis of a set of weighted energy terms which estimates the binding affinity of a complex. The energy can be calculated using Eqn 3.26 as shown below

$$\Delta G = \sum_i W_i . \Delta G_i \qquad \text{[Eqn 3.26]}$$

Where, W_i are corresponding coefficients which are determined by fitting the binding affinity data of a training set of protein–ligand complexes with known three-dimensional structures [Jain, 1996; Head et al., 1996]. The ΔG_i represents different energy terms such as VDW energy, electrostatics, hydrogen bond, desolvation, entropy and hydrophobicity *etc*. Compared to the force field scoring functions, the empirical scoring functions are much faster in binding score calculations due to their simple energy terms. On the basis of fastness, many well-known protein–ligand docking programs have been used in empirical scoring functions, such as FlexX and Surflex. The major challenge for empirical scoring functions is how to avoid double-counting problems with many energy terms. Empirical scoring functions does not have a correct setting to give optimal results, hence there is still a need for a simple empirical function which yields as accurate an estimate of the binding affinity as possible.

(iii) Knowledge-based scoring function

Knowledge-based scoring functions, a third kind of scoring function employs energy potentials that are derivedfrom the structural information embedded in experimentally determined atomic structures [Sippl, 1990]. Knowledge-based scoring functions involves pair wise potentials

which are directly obtained from the occurrence frequency of atom pairs in a database using the inverse Boltzmann relation [Koppensteiner and Sippl, 1998; Thomas and Dill, 1996]. For protein-ligand studies, the potentials are calculated using Eqn 3.27.

$$w(r) = -k_B T \ln [g(r)] \qquad \text{[Eqn 3.27]}$$

$$G(r) = \rho(r)/\rho^*(r)$$

where k_B is the Boltzmann constant, T is the absolute temperature of the system, $\rho(r)$ is the number density of the protein–ligand atom pair at distance r, and $\rho^*(r)$ is the pair density in a reference state where the interatomic interactions are zero. Compared to the force field and empirical scoring functions, the knowledge-based scoring functions offer a good balance between accuracy and speed. However, there is a problem in deriving knowledge-based scoring functions; the calculations of an accurate reference state $\rho^*(r)$ is not achievable and it becomes a venerable difficulty in deriving knowledge-based potentials.

(iv) Consensus scoring

Consensus scoring is not really a specific type of scoring function but a technique in protein-ligand docking. Consensus scoring technique has been introduced to improve the probability of finding correct solutions by combining the scores from multiple scoring functions so that the true modes/ binders can be discriminated from others accordingly [Charifson et al., 1999].

3.9 Gaussian calculations

Gaussian is a computer program for computational chemistry initially released in 1970 by John Pople and his research group at Carnegie-Mellon University as Gaussian 70. After

introducing Gaussian it has been continuously updated and developed for different calculations including cutting-edge research in quantum chemistry and other fields. The current version of the program is Gaussian 09. The name originates from Gaussian type orbitals to speed up calculations compared to those using Slater-type orbitals. The broad range of applications of Gaussian, made it to a popular and widely used theoretical method or model based electronic structure program in the field of computational chemistry.

Theoretical model or method is a way to model a system using a specific set of approximations, which are combined with a calculation algorithm defined by the basis set to compute molecular orbitals and energy. In general, the methods can be separated into four main types: molecular mechanics, semi empirical, *ab* initio and density functional. Mainly, the selection of theoretical model depends on the size of the system and on the level of approximation.

3.9.1 Molecular mechanics

Molecular mechanics (MM) methods approximate atoms as spheres and bonds as springs. For energy calculations MM uses an algebraic equation instead of a wave function or electron density. The constants in the equation are obtained from experimental data or other calculations and are stored in a data library. The combination of constants and equations is called a force fieldused mainly with organic systems.

(i) *Ab initio* methods

Ab initio methods are based on theoretical principles and without considering any experimental data. The numerous methods have the same basic approach, but differ in the

mathematical approximations. These are the most popular type of models, despite the fact that the calculations are time consuming.

Examplesof *Ab initio* methods

Hartree-Fock (HF) is the basic *ab initio* model. It is based on the approximation of Coulombic electron-electron repulsions that takes into account explicitrepulsion interactions (central field approximation). The major drawback of HF method is the exclusion of electron correlation.

(ii) Semi empirical methods

Semi-empirical quantum chemistry methods are Hartree-Fock formalism based methods, but makes many approximations and obtain some parameters from empirical data. Semi-empirical methods are very important in computational chemistry for large molecules with Hartree–Fock formalism. Due to the use of zero differential overlap approximation, these calculations are much faster than their *ab initio* methods. Semi-empirical calculations have been used successfully in the field of organic chemistry, because only a few elements are used extensively and molecules are of moderate size. Usually, semi-empirical methods are used for the big systems, since they can handle large amounts of calculation. However, semi-empirical methods were also applied to the solids and nanostructures but with different parameterization. ZINDO, parameterized to reproduce the electronic spectra to compute the UV transitions and Austin Model 1 (AM1) is a method that is most often used to model the organic molecules.

(iii) Density functional theory (DFT)

DFT methods are most popular, because of its accuracy when compared to the *ab initio* methods. DFT calculations are faster than HF calculations and thus reduces the CPU timebecause, DFT calculations are based on the electron density whereas HF on wave function.

Example of DFT methods

B3LYP is the most popular DFT model and it is a hybrid method, because it uses corrections for both gradient and exchage correlations.

CHAPTER 4

METHODOLOGY

4.1 Capillary electrophoresis

4.1.1 Instrumentation

All separation experiments were performed using Agilent Technologies 7100 CE system equipped with a diode arraydetector (DAD), an auto-sampler and a temperature controller (15–60 ± 0.1 ^{0}C). Instrument control and dataanalysis were carried out by Agilent Chemstation softwareinstalled on a personal computer. A fused silica capillary with 50 μm inner diameter and 363 μm outer diameterwith the total and effective lengths of 64.5 and 56 cm, respectively was employed (Agilent Technologies, SA).

4.1.2 Materials

Individual standards of Reb A and Stv with 98.0 % analytical quality were obtained from Ganzhou Julong High Tech Industrial Co., Ltd, China. L,L and D,D-neotame standards of 97.0% analytical quality were obtained from Hullets,South Africa. SUC standard with 98.0% analytical quality was obtained from Tate & Lyle Company. Sodium dihydrogen orthophosphate, Disodium tetra borate, Heptakis 2,3,6-tri-o-methyl betacyclodextrin (TM-β-CD), Sodium hydroxide, Hydrochloric acid, Methanol,Morpholine, Ethylamine, Piperidine, Triethylaminewere purchased from Capital Lab Supplies CC (KwaZulu-Natal, SA). Deionized water was generated from an aqua MAXTM-basic 360 series water purification system from TRILAB SUPPORT (Durban, SA). All solutions and samples were prepared in deionized water filled in vials with disposable syringes filtering through a 0.45-μm poresize and 25-mm diameter syringe filters

containing cellulose acetate as filter medium supplied from Anatech Instruments (Pty) Ltd. (Durban, SA) before analysis.

4.1.3 Preparation of stock solutions

3mM stevia standard solutions, each containing 98.0% of Reb A and Stv were prepared quantitatively by weighingan equivalent amount in a 5mL volumetric flask and diluting with deionized water. A stock standard solution of L,L and D,D-neotame (5.0 mM) was prepared by weighing an appropriate amount in a 5 mL volumetric flask and diluted with 20% methanol. SUC (5 mM) standard solution was prepared in a 5mL volumetric flask by dissolving an equivalent amount in deionized water. Different concentrations of TM-β-CD was prepared by dissolving an equivalent amount in phosphate buffer in a 10mL volumetric flask at 60 ^{0}C. Phosphate and borate buffers were prepared by dissolving needed amount of sodium dihydrogen orthophosphate and disodium tetra borate with adequate amount of deionized water in a 100 mL volumetric flask, and thenadjusted to desired pH with 1.0 M NaOH/ HCl. All stock solutions were refrigerated at 4 ^{0}C for stability.

Morpholine, ethylamine, piperidine buffers were prepared by dissolving 2ml of each compound with adequate amount of deionized water in a 10 mL volumetric flask. Triethylamine was prepared as 2ml of TEA dissolved in 40% methanol, prior to dilution to the calibration mark with deionized water to get 0.2 M amine buffers and then adjusted to pH 12.0 with 1.0 M NaOH.

Real stevia samples used in this study were purchased from a local supermarket in different forms containing steviol glycosides, tablet samples (Green Canderel, Merisant Company 2, Czech Republic), powder samples (Stevia, Dis-Chem Pty Ltd, SA) and liquid samples (Tantalize, Delite Foods, SA). Specifically, in the preparation of a tablet sample, one tablet was ground into fine

powder and dissolved in the equivalent of 5 mL deionized water. Powdered samples were prepared by dissolving the equivalent amount in a 5 mL volumetric flask with deionized water. Liquid samples were prepared directly by dissolving the equivalent amount in deionized water.

In case of NTM, spiked samples (3.0, 5.0 and 7.0 mM) were prepared with Mango juice (Checkout Manufacturers Pty Ltd, Quilbert-4078, SA), Tab cool drink (SAB Miller House, England) and Bustaorange soft drink (SMJ Beverages SA Pty Ltd, New Germany 3610, SA) were collected from a local supermarket. The spiked samples were prepared by direct dissolution of neotame in 5 mL volumetric flasks with the real samples mentioned above. Spiked NTM samples were prepared, because of unavailability of neotame in the real samples. Three SUC real samples were analysed in this study, powder sample (Canderel yellow, Merisant Company 2, Sarl, 2000 Neuchatel-Switzerland), tablet samples (Canderel yellow, Merisant Company 2, Sarl, 2000 Neuchatel-Switzerland and Hullets equisweet, Tongaat Hullet Sugar, Rossburgh, SA) and SUC spiked samples such as Busta apple drink (SMJ Beverages SA Pty Ltd, New Germany 3610, SA), Refresh cool drink (Little Green Beverages Pty Ltd, 20 Anvil road, Johannesburg, SA), Energade sports drink (Tiger Consumer Brands Limited 3010 W.N. Drive, Bryanston, SA) were used. These samples were purchased at a local super market and all the real samples were used without any further purification. Spiked samples were prepared as different concentrations (3, 5, 7 mM) sucralose dissolved directly with cool drinks in 5 mL volumetric flask. Before the analysis, all the samples were diluted up to optimized dilution level (100-fold) to avoid possible interferences from the other substances.

4.1.4 Capillary electrophoresis procedure

The new capillaries were conditioned at 60 ^{0}C using the following sequence: (1) 7 min rinse with 20% methanol (2) 20 min rinse with 1.0 M NaOH (3) 5 min rinse with deionized water and finally with 20 min rinse with the running buffer. At the beginning of each working day, the capillaries were conditioned by flushing for 10 min with 1.0 M NaOH, 5 min with deionized water and thereafter, treated for 10 min with running buffer solution as the background electrolyte. Between runs the capillary was rinsed with water (100 mbar 1 min), 0.1 M sodium hydroxide (100 mbar 2 min), water (100 mbar 2 min) and filled with the BGE (100 mbar 5 min).

For separation of steviol glycosides and NTM diastereomers using EKC-CE method, 30 mM TM-β-CD in 50mM phosphate buffer was first injected hydrodynamically through the capillary by applying approximately 100 mbar for 10 s followed by ultrafiltrated standard solutions injected at 50 mbar for 4 s. Separation was performed in normal polarity by applying voltage of 20 kV and capillary was thermostated at 30 ^{0}C. The UV detection wavelength was set ranging from 200 to 240 nm for sensitive determination.

For separation of SUC using CZE indirect-UV method, SUC standard solution was injected hydrodynamically by applying 50 mbar for 5 s. The electrophoretic mobility was created by amine buffers under the applied voltage of 22 kV. The capillary was thermostated at temperature of 30 ^{0}C and the UV detection wavelength was set ranging from 220 to 260 nm for sensitive determination. Peak areas corrected by migration times (in order to compensate for velocity discrepancies between peaks) were used as analytical signal.

The resolution factor (Rs) between two peaks was calculated using the equation 4.1:

$$Rs=\frac{2(t_2-t_1)}{w_1+w_2} \qquad \text{[Eqn 4.1]}$$

where

t_1 is the migration time of first elution compound

t_2 is the migration time of second elution compound

w_1 is the peak width of first elution compound at the base

w_2 is the peak width of second elution compound at the base.

The retention factor (K′) and separation factor (α) was calculated using equation 4.2:

$$\text{Retention factor (K}') = \frac{(t_r - t_0)}{t_0\ (1 - \frac{t_r}{t_m})} \qquad \text{[Eqn 4.2]}$$

Where t is the retention time of the solute, t_0 is the retention time of the unretained solute and t_m Pseudostationary phase retention time

Separation factor (α) = K_2'/K_1'

k_1' and k_2' are the retention factors of the first and second eluted analytes respectively.

4.2 Biosensor/ Electroanalytical chemistry

4.2.1 Instrumentation

All electrochemical measurements were performed using a 797 VA computrace from Metrohm (Herisau, Switzerland), operated with a PC equipped by 797 VA computrace 1.3.1 software. Voltammograms were recorded at room temperature using a three-electrode system consisting of a working electrode (GCE, Pt, Au electrodes), Ag/AgCl as a reference electrode, and the platinum wire as a counter electrode. All the solutions examined by electrochemistry were initially purged with purified nitrogen gas for 10min. All solutions were cleaned before analysis using 0.45 μm poresizecellulose acetate filter medium.

Morphological and characterization studies were performed using Transmission electron microscope (TEM) model JEM 2100 equipped with a LaB_6 emitter (MAX OXFORD instruments)

for TEM analysis. Varian 800 FT-IR Scimitar Series supplied by SMM Instruments (Durban, South Africa (SA) for IR analysis with KBr disks was employed. UV–vis absorption spectra were performed using a UV2450 spectro-photometer (Shimadzu). Isothermal titration calorimetric studies were performed using VP-ITC MicroCal titration calorimeter. The STAR^e system of TGA/DCS 1 SF/1346 model was supplied with a STAR^e software version 9.20 by METTLER TOLODO (Johannesberg, South Africa). Compositional and phase identification was performed on an X-ray diffractometer D8 Advance equipped with a Co-Kα radiation, operated at 35 mV and 30 mA. The measurements were taken with 2 Theta (2θ) angle ranging from 5 to 90^0, with a scanning rate of 0.02 S^{-1}. The recorded X-ray diffractograms were processed using Eva/Origin software. All solutions weresonicated using an Ultra sonic (Labcon 5019 U model) supplied by Lasec (Durban, SA). All pH-metric measurements were made on a CRISON micro pH 2000 digital pH meter which was previously calibrated with a precision of 0.1 pH units using buffers of known pH.

4.2.2 Materials

p-aminothiophenol, Graphene oxide, Auric chloride ($HAuCl_4$), Ascorbic acid, Carbon disulfide, Ammonium hydroxide, Copper chloride dihydrate, Copper sulphate dihydrate, Zinc chloride dihydrate, Zinc acetate dihydrate, Nickel chloride dihydratewere purchased from Capital Lab Supplies CC (KwaZulu-Natal, SA). 20-30% MWCNTs basis, O.D × L 7-12 nm × 0.5-10 μm (cas no. 308068-56-6) were purchased from Aldrich (Durban, SA). Horse heart Cytochrome c (96%), Laccase derived from *Trametesversicolor* (51639) and 2,2,6,6-tetramethylpiperidine-1-oxyl (TEMPO) were obtained from Sigma and used without any further purification. Nitrogen of 99.9% purity was obtained from AFROX (Durban, SA). Alumina powder ≤ 3 μm was supplied by

Metrohm (Durban, SA). Deionized water was generated from an aqua MAXTM-basic 360 series water purification system from TRILAB SUPPORT (Durban, SA). All solutions and samples were prepared in deionized water filled in vials with disposable syringes filtering through a 0.45-μm poresize and 25-mm diameter syringe filters containing cellulose acetate as filter medium supplied from Anatech Instruments (Pty) Ltd. (Durban, SA) before analysis.

4.2.3 Preparation of stock solutions

Standard solutions of steviol glycosides, NTM diasteriomers and SUC were prepared as mentioned in section 4.1.3. Horse heart Cytochrome c (96%) and laccase were prepared as, 0.01 g of each Cyt c and laccase dissolved in 10 mL volumetric flask with 0.1 M borate and phosphate buffers respectively. Phosphate and borate buffers were prepared by dissolving needed amount of sodium dihydrogen orthophosphate and disodium tetra borate with adequate amount of deionized water in a 100 mL volumetric flask, and then adjusted to desired pH with 1.0 M NaOH/ HCl. All stock solutions were refrigerated at 4 ^{0}C for stability. Same real samples mentioned in section 4.1.3 were used for analysis with biosensor.

4.2.3.1 Synthesis of NTM-metal complexes

The NTM-metal complexes were prepared as mononuclear complexes. A solution of $CuCl_2.2H_2O$ (1mM), $NiCl_2.2H_2O$ (1mM) and $ZnCl_2.2H2O$ (1mM) in 20 mL methanol was added to a solution containing NTM (2mM) in 30 mL methanol, and the pH of the resulting mixture was adjusted to 5.5. Further, the mixture was stirred at room temperature (RT) for 4 h and then left at RT for 6 h to get dry. Finally, a green [NTM-Cu^{2+}], white [NTM-Ni^{2+}, NTM-Zn^{2+}] crude solids were obtained.

4.2.4 Preparation methods for nanocomposites

4.2.4.1 Preparation and fabrication of CuNPs-APDC-MWCNTs-β-CD nanocomposite for NTM analysis

Synthesis of ammonium piperidine dithiocarbamate (APDC) was carried out as previously reported [Kanchi et al., 2014]. CuNPs were prepared from the previously reported methods [Kobayashi et al., 2013], briefly 0.5 mM of hydrazine was added to the aqueous solution of 0.5 mM of copper sulphate followed by drop by drop addition of ascorbic acid under vigorous stirring at room temperature under nitrogen gas bubbling about 30 min. Then this solution was left 3 h under continueous stirring results in the dark red colour solution, indicates formation of CuNPs. The preparation of functionalized CuNPs was prepared as follows: To the prepared CuNPs solution, aqueous NaOH was used to control the pH and this solution was heated for 30 min at 85 ^{0}C. Then 20 mL of 0.5 M APDC was introduced slowly into the solution with rapid stirring; the solution was further boiled for 30 min and then cooled to room temperature. In this process, the brick red colloidal solution finally changes to a pale yellow colour. The APDC capped CuNPs was separated by filtration and washed with deionised water followed by vacuum drying. Finally, a paste of MWCNTs was prepared by adding 0.3 g of MWCNTs to 3.0 mL of 0.1 mM β-CD solution followed by the addition of 0.1 g of APDC capped CuNPs powder. The resulting mixture was ultrasonicated for 30 min at 60 ^{0}C until a black dispersion of CuNPs-APDC-MWCNTs-β-CD was obtained [Noviandri and Rakhmana, 2012].

A bare GCE was manually polished carefully to a mirror like finish with ≤ 3 μm alumina slurry and then rinsed with distilled water followed by electrochemical cleaning by cycling at a potential range of 0.0 – 1.0 V for 30 cycles in acidified distilled water. This process enabled the removal of any physisorbed or chemisorbed materials from the electrode surface. Thereafter, the GCE was

coated by careful addition of 6µL of nanocomposite and oven dried at 50 ^{0}C for 15 min. After cooling to room temperature, the modified electrode was ready for use.

4.2.4.2 Preparation and fabrication of Cyt c/ AuNPs- GO/ MWCNTs nanobiocomposite for analysis of Reb A

The AuNPs in aqueous system was prepared in a 100 mL flat bottom flask. Approximately 50 mL of 0.01% $HAuCl_4$ solution was boiled with vigorous stirring and 50 mM ascorbic acid was added drop wise until a colour change from pale yellow to blue. The colour change persisted until a red–violet appeared in about 60 s. Solutions were allowed to boil while stirring for another 10 min. AuNPs decorated GO was prepared as: 1 mL of GO was dissolved in 10 mL of deionized water and to this solution 5 mL of previously prepared AuNPs solution was added and subjected to ultrasonication for 1 h to get AuNPs-GO material. To prepare MWCNTs/Au NPs-GO nano composite, MWCNTs was added to the 5 ml of AuNPs-GO solution and sonicated for 45 min to produce a homogenous dispersion of MWCNTs/Au NPs-GO [Cheemalapati et al., 2013]. Finally, the obtained MWCNTs/AuNPs-GO dispersion was centrifuged at 3000 rpm to separate loosely bound MWCNTs and washed several times with deionized water. The resulted black dispersion was used for the fabrication of GCE. Cytochrome c (from horse heart) solution was prepared as, 0.01 g of Cyt c dissolved with 0.1 M borate buffer in 10 ml volumetric flask.

For fabrication, a bare Pt electrode was manually polished carefully to a mirror like surface with ≤ 3 µm alumina slurry and then rinsed with distilled water followed by electrochemical cleaning procedure with cycling at a potential range of -0.4 – 1.0 V for 30 cycles in distilled water with 3 to 5 drops of concentrated nitric acid. This process enabled the removal of any physisorbed or

chemisorbed materials from the electrode surface. Thereafter, the Pt electrode was coated with 6 µL of prepared AuNPs-GO/MWCNTs material by dropping carefully onto the widely spread tip of the electrode and allowed to dry in room temperature for 12 h to form an AuNPs-GO/MWCNTs/GCE. Then the modified electrode was dipped in Cyt c solution for another 6 h at 4 ^{0}C to adsorb Cyt c on to the coated layers, as a result fully fabricated (Cyt c/AuNPs-GO/MWCNTs/) Pt was created.

4.2.4.3 Preparation and fabrication of Graphene oxide- *p*-aminothiophenol-ZnO NPs-Laccase nanobiocomposite for analysis of SUC

The method for the synthesis of ZnO NPs was adapted from previously reported method [Sharma et al., 2011]. Briefly 50 mL of $ZnSO_4 \cdot 7H_2O$ and 50 mL of NaOH in 1:4 molar ratio was mixed instantly and the resulted mixture was stirred continuously for 15 min. The white product obtained was washed with deionized water and dried at 40 ^{0}C in an oven for 4 h. Aminothio phenol-graphene oxide (ATP-GO) mixture was prepared as: 3 mL of GO was dissolved in 5 mL of ethanol: water (50:50%) with the aid of ultrasonic agitation for 1 h, resulting in a homogeneous black suspension. To ensure the surface activation of carboxylate groups of GO, the GO suspension was interacted with 0.2 M 1-Ethyl-3-(3-dimethylaminopropyl) carbodiimide (EDC) solution for 8 h [Yola et al., 2013]. The activated GO suspension was well mixed with 1.0 mM ATP at a 1:1 volume ratio for 2 h (ATP-GO). Finally, the self-assembly of prepared ZnO NPs to ATP-GO was as follows: the aqueous dispersion of ZnO NPs (1 mg/ mL) was mixed with the aqueous dispersion of ATP-GO sheets (0.1 mg/ mL) at a 1:1 volume ratio and sonicated for 15 min to form a homogeneous mixture (ZnO NPs–ATPGO). The mixture was then kept undisturbed

under ambient condition for12 h. The resulted pale yellowish color dispersion was used for the fabrication of GCE.

For immobilization of laccase/TEMPO on ZnO NPs–ATP-GO composite, a bare GCE was manually polished carefully to a mirror like surface with ≤ 3 μm alumina slurry and then rinsed with distilled water followed by electrochemical cleaning procedure with cycling at a potential range of -0.4 – 1.0 V for 30 cycles in distilled water with 3 to 5 drops of concentrated nitric acid to remove any physisorbed or chemisorbed materials from the electrode surface. Thereafter, the GCE was coated with 6 μL of prepared ZnO NPs–ATP-GO material by dropping carefully onto the widely spread tip of the electrode and allowed to dry in oven at 50 ^{0}C for 10 min to form an ZnO NPs-ATP-GO/GCE. Thereafter the modified electrode was dipped in laccase/TEMPO solution for 6 h at 4 ^{0}C to adsorb laccase on to the coated layers, as a result fully fabricated (Laccase/ ZnO NPs-ATP-GO/) GCE was created.

4.2.5 Procedure for the electrochemical measurements with biosensors

Approximately 10 mL of the phosphate/borate buffer was introduced into the electrochemical cell in which either bare or fabricated working electrode (GCE or Pt or Au) were immersed prior to electrochemical measurements. Several cyclic sweeps were applied until a low background current was achieved. An aliquot of the analyte solution was then introduced into the electrochemical cell, and a pre-concentration potential was applied to the working electrode while the solution was stirred at 400 rpm. At the end of the pre-concentration time, stirring was stopped and a 5 s equilibration period was allowed for the solution to become inert. The voltammograms were then recorded using the bare or the modified working electrode by scanning the potential towards the positive direction using differential pulse or linear sweep potential at a scanning rate

of 0.1 V/s. Following each measurement, the working electrode was removed from the system and rinsed with deionized water.

Isothermal titration calorimetric measurements were carried out at 25 ^{0}C as follows; 2 mM of different metal solutions titrand (Ni^{2+}, Cu^{2+} and Zn^{2+}) were placed in a cell containing the phosphate buffer at pH 5.5. 2 mM NTM (titrant) was added to the titrand by an automatic titration. For a typical experiment 10 µL of the titrant were added to the cell solution to achieve complete equilibration with intervals of 240 s between injections with stirring speeds of 300 revolutions per min. The net reaction heat value measured by the injection of the titrant to the buffer solution was subtracted from each titration to obtain the heat of dilution.

4.3 Computational modelling

Material studio 5.0 (Accelrys) and Gauss View programs were used for the construction and minimization of ligands. The docking calculations were performed using Discovery studio 3.0 (Accelrys). Density functional theory (DFT) calculations for molecular structures of ligand and metal-ligand complexes were performed at B3LYP/6-31g** and LANL2DZ level using Gaussian 09.

4.3.1 Docking procedure

In this study, docking calculations were performed to calculate the binding energies of inclusion complexes of heptakis 2,3,6- tri-o-methyl betacyclodextrin (TM-β-CD) and steviol glycosides/neotame diastereomers. The obtained results were applied to explain the observed elution order in capillary electrophoresis.

Major steps in molecular docking

Step I – Building the Receptor

In this study heptakis 2,3,6- tri-o-methyl betacyclodextrin (TM-β-CD), Cytochrome c (Cyt c) and laccase were considered as docking receptors. Due to the absence of the X-ray structure for TM-β-CD the atomic coordinates of β-cyclodextrin_hemolysin complex crystal (pdb id: 3M3R) were retrieved from the protein data bank [Banerjee et al., 2010] and were used as a reference to construct the 3D structure of TM-β-CD. The crystal structure of Cyt c (pdb id: 3cyt) [Takano and Dickerson, 1980] and Lac (pdb id: 3cg8) [Skálová et al., 2009] were retrieved from the protein data bank (http://www.rcsb.org). The water molecules and native ligand were removed and single chain was selected. The protein was protonated at physiological pH using the Prepare Protein Algorithm in DS, and minimized using the Conjugate gradient algorithm.

Step II – Identification of the active site

After the receptor is built, the active site within the receptor should be identified. The receptor may have many active sites but the one site of the interest should be selected. Most of the water molecules and heteroatom if present should be removed. Prior to docking, a binding sphere of dimensions 30.4, 32.5 and 21.0 Å covering the whole TM-β-CD and a binding sphere covering all the active site residues in Cyt c with dimensions of 42.774, 26.591 and7.72 Å and Lac with dimensoions of 56.34, 31.42, 11.35 Å were created using the Define and Edit Binding Site modules in discovery studio (DS).

Step III – Ligand preparation

Ligands can be obtained from various databases like ZINC, PubChem or can be sketched using tools Chemsketch or Material Studio. The Molecular Mechanics Force Field (MMFF) was used for the development of partial atomic charges. The unreasonable bond distances and angles of both ligands which are steviol glycosides (Stv and Reb A) and neotame distereomers (L,L and D,D) were adjusted by optimization process using the Forcite module in Materials Studio (MS) [Accelrys, 2006]. The ionic states of steviol glycoside ligands were determined at pH 8.0 and three different ionic states (zwitterions, anion and cation) of both neotame diastereomers were predicted using the "Prepare Ligands" module followed by a conformational search. Conformations modules in DS [Wu et al., 2003] resulted in 40, 22 conformations generated for Stv and Reb A, 38, 46 conformations generated for L,L and D,D neotame and 18 conformations for sucralose respectively. The lowest energy conformation for each ligand was further used for docking simulations.

Step IV- Docking

Here the ligand is docked onto the receptor and the interactions are checked. The scoring function generates score depending on which the best fit ligand is selected. Different ligand conformations were generated using Molecular Dynamics (MD) method and were refined further by grid-based (GRID 1) simulated annealing and a final grid-based minimization. The best docked poses showing efficient host-guest interactions were identified on the basis of the CDOCKER energy (CDE) and CDOCKER interaction energy scoring functions. The higher negative value of binding energy (BE) indicates a stronger binding and therefore, a more favorable binding of the

steviol glycosides and neotame diastereomers to TM-β-CD as well as Reb A with Cyt c and sucralose with laccase.

4.3.2 Methodology for HOMO-LUMO and DFT calculations

For sucralose and amine-sucralose complexes HOMO-LUMO calculations and for NTM, NTM-metal complexes DFT calculations were performed to get a deeper understanding of their structural and thermochemical features and to correlate them with the experimental results. The Gaussian 09 program was used for all calculations [Frisch et al., 2009].

(i) Preparation of input

The first step for Gaussian calculations is preparation of Gaussian input file which can be generated directly using gauss view or any pdb structure can convert to Gaussian input file. The initial structures of neotame, neotame-metal complexes, sucralose and its amine derivatives were modelled using the Gauss View program [Nielsen and Holder, 2003].

(ii) Submission of jobs

After generating the input file, based on type of calculations we need to do select particular type of calculation with significant basis set. Here, full geometry optimization with frequency calculations were performed at DFT level using the Becke3 Lee et al [Lee et al., 1988] (B3LYP) functional with 6-31g** basis sets for all studied structures. For better results, in case of neotame-metal complexes mixed basis sets were used than 6-31g**. Moreover, the vibrational analysis was also performed to verify the ground state energy minima of all structures.

(iii) Analysis of output file

The results from the above calculations give an output file with the extension of **.out,** which can be used to calculate the energies and spectroscopic details for neotame and neotame-metal complexes. The molecular orbitals were generated using **.fchk** file in case of sucralose and sucralose-amine complexes and similar procedure was adopted for Reb A molecule.

CHAPTER 5

RESULTS AND DISCUSSION

PART ONE

Micro separation of steviol glycosides, neotame and sucralose

In this chapter, the results obtained from the separation of analytes with capillary electrophoresis and supported computational works are discussed. This chapter is divided into three sections: analytical evaluation of steviol glycosides by capillary electrophoresis supported with molecular docking studies; chiral separation of neotame diastereomers using β-cyclodextrin as a chiral selector and electrophoretic analysis of sucralose in food samples using amines as background electrolyte. Computational work was carried out to get a better understanding of the conformational profile of the inclusion complexes between TM-β-CD and steviol glycosides/ neotame diastereomers. Furthermore, the interaction studies were helpful to validate the elution order observed in capillary electrophoresis. Separation of sucralose with amine buffers was further investigated computationally using HOMO-LUMO calculations.

5.1 Analytical evaluation of steviol glycosides by capillary electrophoresis supported with molecular docking studies

The separation of steviol glycosides is mainly based on the interaction and degree of complex formation with TM-β-CD. The complex formation depends on the type of injection mode used and consequently it affects the net migration velocity and resolution. If the separating agent was directly bound to the capillary surface as a modifier, then the net velocity of the complex would be zero, but if the separating agent was directly added to the buffer, then the net velocity of

the complex would not be zero. Accordingly, three different modes of injection were employed for a better understanding of the interaction of the analytes with TM-β-CD. In first mode, the analytes were injected followed by the separating agent. While in the second mode, the separating agent was injected before the analytes. Finally, in the third mode, the analytes were sandwiched by the separating agents. Results from this study revealed that no separation was achieved in the first mode, due to the higher mobilities of the analytes; hence there were insufficient interaction between the analytes and the separating agent. However, in the second mode, the EOF of the analytes was blocked by the slow moving TM-β-CD leading to some interaction and separation being observed. The weaker hydrophobic interactions between Reb A and TM-β-CD resulted in a less stable complex, whereas Stv formed a more stable complex with TM-β-CD, due to the stronger hydrophobic interactions with the two hydrogen bonds, as confirmed by the molecular docking calculations. Hence, the less stable Reb A-(TM-β-CD) complex with a high EOF and velocity eluted first than Stv-(TM-β-CD) complex. On the other hand, LL-neotame forms less stable complex with TM-β-CD with two hydrogen bonds eluted first than stable DD-neotame-(TM-β-CD) complex. While in the third mode, the hydrophobic interactions between the analytes and the hydrophobic cavity of TM-β-CD were very high due to the presence of TM-β-CD on either side of the analyte (sandwich). Therefore, the resulting complexes were more stable, with longer migration times than the corresponding complexes formed in the second method, but with a similar elution order observed. For this purpose, the second mode was selected for separation of steviol glycosides with better resolution and migration times.

In the partial filling method, capillary is partially filled with the separation solution containing a protein or cyclodextrin as a chiral selector forming a separation zone. The formed separation zone does not reach the detection cell and a sample solution is introduced at the end of the capillary

filled with the separation solution. Finally the injection end is dipped into the running buffer followed by the application of a high voltage. But in the present work simple and efficient method has been adopted which involves the addition of separating agent directly to the BGE to increase the solubility of cyclodextrin. The main advantage of this method is due to the presence of separating agent in buffer it can't escape from the analyte molecules and shows absolute interactions [Conradi et al., 1997; Wang and Ren, 2004; Raczi et al., 2011; Mayer and Schurig, 1994].

Separation mechanism of steviol glycosides

Steviol glycosides are diterpenoids with an aglycone molecule attached to sugar moieties such as glucose and rhamnose which are water soluble. The steviol glycosides can carry a negative charge and form anions in water because of the dissociation of their ester groups [Lovric et al., 2010; Pavlova et al., 2004]. But the separation of steviol glycosides using methylated beta cyclodextrin is mainly depends on the hydrophilic and hydrophobic interactions between hydrogen atoms in cyclodextrin and negatively charged oxygens in analytes. At pH greater than 8.0 the deprotonation capacity of hydroxyl groups were predominant in steviol glycosides results in with increased migration times. Because the electrophoretic migration of the analytes is in a direction counter to the electroosmotic flow. With increase in buffer pH significantly reduces the net migration velocities (towards the cathode) of steviol glycosides. The number of dissociation of hydroxyl groups increases at higher pH values (9.0 to 10.0) with decreasing electroosmotic flow leading to a lower net migration velocity [Kuo et al., 1998; Moreno et al., 2014]. In addition high number of the dissociated hydroxyl groups in steviol glycosides interacts strongly with beta cyclodextrin at higher pHs results in lower migration times [Aturki et al., 2003].

The ionization of analytes can be achieved at a pH that is at least two units above or below the pKa of the analytes [Henk, H. L., and P. R. Gerard, 2010]. In fact the pKa values for the natural glycosides are 9-10 and gives more negatively charged groups at high pHs with longer migration times [Aturki et al., 2003]. Hence in this work one unit below than their pKa values which is pH 8.0 was used with high increase in EOF and migration velocity to achieve shorter migration times.Mauri et al., separated two major steviol glycosides (Reb A and Stv) at pH 8.30 using MEKC method. Hence in this work pH 8.0 was used as the optimum pH for the separation of steviol glycosides. Further the separation mechanism was supported by the docking simulations, it is believed that the more folded docked conformation of Stv brought the hydroxyl groups (-OH) in the vicinity of the side chains of the TM-β-CD and facilitated the hydrogen bonded interactions between them. The conformation of Reb A on the other hand, was comparatively extended and simply penetrated through the cavity of the TM-β-CD. Thus, the proton acceptor/donor sites of Reb A were not close enough to form hydrogen bonds with the cyclodextrin. Finally, the computed CDOCKER energies of Stv (-278.4) was lower than Reb A (-253.8) at pH 8.0, thus confirming the stronger interaction of the former with TM-β-CD than the later. At pH 9.0 the calculated CDOCKER energies of Stv (-263.7) and Reb A (-248.1) were lower than the values at pH 8.0 with same elution order showing the stronger interaction with cyclodextrin.

In this work methanol was used as the EOF marker and the indisputable peaks were shown in below Figure 5.1 (i). The EOF peak was observed at 2.5 min and the electropherograms for steviol glycosides at different concentrations were shown in attached Figure 5.1 (ii-v). As the concentration of the Reb A and Stv increases the peak absorbance increases with correlation coefficient of 0.99 and 0.98.

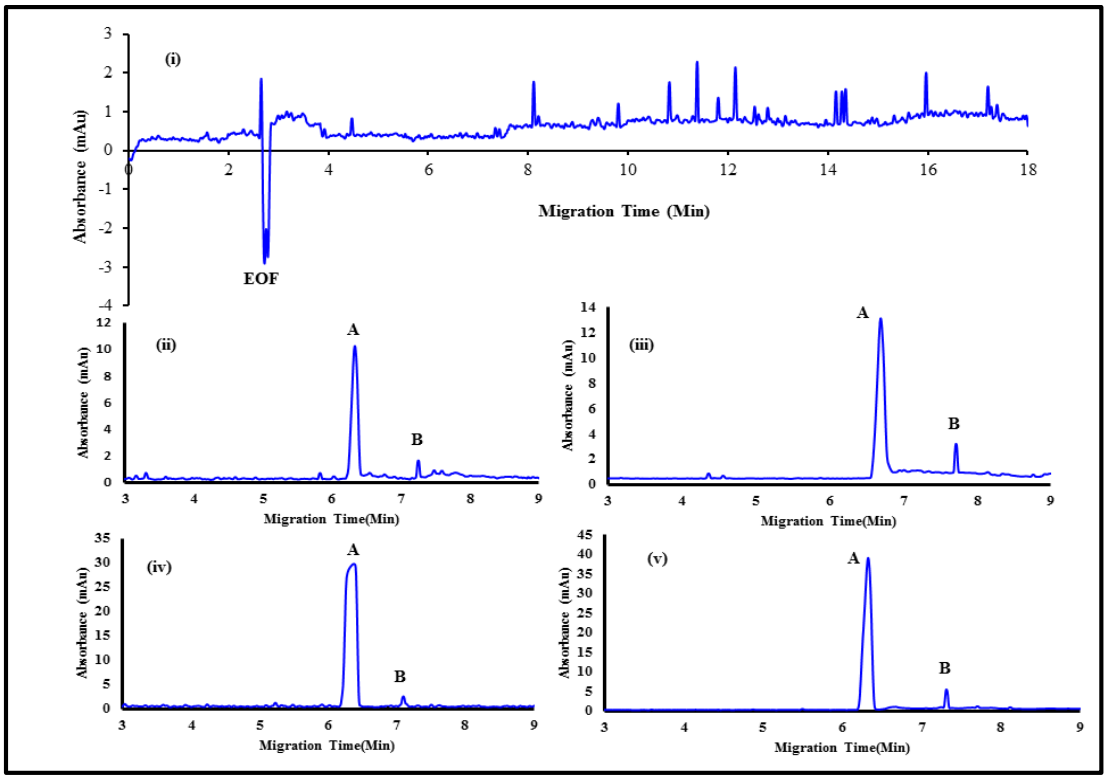

Figure 5.1: The electropherograms for (i) EOF marker methanol and steviol glycosides (A) Rebaudioside A (B) Stevioside at different concentrations (i) 1 mM (ii) 2 mM (iii) 3 mM (iv) 4 mM

For the purpose of this study, the degradant products such as steviol was not considered in contast to those reported in literature [Woelwer-Rieck et al., 2010].

5.1.1 Optimization of separation conditions

5.1.1.1 Effect of pH on resolution and absorbance

The pH of the running buffer plays a pivotal role in the separation mechanism because it affects the EOF, zeta (ζ) potential and the overall charge of the analytes [Chen et al., 2001]. Accordingly, in this study, the influence of pH ranging from 3.0 to 10.0 (using a 50 mM phosphate buffer) on the migration times and resolution of Reb A and Stv were investigated. Poor resolution and longer migration times with a noisy baseline were observed at pH values ranging from 3.0 to

3.9 whereas good resolutions on the peaks were observed at pH 4.0. A further increase in pH from 4.0to 8.0 resulted in shorter migration times, greater absorbances and good resolution between Reb A and Stv. At higher pH values, the deprotonation of the hydroxyl groups were favored [Chen et al., 2001, Peng et al., 2005], as it promotes the complex formation between the negatively charged oxygen atoms in steviol glycosides with the hydrogen atoms in TM-β-CD, resulting in better resolution and absorbances as shown in Figure 5.2a-b.

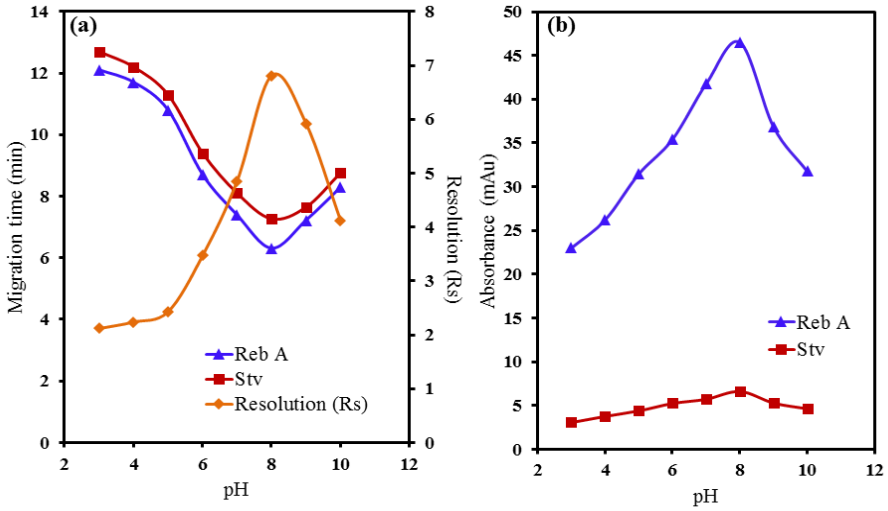

Figure 5.2: (a) Effect of buffer pH (b) absorbance on migration time and resolution (Conditions: 50 mM phosphate buffer, 30 mM TM-β-CD, 18 kV applied voltage, 30 ^{0}C temperature, 200 nm wavelength)

However, no significant differences were observed at pH > 8.0 in resolution capacities and migration times. Consequently, 50 mM phosphate buffer at pH 8.0 was selected as the running buffer in this study.

To have the best sensitivity, steviol glycosides were analysed at a shortest possible wavelength of 200 nm [Jaitak et al., 2008; Liu and Li, 1995]. At this wavelength the significant peak differences were observed between Reb A and Stv due to the variation in their molar masses. The molecular

weights of Reb A and Stv are 967.03 and 804.88, hence the aborbance of analytes will change with the amount used for analysis. In addition the calculated molar absorptivity values for Reb A and Stv were 278.4 and 38.6 $cm^{-1}g^{-1}$ using Beer's law shows the significant absorption capacities [Lauer and Rozing, 2010].

$$\mathbf{A = b\ C\ \varepsilon}$$

Where b= optical path length,

C= concentration

ε= molar absorptivity

The peak absorbance mainly depends on the pH of the running buffer, as the pH of the running buffer increases the dissociation of hydroxyl groups increases results in the increase in peak absorbance.

5.1.1.2 Effect of buffer concentration

The viscosity coefficient of the solution, diffusion coefficient of the analytes and the zeta (ζ) potential of the inner surface of the capillary are mainly dependent on the concentration of running buffer which in turn affects the peak resolution, migration time and the absorbance of the analytes. Accordingly in this experiment, different concentrations of the buffer ranging from 20 to 100 mM were examined on the resolution of Reb A and Stv.

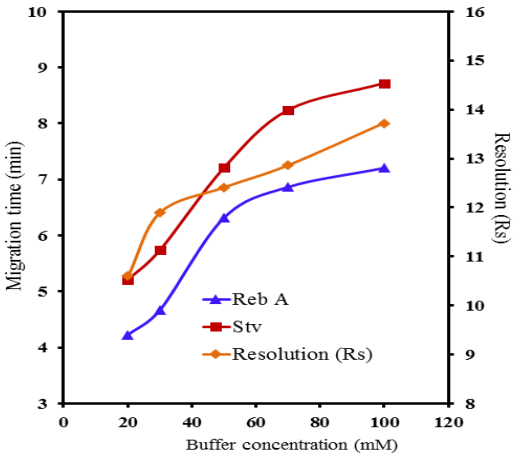

Figure 5.3: Effect of buffer concentration on migration time and resolution (Conditions:30 mM TM-β-CD with pH 8.0, 18 kV applied voltage, 30 ^{0}C temperature, 200 nm wavelength)

Figure 5.3 shows the influence of the buffer concentration on the resolution and migration time of Reb A and Stv. At low concentrations (<50 mM of phosphate buffer), low instrumental currents were observed at an applied voltage of approximately 18 kV. However, at higher concentrations of phosphate buffer (>50 mM), joule heating becomes more pronounced resulting in a negative effect on the LOD values. The maximum resolution values were obtained with a 50 mM phosphate buffer at pH 8.0 and therefore chosen as the running buffer for further studies.

5.1.1.3 Effect of applied voltage

The applied voltage mainly affects the resolution, migration time and the peak shapes of the analytes. Shorter migration times with a good resolution between analytes were observed with higher voltages and EOF's as shown in Figure 5.4.

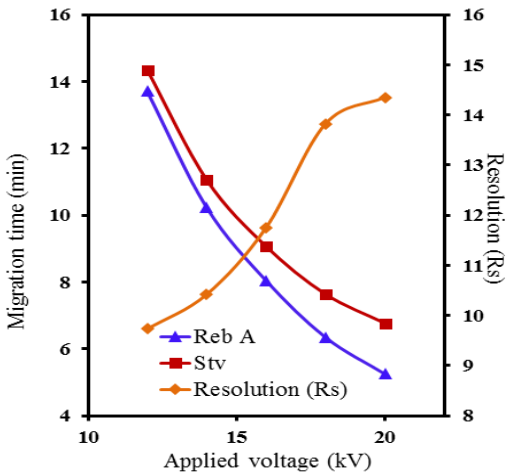

Figure 5.4: Effect of separation voltage on migration time and resolution (Conditions: 50 mM phosphate buffer, 30 mM TM-β-CD with pH 8.0, 30 ^{0}C temperature, 200 nm wavelength)

However, higher voltages are not preferred due to the increased joule heating generated from the capillary walls. Therefore in this study, the effect of the applied voltages ranging from 12 to 20 kV were examined. Application of a higher voltage (20 kV) resulted in a noisy baseline with a maximum peak resolution and poor detection limits. On the other hand, the use of a lower voltage (12 kV) resulted in better baseline resolved peaks, but with longer migration times. Consequently the optimum voltage for this analysis was chosen at 18 kV.

5.1.1.4 Effect of cassette temperature

In this study, the effect of cassette temperature ranging from 20 to 40 ^{0}C on the baseline resolution was examined. As the capillary temperature increased the viscosity of the buffer decreased and the EOF of the buffer increased, resulting in shorter migration times but with good resolutions achieved. As a consequence of this, the optimum temperature of 30 ^{0}C was selected to sustain a baseline resolution with a shorter migration time and good peak shapes for both Reb A and Stv [Figure 5.5].

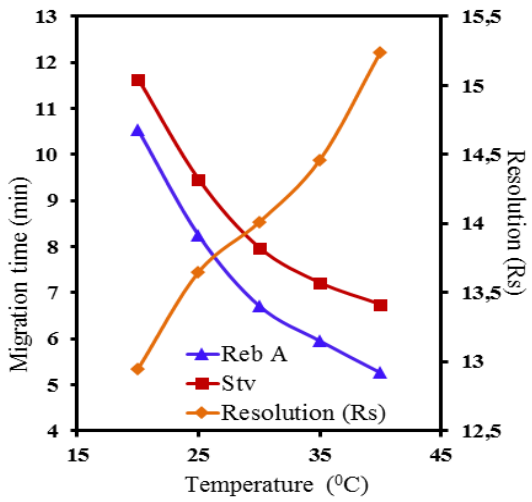

Figure 5.5: Effect of cassette temperature on migration time and resolution (Conditions: 50 mM phosphate buffer, 30 mM TM-β-CD with pH 8.0, 18 kV applied voltage, 200 nm wavelength)

5.1.1.5 Effect of sample injection time

The effect of sample volume on the separation of Reb A and Stv was studied by changing the injection times ranging from 2 to 10 s. It was observed that the resolution between the two peaks decreased while the migration times of the two analytes increased with an increase in injection times of the samples. Increasing the injection time beyond 4 s resulted in a peak broadening, hence lowering of the resolution between the two peaks. Therefore, 4 s was selected as an optimum injection time to enhance the separation of Reb A and Stv [Figure 5.6].

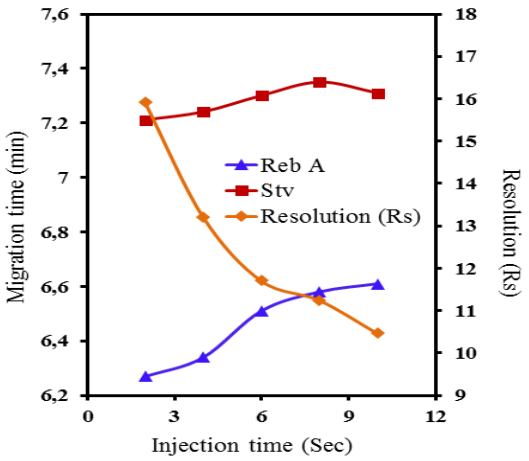

Figure 5.6: Effect of injection time of sample on migration time and resolution (Conditions: 50mM phosphate buffer, 30 mM TM-β-CD with pH 8.0, 18 kV applied voltage, 30 ^{0}C temperature, 200 nm wavelength)

5.1.1.6 Effect of concentration of TM-β-CD

Figure 5.7 shows the influence of the concentration of TM-β-CD ranging from 5 to 50 mM. The separation of steviol glycosides with and without TM-β-CD are depicted in Figure 5.8 a-b respectively. Clearly, the migration times and the resolution between Reb A and Stv reached a maximum value at a concentration of 30 mM and for this reason 30 mM of TM-β-CD was chosen as the optimum concentration.

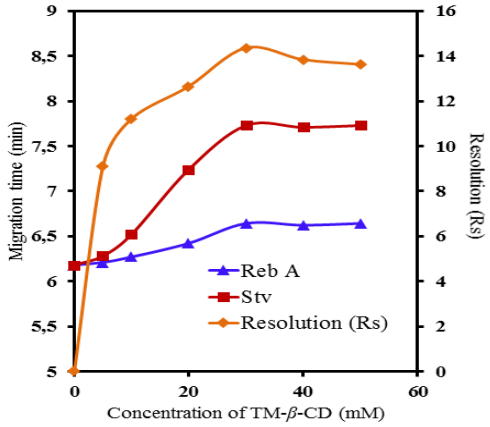

Figure 5.7: Effect of concentration of TM-β-CD on migration time and resolution of compounds (Conditions: 50 mM phosphate buffer with pH 8.0, 18 kV applied voltage, 30 ^{0}C temperature, 200 nm wavelength)

5.1.2 Repeatability and reproducibility

Repeatability and reproducibility in terms of the relative standard deviation of this method were studied on three types of stevia real samples described above. The reproducibility mainly depends on the dissociation of the silanol groups present on the inner walls of the capillary. To achieve a good reproducibility between the consecutive runs, the capillary was equilibrated. For this purpose, the capillary was flushed sequentially with deionized water for 2 min, 1 M NaOH for 2 min to refresh the silanol groups, and finally with the separation buffer for 2 min. Repeatability was evaluated by performing five replicates with the pH 8.0 buffer solution resulting in the percentage relative standard deviations (%RSD n = 5) of ±1.13 and±1.43 % for migration time and 0.94 and 1.38 % for peak area as shown in Figure 5.8.

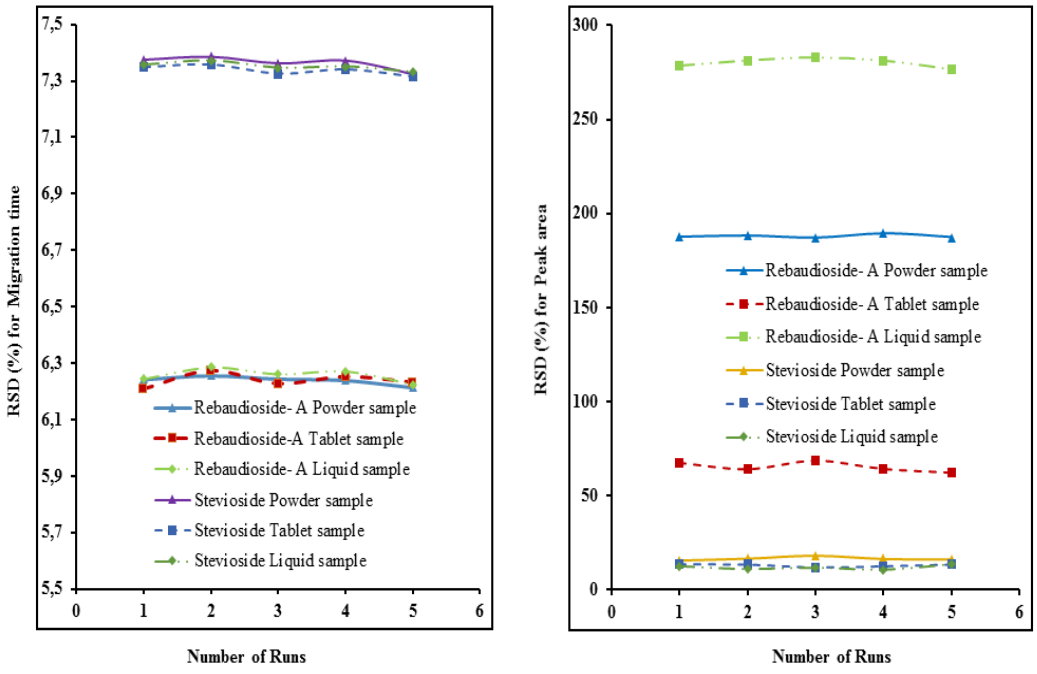

Figure 5.8: Reproducibility for the separation of steviol glycosides in real stevia samples showing (a) migration time (b) peak area (Conditions: 50 mM phosphate buffer, 30 mM TM-β-CD with pH 8.0, 18 kV applied voltage, 30 ^{0}C temperature, 200 nm wavelength

5.1.3 Calibration curve and detection limit

For calibration studies, 98 % of Reb A and Stv standards were used with different concentrations ranging from 1 to 5 mM. The detection limits were calculated using individual standards at the following optimum conditions: 50 mM phosphate buffer, 30 mM TM-β-CD with pH 8.0, 18 kV applied voltage, 30 ^{0}C cassette temperature and 4 s of sample injection. From the calibration plots, the analytical figures of merit for the separation of Reb A and Stv are represented in Table 5.1.

Table 5.1: Analytical figures of merit for the separation of RebA and Stv

Sample	*y=a+bx*	Correlation coefficient	LOD (M)	LOQ (M)
Reb A	y = 12669x + 27.05	0.9935	2.017×10^{-5}	6.114×10^{-5}
Stv	y = 4079.6x - 16.46	0.9850	7.386×10^{-5}	2.2881×10^{-4}

Regression equation (*y=a + bx)* where y is the peak areas of Reb A and Stv and *x* is the concentration in mM, r= correlation coefficient.
LOD's and LOQ's are calculated according to signal to noise ratio *S/N*=3 and *S/N*=10 respectively

5.1.4 Interference studies

To test the selectivity of the developed method, the effect of foreign species were performed in this study. According to the manufacturer's label, the tablet, liquid and powder samples contain lactose, fructose, citric acid, sorbic acid, natural flavors, colorants, wheat and gluten along with steviol glycosides. To discriminate the interferences from other foreign species, the dilution method was adapted to determine the optimum dilution level that would minimize the amount of fructose, lactose, citric acid, sorbic acid in the capillary, while maintaining a measurable amount of steviol glycosides. The following dilutions: 2-, 10-, 50-,100-, 500- and 1,000-fold were tested. A 100-fold dilution was optimized to measure steviol glycosides for all the studied real samples without any interference.

5.1.5 Analytical applications

The developed method worked well under laboratory conditions and was successfully applied to Reb A and Stv with no significant separation observed in the absence of the separating agent (TM-β-CD) [Figure 5.9]. To evaluate the accuracy of the developed method, real stevia samples in tablet, powder and liquid forms as described in the chapter 4 under section 4.1.3 were purchased and analyzed. The obtained electropherograms for the real samples are shown in Figure 5.10. The percentages of Reb A and Stv ranged from 92.78 to 99.08 % and 84.57 to 98.13 %while their % RSD was 1.10 and 1.17 %, respectively, are depicted in Tables 5.2 and 5.3.

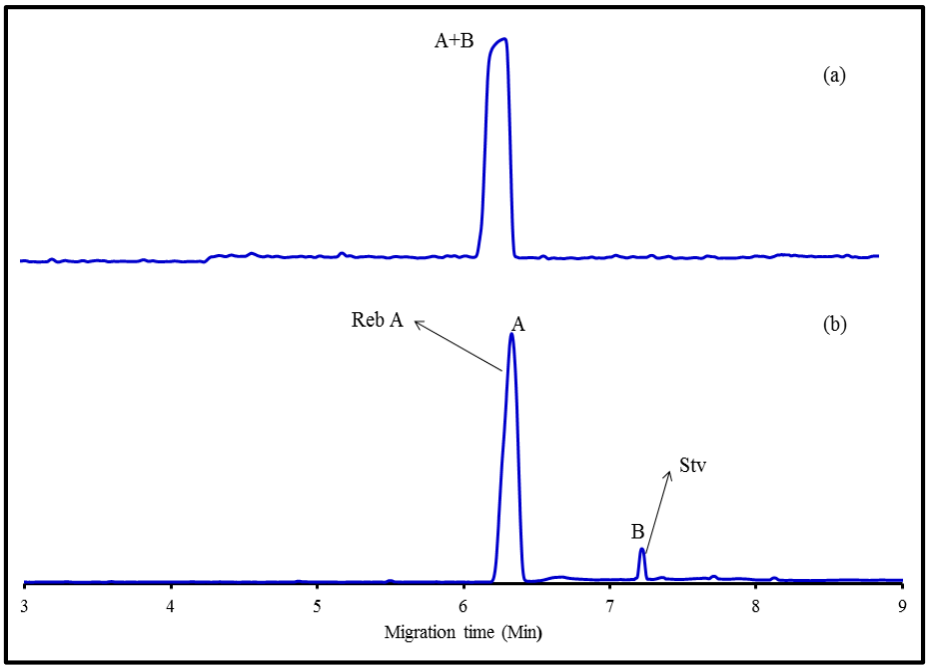

Figure 5.9: Electropherograms showing the effect of TM-β-CD on the resolution of steviol glycosides (a) without TM-β-CD and (b) with TM-β-CD of (A) Reb A and (B) Stv (Conditions: 50 mM phosphate buffer, 30 mM TM-β-CD with pH 8.0, 18 kV applied voltage, 30 ^{0}C temperature, 200 nm wavelength)

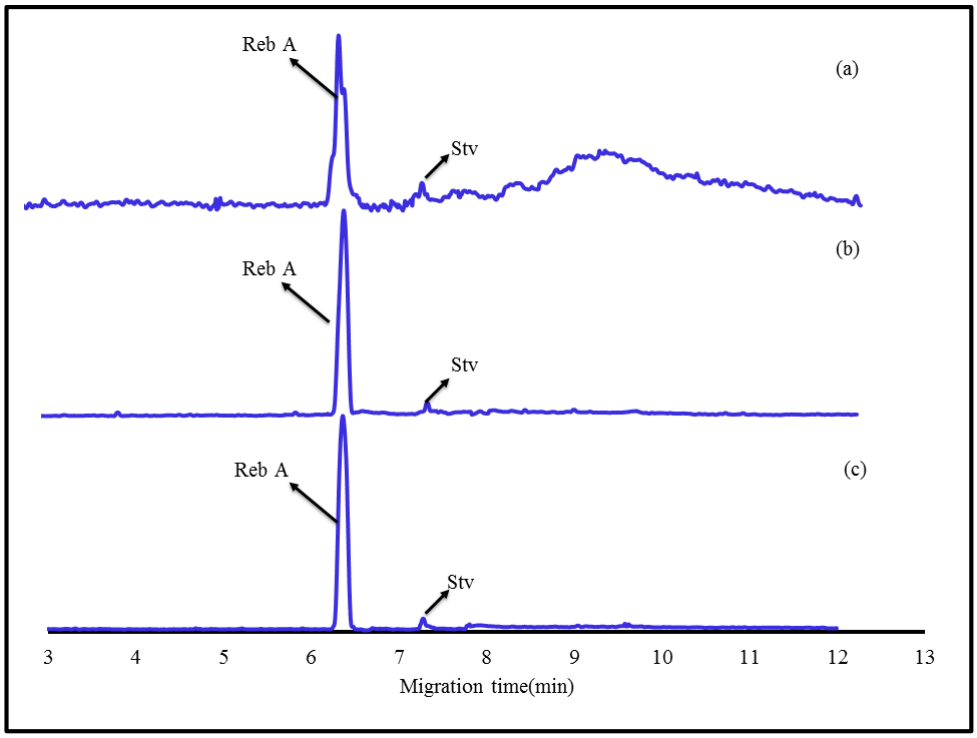

Figure 5.10: Electropherograms for Reb A and Stv in real samples (Conditions: 50 mM phosphate buffer, 30 mM TM-β-CD with pH 8.0, 18 kV applied voltage, 30 ^{0}C temperature, 200 nm wavelength)

Table 5.2: Analytical data for the determination of steviol glycosides from the spiked samples

Sample	Concentration added (mM)					
	1mM		2 mM		3 mM	
	Found	Recovery±RSD[a]	Found	Recovery±RSD[a]	Found	Recovery±RSD[a]
Reb A	0.00392	97.51±1.10	0.00746	92.78±1.32	0.01195	99.08±1.28
Stv	0.00384	95.52±1.25	0.00789	98.13±1.68	0.0102	84.57±1.17

[a]Relative standard deviation for five individual determinations

Table 5.3: Determination of Reb A and Stv in food samples

Sample	Available form	Active Ingredients	Stevia glycoside concentration (g)	RSD[d]
			Found	
Green Canderel[a]	Tablet	Reb A	0.0119	1.15
		Stv	0.0112	1.53
Stevia[b]	Powder	Reb A	0.0118	1.46
		Stv	0.0102	1.57
Tantalize[c]	Liquid	Reb A	0.0125	1.55
		Stv	0.0114	1.87

[a]Merisant Company 2, Sarl, Czech Republic,
[b]Dis-Chem Pty Ltd, South Africa,
[c]Delite Foods, South Africa
[d]Relative standard deviation for five individual determinations

5.1.6 Computational discussion

To get a deeper understanding of the host–guest interactions of Reb A and Stv with TM-β-CD, molecular docking simulations were performed using the CDOCKER module of Discovery Studio 3.1 [Wu et al., 2003]. The docked complexes of Reb A and Stv with TM-β-CD are diagrammatically depicted in Figure 5.11 a-b, respectively. In contrast, a closer inspection of Figure 5.10reveals that both ligands (Reb A and Stv) penetrated the cavity of the TM-β-CD, thereby stabilizing their geometries, probably due to the hydrophobic interactions between their aliphatic functional groups and the hydrophobic cavity of the TM-β-CD ring. Apart from these hydrophobic interactions, two additional hydrogen bonds between the hydroxyl (–OH) groups and the oxygen atoms of the glucopyranose rings were observed in the case of Stv [Figure 5.11 b; Table 5.4], which accounts for their strongerinteraction with the TM-β-CD than the Reb A [Figure 5.11 a] as evidenced by its lower CDOCKER energy (CDEscore = -278.4). Moreover, it is believed that the more folded docked conformation of Stv [Figure 5.11b] brought the hydroxyl groups (-

OH) in the vicinity of the side chains of the TM-β-CD and facilitated the hydrogen-bonded interactions between them. The conformation of Reb A [Figure 5.11a] on the other hand, was comparatively extended and simply penetrated through the cavity of the TM-β-CD. Thus, the proton acceptor/donor sites of Reb A were not close enough to form hydrogen bonds with the cyclodextrin. Finally, the computed binding energy (energy of complex-energy of ligand-energy of TM-β-CD) of Stv was lower than Reb A, thus confirming the stronger interaction of the former with TM-β-CD than the later [Table 5.4]. Moreover, the lower migration times of Stv observed in our CE experiments can also be explained on the basis of its stronger interaction with TM-β-CD [Table 5.4], resulting in its slower movement towards the anodic end of the CE system compared to the Reb A–TM-β-CD complex, under the influence of EOF.

Table 5.4: Docking results of Stv and RebA with TM-β-CD using docking studies

Compound	CDocker Energy (CDE) score	Binding Energy ($kcalmol^{-1}$)	Migration Time(min) in CE	Number of H-bonds	H-Bond Distance (Å)
Stv	-278.4	-34.9	7.21	2	2.39, 2.35
Reb A	-175.4	-25.4	6.32	0	--

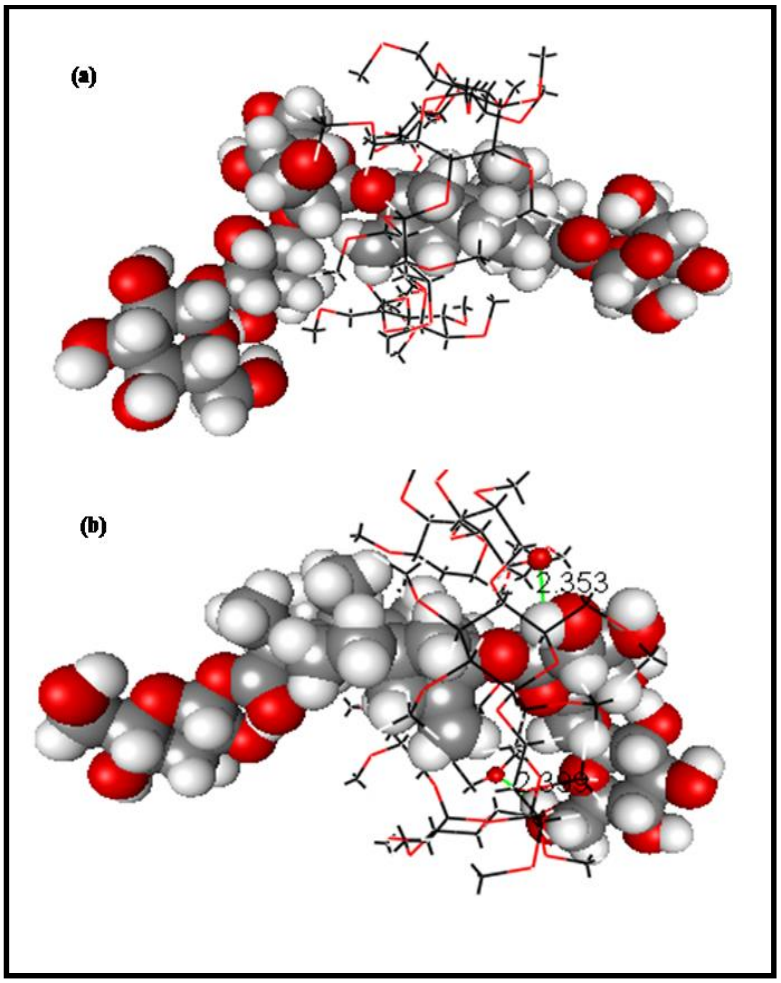

Figure 5.11: Docked conformation of (a) Reb A and (b) Stv with TM-β-CD. Both ligands are shown in CPK format, while the TM-β-CD is shown in line format. Oxygen atoms of TM-β-CD participating in hydrogen bonding are shown in ball format. Hydrogen bonds are presented in green

5.2 Chiral separation of neotame diastereomers using β-Cyclodextrin

5.2.1 Optimization of separation conditions

5.2.1.1 Effect of pH

The electro-osmatic flow (EOF), the zeta potential (ζ) and the charge of the analytes depends mainly on the acidity of the running buffer. The separation capacity and changes inmigration time and the resolution of the analytes also depends on the pH of the running buffer. In this work, the effect of pH on the migration times and the resolution of the analytes were investigatedusing 50 mM phosphate buffer at pH ranging from 3.0 to 8.5, and the results are depicted in Figure 5.12. Based on the *pKa* values (*pK1* 3.01 and *pK2* 8.02; isoelectric point 5.5) neotame (NTM) exhibits a cationic form due to the protonation of the amino groups below pH 3.01 [Nofre and Tinti, 2000]. At this pH the D,D-cationic form eluted later due to the higher stability complex (D,D-cat-TM-β-CD) compared to the corresponding L,L-cationic form. As the pH increased from 3.01 to 5.5, a gradual decrease in migration times were observed. At the isoelectric point (5.5) NTM exhibited a zwitterionic form with a (+ve) charge on the amino group and a (–ve) charge on the carboxyl group. The charged groups present in the L,L-zwitterionic form, resulted in a weak hydrophobic interactions or hydrogen bonds with the hydrophobic cavity of TM-β-CD, hence it eluted first in contrast to the D,D-zwitterionic form. At this pH, a baseline separationwas achieved with shorter migration times with respect to both the cationic and anionic forms.However, a further increase in pH from 5.5 to 8.5, resulted in the conversion of the zwitterionicform to the anionic form, due to deprotonation of the amino group. Furthermore, the gradualincrease in migration times were observed with an increase in pH due to an increase in the stability of the anionic NTM-TM-β-CD complex. Similar elution patterns were observed inthe two ionic forms described above. The L,L-anionic form eluted first due to thepresence of weaker

hydrogen bonds present in L,L-anionic-TM-β-CD complex, than the corresponding D,D-anionic complex. The effect of pH on the separation, resolution and the retention factors were also explored in this work. The separation and resolution factor values at pH 3, 5.5, and 8.5 were 1.15, 2.43, 1.39 and 4.88, 9.67, 8.12 respectively. These results suggest a maximum separation, resolution and peak absorbance were obtained at pH 5.5.

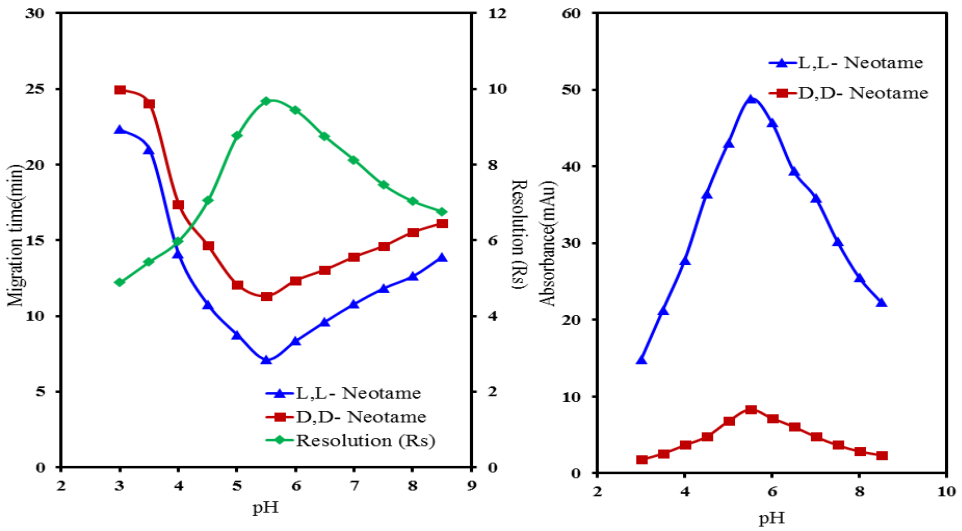

Figure 5.12: Effect of buffer pH on migration time and absorbance (Conditions:50 mM phosphate buffer, 30 mM TM-β-CD, 20 kV applied voltage, 30 ^{0}C temperature, 200 nm wavelength

5.2.1.2 Effect of buffer concentration

The viscosity coefficient of the solution, diffusion coefficient of analytes and the ζ - potential of the inner surface of the capillary tube were dependent on the concentration ofthe running buffer. In this work buffer concentrations ranging from 30 to 100 mM were examined in relation to the migration times and the resolution of analytes. The migration times and resolution of the analytes increased with increasing concentration of the running buffer as shown in Figure 5.13.

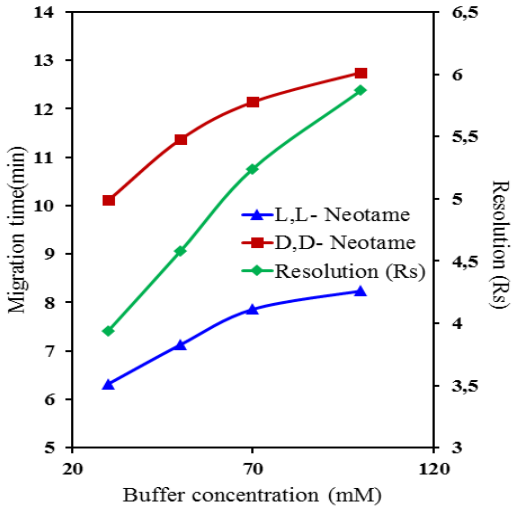

Figure 5.13: Effect of buffer concentration on migration time and resolution (Conditions:50 mM phosphate buffer, 30 mM TM-β-CD, 20 kV applied voltage, 30 ^{0}C temperature, 200 nm wavelength)

Low concentrations of the phosphate buffer (30 mM) resulted in low instrumental current (15-20 mA) at an applied voltage of 20 kV. While at higher concentrations (> 50 mM), the joule heating effect was more pronounced and thus decreased the peak area, resulting in negative effects on the LODvalues. The retention factors (k_1' and k_2') gradually increased from 0.533 to 1.999 with acorresponding decrease in separation factors from 2.729 to 1.999. The resolution factors alsoincreased from 3.97 to 5.87 with a corresponding increase in buffer concentrations. At lower concentrations, good resolutions were observed between two peaks with shorter migration times. Hence, 50 mM phosphate buffer at pH 5.5 was chosen as the running buffer for further studies.

5.2.1.3 Effect of applied voltage

In this work the effect of applied voltages on the resolution, migration times and separationfactors were investigated at voltages ranging from 14 to 22 kV. At higher voltages, the EOF of the mobile phase increased, and thus shorter migration times were obtained as shown in Figure 5.14.

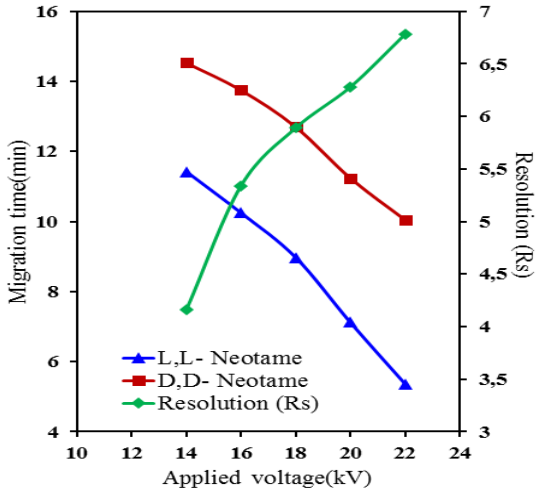

Figure 5.14: Effect of applied voltage on migration time and resolution (Conditions:50 mM phosphate buffer, 30 mM TM-β-CD, 20 kV applied voltage, 30 ^{0}C temperature, 200 nm wavelength)

To achieve stable baselines and appropriate peak shapes, the applied voltages were reduced from 22 to 14 kV. At lower voltages longer migration times were observed with satisfactory baseline separations. However, a careful consideration of migrationtimes, resolution and peak shapes suggested that lower voltages were not desirable; therefore 20kV was selected as the optimum voltage. Retention factors for L,L-neotame and D,D-neotame were significantly decreased from 1.287 to 0.545 and from 2.282 to 1.365 respectively. The resulting separation factor increased from 1.773 to 2.504 and the resolution factor also increased from 4.16 to 6.78

with an increase in voltage, suggesting that the resolution between two peaks were better at higher voltages.

5.2.1.4 Effect of cassette temperature

The viscosity and EOF of the running buffer depends on the cassette temperature. At higher temperatures, the viscosity decreased and the EOF increased resulting in shorter migration times. Since the kinetic effect influences the viscosity and diffusion coefficient of the solute, and the thermodynamic effect (enthalpy and entropic contributions) influences the transfer of the Gibbs free energy change (ΔG) between buffer systems including chiral selector and analyte [Peter et al., 2002]. The kinetic effects of the cassette temperature on the migration times and resolution were evaluated from 15 to 40 ^{0}C. Clearly above 30 ^{0}C, the excess joule heating generated from the inside of the capillary resulted in a noisy baseline with peak splitting, while longer migration times and broader peaks were observed below 30 ^{0}C [Figure 5.15].

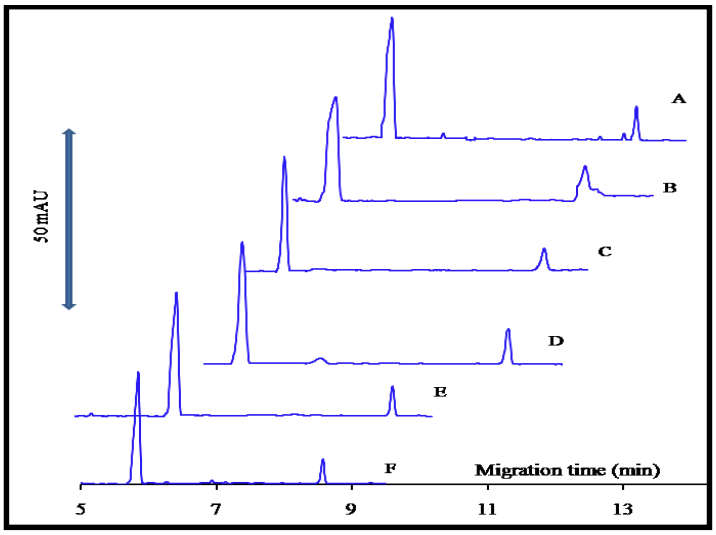

Figure 5.15: Influence of the temperature on the chiral separation of neotame(Conditions: Temperature A(15^{0}C), B(20 ^{0}C), C(25 ^{0}C), D(30 ^{0}C), E(35 ^{0}C), F(40 ^{0}C), 50 mM phosphate buffer, 30 mM TM-β-CD, 20 kV applied voltage, 200 nm wavelength)

The retention factors for both L,L and D,D diastereomers were increased from 0.4169 to 2.2444 and from 1.001 to 3.755 respectively, with a corresponding increase in temperature from 15 to 40 ^{0}C. However with an increase in temperature, the separation and resolution factors gradually decreased from 2.4010 to 1.6733 and 8.23 to 5.24 respectively. These results suggests that the gaps between the two peaks (resolution) and the migration time decreases with an increasing temperature, as depicted in Table 5.5. Accordingly, the cassette temperature for a baseline separation was selected at 30 ^{0}C. An acceptable mathematical model describing the thermodynamic effects based on the enthalpy and entropy contributions are derived from the van't Hoff equations:

$$\ln k = \frac{-\Delta H}{RT} + \frac{\Delta S}{R} + \ln\phi \qquad \text{and} \qquad \ln\alpha = \frac{\Delta_{R,S}\Delta H^\circ}{RT} + \frac{\Delta_{R,S}\Delta S^\circ}{R}$$

where, ΔH and ΔS are the standard enthalpy and entropy of transfer of the solute from the mobile phase to the stationary phase; $\Delta_{R,S}\Delta H°$ and $\Delta_{R,S}\Delta S°$ are the differences of $\Delta H_2 - \Delta H_1$ and $\Delta S_2 - \Delta S_1$respectively. From the above expressions, linear graphs were obtained by plotting lnk versus 1/T and lnα versus 1/T with slopes of $-\Delta H/R$, $\Delta_{R,S}\Delta H/R$ and intercepts of $\Delta S/R + \ln\phi(\Delta S^*)$, $\Delta_{R,S}\Delta S/R$ respectively. lnα versus 1/T plots were constructed at 15–40 ^{0}C for L,L-neotame and D,D-neotame. Thermodynamic parameters for the two compounds were calculated and the van't Hoff isotherms were found to be linear (r^2>0.93) [Figure 5.16].

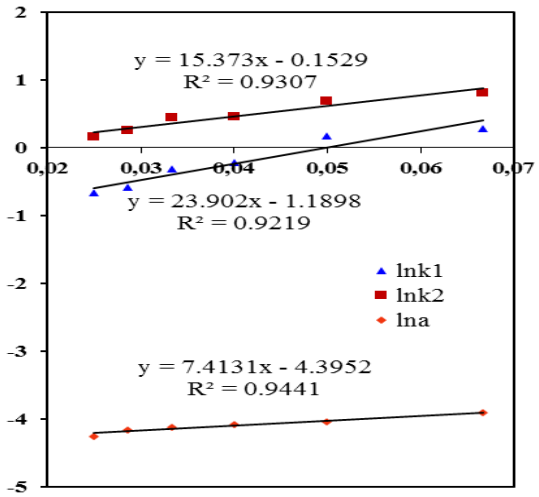

Figure 5.16: Van'tHoff plots for L,L- neotame and D,D- neotame

At lower temperatures the resolution factors were higher because the transfer of the Gibbs free energy (ΔG) between the buffer systems to the analyte was low. However, the resolution and separation factors decreased with an increasing temperature. At optimum temperature the transfer of energies were -21.7464 and -23.0431 for L,L-neotame and D,D-neotame respectively. Our results suggested that the resolution and elution order of the analytes controlled by the enthalpy were due to weaker interactions of the L,L-neotame with the stationary phase (TM-*β*-CD) in contrast to D,D-neotame. As a consequence of this, L,L-neotame eluted prior to D,D-neotame. For this purpose 30 ^{0}C was considered as the optimum working temperature.

Table 5.5: Effect of Temperature (^{0}C) on Retention, Separation and Resolution factors (K′, α, Rs).

Temperature (°C)	Migration time (min)		Retention factor (K′)		Separation factor (α)	Resolution factor (Rs)	van't Hoff equation (R^2)	$\Delta H/\Delta_{R,S}\Delta H$ kJ mol^{-1}	$\Delta S^*/\Delta_{R,S}\Delta S$ kJ mol^{-1}
	L,L	D,D	K_1'	K_2'					
15	9.21	13.01	0.416	1.001	2.401	8.23	$Lnk_1 = 23.902/T - 1.1892(0.92)$	-21.7464	-1.1892
20	9.03	12.32	0.556	1.124	2.018	7.89	$Lnk_2 = 15.373/T - 0.1529(0.93)$	-23.0431	-0.1529
25	7.42	10.67	0.725	1.481	2.041	7.12	$Ln\alpha = 7.413/T - 4.3952(0.94)$	-19.0502	-4.3952
30	7.13	11.24	1.376	2.746	1.995	6.65			
35	6.42	9.44	1.918	3.290	1.715	5.91			
40	5.84	8.56	2.244	3.755	1.673	5.22			

5.2.1.5 Effect of injection time

The effect of injection times on the migration and resolution were investigated by changing the injection times of the analyte ranging from 2 to 8 s. An increase in injection time of the sample resulted in peak broadening and a slight shift in the peaks towards the right hand side resulted in longer migration times as shown in Figure 5.17.

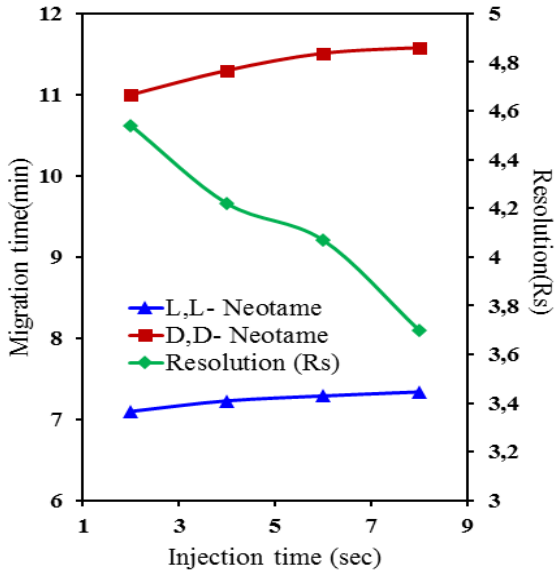

Figure 5.17: Effect of injection time of sampleon migration time and resolution(Conditions:50 mM phosphate buffer, 30 mM TM-β-CD, 20 kV applied voltage, 30 ^{0}C temperature, 200 nm wavelength)

On the other hand, an increase in migration time resulted in a decrease in the resolution between two peaks from 4.54 to 3.70. Injection times beyond 4 s affected the peak broadening and ultimately resulted in lower resolutions. For this purpose, 4 swas chosen as the optimum injection time of the sample into the capillary.

5.2.1.6 Effect of concentration of heptakis 2, 3, 6 tri-*o*-methylbetacyclodextrin

The electrophoretic mobility mainly depends on the concentration of the chiral selector. In CE the process responsible for the separation is the formation of complexes between

the neotame diastereomers and the chiral selector. The presence of additives such as cyclodextrins in the electrophoresis buffer changes the viscosity of the media, which in turn affects the effective electrophoretic mobilities. The corrected electrophoretic mobility ($\mu_{corrected}$) of neotame diastereomers in the presence of TM-β-CD at different concentrations are reported in Table 5.6.

The observed electrophoretic mobility is given by the following equation [Eqn 5.1]:

$$\mu(obs) = \mu(EOF) + [\mu(f) \times x(f)] + [\mu(c) \times x(c)] \quad \text{[Eqn 5.1]}$$

where μ(obs) is the observed mobility, μ(EOF) is the electro-osmotic mobility and *x* are the molarfractions, whereas *f* and *c* represents the free and the complexed (by the chiral selector) analyte, respectively. In general, μ(EOF) is equal for both the diastereomers to be separated in the sameelectrophoretic run and, dealing with chiral separations, μ(f) must be equal for the two diastereomers [Giuffrida et al., 2012]. Thus the resulting equations are [Eqn 5.2]:

$$\Delta(\mu(obs)) = \Delta[(\mu(c)) - \mu(f) \times x(c)]$$

$$\mu_{corr} = \mu_{obs} - \mu_{EOF} \quad \text{[Eqn 5.2]}$$

This equation shows that two different factors i.e., the difference in the electrophoretic mobility between the free and the complexed analyte and the difference in their degrees of formation are responsible for the separation. At optimum pH 5.5, neotame formed complexes with TM-β-CD in the zwitterionic state and thus formed a less stable anionic complex as shown by the mobility values. However, the mobility value increased with an increasing concentration of the chiral selector. Furthermore, the complexes are significantly more bulky than the free analytes, resulting in an increase of the selector concentration. The chiral selector therefore plays an important role in the separation of diastereomers. It is widely believed that a combination of interactions such as hydrogen bonding, hydrophobic interactions, dipole–dipole interactions, and charge transfer complexes (π-π) might be a key for the chiral recognition [Aboul-Enein, 2001], where the main

chiral absorbing sites are the methoxy groups for TM-β-CD. Our results revealed that at an optimum pH 5.5, the concentration of TM-β-CD affected the resolution of the peaks, while at lower concentrations less than 20 mM of TM-β-CD the separation factor was 1.281 and resolution factor was 0.80, indicating that the capacity of separation was very low. When the concentrations increased from 20 to 30 mM the separation factors increased to 2.409 and the resolution factor increased to 3.79. Thus, the capacity of separation increased up to 30 mM and a further increase in concentration of TM-β-CD showed no specific changes either on the separation or the resolution factors. Higher concentrations of TM-β-CD affected peak shapes and baseline separations, as depicted in Table 5.6.

Table 5.6: Effect of concentration of TM-β-CD on Retention, Separation and Resolution factors (K′, α, RS)

Concentration of TM-β-CD	Migration time(min)		Retention factor(K')		Separation factor(α)	Resolution factor(Rs)	$\mu_{corrected}$ (10^{-9} m^2 V^{-1} s^{-1})	
	L,L	D,D	K_1'	K_2'			L,L	D,D
0	6.85	6.85	0.662	0	1	0	-4.05	
5	6.93	7.72	0.682	0.80	1.281	0.80	-3.52	-3.84
10	7.08	8.26	0.718	1.71	1.398	1.71	-3.33	-3.48
20	7.19	9.95	0.745	2.52	1.902	2.52	-2.95	-3.24
30	7.12	11.35	0.728	3.79	2.409	3.79	-2.61	-2.87
40	7.16	11.31	0.737	3.98	2.367	3.98	-2.53	-2.75
50	7.15	11.33	0.735	4.06	2.380	4.06	-2.41	-2.64

A closer inspection of Figure 5.18 shows the effect of concentration of TM-β-CD on the resolution between the two analytes. Based on the separation and resolution factors, 30 mM was considered as optimum concentration for TM-β-CD.

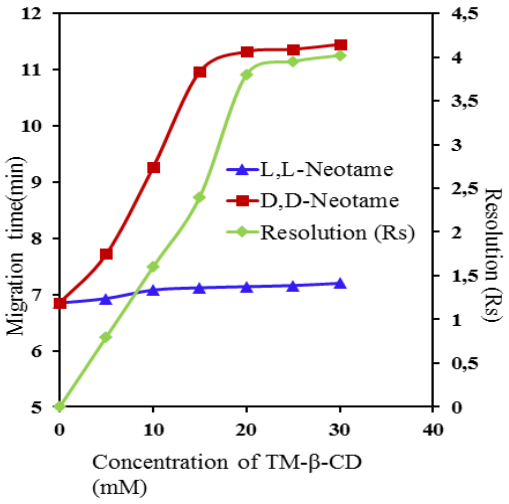

Figure 5.18: Effect of TM-β-CD concentration on migration time and resolution of compounds (Conditions:50 mM phosphate buffer, 30 mM TM-β-CD, 20 kV applied voltage, 30 ^{0}C temperature, 200 nm wavelength)

5.2.2 Interaction mechanism of TM-β-CD with neotame

The chiral separation of neotame diastereomers (L,L and D,D) with TM-β-CD is mainly governed by the relative mobilities of the isomers in the applied electric field, which are a function of their charge, mass and shape. The interaction of isomers with TM-β-CD depends on the complex formation inside the capillary with the electro-osmatic flow (EOF) of the buffer. Due to the injection of TM-β-CD into the capillary followed by neotame isomers, the movement of the isomers blocked by the slow moving TM-β-CD leading to some interaction with isomers. Even though TM-β-CD is a neutral molecule the complex formation and elution of analyte-TM-β-CD complex varies with changing in pH of the running buffer. Accordingly, in this work the separation

of neotame diastereomers were studied at different pH ranges, at pK_1 (3.01) and pK_2 (8.02) neotame isomers exhibits in cationic and anionic forms. At pH greater than 6.0, due to the deprotonation of the amino group neotame exhibits in an anionic form resulted in with increased migration times. Because the electrophoretic migration of the analytes is towards the cathode and with increase in buffer pH significantly reduces the net migration velocities of neotame diastereomers. In addition the negatively charged species interacts strongly with beta cyclodextrin at higher pHs results in lower migration times and resolution between peaks [Aturki et al., 2003]. According to theory the cationic form of neotame diastereomers at pH 3.0 should elutes quick but interestingly observed at longer migration times. To better understand the interaction mechanism and elution orders docking studies were performed and the obtained results shows the cationic and anionic isomers showing strong interaction with TM-β-CD as a result stable cationic and anionic-TM-β-CD complexes were formed and elutes at longer migration times. In the case of zwitter ionic form at pH 5.5, the elution of isomers observed at shorter migration times because neotame in zwitter ionic form showing weak interaction with TM-β-CD and forming less stable complex than cationic and anionic forms as a result elutes quickly. Computationally, H-bonded lengths in cationic, anionic and zwitterionic-TM-β-CD complexes were calculated and these results supporting the observed experimental elution orders. In case of cationic and anionic complexes shorter hydrogen bond lengths observed than hydrogen bond lengths in zwitter ionic form it is suggesting stronger interaction and longer migration times.

In this work methanol was used as the EOF marker and the indisputable peaks were shown in below Figure. The EOF peak was observed at 4.12 min and the electropherograms for neotame diastereomers at different concentrations were shown in attached Figure 5.19 (i). As the

concentration of the LL and DD-neotame increases the peak absorbance increases with correlation coefficient of 0.99 and 0.98 [Figure 5.19 (ii)].

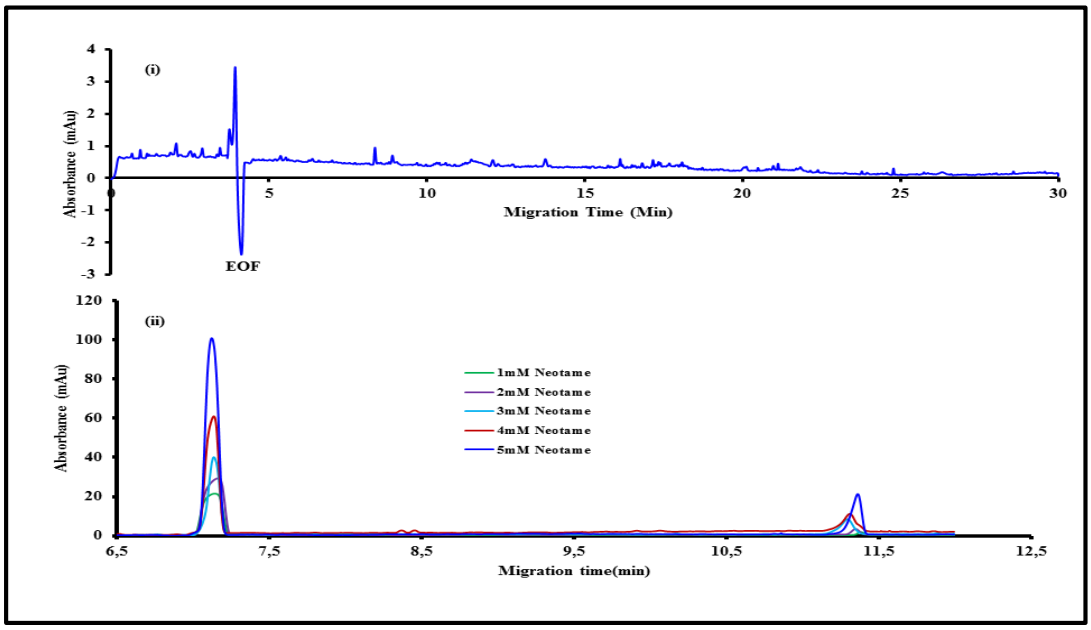

Figure. 5.19: The electropherograms for (i) EOF marker methanol and (ii) neotame diastereomers at different concentrations (Conditions: 50 mM phosphate buffer, 30 mM TM-β-CD with pH 5.5, +20 kV applied voltage, 30 ^{0}C temperature, 200 nm wavelength.

5.2.3 Repeatability and reproducibility

In order to achieve good reproducibility between consecutive runs the capillaries were flushed with deionized water for 2 min and thereafter with NaOH for 2 min to replenish the silanol groups, and the separation buffer was used to equilibrate the capillaries. On the other hand, to get good reproducibility for the developed method in terms of migration time and peak absorbances, five successive runs with TM-β-CD/phosphate buffer of pH 5.5 were carried out with the same solutions. The repeatability was evaluated by performing five determinations with the same solution resulting in the percentage relative standard deviations (%RSD n = 5) of ±1.20, ±1.45 %

with respect to migration time and 1.17 %, 1.28 % for peak area for L,L and D,D-neotame, respectively.

5.2.4 Calibration curve and detection limits

L,L and D,D-neotame were determined using EKC-CE under the following optimum conditions: 50 mM phosphate buffer/30 mM TM-β-CD with pH 5.5, 20 kV applied voltage, 30^0C cassette temperature, 4 s sample injection. The regression equations and the correlation coefficients were y = 44837x + 70.214, y = 11511x - 3.8789 and 0.9977, 0.9887 for L,L-neotame and D,D-neotame respectively. The LOD and LOQ (signal to noise ratio *S/N*=3 and *S/N*=10) were 0.01857; 0.08214 mM and 0.07428; 0.24891 mM for L,L-neotame and D,D-neotame respectively.

5.2.5 Analytical applications

Figure 5.20 shows the chiral separation and determination of neotame in standard samples were carried out according to the procedures described above and good separations with satisfactory resolutions between peaks were observed.

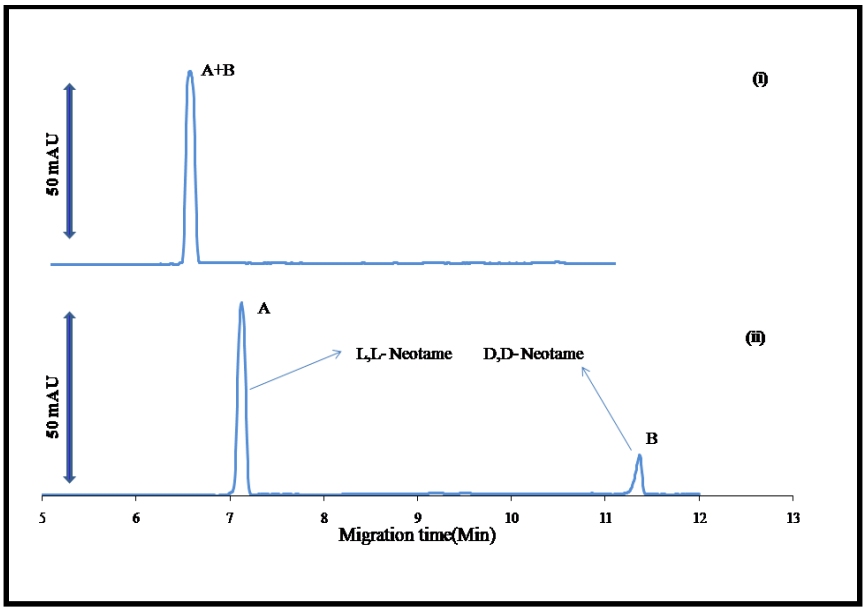

Figure 5.20: Electropherogram of standard mixture (i) without TM-β-CD and (ii) with TM-β-CD of of (A) L,L-neotame and (B) D,D-neotame (Conditions: 50 mM phosphate buffer, 30 mMTM-β-CD with pH 5.5, +20 kV applied voltage, 30 ^{0}C temperature, 200 nm wavelength

The accuracy of this method was tested using three different neotame spiked samples under the same optimum conditions and the resulting electropherograms are illustrated in Figure 5.21. Intra and inter-day precision and accuracy were evaluated by analyzing three sets of spiked food samples at three concentration levels (3.0, 5.0 and 7.0mM) on three separate days. The overall intra and inter-day variations (%RSDs) of the two analytes in three samples were found to be1.20% and 1.50% respectively, with the recoveries ranging from 95.66 - 99.00% as shown in Table 5.7.

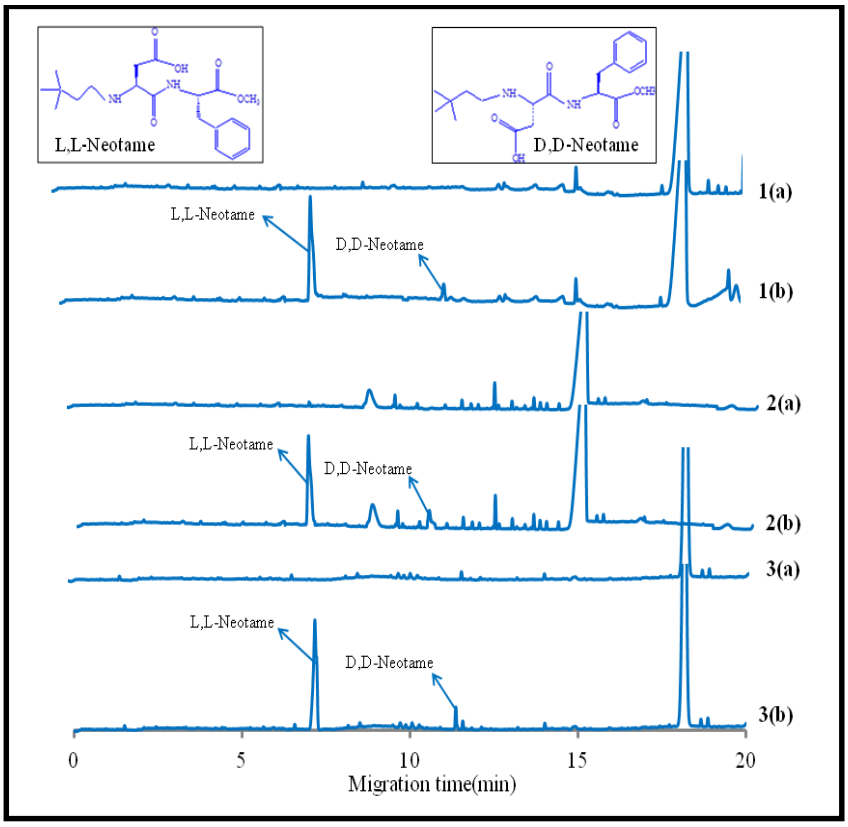

Figure 5.21: Electropherograms (1a) blank mango juice (1b) spiked mango juice (2a) blank busta orange drink (2b) spiked busta orange drink (3a) blank tab cool drink (3b) spiked tab cool drink for L,L-neotame and D,D-neotame (Conditions: 50 mM phosphate buffer, 30 m MTM-β-CD with pH 5.5, 20 kV applied voltage, 30 ^{0}C temperature, wavelength 200nm.

Table 5.7: The intra-day and inter-day precision and accuracy for the determination of NTM (n=5)

Sample	Active components	NTM conc. Added (g)	Intra-day (n=5)		Inter-day (n=3)	
			[b]RSD (%)	Recovery (%)	RSD (%)	Recovery (%)
[a]SS-1	L,L-Neotame	0.00378	1.9	96.67	1.2	97.33
	D,D-Neotame		2.3	97.66	1.8	95.66
SS-2	L,L-Neotame	0.00567	2.1	98.21	1.3	97.26
	D,D-Neotame		1.5	97.40	2.0	98.41
SS-3	L,L-Neotame	0.00756	1.7	99.0	2.2	98.39
	D,D-Neotame		2.0	97.71	1.9	98.87

[a]SS= Spiked sample
[b]RSD= Relative standard deviation for five and three individual runs

5.2.6 Docking discussion

The geometric aspects and the binding interactions of neotame diastereomers with TM-β-CD were studied using docking simulations. Accordingly, three different ionic states (cation, anion, zwitterion) of D,D-neotame and L,L-neotame were chosen based on the experimental pH. For expediency, the ionic states of D,D-neotame are labeled as $DD_{zwitterion}$, DD_{cation} and DD_{anion}, while $LL_{zwitterion}$, LL_{cation} and LL_{anion} represents the ionic states of the L,L-neotame. The inclusion complexes of neotame with TM-β-CD showed important host-guest interactions and the detailed docking results are summarized in Figure 5.22 and Table 5.8. A closer inspection of Figure 5.22 revealed that both the electrostatic and hydrophobic interactions were very important in locking the geometries of the ligands in the cavity of the TM-β-CD ring.

Table 5.8: Docking results of NTM diastereomers with the TM-β-CD

NTM ionic form	Migration time(min)	CDOCKER energy	CDocker interaction energy	Number of H-bonds	H-bond distance (in Å)
L,L-CATIONIC	20.5	- 13.9488	-20.1	2	1.959, 2.139
L,L-ANIONIC	16.4	-7.308	-22.4	2	2.079, 2.406
L,L-ZWITTER IONIC	7.1	- 16.562	-19.5	2	1.978, 2.146
D,D-CATIONIC	23.1	-14.731	-23.2	2	1.80, 2.082
D,D-ANIONIC	18.7	-9.4013	-23.3	2	1.959, 1.865
D,D-ZWITTERIONIC	11.3	-19.003	-22.7	3	2.108, 1.786, 1.967

Specifically, both zwitterions ($DD_{zwitterion}$ and$LL_{zwitterion}$) in addition to hydrophobic interactions formed inter-molecular hydrogen bonds with the TM-β-CD atoms. The structure in the case of $DD_{zwitterion}$ was more folded due to an additional intramolecular hydrogen bond formed between its carbonyl oxygen and the aminic hydrogen. Moreover, the hydrogen bond distances in the case

of $DD_{zwitterions}$ were comparatively shorter, suggesting stronger interactions with the TM-β-CD than the $LL_{zwitterions}$ variants [Table 5.8]. The cationic forms, DD_{cation} and LL_{cation} of both neotame isomers also interacted comfortably with the TM-β-CD through two hydrogen bonds formed between their nitrogen and oxygen atoms of the TM-β-CD ring. Although both complexes of DD_{cation} and LL_{cation} with TM-β-CD exhibited equal number of hydrogen bonds, the computed hydrogen bond lengths were shorter in the former than the latter, suggesting its stronger interaction with the TM-β-CD. Similarly, the DD_{anion} compared to its structural isomer LL_{anion} also exhibited stronger interactions with the TM-β-CD ring through two stronger hydrogen bonds as evidenced by their shorter distances. The results were further substantiated on the basis of two scoring functions, C-Docker energy (CDE) and C Docker interaction energy (CDIE), as shown in Table 5.8.

Clearly, the computed CDE and CDIE for DD-neotame were comparatively lower than LL-neotame, irrespective of their ionic states [Table 5.8], supporting the better fitting of the former in the TM-β-CD cavity. Moreover, a very good relationship between the scoring functions (CDE and CDIE) and migration times in CE were observed. Specifically, all ionic states of DD-neotame exhibited lower values of CDE and CDIE compared to their structural isomers. TM-β-CD, owing to its larger size migrated slower in the capillary under CE conditions. It is believed that the stronger bonding of DD-neotame with the TM-β-CD restricted its movement towards the anodic electrode, and is probably responsible for its greater migration time in CE than its structural diastereomer LL-neotame.

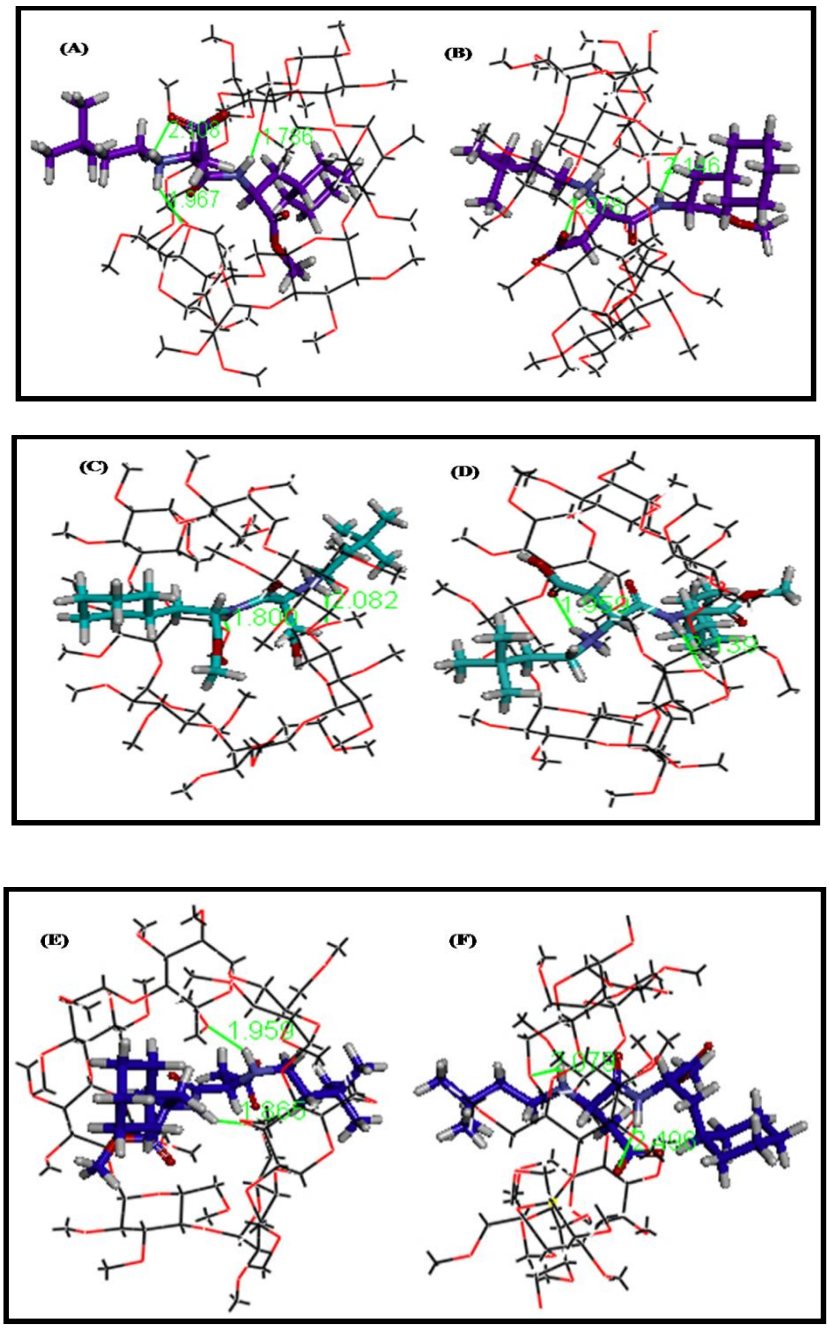

Figure 5.22: The inclusion complexes of (A) $DD_{zwitter}$ (B) $LL_{zwitter}$ (C) DD_{cation} (D) LL_{cation} (E) DD_{anion} (F) LL_{anion} with the TM-β-CD. Ligands are presented in stick form while the host ring is shown in lines format. Hydrogen bonds are depicted as green lines.

5.3 Electrophoretic analysis of sucralose in food samples using amines as BGE

5.3.1 Optimization of separation conditions

5.3.1.1 Comparison of back ground electrolyte for separation

The principle of indirect UV method is based on the strong UV absorption of the back ground electrolyte (BGE) when passed through a UV detection window with an analyte, the absorbance decreases corresponding to the concentration of the analyte and detected as a negative peak [Yoshikawa et al., 2011]. Although no absorbing analytes were present in the UV and visible ranges resulting in optimal sensitivity achieved, rendering this as an effective method considering its ability for the simultaneous analysis of organic and inorganic analytes.

The effect of BGE on separation behavior was studied using different amine compounds such asethylamine (EA), piperidine (Pip), morpholine (Mor) and triethylamine (TEA). Other operating conditions: BGE pH 12.0, capillary temperature 30 ^{0}C, applied voltage 20 kV, and injection time of sucralose 6 s for 50 mbar and signal wavelength 230 nm were implemented. The typical electropherograms for separation of sucralose (SUC) with different BGE's are shown in Figure 5.23. When EA was used as an absorbing buffer, it was not able to detect the sucralose (SUC) at low concentrations (0.2-0.3 M). With an increase in the concentration of EA to 0.4 M, the separation was achieved with a migration time of 7 min. But, higher concentrations resulted in the disruption of a baseline stability. In the case of Pip, the baseline became stable and the separation was attained with a lower concentration (0.2 M), but with migration time of SUC achieved at 15 minutes. When TEA was used as a buffer at the same concentration (0.2 M) the separation was observed with a stable baseline but with a migration time of 25 min for SUC. Even though the concentrations of Pip and TEA were changed, no significant changes were noted in the migration times of SUC. In contrast, SUC separation was successfully achieved when Mor was used as a

buffer with similar concentration (0.2 M) and improved migration time of 7.62 min. Moreover, the stability of the baseline and the sensitivity of the detection were favorable and consequently Mor was used as BGE for further studies.

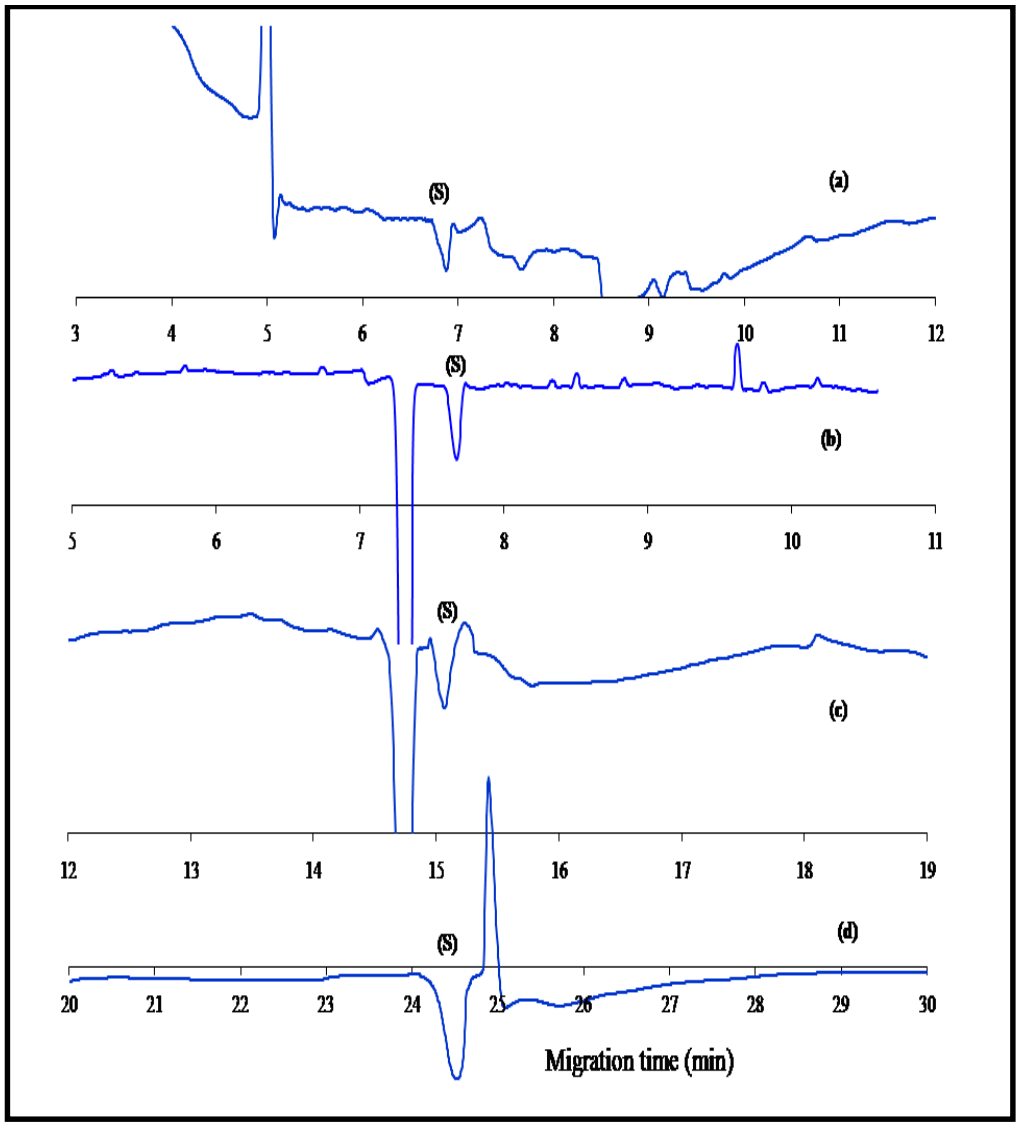

Figure 5.23: Electropherograms for separation of sucralose (s) with (a) EA (b) Mor (c) Pip (d) TEA (Conditions: pH 12.0, 20 kV applied voltage, 30 ^{0}C temperature, 230 nm wavelength)

5.3.1.2 Comparison of indirect UV detection wavelength

The effect of the detection wavelength was studied over the range of 200–260 nm, with different solutions of 0.2 M amine buffers at pH 12.0. Below 230 nm wavelength, the baseline was unstable and the detection sensitivity was unsatisfactory due to the absorption difference between SUC and BGE. In contrast, above 230 nm the detection sensitivity of SUC was lowered as the absorption of amine buffers decreased with an increasing wavelength and it was not suitable for indirect UV detection. As a result, the optimum reference wavelength was determined at 230 nm on the basis of the detection sensitivity of analytes and the stability of the baseline.

5.3.1.3 Effect of concentration of BGE (Morpholine)

The viscosity co-efficient of the solution and the zeta (ζ) potential of the inner surface of the capillary are mainly dependent on the concentration of the running buffer which in turn affects the migration time and absorbance of the analytes. The concentration of the BGE on the migration times and peak absorbances were examined over the range of 0.05 to 3 M and the results were shown in Figure 5.24a.

At low concentrations (0.05-0.15 M) longer migration times (8.5-10 min) were observed with poor peak absorbances and peak shapes. When the concentration increased from 0.15 to 0.2 M, the migration time shifted to 7.6 min, with a stable base line and a fair peak shape at an applied voltage of 20 kV. Beyond the concentration of 0.2 M, no significant difference was observed in the migration time. However, lower concentrations of Mor resulted in poor sensitivity, while higher concentrations resulted in the instability of the baseline. As a result the optimum concentration of Mor was chosen as 0.2 M for further studies.

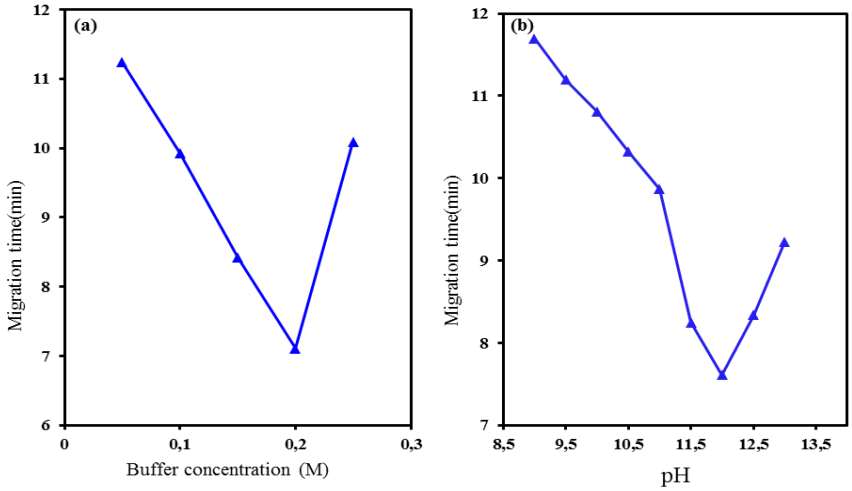

Figure 5.24: Effect of (a) buffer concentration (b) pH on migration time (Conditions: 0.2 M Mor buffer, pH 12.0, 20 kV applied voltage, 30 ^{0}C temperature, 230 nm wavelength)

5.3.1.4 Effect of pH

The separation of carbohydrates or sucralose mainly depends on the pH, especially in an alkaline environment in which sucralose easily undergoes ionization inside the capillary resulting in a separation [Stroka et al., 2003]. At pH below the pKa values (EA-10.70, Mor-8.33, Pip-11.12 and TEA-9.80), amines predominantly undergo protonation, resulting in the ionic form. Whereas, pH above the pKa values amines undergo deprotonation and results in the non-ionized state. However, pH less than pKa values of amines were not favorable for the separation of sucralose. Consequently, the pH of all amines were maintained above the pKa values in this investigation. The effect of pH on the migration times and peak absorbances of SUC were studied at different pH values ranging from 9.0 to 13.0 using 0.2M Mor buffer. At pH values of 9.0 to 11.5, longer migration times and noisy baseline with low peak absorbance were observed due to poor ionization capacity. Further, increase in pH from 11.5 to 12.0 resulted in a baseline separation with shorter migration times and immense peak absorbance as shown in Figure 5.24b. The capacity

of ionization increased with an increase in the pH, as a result SUC effectively interacted with the buffer. Beyond the pH 12.0, significant changes in migration times and peak absorbances were not observed. At optimum pH and detection wavelengths the order of peak absorbances for SUC with different amines were as follows: TEA >Pip >Mor >EA. These results indicated that the interaction ability of amines gradually decreased from TEA to EA, resulting in shorter migration times. Therefore a pH 12.0 was considered as an optimum pH for the separation studies.

5.3.1.5 Effect of cassette temperature

Shorter migration times were possible at high cassette temperatures because the viscosity decreased and the EOF of the buffer increased with a gradual increase in temperature. In this study, the effect of cassette temperature on the migration times were examined in the range of 10 to 40 ^{0}C. At low temperatures (< 30 ^{0}C) longer migration times (between 20.8-13.7 min) were achieved with a stable baseline. At 30 ^{0}C the baseline separation (12.1 min) was obtained and further increases in temperature to 40 ^{0}C with shorter migration times (11.5-10.2 min) [Figure 5.24c] with noisy base line and peak broadening were observed. Considering the baseline and peak shapes high temperatures were not favorable for the separation even though shorter migration times could be achieved. Therefore, a temperature of 30 ^{0}C was maintained as an optimum temperature for further studies.

5.3.1.6 Effect of applied voltage

Migration and peak shape of the analytes mainly depends on the applied voltage. The EOF of the mobile phase increased with an increase in the applied voltage hence, remarkable decrease in migration times were observed. In this study, the effect of applied voltages on the

separation were studied ranging from 14 to 22 kV. At low applied voltages (14), the EOF was low and the analyte moved slowly, which resulted in the longer migration times [Figure 5.24d]. When the applied voltage increased from 14 to 22, the EOF of the mobile phase increased and the analyte moved rapidly. High applied voltages are not recommended, because high joule heat released from the capillary walls and leads to irregular peak shapes and noisy baseline. Considering migration time and peak shapes, 20 kV was used as an optimal applied voltage for baseline separation.

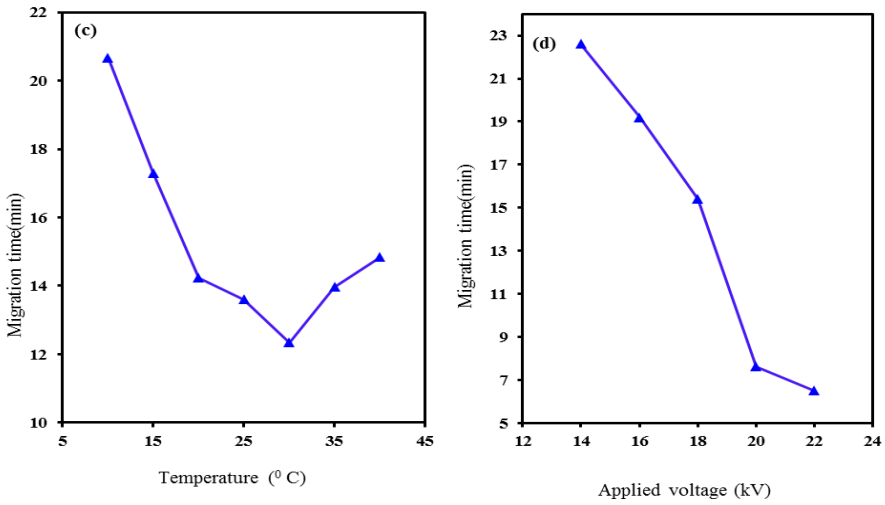

Figure 5.24: Effect of (c) cassette temperature (d) applied voltage on migration time (Conditions: 0.2 M Mor buffer, pH 12.0, 20 kV applied voltage, 30 ^{0}C temperature, 230 nm wavelength)

5.3.1.7 Effect of injection time of standard on absorbance

The effect of injection time on the migration times and peak absorbances were investigated by changing the injection time of analyte ranging from 2–10 s. Increase in injection time of SUC, resulted in the peak broadening and a slight peak shift towards the right side resulting in longer migration times. Injection time beyond 6 s affected the peak broadening and ultimately resulted in longer migration times [Figure 5.25]. The peak absorbances were gradually increased

with increase in injection times. Considering the migration times and peak absorbances the optimum injection time was selected as 6 s for further studies.

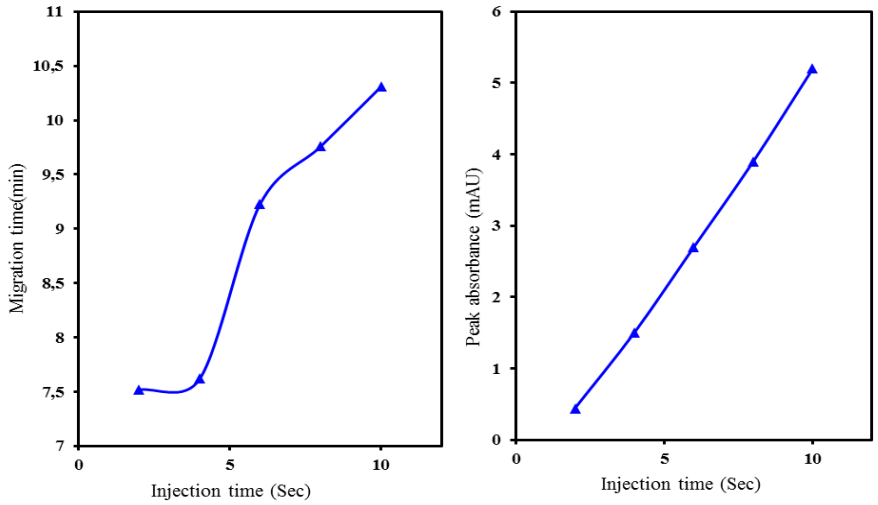

Figure 5.25: Effect of injection time on (a) migration time and (b) peak absorbance (Conditions: 0.2 M Mor buffer, pH 12.0, 20 kV applied voltage, 30 ^{0}C temperature, 230 nm wavelength)

5.3.2 Mechanism for the separation of sucralose

The separation of SUC was achieved with four different amine buffers (1^0, 2^0 and 3^0) at an optimum pH 12.0. The mechanism behind the separation of sucralose was due to the presence of the chlorine atoms in SUC, as it behaves like an alkyl halide which easily undergoes ionization in a strong nucliophilic environment as shown in Scheme 5.1. The ionization occurs via dehalogenation followed by substitution reaction, where the chlorine atoms present in sucralose undergoes substitution with nucliophiles (electron rich species) present in alkaline buffer as an S_N2-type mechanism [Motwani et al., 2011].

The chlorine atoms present in fructose and galactose portion of the SUC molecule are primary and secondary halides in nature respectively. The steric congestion around the carbon atoms attached

to the chlorine atoms in the fructose portion were less when compared to carbon atom in the galactose portion, due to the presence of primary chlorine atoms. The bond distance between the carbon and chlorine atoms in the fructose portion were nearly 1.781 and 1.786 which are longer than carbon and chlorine atom in galactose portion [Wu and Zhang 2011; Brizuela et al., 2013]. Based on the steric congestion and bond lengths, primary chlorine atoms in fructose portion are more favorable to undergo substitution with amines than secondary chlorine atom in the galactose portion.

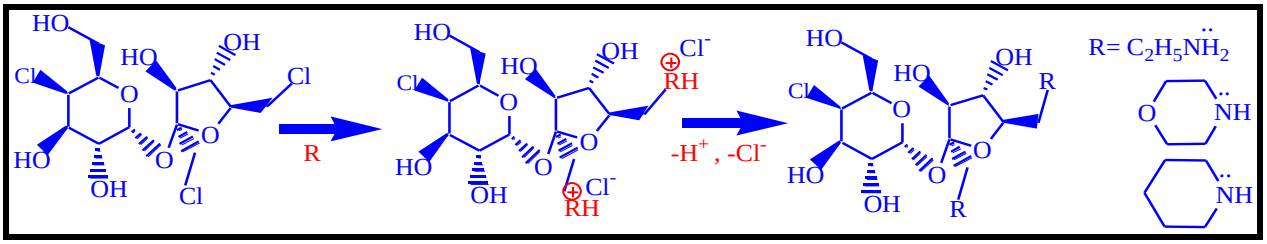

Scheme 5.1: Mechanism for the interaction of SUC with amines

In order to better understand the coordination behaviour of amines with SUC, FT-IR analysis was carried out for SUC and SUC-amine complexes [Figure 5.26]. The IR measurements were done using KBr disks and preheated SUC (at 70 ^{0}C) [Bannach et al., 2009]. However, the IR spectra for pure SUC showed sharp stretching peaks at 710 cm^{-1}, 745 cm^{-1} and 768 cm^{-1} for a single chlorine atom present at the galactose portion and the two chlorine atoms present at the fructose portion. The broader absorption peak at 3450 cm^{-1} is assigned to the –OH stretching mode. Even though SUC has no carbonyl groups, due to the heating at 70 ^{0}C it showed stronger absorption peaks at 1652.703 cm^{-1} and 1734.036 cm^{-1}, which are assigned to the carbonyl stretching while the peak around 1151.801 cm^{-1} is assigned to the ether linkage [Bannach et al., 2009].

However, in the case of SUC-amine complexes (SUC-Mor, SUC-Pip, SUC-EA and SUC-TEA) the IR spectras showed significant structural changes. Especially, two stretching peaks at 745 cm^{-1} and 768 cm^{-1} observed for the two chlorine atoms present at the fructose portion which disappeared indicating the participation of these chlorine atoms in the formation of the complex. The sharp peak at 710 cm^{-1} corresponds to the single chlorine atom at the galactose portion shifted nearly -15 cm^{-1}, -10 cm^{-1}, -13 cm^{-1} and -10 cm^{-1} in SUC-Mor, SUC-Pip, SUC-EA and SUC-TEA complexes respectively as shown in Table 5.9. In all complexes a new absorption peak was observed ranging from 990 to 1025 cm^{-1} next to 1030 to 1041cm^{-1} (C-N stretch in EA, Mor, Pip, TEA) which corresponds to the C-N stretch of the complex. This main change suggests that the amine undergoes S_N2 type reaction involving the replacement of two chlorine atoms with SUC.

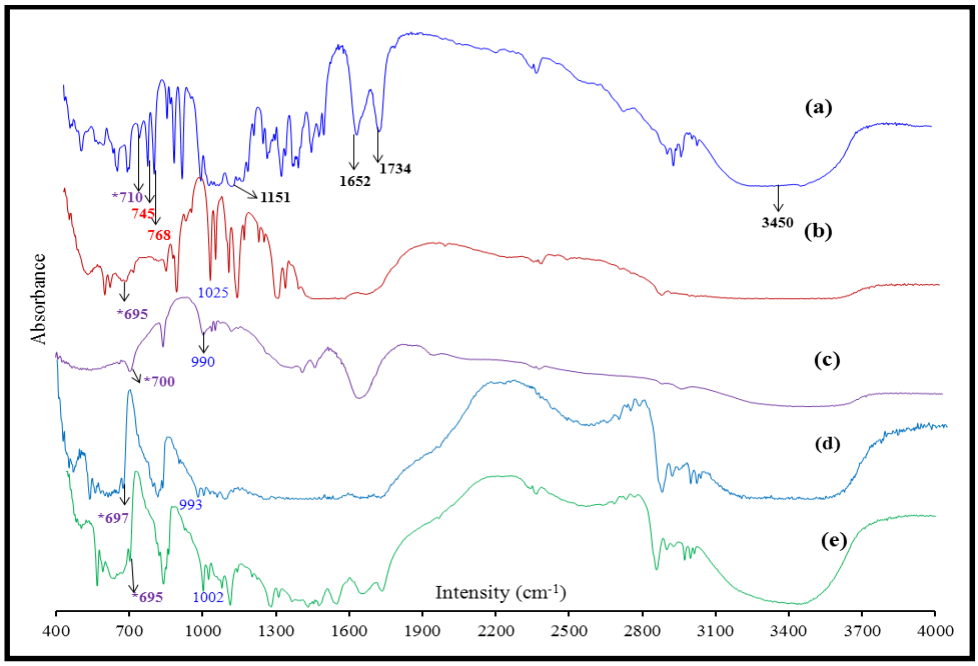

Figure 5.26: FTIR spectras for (a) SUC (b) SUC-Mor complex (c) SUC-Pip complex (d) SUC-EA complex (e) SUC-TEA complex

Table 5.9: FT-IR results obtained from computational calculations (DFT level 6-31 G basis set)**

System	C-Cl (fructose) (cm^{-1})	C-Cl (galactose) (cm^{-1})	C-N stretch (cm^{-1})	OH stretch (cm^{-1})
SUC	730, 754	705	absent	3843, 3817
SUC-EA complex	absent	697	1007	3835, 3815
SUC-Morcomplex	absent	692	1016	3844, 3817
SUC-Pip complex	absent	685	1010	3844, 3816
SUC-TEA complex	absent	694	1021	3842, 3816

5.3.3 Analytical precision

Sucralose was determined by indirect UV method under the following optimum conditions: 0.2 M Mor buffer with pH 12.0, 20 kV applied voltage, 30 ^{0}C cassette temperature, 6 s sample injection. For calibration different concentrations ranging from 2 to 10 mM standard solutions were used. From the calibration plots the regression equations and the correlation coefficients were y = 167.27x + 0.3794 and 0.9942 respectively. The LOD's and LOQ's (signal to noise ratio *S/N*=3 and *S/N*=10) were 0.3804 mg/ L and 1.2550 mg/ L respectively. The repeatability and reproducibility was evaluated by performing five determinations with the same solutions resulting in the percentage relative standard deviations (%RSD n = 5) of ±1.27 and 1.19 %with respect to migration times and peak areas.

5.3.4 Application to food samples

Under the optimum conditions, the separation and determination of SUC in standard sample was carried out according to the procedure described above and achieved good separation with satisfactory analytical figures. Typical electropherograms of the standard with different amine buffers are depicted in Figure 5.23.

To evaluate the accuracy of this method, three real SUC samples with three spiked samples were analyzed on an intra and inter-day basis. The analyzed real samples were in powder form (Yellow canderel), tablet form (Yellow canderel, Hullets equisweet) and spiked samples (Busta apple drink, Refresh cool drink, Energade sports drink) were prepared with three different concentrations (3, 5, 7 mM). Figure 5.27 (1) and (2) showed the electropherograms of three real and spiked samples. The recovery percentages of the real and spiked samples (n=5) with relative standard deviation% RSD are shows in Table 5.10. From this method the recoveries obtained ranged from 96.45 to 98.41% on an intra and 94.14 to 99.12% on an inter-day basis with RSDs of 1.60 and 1.26 % respectively.

Table 5.10: Determination of SUC in different real and spiked food samples

Sample	SUC concentration analyzed (mM)	Intra-day (n=5)		Inter-day (n=3)	
		RSD[a] (%)	Recovery (%)	RSD (%)	Recovery (%)
RS-1	3	1.50	98.41	1.15	97.74
RS-2	5	1.72	96.87	1.55	98.27
RS-3	7	1.41	98.65	1.46	98.82
SS-1	3	2.10	94.45	1.53	97.32
SS-2	5	1.93	97.91	1.60	96.14
SS-3	7	1.64	95.33	1.55	98.06

RS= Real sample, SS=Spiked sample, [a]Relative standard deviation for five individual determinations, RS-1 (powder sample- Canderel yellow), RS-2 (tablet sample- Canderel yellow), RS-3 (tablet sample- Hulletsequisweet), SS-1 (Busta apple drink), SS-2 (Refresh cool drink), SS-3 (Energade sports drink)

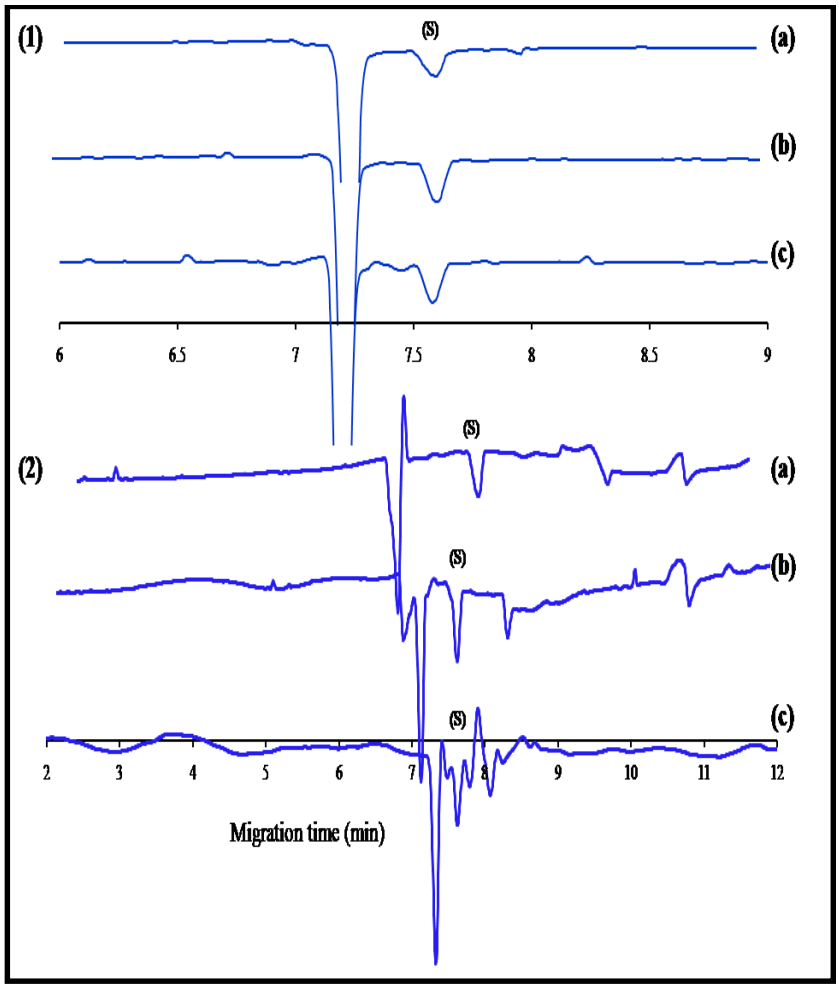

Figure 5.27: Electropherograms for SUC (S) in (1) real samples (1a) powder sample (Canderel yellow, Merisant Company 2, Sarl, 2000 Neuchatel-Switzerland), (1b) tablet sample (Canderel yellow, Merisant Company 2, Sarl, 2000 Neuchatel-Switzerland) and (1c) tablet sample (Hulletsequisweet, TongaatHullet Sugar, Rossburgh, SA), (2) spiked samples (2a) Busta apple drink (SMJ Beverages SA Pty Ltd, New Germany 3610, SA) (2b) Refresh cool drink (2c) Energade sports drink (Tiger Consumer Brands Ltd, 3010 W.N. Drive, Bryanston, SA) (Conditions: 0.2 M Mor buffer, pH 12.0, 20 kV applied voltage, 30 ^{0}C temperature, 230 nm wavelength)

5.3.5 Computational results

Based on the experimental FT-IR results, dichloro substituted products of the SUC were optimized at the density functional theory (DFT) level. The aim of the computational calculations was to get a deeper understanding of their structural and thermochemical features and

to correlate them with the experimental results. The nature of the stationary points of all structures were checked by calculating the vibrational wave numbers. The optimized structures of SUC and its Mor, Pip, EA and TEA analogues are diagrammatically represented in Figures 5.28a-e respectively, whereas their computed FT-IR vibrational frequencies are depicted in Table 5.10. A closer inspection of Table 5.10 revealed that the computed harmonic vibrational frequencies for dichloro-substituted products were in good agreement with the experimental FT-IR results irrespective of the nature of amine. Specifically, the disappearance of the two characteristic C-Cl peaks supported the substitution of the chloro groups attached to the five membered fructose rings. Shift in absorption peaks at 692, 685, 697 and 694 cm^{-1} for Mor, Pip, EA and TEA complexes respectively, also suggested the presence of a C-Cl bond attached to the galactose ring [Table 5.9]. The steric hindrance caused by the neighbouring hydroxyl functionalities (-OH) on the glucopyranosyl rings could probably have been avoided by the amine nucleophiles.

The frontier molecular orbitals were calculated for SUC and its amine derivatives in order to get a deeper understanding of their chemical reactivity and electrochemical behaviour on the basis of their HOMO-LUMO band gap energy. The results clearly show that the HOMO-LUMO band gaps were highest in the case of SUC molecule, and decreased in the presence of the amine moiety irrespective of its nature. An inverse relationship existed between the absorbance of CE peaks and the HOMO-LUMO band gaps. The SUC-EA compound, for instance, showed the lowest absorbance yet exhibited a greater HOMO-LUMO band gap (6.0 eV), whereas the SUC-TEA molecule with a maximum absorbance showed a minimum band gap (5.5 eV) [Table 5.11]. These results suggests that the movement of electrons between and across the orbitals were more efficient in the SUC-TEA molecule leading to a greater current response observed under CE conditions. Additionally, the order of the computed HOMO-LUMO band gaps were also consistent with the

migration times of the analytes. The HOMO and LUMO orbitals of the SUC and its amine derivatives were further visualized and are pictorially depicted in Figure 5.29. Clearly, the electron density, in case of SUC, was localized on its glucopyranosyl ring, and probably have shifted the nucleophilic attack of the amines to the more exposed electron deficient C-Cl bonds of the glucofuranosyl ring. Interestingly, the HOMO in case of SUC amine compounds were present only on a single amine functionality, irrespective of the nature of the amine present, whereas the corresponding LUMO were localized on the C-Cl bond of their glucofuranosyl ring. This distribution clearly indicates that the direction of charge transfer from the amine functionality to the glucofuranosyl ring in each amine derivative of SUC.

Table 5.11: HOMO-LUMO energies obtained from 6-31g basis set compared with CE migration time**

System	CE migration time	Absorbance	$E_{HOMO-LUMO}$ (a.u)	$E_{HOMO-LUMO}$ (eV)
SUC	-	-	0.261	7.0
SUC-EA complex	6.8	9.2	0.223	6.0
SUC-Mor complex	7.6	24.7	0.221	5.9
SUC-Pip complex	15.2	47.2	0.212	5.7
SUC-TEA complex	24.5	85.6	0.204	5.5

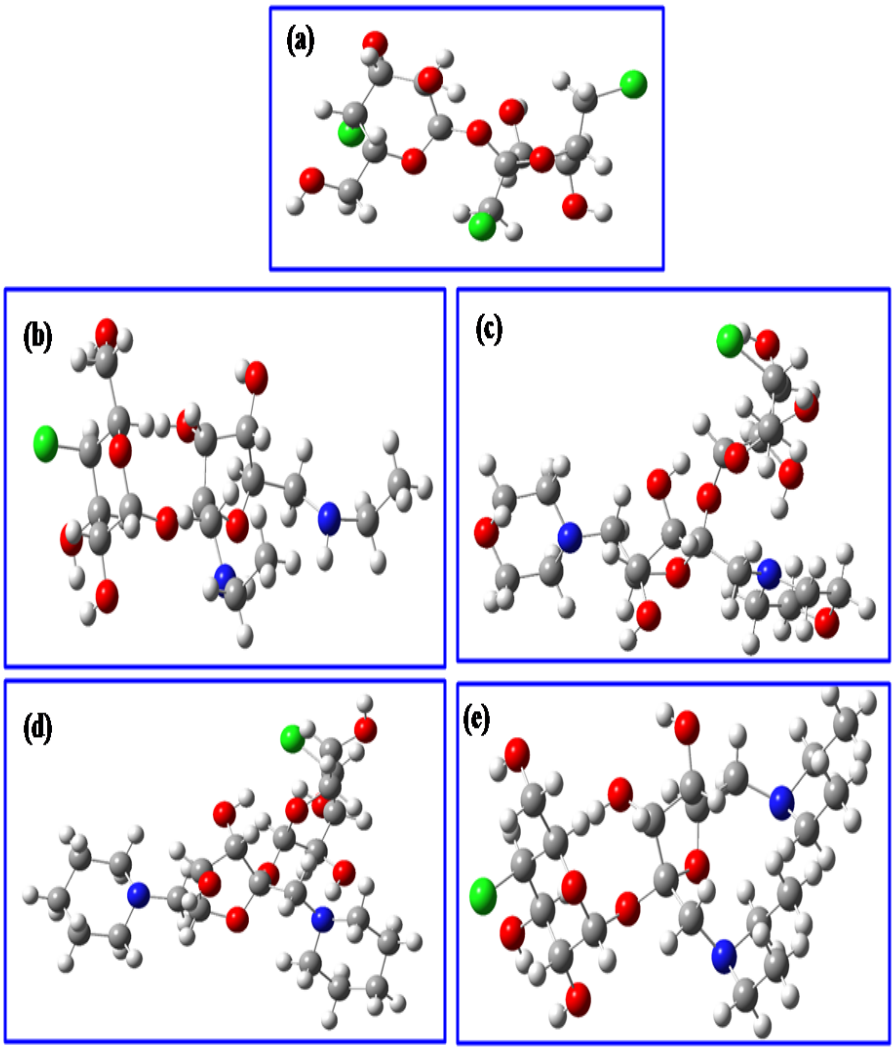

Figure 5.28: Structures of (a) SUC (b) SUC-EA (c) SUC-Mor (d) SUC-Pip (e) SUC-TEA were optimized at DFT level using 6-31g basis set.**

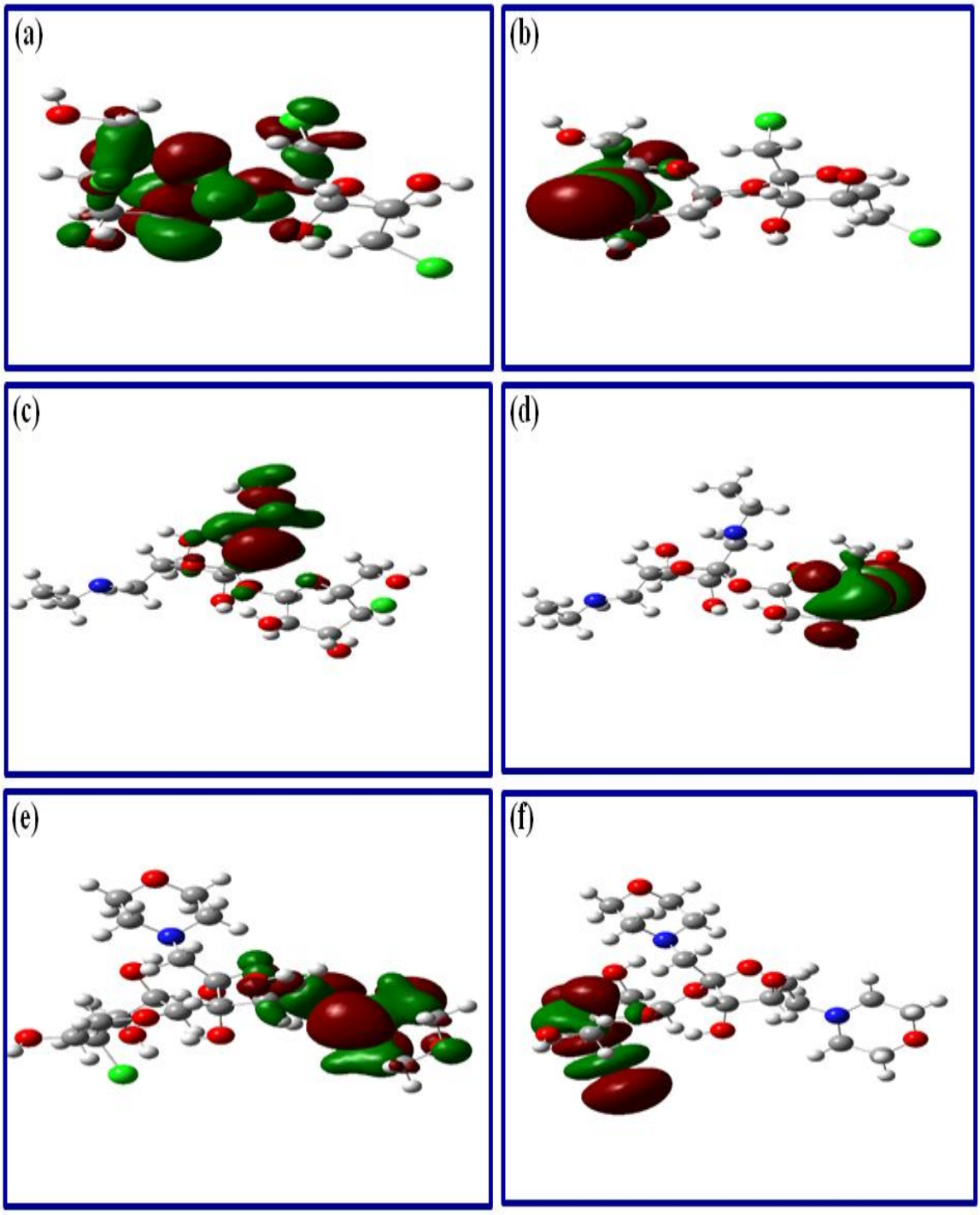
(a)
(b)
(c)
(d)
(e)
(f)

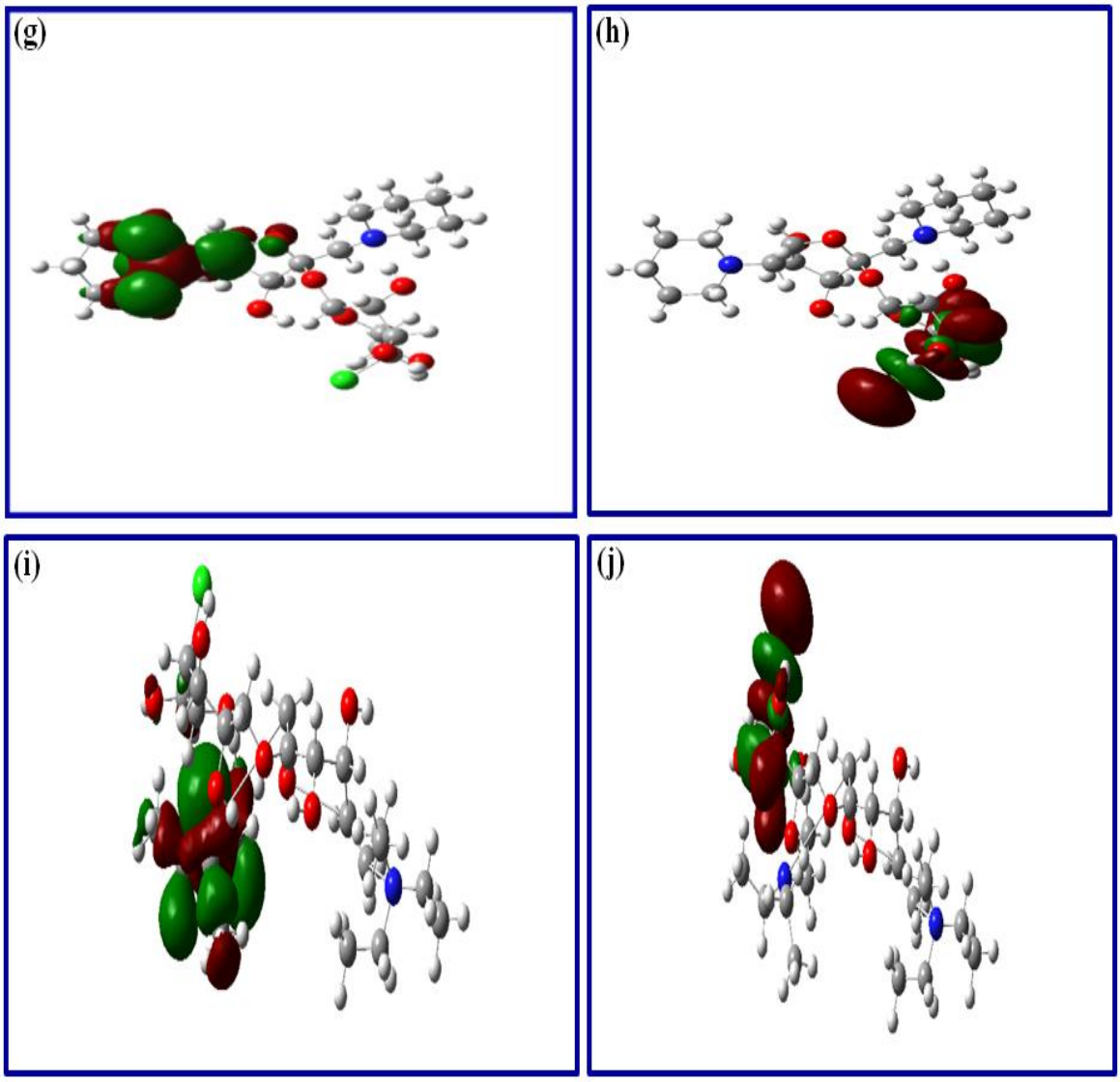

Figure 5.29: Highest occupied molecular orbital (HOMO) for (a) SUC (c) SUC-EA (e) SUC-Mor (g) SUC-Pip (i) SUC-TEA and Lowest occupied molecular orbital (LUMO) for (b) SUC (d) SUC-EA (f) SUC-Mor (h) SUC-Pip (j) SUC-TEA

CHAPTER 6

RESULTS AND DISCUSSION

PART TWO

Electrochemical characterization and detection of neotame, rebaudioside A and sucralose

This chapter deals with the results obtained from the experimental and computational part of the electrochemical work. The experimental work mainly divided into three sections: nanocomposite electrochemical sensor for the detection of neotame: experimental and computational studies of metal ion affinity for biological applications, development of cytochrome c (Cyt c) based biosensor for the analysis of natural sweetener rebaudioside A (Reb A) and analysis of sucralose using laccase-TEMPO based biosensor as discussed.

Computationally, the metal ion affinities were calculated for neotame with divalent metal ions as a biological application. Accordingly, density functional theory calculations were performed for neotame-metal complexes and the obtained results were compared with the experimental results. Docking simulations were further performed to predict the binding affinity of Cyt c and laccase with the Reb A and sucralose to establish their host-guest relationships.

6.1 Nanocomposite electrochemical sensor for the detection of neotame

In this work β-cyclodextrin (β-CD) was utilized in the modification of the glassy carbon electrode using copper nanoparticles (CuNPs) anchored with ammonium piperidine dithiocarbamate (APDC) on the multiwalled carbon nanotubes (MWCNTs). The purpose of the (MWCNTs) was to facilitate electron transfer between the electroactive species and the electrode, while β-CD was used as a dispersing reagent for the carbon nanotubes [Jia et al., 2011]. Moreover, APDC capped CuNPs were added onto the MWCNTs to generate additional electro-catalytic sites

and to increase the sensitivity and detection limits of the electrodes. To the best of our knowledge, this is the first electro-analytical attempt using CuNPs-APDC-MWCNTs-β-CD for the detection of neotame (NTM). Further studies involving the electrochemical behaviour of NTM with Ni^{2+}, Cu^{2+} and Zn^{2+} ions were investigated in terms of metal ion affinities (MIA) using isothermal titration calorimetry and supported by density functional theory (DFT) calculations.

6.1.1 Characterization of CuNPs-APDC-MWCNT–GCE

Figure 6.1A–D shows the typical TEM image of the pure MWCNTs, MWCNTs-CuNPs, MWCNTs-CuNPs–APDC and MWCNTs–CuNPs–APDC-β-CD respectively. The morphological structure of MWCNTs where the crystalline tubular structure of nanotubes are observed in Figure 6.1A, with the nanotubes having clear inner channels. Figure 6.1B displays the TEM images of MWCNTs decorated with CuNPs, showing the morphology and the size distribution of CuNPs. It can be seen that the size of nanoparticles are distributed from 10.5 to 80 nm, with a mean particle size of about ~50 nm. The CuNPs were covalently bonded to the APDC through the strong chelating undefined atoms, resulting in a uniform size of the nanoparticles on the outer surface of the MWCNTs [Figure 6.1C-D].

Thermogravimetric analysis (TGA) was used to determine the thermal stability of the material by monitoring the change in weight as a function of temperature. The amount of CuNPs, APDC and β-CD grafted on the MWCNTs was estimated by TGA analysis. Samples were analyzed in successive stages starting with the pure MWCNTs. The TGA curve for MWCNTs shown in Figure 6.1E (i) exhibited a well-defined step at 630 ^{0}C which can be associated with the oxidation of the carbon atom. On the other hand, CuNPs decorated MWCNTs showed a different TGA profile, with two drop downs at 173 ^{0}C and 440 ^{0}C as shown in Figure 6.1E(ii). The mass percentage of

CuNPs on the MWCNTs calculated as about 36.07%, which is probably due to the stronger electrostatic effects between the CuNPs and MWCNTs. In addition, the mass percentage of APDC and β-CD loaded on the MWCNTs was estimated to be 12.98% and 13.84% respectively as depicted in Figure 6.1E (iii and iv). The high mass loss in CuNPs– MWCNTs is probably due to the oxidation of Cu to CuO in the absence of the APDC and β-CD. Certainly, the TGA analysis also confirmed the presence of the CuNPs on the MWCNTs. However, an improvement of the thermal stability of the CuNPs–MWCNTs with the addition of APDC and β-CD were observed.

The FT-IR studies helped to understand the role of the APDC in the formation of the homogeneous nanoparticles. The FT-IR spectra [Figure 6.2a] for APDC capped CuNPs showed a strong intensity band in the range 1025–1009 cm^{-1}, which may be attributed to the (C–S) vibrations with a stronger intensity band observed around 1438–1497cm^{-1}, corresponding to the thiuride (C–N) vibrations. On the other hand, the free APDC (without CuNPs) showed a positive shift of around 10–35 cm^{-1} for the (C–S) bands and with no significant changes observed for the (C–N) bands. This suggests that the CuNPs were capped with APDC through an exohedral conjugation with their thiol (–SH) groups instead of the nitrogen atoms [Figure 6.2b].

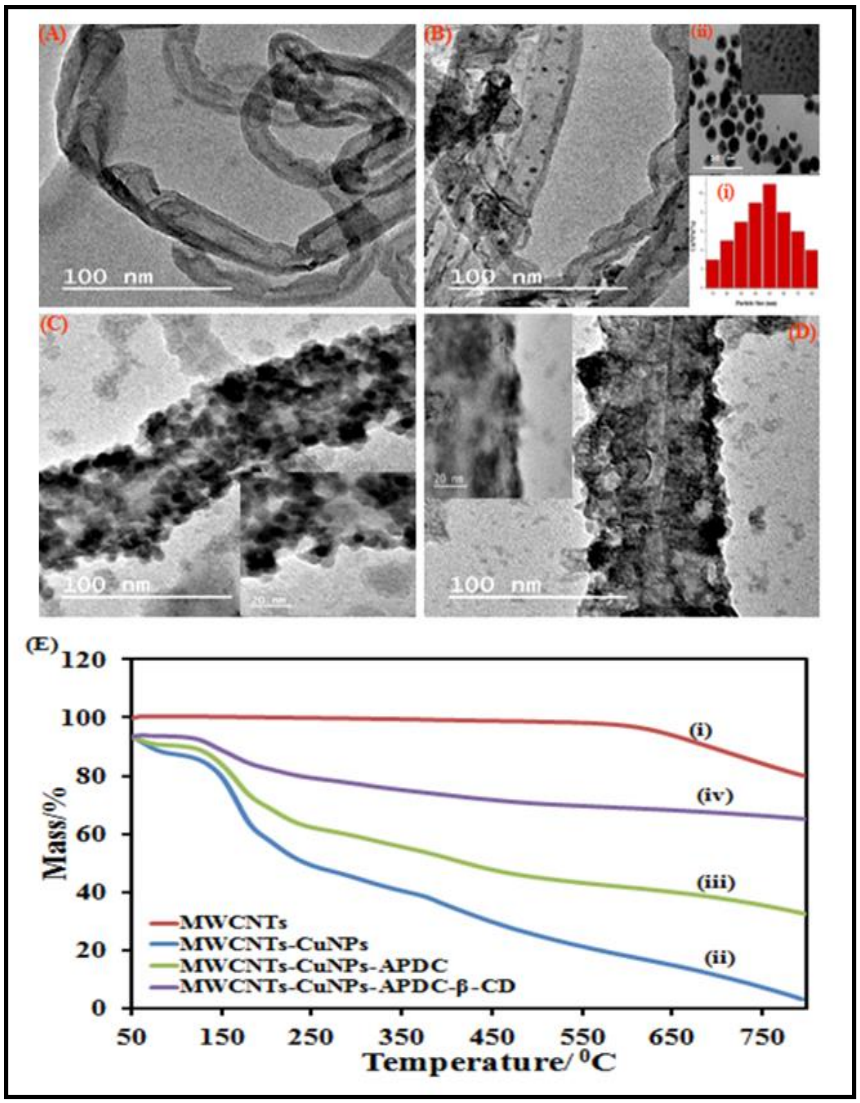

Figure 6.1: TEM images of (A) pure MWCNTs (B) MWCNTs–CuNPs (C) CuNPs–APDC–MWCNTs (D)CuNPs–APDC–MWCNTs-β-CD (E) TGAcurves (i)MWCNTs (ii) CuNPs–MWCNTs (iii) CuNPs–APDC–MWCNTs (iv) CuNPs–APDC–MWCNTs-β-CD

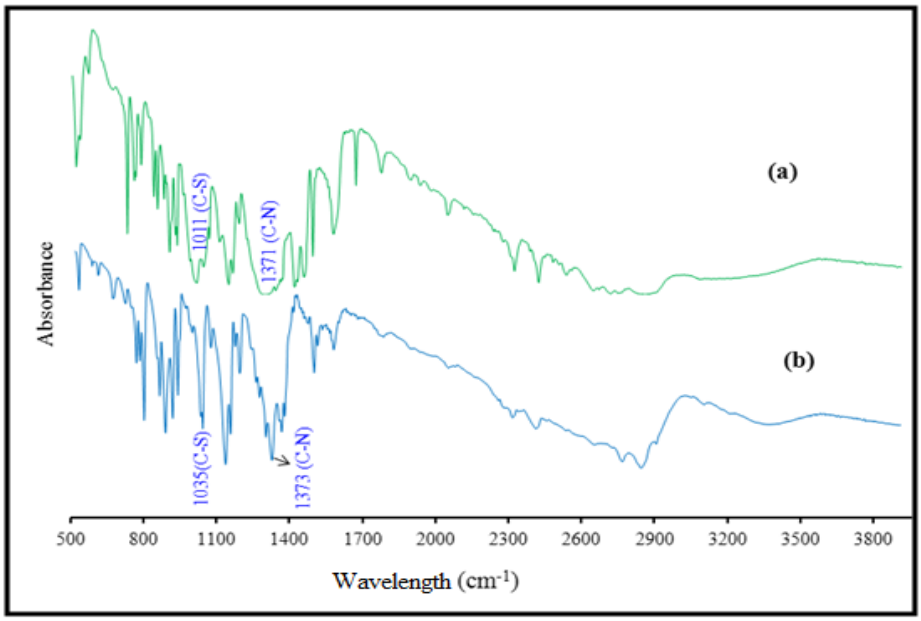

Figure 6.2: FT-IR spectras of (a) CuNPs capped APDC (b) Pure APDC

Furthermore, XRD analysis carried out to confirm the presence of CuNPs on the surface of MWCNTs, is depicted in Figure 6.3. The XRD patterns of Cu/MWCNT over the range of angle shift values of 10^0- 80^0. In the diffraction pattern (2θ) of Cu/MWCNT, with a single small peak observed approximately at 26.5 and three prominent peaks were observed at 43.5, 50.6 and 64.2, respectively. The smaller peaks correspond to MWCNTs (002) and the remaining three peaks were related to (111), (200) and (220) planes of face-centric-cubic (FCC) of copper metal. Our XRD results clearly confirm that MWCNTs are coated with CuNPs [Lin et al., 2013; Peng and Chen, 2009]. The average crystalline size of CuNPs was calculated according to the Scherrer's equation [Eqn 6.1] [Martins et al., 2014].

$$D = \frac{0.9\,\lambda}{\beta \cos\theta} \qquad \text{[Eqn 6.1]}$$

where D is the crystallite size, λ represents the X-ray wavelength of 1.54 Å, 0.9 is an approximated constant for sphere samples, θ represents the Bragg diffraction angle and β represents the full width at half maximum (FWHM) of the peak.

The Williamson-Hall equation is given by Eqn 6.2:

$$\beta \cos\theta = \frac{0.9\,\lambda}{D} + 2\,\mathcal{E}\sin\theta \qquad \text{[Eqn 6.2]}$$

where β is the full width at half maximum (FWHM) of the XRD all peaks, D is the crystallite size, 0.9 (K) is Scherrer's constant, λ the wavelength of the X-ray, ε the lattice strain, and θ the Bragg angle. $\beta \cos\theta$ is plotted against 2 sin θ along y and x axis respectively. The crystallite size is given by the intercept $K\lambda/D$ and the strain (ε) is given by the slope. The crystallite size estimated from different peaks in the XRD patterns is in the order of 22–40 nm, resulting in average size of 31.4 nm from all the peaks.

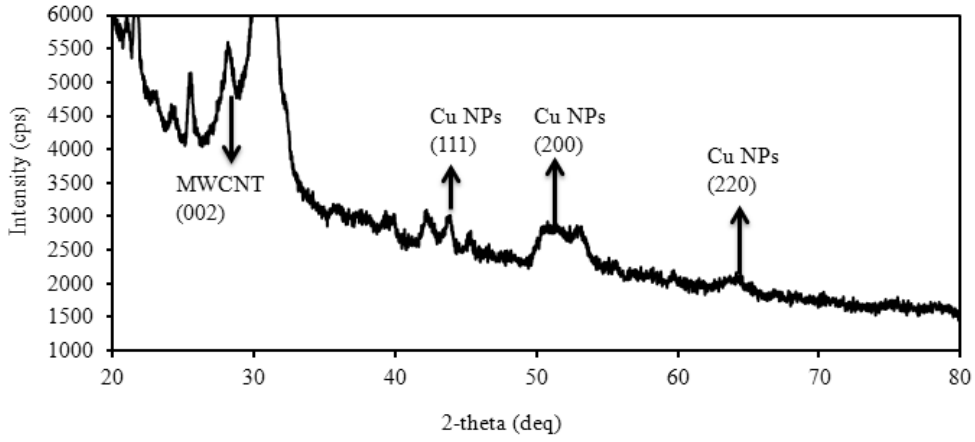

Figure 6.3: XRD patterns of CuNPs fabricated MWCNTs nanocomposite

6.1.2 Electrochemical characterization of the sensor and NTM behaviour to CuNPs-APDC-MWCNT- β-CD –GCE

The developed electrochemical sensor was characterized by cyclic voltammetry (CV), using $K_3Fe(CN)_6$ as a probe in a 1 M solution. The microscopic areas of the CuNPs–APDC–MWCNTs-β-CD modified and the bare GCE were obtained at different scan rates [Kaur et al., 2013] according to the Randles–Sevcik equation [Eqn 6.3],

$$i_{pa} = 2.69 \times 10^5 A C_0 n^{3/2} D_R^{1/2} v^{1/2} \quad \text{[Eqn 6.3]}$$

where i_{pa} is the anodic peak current, A is the surface area of the electrode, C_0 is the concentration of the $K_3Fe(CN)_6$, n is the number of electrons transferred, D_R is the diffusion coefficient, and v is the scan rate. The diffusion coefficient (D_R) of $6.9X10^{-6}$ cm^2s^{-1} was calculated from the slope of the i_{pa}–$v^{1/2}$ graph. In the case of CuNPs–APDC–MWNTs-β-CD modified GCE, the electrode surface area was $0.674cm^2$, while the bare GCE was nearly five times smaller than the modified electrode. The electrochemical performance of the CuNPs–APDC–MWCNTs-β-CD-GCE towards the detection of NTM was evaluated by measuring the current–potential responses. First, a comparative study on the behavior of the bare GCE and the MWCNTs-β-CD-GCE was investigated using CV in a 10 mL phosphate buffer (pH3.0) at a scan rate of $0.11Vs^{-1}$.

The mechanism for the oxidation of NTM involved a single proton and electron to produce hydroxylamine and an aldehyde, resulting in the appearance of an irreversible oxidation peak at 1.30 V (versus Ag/AgCl) in the potential ranging from -0.2 to 2.0V [Scheme 6.1] as reported in the literature [Medeiros et al., 2007, 2008; Elmer et al., 1978].

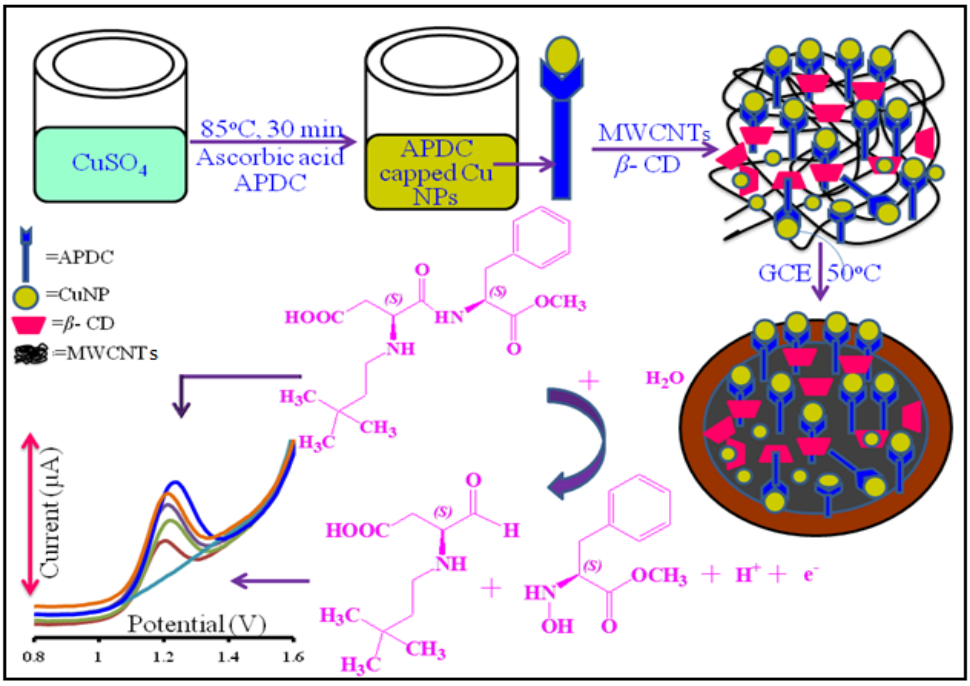

Scheme 6.1: A schematic representation of the typical electrooxidation of NTM at CuNPs-APDC-MWCNTs-β-CD modified GCE

Figure 6.4A shows the response of NTM with the GCE (curve a), MWCNTs-β-CD-GCE (curve b) and CuNPs–APDC–MWCNTs-β-CD (curve c). However, curve d in Figure 6.4A represents the response of a CuNPs–APDC–MWCNTs-β-CD electrode in a blank solution. The oxidation peak for the bare GCE was sluggish, broad and much smaller. In contrast to the bare GCE, well-defined peaks observed with good responses for the MWCNTs-β-CD-GCE and CuNPs–APDC–MWCNTs-β-CD electrodes. The bar-graph [inset of Figure 6.4A] shows a comparative current response for the three electrodes, with the peak currents of NTM recorded at the bare GCE (curve a) and the MWCNTs-β-CD-GCE (curve b). Clearly, the peak currents recorded for CuNPs–APDC–MWCNTs-β-CD (curve c) were higher than the currents obtained for a bare electrode and the MWCNTs-β-CD-GCE (curves a-b). On this basis, the nanometer dimensions and the topological effects of the MWCNTs, CuNPs–MWCNTs surfaces [Kara et al., 2010; Pilehvar et

al., 2014] resulted in a significant catalytic effect for the electrochemical oxidation of NTM in-terms of peak currents.

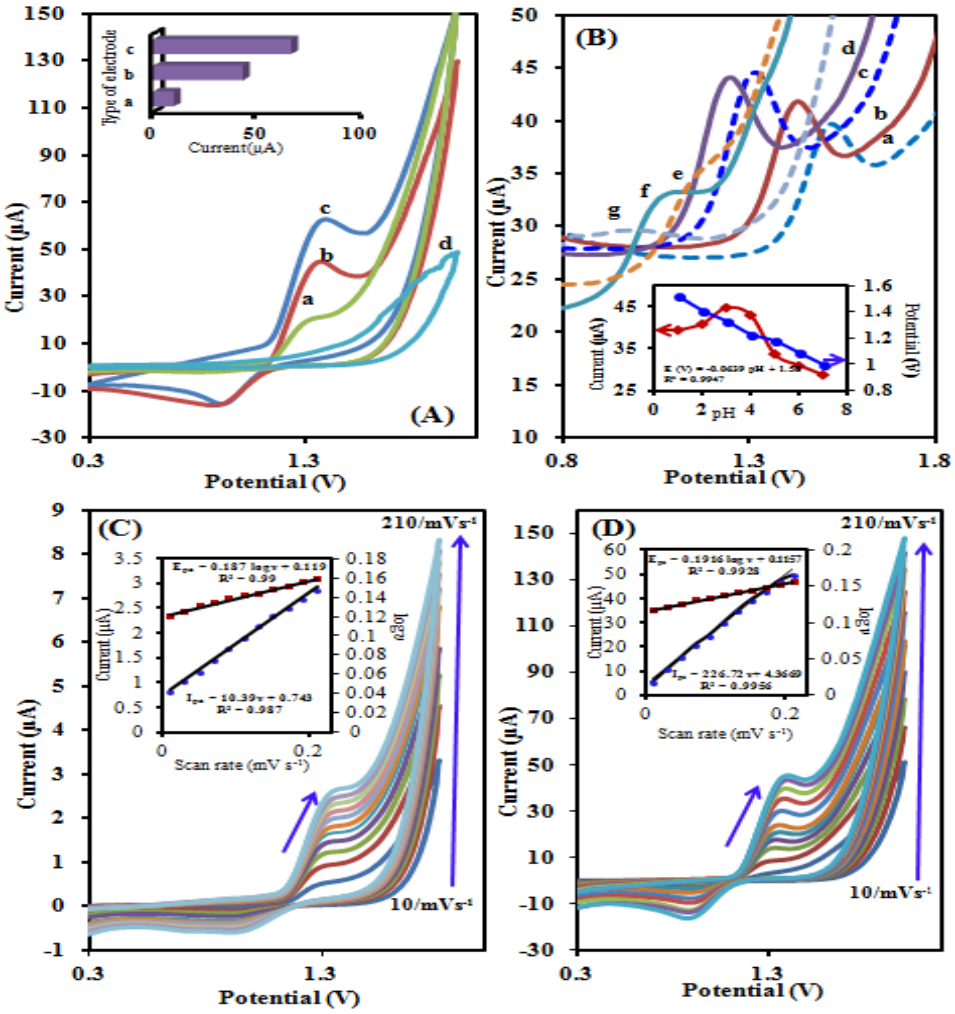

Figure 6.4: (A) Cyclic voltammograms of 0.5 mM NTM at (a) bare GCE (b) MWCNTs-GCE and (c) CuNPs-APDC-MWCNTs-β-CD-GCE, inset: current comparison among three electrodes. (B) DPV responses of 0.5 mM NTM at Cu NPs-APDC-MWCNTs-β-CD-GCE at different pHs: a (1), b (2), c (3), d (4), e (5), f (6), g (7), inset: The plot of pH verses peak current and peak potential in phosphate buffer (pH 3.0), Scan rate: 0.11 V s^{-1}. Cyclic voltammograms of (C) bare GCE and (D) CuNPs-APDC-MWCNTs-β-CD-GCE at different scan rate. The scan rate from inner to outer are 0.01, 0.03, 0.05, 0.07, 0.09, 0.11, 0.13, 0.15, 0.17, 0.19, 0.21 V s^{-1}, respectively. Inset is the plot of scan rates versus anodic peak currents and log *v*.

6.1.3 Effect of pH and scan rate on the peak potentials and peak current

In this study the effect of pH ranging from 1.0 to 7.0 was investigated on the anodic peak potentials and peak currents of NTM using the DPV method in a solution containing 0.5 mM NTM. Figure 6.4B shows the electrochemical behavior of NTM on the CuNPs–APDC–MWCNTs-β-CD electrodes at different pHs. Clearly, the peak potentials linearly decreased with the increase in pH with a slope [inset Fig. 6.4B] of 63.9mV/pH. Our results are similar to those reported in literature [Medeiros et al., 2007, 2008], suggesting that equal number of protons and electrons were involved in the overall oxidation process. In this study the electrochemical response (i_{pa}) for the detection of NTM due to the CuNPs–APDC–MWCNTs-β-CD electrodes were pH dependent. The maximum peak currents observed at pH 3.0 [Figure 6.4B inset], due to the dissociation of the amide bond into two molecules, resulting in higher current signals. Consequently, the phosphate buffer at pH 3.0 was selected as the optimum for the determination of NTM.

The effect of scan rate on peak currents and potentials were investigated using 0.5 mM NTM ranging from 0.01 to 0.21 Vs^{-1}. The CVs of NTM at pH 3.0 on the bare GCE and the CuNPs–APDC– MWCNTs-β-CD electrodes at different scan rates are depicted in Figure 6.4C-D. The oxidation peak current gradually increases with an increase in scan rate on the bare and the modified electrode. In case of both bare and modified GCEs, a maximum scan rate of 0.21Vs^{-1} resulted in peak currents of 2.6 and 48 mA respectively, indicating a linear relationship with scan rate between NTM and the modified electrode surface [inset Figure 6.4C-D]. The peak potential of NTM shifted linearly towards the more positive values with increasing scan rates, hence the optimum scan rate of 0.11 Vs^{-1} was selected in this study. At this scan rate the electron transfer rate constant, *Ks* for CuNPs–APDC–MWCNTs-β-CD/GCE electrode surface were calculated

based on the Laviron's equation [Zhou et al., 2013] [Eqn 6.4]. The average *Ks* values for the bare and modified GCEs were 1.14s^{-1} and 5.78s^{-1} respectively.

$$E_{pa} = E^0 + \frac{RT}{(1-\propto)nF}\ln v$$

$$\log ks = \alpha \log (1\text{-}\alpha) + (1\text{-}\alpha) \log \alpha - \log \frac{RT}{nFv} - \frac{(1-\alpha)\alpha nF\Delta E_p}{2.3\ RT} \quad \text{[Eqn 6.4]}$$

6.1.4 The DPV technique for quantitative determination of NTM

Based on the higher current sensitivity and better peak separation, DPV was used for the sensitive detection of NTM using CuNPs–APDC–MWCNTs-β-CD/GCE [Zhou et al., 2013], and the optimized parameters were tabulated in Table 6.1. Figure 6.5A shows the DPV response for the various concentrations of NTM in two intervals for the modified electrode in 0.1 M phosphate buffer (pH 3.0). The results illustrate a linear relationship between the concentration of NTM and anodic peak currents observed in the concentration ranging from 0.03 to 2.0 mM. The anodic peak current at 1.2 V increased with an increasing concentration of NTM, the first (a-e) and second (f-o) interval calibration curves (insets i and ii) were obtained at low concentrations ranging from 0.03 to 0.15 mM and from 0.2 to 2.0 mM with a detection limit of 0.013 mM. The results were compared with CE in terms of detection limits at different concentrations ranging from 0.05 to 2 mM as shown in Figure 6.5B. From the obtained analytical outputs, it is clear that the proposed electrochemical method showed lower limits of detection than the CE method. These results suggest that the developed electrochemical sensor is suitable and efficient for the detection of NTM in food samples.

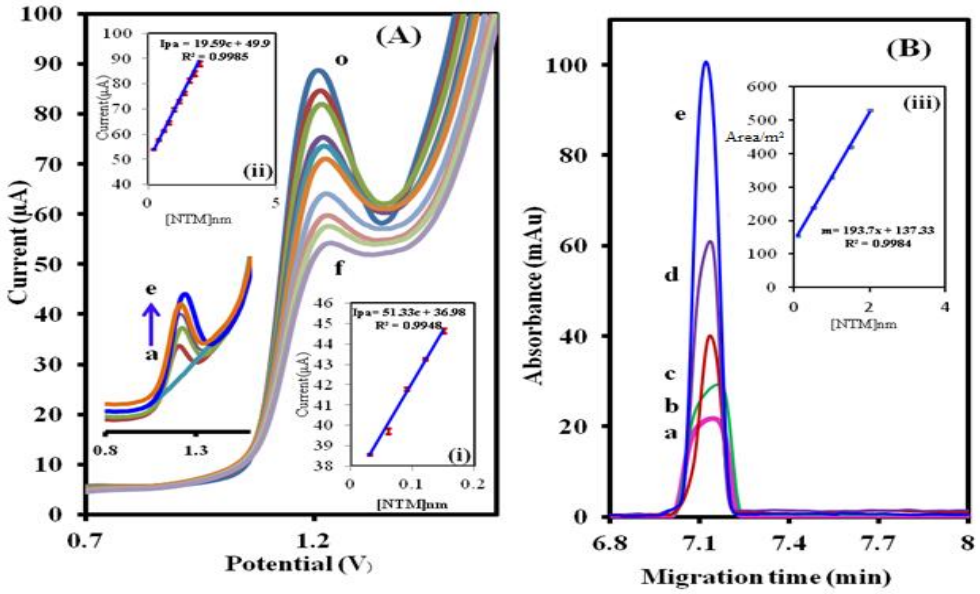

Figure 6.5: (A) DPVs recorded at CuNPs-APDC-MWCNTs-β-CD-GCE at different concentrations of NTM a→e (0.03 to 0.15 mM) and f→o (0.2 mM to 2mM), inset: plots (i) and (ii) shows for linear dependence of I_{pa}vs [NTM]. (B) Electropherograms obtained using CE method at different concentrations of NTM a→e (0.05 to 2 mM), inset shows calibration curve for [NTM] vs peak area at pH 3.0, accumulation time: 30 s, accumulation potential: 0.11 V s^{-1}, pulse amplitude: 50 mV, voltage step: 2 mV and voltage step time: 0.4 s

Table 6.1: Experimental results of the optimized parameters containing 0.1 mM NTM

Parameters	Peak response i_{pa}(µA)						
pH	1.0	2.0	3.0	4.0	5.0	6.0	7.0
i_{pa}(µA)	39.3	40.8	44.6	42.9	33.6	31.0	28.7
Depostion time (s)	5	10	15	20	25	30	35
i_{pa}(µA)	40.2	41.5	42.1	42.9	43.8	44.5	45.1
Deposition potential (V)	-0.5	-0.3	-0.1	0.0	0.1	0.3	0.5
i_{pa}(µA)	38.6	39.8	40.7	41.2	42.8	43.1	43.6
Pulse amplitude (V)	0.01	0.02	0.03	0.04	0.05	0.06	0.07
i_{pa}(µA)	25.3	31.6	35.4	39.7	43.3	42.1	42.9
Voltage step (V)	0.005	0.01	0.02	0.03	0.04	-	-
i_{pa}(µA)	43.0	43.2	46.9	46.5	45.8	-	-
Voltage step time (s)	0.2	0.3	0.4	0.5	0.6	0.7	0.8
i_{pa}(µA)	32.1	40.7	45.8	44.2	43.7	39.8	37.2

6.1.5 Stability, recovery, accuracy and precision studies

The stability of the sensor was tested using CV in a phosphate buffer at pH 3.0, resulting in a 4.1% decrease in the current response after 50 cycles. The long term stability of the sensor was observed by measuring the responses in 0.5 mM NTM over a range of ten runs over three days using the same coating. The sensor maintained 83.0% of the original response on the third day, clearly suggesting that the sensor retained its activity to a large extent. The analytical parameters in terms of accuracy, precision and recovery were estimated by analyzing three different concentrations of standard NTM in triplicate on one day ranging from 0.05 to 0.15 mM. The range of values for the relative error (bias) and %RSD were -0.109 to -0.038 and 0.71 to 1.36 respectively, indicating a higher accuracy and precision of the developed method [Table 6.2]. The percentage recoveries of NTM from the fabricated sensor ranged from 89.0% to 96.0%. On the other hand, the reproducibility of the sensor was studied by assaying the CV peak currents using 0.5 mM NTM on three different modified GCE for three replicate measurements. A %RSD of 1.89 suggests an acceptable reproducibility of the developed sensor.

Table 6.2: Analytical parameters (stability, accuracy, precision and recovery (n=3)) obtained for NTM at CuNPs-APDC-MWCNTs-β-CD-GCE

Stability		Analytical parameters				
Day	Peak response[a] (I_{pa})	Added (mM)	Found (mM)	Bias[b]	Recovery (%)	RSD[c] (%)
1	55	0.1	0.089	-0.109	89	0.71
2	51	0.2	0.192	-0.038	96	1.24
3	46	0.3	0.276	-0.078	92	1.36

[a]Average of three determinations,
[b]Bias= (found-added/added)× 100,
[c]Relative standard deviation for three individual determinations

6.1.6 Real sample analysis

The applicability of the developed sensor was tested under the optimum conditions using three different NTM spiked samples described in the methods section 4.1.3. Furthermore, the obtained results were validated with the CE method, three sets of spiked food samples (0.05, 0.10 and 0.15 mM) were studied using voltammetric and CE methods. The % RSDs of NTM in three samples were 1.3 to 2.1 % and 1.1 to 1.9 % and recoveries ranging from 94.33 to 98.97 % and 95.66 - 98.14 % with relative errors -2.0 to -5.7 and 1.87 to -2.98 for voltammetric and electrophoretic methods respectively as shown in Table 6.3.

The validation of the CE and voltammetric techniques was accomplished by applying the paired *t*-test [Anderson, 1987]. It was found that all results are in agreement at the 96% confidence level. The calculated *t*-test value of 2.53 was less than that of the theoretical value 2.81 for *t*-test. Also, from the Table 6.3 it was observed that there were no significant differences between the amount of NTM obtained by the voltammetric and the CE methods, showing the validity of the developed method. Thus suggesting that, the determination of NTM can be carried out with great confidence in food samples by the proposed method.

Table 6.3: Results obtained for the determination of NTM in spiked food samples analyzed by DPV and CE methods

Sample	NTM added (mM)	Recovered by DPP[a]	Recovered by CZE[a]	Relative error 1 (%)[b]	Relative error 2 (%)[c]
SS-1	0.05	98.97 ±1.3	96.23 ±1.9	-2.0	1.87
SS-2	0.10	94.33 ±2.1	95.66 ±1.5	-5.7	-1.35
SS-3	0.15	95.24 ±1.7	98.14 ±1.1	-4.8	-2.98

SS=Spiked sample,[a]Average of 3 measurements.
[b]Relative error 1 (%) = 100×(DPP value−added value)/added value.
[c]Relative error 2 (%) = 100×(DPP value−CZE value)/CZE value.

6.1.7 Effect of potential interferents

The selectivity of the proposed method was studied by the simultaneous addition of possible interferents like acesulfame K, saccharine, aspartame, cyclamate, tryptophan, tyrosine, sodium benzoate, silicon dioxide, sunset yellow, tartrazine and brilliant blue to 0.05 mM NTM standard solution. The anodic peak potentials of the intereferents, aspartame (0.9 V), tartrazine (1.6 V), cyclamate (1.9 V) and acesulfame K (2.2 V) were observed for CuNPs-APDC-MWCNT-GCE using DPV. The applied tolerance limits for the interfering species were the maximum concentration that resulted in a relative error of ±5%. From such studies, 50-fold tryptophan, tyrosine, sodium benzoate, silicon dioxide, sunset yellow, tartrazine and brilliant blue and 10-fold acesulfame K, saccharine, aspartame, cyclamate showed no effect on the determination of NTM. These results suggest that, the determination of NTM in food samples should not significantly be affected by the potential common interferents mentioned above.

6.1.8 Biological applications: Voltammetric behaviour of NTM with metals

The cell wall selectively allow ions based on the charge, size and nature of the ligand. The cell membrane on the other hand mediates the movement of the ligands and ions from external environments to the cellular fluids. In the case of anions and gases, the energy barrier to penetrate through the hydrophobic environment is lower, due to smaller charge-radius ratio and a lower charge density than cations. Hence, anions penetrate directly through the cell membrane than cations [Cowan, 1993]. To overcome this drawback, NTM-metal complexes were investigated to better understand the metal ion affinities of Ni^{2+}, Cu^{2+} and Zn^{2+} with interesting application for biological systems.

6.1.8.1 Cyclic and differential pulse voltammetric analysis of NTM-Ni^{2+} complex

The cyclic voltammogram of 2 mM nickel chloride resulted in a cathodic peak (P1) at -1.5 V in the absence of NTM. The peak at -1.5 V inferred from the reduction of hydrated Ni^{+2} ions. The addition of NTM to 2 mM hydrated Ni^{+2} at pH 5.5 led to the formation of a new peak at positive potentials than that of hydrated Ni^{+2} ions [Figure 6.6A]. This new peak probably related to the complexation of NTM and the hydrated Ni^{+2} ions. At lower concentrations of NTM, the new peak was observed at -1.35 V and with increase in the concentration of NTM, the peak predominantly shifted towards the more positive potential. The well-defined peak shape was observed with two fold concentration of NTM at -1.24 V, further increased in the concentration of NTM with no significant potential changes observed.

Similar results were observed with DPV, without NTM hydrated Ni^{+2} ions undergoing reduction at -1.5 V (P1). The addition of NTM caused a decrease in overvoltage of Ni^{+2} ions and reduction occurred at more positive potentials. Hence, for NTM-Ni^{+2} complex reduction peak observed at -1.25 V (P2). With an increase in concentration of NTM, the current of P1 decreased while an increase in the current of P2 was observed [Figure 6.6D].

6.1.8.2 Cyclic and differential pulse voltammetric analysis of NTM-Cu^{2+} complex

The cyclic voltammogram of 2 mM copper chloride in 0.1M phosphate buffer (pH 5.5) resulted in a reversible peak with two electron reaction [$Cu^{+2} \leftrightarrow Cu^{0}$] at -0.008 V. Based on the structure of the coordinating ligand, copper undergoes one step or two step reduction [Crow, 1969]. In the presence of NTM, copper ion shows two quasi-reversible peaks at 0.07 V (P1) and -0.28 V (P2) and one irreversible peak at -0.41 V (P3) as shown in Figure 6.6B. The peaks at 0.07 V (Cu^{+2}

$\rightarrow Cu^{+1}$) and -0.28 V ($Cu^{+1} \rightarrow Cu^{0}$) specify the reduction reaction was in two steps and the peak at -0.43 V attributed to NTM-Cu^{+2} complexes.

Similar results were obtained with DPV, in absence of NTM copper ions undergo reduction at -0.08 V and the addition of NTM resulting in two quasi-reversible steps (0.07 V and -0.28 V). The irreversible reduction reaction of NTM-Cu^{+2} complexes observed at -0.43 V. Both forms of Cu^{+1} and Cu^{+2} shows complexes with NTM, due to d–π interactions between the copper d- orbitals and the aromatic π-system stabilization occurs for NTM-Cu^{+1} complex rather than the binding of the metal with the carboxylate group for NTM-Cu^{+2} complex. With an increase in the concentration of NTM, the peak currents at -0.43 V increased because, the concentration of Cu(II)L_2 increased while those of first and second decreased [Figure 6.6E].

6.1.8.3 Cyclic and differential pulse voltammetric analysis of NTM-Zn^{2+} complex

The cyclic voltammogram of 2 mM zinc chloride showed one peak (P1) at -1.13 V due to the reduction of the free Zn^{+2} in the absence of NTM. The addition of high concentrations of NTM (6 fold compared to Zn concentration) into the cell containing 0.1 M phosphate buffer at pH 5.5 and 2 mM Zn^{+2} resulted in a new irreversible cathodic peak (P2) at -0.83 observed, due to the reduction of NTM-Zn^{+2}complexes as illustrated in [Figure 6.6C].

Similar results were observed using DPV studies, a cathodic peak at -1.13 V was observed for reduction of free Zn^{+2} without NTM. With an increase in the concentration of NTM, the peak currents of free zinc at -0.11 V (P1) decreased while the peak currents of NTM-Zn^{+2} complexes at -0.85 V (P2) increased as presented in Figure 6.6F.

6.1.9 FT-IR characterization of NTM-metal complexes

NTM and metal complexes were characterized using FT-IR and the data are shown in Table 6.4. The significant absorption peaks observed in NTM at 1691 cm^{-1}*(s)*,1729 cm^{-1}*(s)* and 1598 cm^{-1}*(s)* corresponds to the amide carbonyl (-C=O), ester carbonyl (-C=O) and carboxylic carbonyl (-C=O) group in zwitterionic form, respectively. A small peak observed at 1544 cm^{-1}*(b)* was attributed to the β-amino group (-NH) in NTM. Whereas in NTM-metal complexes,the carboxylic carbonyl (-C=O) (1544 cm^{-1}) and β-amino groups (-NH) (1598 cm^{-1}) were drastically shifted to 1627 and 1568 cm^{-1} respectively. This indicates that, the carboxyl carbonyl (-C=O) group and β-amino groups (-NH) were participating in coordination with metals as shown in Figure 6.7.

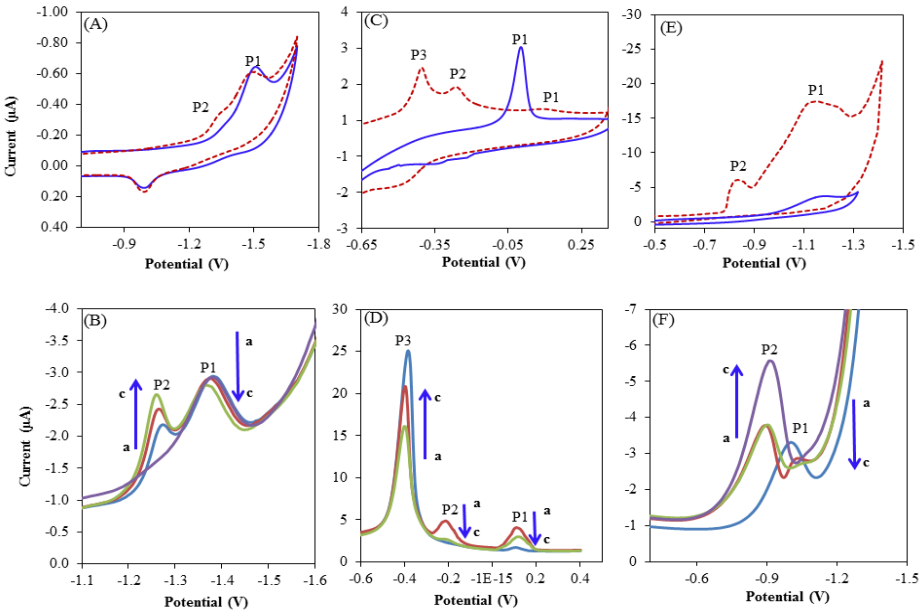

Figure 6.6: Cyclic voltammograms for (A) 2 mM $NiCl_2$ (—) and 5mM NTM solution containing 2mM $NiCl_2$ (---) (B) 2 mM $CuCl_2$ (—) and 4 mM NTM solution containing 2 mM $CuCl_2$ (---) (C) 2 mM $ZnCl_2$ (—) and 6 mM NTM solution containing 2 mM $ZnCl_2$. DPVs recorded for (D) $NiCl_2$ (P1) and NTM-Ni complex (P2) (E) $CuCl_2$ (P1) and NTM-Cu complex (P3) (F) $ZnCl_2$ (P1) and NTM- Zn complex (P2) at pH 5.5 scan rate 0.11 V s^{-1}

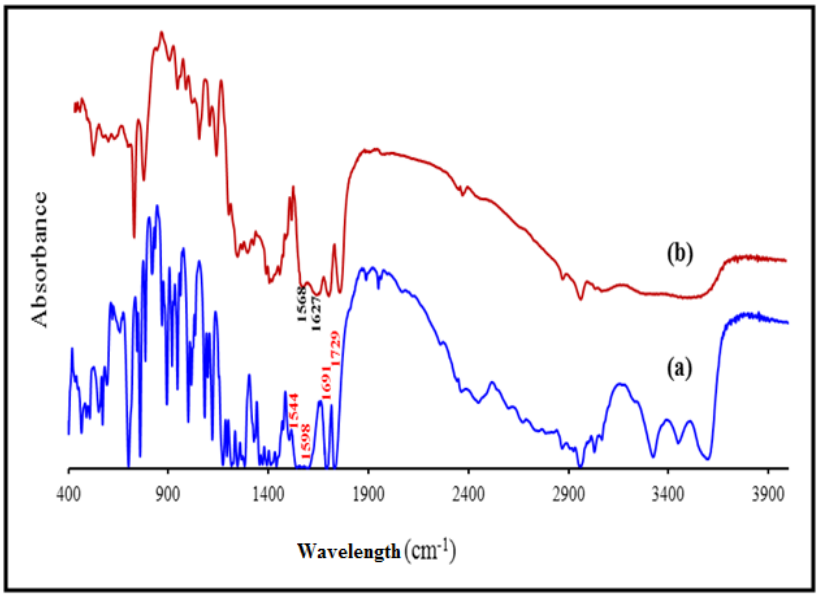

Figure 6.7: FT-IR spectras obtained for (a) Pure NTM (b) NTM in presence of divalent cation (Zn^{2+})

6.1.10 Composition and stability of NTM-metal complexes

The stoichiometry and formation or the stability constants of the neotame with metals were determined using UV-vis spectroscopy. NTM and its metal complexes showed several absorption maxima in the UV–vis region. The position of the absorption bands and the stability constants of NTM and its complexes are given in Table 6.4. The data in Table 6.4 suggests that, the UV absorptions bands (Band I) of the complexes can be assigned to the metal–ligand charge transfer bands while their absorptions (Band II) in the visible region are attributed to the d–d transitions. The plot of absorbances versus the molar ratios of NTM to metals were attained by changing the concentration of NTM, showed a variation at molar ratio 1.0 as shown in Figure 6.8. This indicates that one NTM molecule participating in the coordination with metals and with the

stoichiometry ratio of 1:1. Moreover, Job's method showed similar stoichiometry with the metals for the dipeptide esters [Cakir et al., 2003]. The conditional formation constant (log K) were calculated using Harvey and Manning equation [Harvey and Manning, 1950] [Eqn 6.5],

$$K_n = \frac{(A/A_m)}{(1 - A/A_m)^{n+1} C_R n^2} \qquad \text{[Eqn 6.5]}$$

where *Kn* is the formation constant, C_R is the reagent concentration, *A* is the absorbance of C_R, A_m is the maximum absorbance and *n* is the stoichiometric ratio obtained from molar ratio method. The formation constant results obeys the Irwing–Williams series (Ni<Cu>Zn) [Martin, 1973] which explains the metal complexation stabilities.

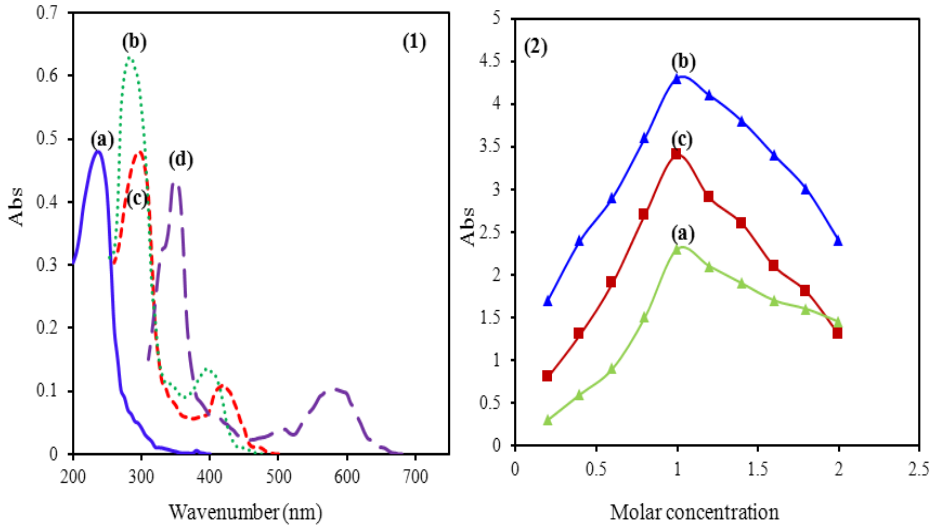

Figure 6.8: (1) UV spectras obtained for (a) NTM (b) NTM-Cu^{2+} (c) NTM-Ni^{2+} (d) NTM-Zn^{2+} complexes. (2) Molar ratio plots (a) NTM-Cu^{2+} (b) NTM-Zn^{2+} (c) NTM-Ni^{2+}

Table 6.4: FT-IR charectarization and UV-Spectroscopy results for NTM and NTM-metal complexes

FT-IR Analysis					UV-Spectroscopy			
Component	Carboxyl carbonyl	Ester carbonyl	Amide carbonyl	β-amino group	Band I	Band II	Molar Ratio (M:L)	Log (k)
NTM	1598	1729	1691	1544	220			
NTM-Ni^{+2} complex	1654	1731	1679	1583	351	573	1:1	7.12
NTM-Cu^{+2} complex	1637	1718	1711	1573	294	437	1:1	8.25
NTM-Zn^{+2} complex	1627	1742	1682	1568	276	415	1:1	4.09

6.1.11 Isothermal titration calorimetry

The principle of isothermal titration calorimetry (ITC) involved measuring not only the binding stoichiometry (n) and enthalpy changes (ΔH), but also the binding affinity constant (K). The entropy changes (ΔS) and Gibbs energy changes (ΔG) are derived from the thermodynamic relationships:

$\Delta G = -RT\ InKa = \Delta H - T\Delta S$ (R is the gas constant and T is the absolute temperature). Traditionally, ITC experiments were performed using an incremental titration method, whereby a fixed volume of the titrant is added to a solution at specific time-intervals [Demarse and Quinn, 2011]. The peak areas were then integrated and the binding affinities, enthalpy and stoichiometry for the interactions were calculated.

In the traditional incremental-ITC experiments, different metals were titrated with the ligand NTM and an exothermic interaction (n = 1) was obtained, corresponding to the formation of NTM-metal

complex. The heat flow for the metals were increased until saturation point, and then gradually decreased, resulting in the heat of dilution being measured. The peak areas plotted against the molar ratio (titrant: titrand) [Chekmeneva et al., 2010] are illustrated in Figure 6.9. The data analysis revealed that the association constant (Ka) of 1.23 $\times 10^2$ and the binding affinity values for Ni^{2+}, $Cu^{2+}$and Zn^{2+}were found to be 371.08, 351.12 and 259.04 kcal/mol with a stoichiometry ratio of 1:1. The binding affinity values obtained from the experiment were in similar trend with DFT calculations.

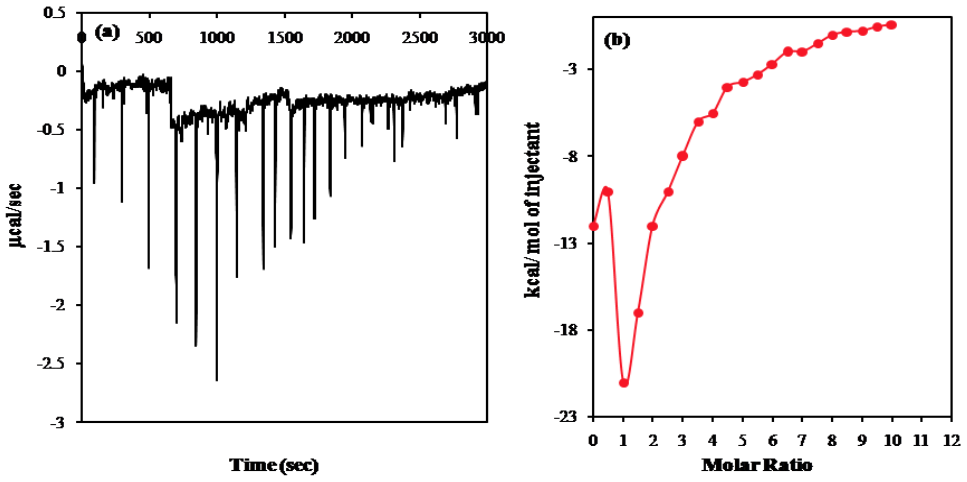

Figure 6.9: Isothermal titration curve obtained during the titration of divalent ions (Ni^{2+},Cu^{2+}, Zn^{2+}) with NTM (a) at 25 ^{0}C in 0.1 mol/ L phosphate buffer at pH 5.5. Molar ratio plot calibrated from peak areas of NTM-Metal titrations.

6.1.12 Computational discussion

Initially, the conformational profile of NTM was explored using the Generate conformations [Li et al., 2007] module embedded in Discovery Studio (DS) 4.0 modelling software program. Of the 100 conformations obtained, 20 conformations with energies less than 10 kcal/ mol were partially optimized using the Energy minimization module in DS. The lowest energy conformation depicted in Figure 6.10 was further re-optimized using the Gaussian 09 program [Frisch et al., 2009] at the density functional theory (DFT) level in combination with the 6-31g** basis set. A closer inspection of Figure 6.10A revealed the presence of two potential co-ordination sites for the metals through its amide nitrogen and the acid carbonyl oxygen, similar to those identified for its structural analogue aspartame [Rashidian and Fattahi, 2009]. Accordingly, the optimization of NTM with the metals Ni^{2+}, Cu^{2+} and Zn^{+2} were performed using both binding sites at the DFT level using mixed basis sets, and the results are pictorially depicted in Figure 6.10. All optimized structures in their ground state minima, were verified by the second derivative frequency calculations.

The computed inter-atomic distances between the donor atoms of NTM and the Ni^{2+}centres in their respective complexes (N-Ni^{2+}=1.93, CO-Ni^{2+}=1.99) were comparatively shorter than those present in the complexes of NTM-Cu^{2+} (N-Cu^{2+}=1.94, CO-Cu^{2+}=2.05) and NTM-Zn^{2+} (N-Zn^{2+}=2.0, CO-Zn^{2+}=2.3) clearly suggesting a compact nature of the complexes with a tighter binding energy in case of the NTM-Ni^{2+}complex followed by NTM-Cu^{2+} and NTM-Zn^{2+} complexes. The additional electrostatic interaction energy of the copper and nickel metals with the aromatic π-electrons of NTM could be a contributing factor in the stabilization of their complexes. However, the *trans* orientation of the phenyl ring of the metal prohibited this interaction in the case of NTM-Zn^{2+} complex. The bidendate co-ordination nature through the

nitrogen and oxygen atoms of the amino acids observed in this study are consistent with those reported in literature [Rashidian and Fattahi, 2009].

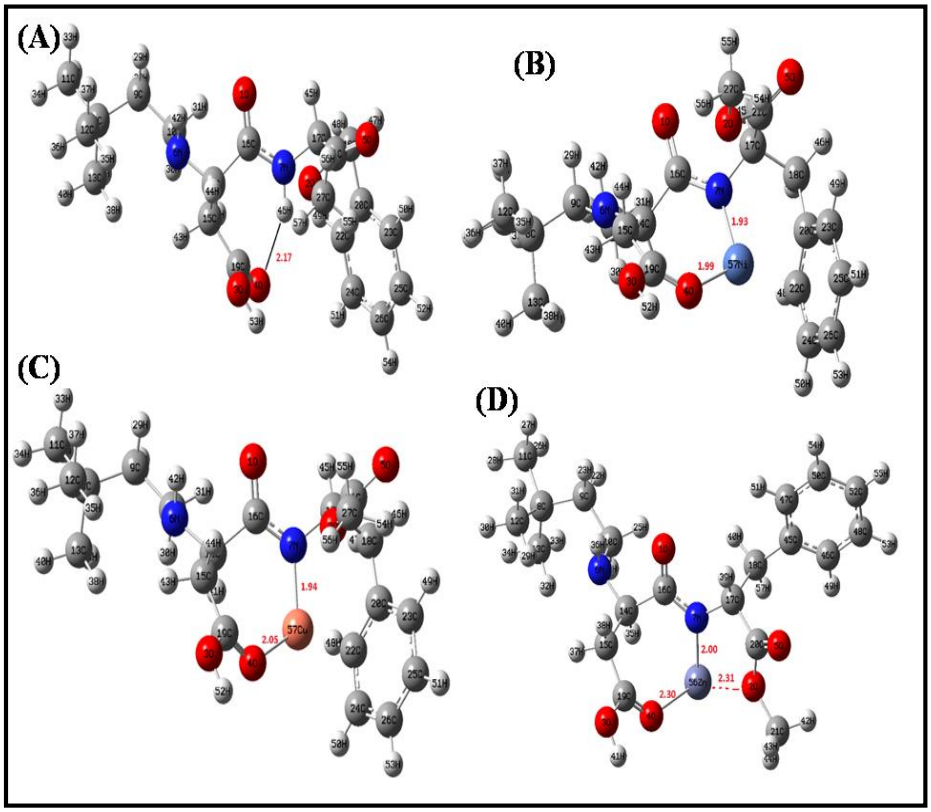

Figure 6.10: (A) The optimized geometry of NTM at B3LYP level. The complexes of (B) Ni^{2+}, (C) Cu^{2+} and (D) Zn^{2+} with NTM, optimized at B3LYP level using lanl2dz/tzvp mixed basis sets

Furthermore, the gas phase metal ion affinities (MIAs) of NTM with Ni^{2+}, Cu^{2+} and Zn^{+2} were computed at the DFT level using the B3LYP exchange-correlation functional according to the following equation [Eqn 6.6],

$$B+M \Longrightarrow BM^{+}$$

$$MIA = - [E_{el}(BM^{+}) - E_{el}(B) - E_{el}(M^{+}) + (E_{vib}(BM^{+}) - E_{vib}(B))] \quad \text{[Eqn 6.6]}$$

where B= NTM, M=metal, E_{el} = electronic energy obtained from the SCF computation

E_{vib} = zero point energy+ temperature corrections

The electronic energies of NTM and its metal complexes along with MIA are depicted in Table 6.5. Clearly, NTM exhibits a stronger affinity with Ni^{2+} (380 kcal/mol) followed by Cu^{2+} (345 kcal/mol) and Zn^{2+} (264 kcal/mol), in agreement with the inter-atomic distance analysis described above. Additionally, the DFT predicted MIA energies also exhibited good agreement with the experimental binding affinity data obtained using ITC method [Table 6.5]. The presence of the incomplete d-shells in nickel (d^8) and copper metals (d^9) could probably have increased their electron exchange with NTM, leading to a more efficient bonding and stabilization energies of their complexes.

Table 6.5: Metal ion affinity (MIA) of NTM with different metals obtained from computationally and experimentally

System	Metal	Electronic energy ($E_{el)\ (Hartree)}$	MIA (Kcal/mol) B3LYP-lanl2dz/tzvp	MIA (Kcal/mol) ITC_{Exp}
NTM	Ni^{+2}	-2772.2	380	371
	Cu^{+2}	-2904.4	345	351
	Zn^{+2}	-3043.2	264	259

6.2 Development of Cyt c/AuNPs-GO/MWCNTs modified platinum electrode for the analysis of natural sweetener rebaudioside A (Reb A)

In this work, cytochrome c (Cyt c) immobilized on AuNPs decorated graphene oxide (GO)/multiwalled carbon nanotubes (MWCNTs) were explored to modify platinum electrodes. Even though GO sheets have a higher edge density (ρ_L), in 3D arrangement lacks to maximize their edge density. On the other hand MWCNTs have high surface area in 3D arrangement, but with lower surface charge density. When compared to these two materials, the combination of GO/MWCNTs nanocomposite provides high edge density from GO and higher surface area from MWCNTs, results in higher edge density per unit nominal area [Cheemalapati et al, 2013]. Recently, Patila et al., reported kinetic studies involving nanomaterials and Cyt c, the catalytic efficiency of Cyt c was 2.5-fold in the presence of MWCNTs and 78-fold in the presence of mixture of GO and MWCNTs. Additionally, the use of MWCNTs/GO nanocomposite enhanced the thermal stability and activity of Cyt c over a wider range of pH's [Patila et al., 2013]. The presence of AuNPs on the surface of GO/ MWCNTs gave a higher surface to volume ratio to immobilize higher quantity of Cyt c on the electrode surfaces. Moreover, Cyt c was adsorbed tightly onto the surface of the modified electrode and showed an enzyme-like activity [Wu et al., 2010] for the reduction of Reb A. Hence, the exceptional properties of Cyt c/AuNPs-GO/ MWCNTs nano composite enhance the electron transfer for the electro catalytic reduction of Reb A than with GO or MWCNTs. These nanocomposite were applied for the determination of Reb A and exhibited good sensitivity and low detection limits. Finally, docking simulations were employed to get a deeper understanding of the interactions between Reb A and Cyt c. However, AuNPs and GO/MWCNTs could not be considered in the present docking study due to software limitations and the results obtained from the present docking were thought to be adequate and

helpful to get some basic understanding of the nature of Cyt c-Reb A interactions taking place at a molecular level.

6.2.1 Characterization of Cyt c/AuNPs-GO/ MWCNTs/Pt electrode

Surface morphological characterization of AuNPs-GO/MWCNTs nanocomposite was studied using TEM. Figure 6.11A shows characteristic morphology of pure MWCNT with clear hollow cylindrically shaped shells, while in Figure 6.11B ultra-thin sheet of pure GO with a diameter of nano to sub micro meter was observed. The TEM image of MWCNT/GO nano composite [Figure 6.11C] showed, the MWCNT walls were well incorporated with ultra-thin sheets of GO [Zhang et al., 2011; Zhang et al., 2011] due to π-π interactions between the side walls of MWCNT and the hydrophilic functionalities of GO. Figure 6.11D shows the AuNPs-GO/MWCNTs nano composite and the AuNPs were well distributed in a uniform size on the GO thin sheet and with the outer surface of the MWCNTs. The higher magnification of AuNPs (10 nm) and EDS [Figure 6.11 E-F] showed the coated AuNPs were evenly distributed on the surfaces with a tendency of the aggregation being reduced by the presence of hydrophilic functionalities of GO.

Furthermore, the nanocomposites were characterized by UV-Vis spectroscopy and the results showed that GO exhibited two characteristic peaks at 230 mm and a broader peak at 311 nm associated with π-π* and n-π* transitions respectively. While, AuNPs-GO/MWCNTs composite also exhibited two similar peaks, but the positions of π-π* peaks bathochromically shifted to 262 nm respectively. This confirmed the formation of the π-π interactions between the side walls of MWCNT and the AuNPs of GO as shown in Figure 6.12A.

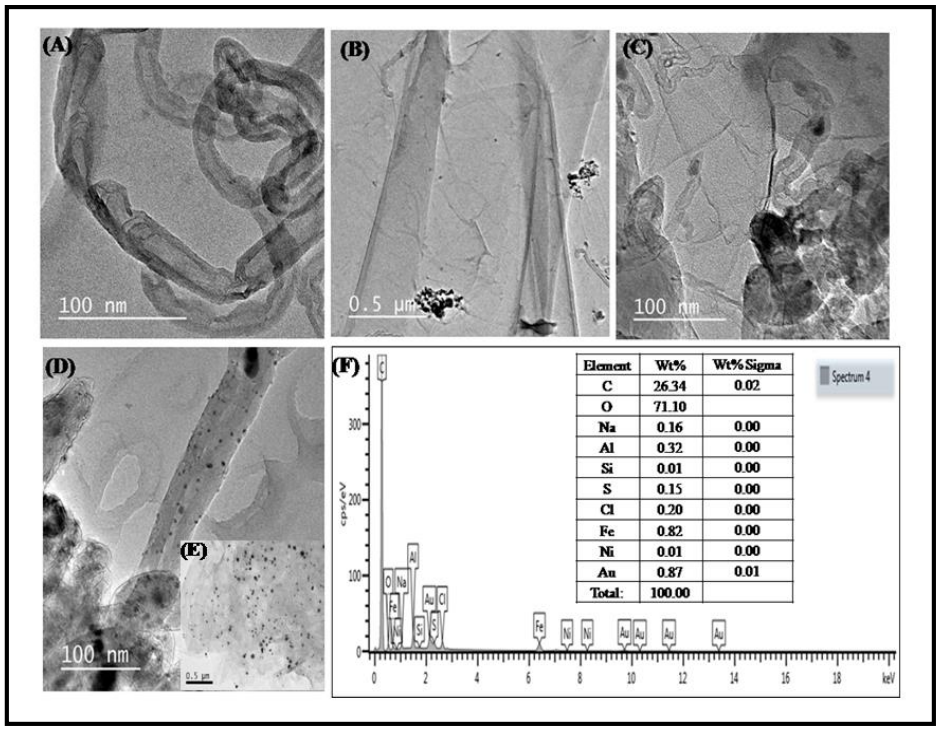

Figure 6.11: TEM images for (A) pure MWCNTs (B) pure GO (C) MWCNTs on surface of GO (D and E) AuNPs decorated on MWCNTs and GO surface (F) EDS showing presence Au NPs in nanocomposite

The crystalline characterization of the AuNPs-GO/MWCNT nanocomposite was performed by XRD shownin Figure 6.12B. The diffraction peaks observed around $2\theta = 23^0$ and 27^0 were assigned to the (002) plane of carbon materials such as MWCNTs and GO respectively [Prabakaran and Pandian, 2015]. All the other peaks, $2\theta = 39^0$, 44.6^0 and 64.7^0 were assigned to the Au planes of (111), (200) and (220), respectively [Li et al., 2015; Dharuman et al., 2013; Pruneanu et al., 2013]. According to the Scherrer and Williamson-Hall formula all XRD patterned peaks were considered to calculate the average crystallite size of the AuNPs. The calculated average size of the AuNPs present in the nanocomposite ranging from 10-33 nm for different peaks and the average crystalline size was found to be 23.7 nm with a face-centered-cubic (fcc) crystal structure [Shimizu et al., 2003].

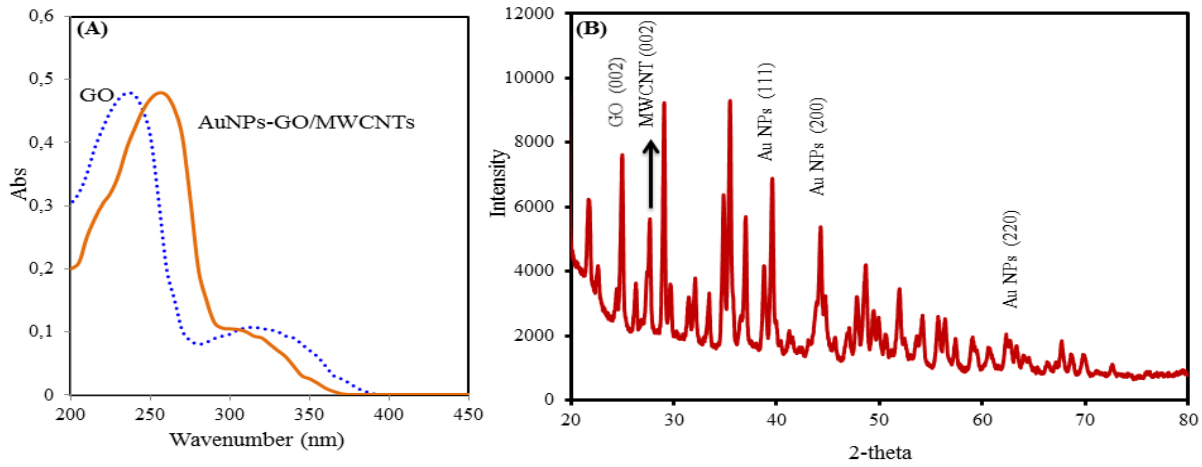

Figure 6.12: (A) UV spectras for GO and AuNPS-GO/MWCNTs nanocomposite (B) XRD patterns of AuNPs fabricated GO/MWCNTs nanocomposite

The thermal behaviour and stability of the prepared nanocomposites were investigated by thermo gravimetric analysis (TGA). Figure 6.13 showed the TGA curves for MWCNTs (curve i), GO (curve ii), MWCNTs-GO composite (curve iii) and MWCNTs-GO-AuNPs composite (curve iv). MWCNTs showed two significant decreases in the mass around 322 and 650 ^{0}C [Figure 6.13 curve i]. In the first peak, a 6 % weight loss was observed due to the evaporation of the total moisture content and the second decrease was due to the oxidation of carbon into gaseous carbon dioxide at a temperature range of 450–680 ^{0}C and the calculated weight loss was 11% [Liu et al., 2014]. GO started to lose weight form 60 ^{0}C and the main weight loss took place around 90 ^{0}C with a total weight loss of 98% [Figure 6.13 curve ii]. These weight loses were due to the pyrolysis of the labile oxygen atoms containing functional groups such as –OH, -COOH to CO, CO_2 and steam [Stankovich et al., 2007; Pham et al., 2011]. The TGA curve for MWCNTs-GO composite showed two significant drops around 100-258 ^{0}C and 420-560 ^{0}C, in the first zone the decrease of weight is 8.86%, which can be attributed to the oxidation of the GO functionalities. The second weight loss of 5.2% corresponds to the MWCNTs, indicating the thermal stability of the GO increased in

presence of MWCNTs, due to the incorporation of MWCNTs with GO. The MWCNTs-GO-AuNPs composite thermogram shows two significant mass drops at 319 and 510 ^{0}C with weight loss of 19%. The percentage AuNPs loaded on to the surface of MWCNTs-GO was found to be 27%. The presence of AuNPs increased the thermal stability of the nanocomposites [Jia et al., 2013].

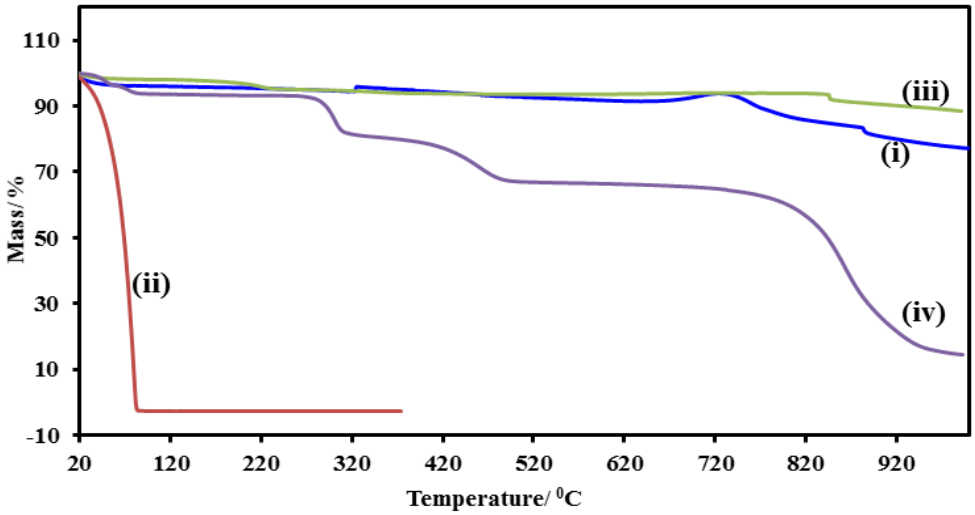

Figure 6.13: TGA curves for (i) MWCNTs (ii) GO (iii) MWCNTs-GO and (iv) MWCNTs-GO-AuNPs nanocmposite

6.2.2 Electrochemical characterization of the developed sensor and Reb A behaviour to Cyt c/AuNPs-GO/ MWCNTs/Pt

The microscopic areas of the developed biosensor were characterized using cyclic voltammetry (CV) with 1 M $K_3Fe(CN)_6$ as a probe solution. The $[Fe(CN)6]^{3-/4-}$showed heterogeneous one-electron transfer (n=1) reactions and one of the most broadly studied redox couples in electrochemistry. The anodic and cathodic peak currents of $[Fe(CN)6]^{3-/4-}$reaction linearly increased, while the peak potentials of the anodic and cathodic peaks shifted to positive

and negative sides with an increase in scan rate from 10 to 210 mV/ s. The microscopic areas for bare Pt and modified Pt were studied using Randles–Sevcik equation [Kaur et al., 2013] [Eqn 6.3].

In that equation, I_P refers to the peak current, A is the surface area of the electrode, C_0 is concentration of the $K_3Fe(CN)_6$, n is number of electrons transferred, D_R is the diffusion coefficient and v is the scan rate. The diffusion coefficient (D_R) of 6.7×10^{-6} cm^2 s^{-1} was calculated from the slope of the i_{pc}–$v^{1/2}$ graph. In the case of Cyt c/AuNPs-GO/ MWCNTs/Pt, the electrode surface area was calculated as 0.842 cm^2, while the bare Pt was nearly six times smaller than the modified electrode.

The electrochemical performance of the Cyt c/AuNPs-GO/ MWCNTs/Pt towards the detection of Reb A in food samples were studied by measuring the current-potential responses. The calculated microscopic areas of the electrodes were mainly effected the peak responses of Reb A, a comparative study among different modified electrodes were studied on peak currents (i_{pa}) using CV in a 10 mL borate buffer (pH 11.0) at a scan rate 70 mV/s. The peak currents were directly proportional to the coating of electrode material, due to an increase in electro active surface area. Figure 6.14A shows the electrochemical responses of Reb A at -0.1 V with the bare Pt (curve a), AuNPs-GO/Pt (curve b) AuNPs-GO/ MWCNTs/Pt (curve c) and Cyt c/AuNPs-GO/ MWCNTs/Pt (curve d). The bare Pt (curve a) showed a broad and weak intensity peak due to the slower electron transfer kinetics of the reduction process. In contrast, well-defined sharp peaks were observed with fair responses for the different modified electrodes. The bar graph [inset Figure 6.14A] showed comparative current responses of four studied electrodes, clearly indicating that the peak currents at Cyt c/AuNPs-GO/ MWCNTs/Pt were significantly higher than the currents obtained at the bare Pt, Au NPs-GO/Pt and AuNPs-GO/ MWCNTs/Pt. This indicated that the addition of Cyt c showed excellent catalytic activity towards the reduction of Reb A.

Considering the structure of Reb A, the electrode reaction attributed to the reduction of the carboxyl groups with one electron transfer [scheme 6.2], resulting in the appearance of a quasi-reverisible reduction peak at -0.1 V (versus Ag/AgCl) [Lovric et al., 2010]. Similar types of reactions were also observed in the case of cocaine [Pavlova et al., 2004], nalidixic acid [Ibrahim et al., 2002].

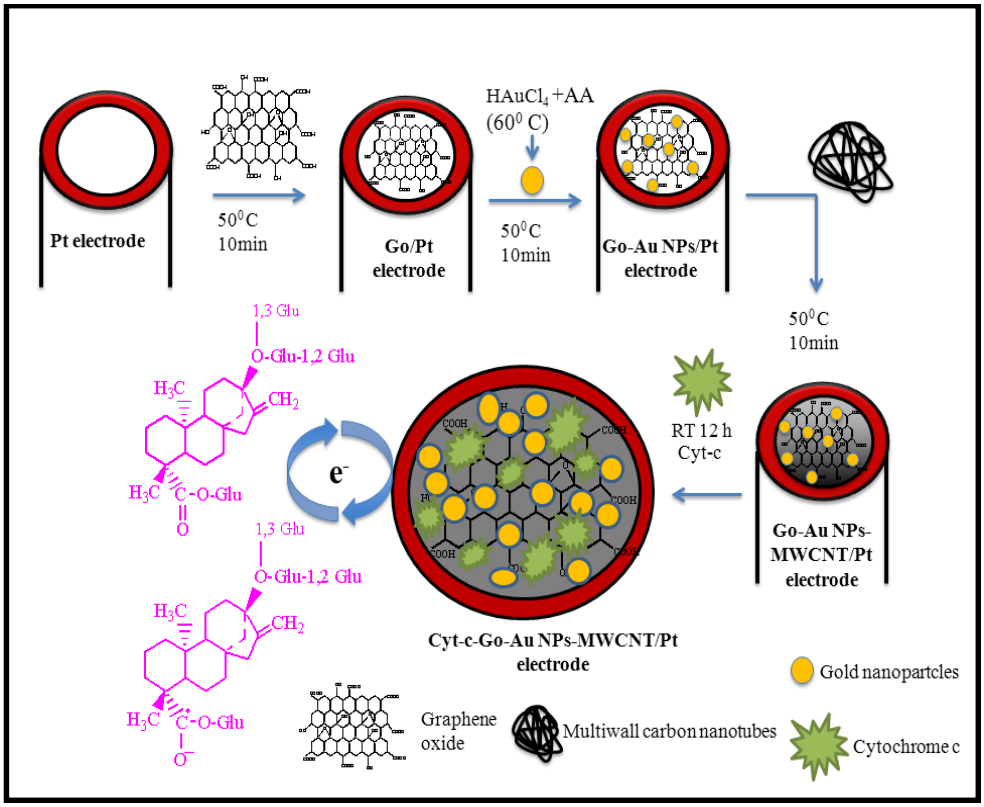

Scheme 6.2: **Fabrication of Pt electrode with nanocomposite and electrochemical mechanism for Reb A**

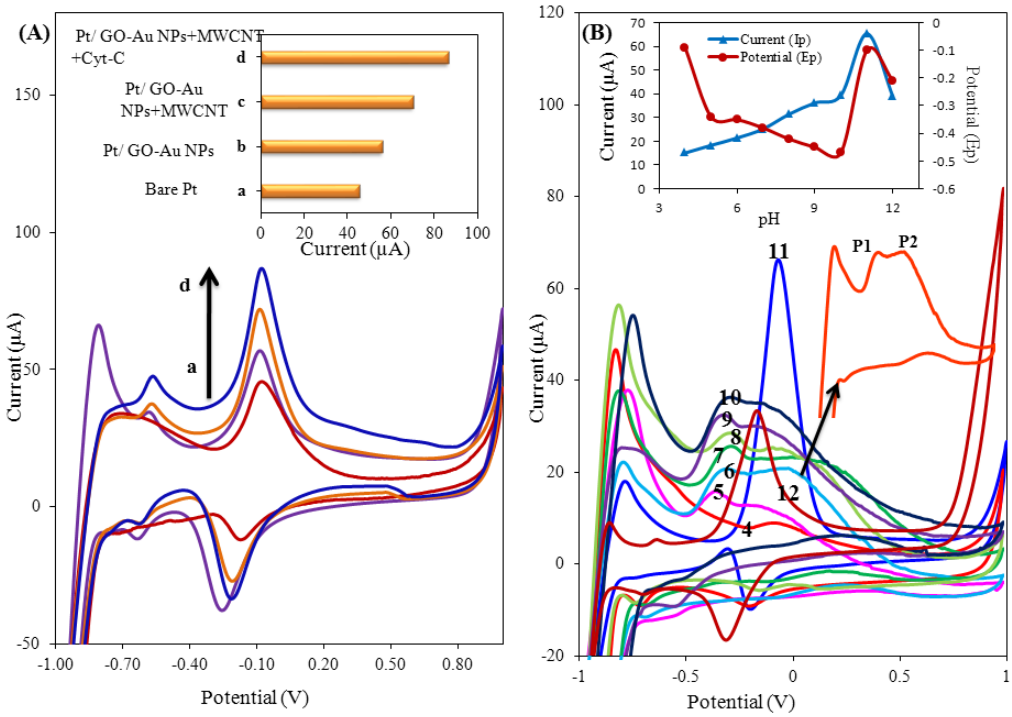

Figure 6.14: (A) Cyclic voltammograms recorded at (a) bare Pt (b) GO-AuNPS modified Pt (c) GO-AuNPS-MWCNTs modified Pt (d) Cyt c-GO-AuNPS-MWCNTs modified Pt (B) Cyclic voltammograms recorded at different pHs (4.0 to 12.0) with 0.3 mM Reb A, scan rate 70 mV/s and in inset shows the effect of pH on peak current and potentials

6.2.3 Effect of pH and scan rate on the peak currents and peak potentials

A 0.3 mM Reb A solution was used to find the optimum pH of the supporting electrolyte by Cyt c/AuNPs-GO/ MWCNTs/Pt. The effect of pH on the reduction peak currents of Reb A were studied ranging from 4.0 to 12.0 in a 0.1 M borate buffer using cyclic voltammetry. According to Figure 6.14B as pH of the electrolyte increased the peak current increased and the maximum peak current was observed at 11.0, due to the higher electron transfer between modified electrode and Reb A.

The effect of pH on the peak potentials were investigated and Figure 6.14B showed the recorded peak potentials were mainly pH dependent, due to the reduction capacity of the carboxylic group with changes in pH. It was also found that the peak potential shifted towards a more negative value with an increase in pH. Interestingly, from pH 4.0 to 9.0 two peaks were observed in a voltammogram (indicated as P1 and P2), the first peak related to the reduction of the carboxyl group and the second peak corresponding to hydrogen evolution interfered with the negatively charged oxygen. In a more basic medium 10.0 to 12.0, the appearance of second peak decreased and merged as a single peak due to a decrease in the effect of the hydrogen evolution. Thus, based on the peak currents and the less negative potentials, the phosphate buffer at pH 11.0 was considered as the optimum for determination of Reb A.

To obtain the kinetic parameters, the effect of scan rates on peak currents were studied using 0.3 mM concentration of Reb A on a bare Pt and Cyt c/AuNPs-GO/ MWCNTs/Pt using CV. Figure 6.15A-B shows, the anodic and cathodic peak currents linearly increased with an increase in scan rate from 10 mV/s to 210 mV/s, indicating the reduction process were adsorption controlled. Hence, Reb A first adsorbed and accumulated on the electrode surface and then followed by an electrochemical reduction reaction. The adsorbed amount of Reb A on the electrode surfaces were calculated using the following equation [Eqn 6.7].

$$I_p = \frac{nFQv}{4RT} = \frac{n^2F^2A\Gamma_T v}{4RT} \qquad \text{[Eqn 6.7]}$$

where n is the number of electron transferred, F (C mol^{-1}) is the Faraday's constant, Q (C) is the quantity of charge consumed during the electro-reduction reaction and v (V s^{-1}) is the scan rate. A (cm^2) is the area of the electrode, Γ_T (mol cm^{-2}) is the surface concentration of the electroactive

Reb A. An integration of the peak area of both bare and modified Pt electrodes, resulted in a straight line with a slope of 0.8976 and 0.9112 within the same scan range. From above equation the values of *n* and I_T were obtained and the results are 1.17 and 2.3 X 10^{-6} respectively. At an optimum scan rate of 70 mV/s, Cyt c/AuNPs-GO/ MWCNTs/Pt showed 52 µA of the peak current which was 10 fold compared to peak current measured at bare Pt electrode (4.8 µA) indicates the fair catalytic activity of nanocomposite materials.

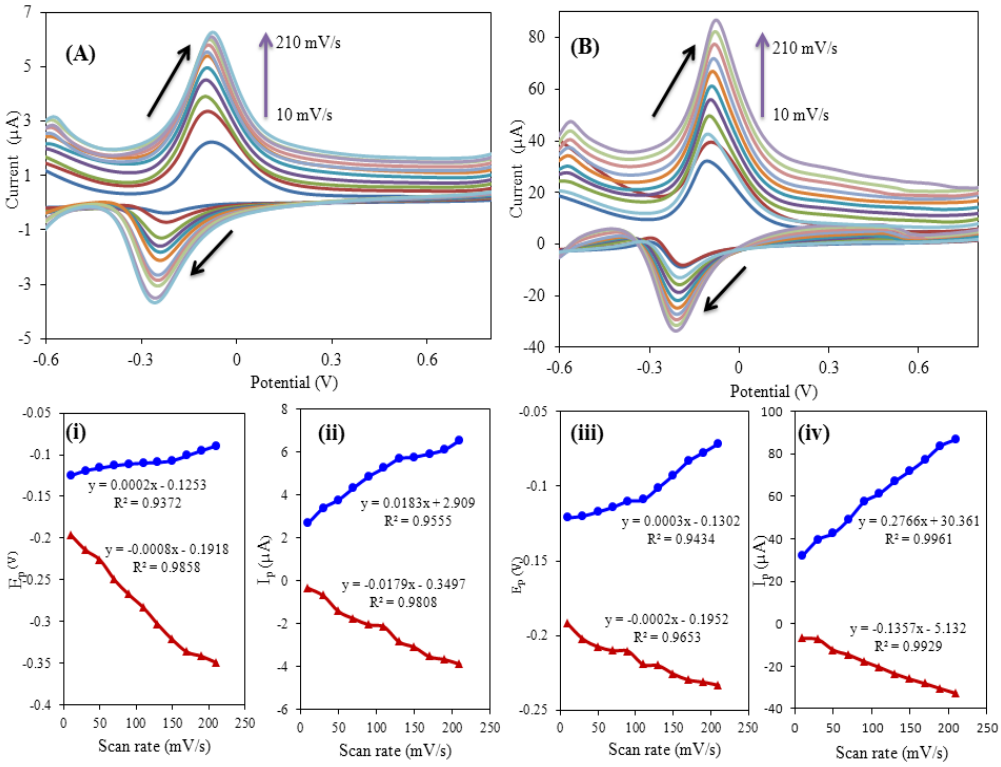

Figure 6.15: Cyclic voltammograms recorded at different scan rates (A) bare Pt and (B) Cyt c-GO-AuNPs-MWCNTs/Pt. The scan rate from inner to outer are 10, 30, 50, 70, 90, 110, 130, 150, 170, 190, 210mV/ s, respectively. The plots of scan rate versus peak potentials (i) bare Pt (iii) modified Pt and peak currents (ii) bare Pt (iv) modified Pt

The effect of scan rate on the peak potentials were studied with the same concentration of Reb A and the anodic peak potential shifted to a more positive side and the cathodic peaks shifted to a more negative potential with an increase in the scan rate. The linear regression equations were constructed between the peak potentials and the scan rates (v) at the bare and modified Pt electrodes are shown in Figure 6.15.

From the regression equation the electrochemical parameters, electron transfer coefficient (α) 0.58 and the electrode reaction standard rate constant (k_s) 4.71 s^{-1}were calculated using Laviron's equation [Eqn 6.4] at modified electrode.

6.2.4 Effect of accumulation time and potential

The optimization of accumulating conditions for the adsorption process of Reb A on the modified electrode were studied using 0.5 mM Reb A by differential pulse voltammetry (DPV) technique. The influence of the accumulation time on the reduction of Reb A at Cyt c/AuNPs-GO/ MWCNTs/Pt were studied ranging from 0 to 50 s. The peak currents gradually increased with an increase in accumulation time from 10 to 30 s. However with further increase in accumulation time no significant changes in peak current were observed thus indicating that the electrode surfaces were saturated. Hence, 30 sec was considered as the optimum accumulation time for further studies [Figure 6.16a].

The accumulation peak potential on peak currents was studied ranging from -50 to 20 mV vs. Ag/AgCl. The maximum peak currents were observed at -30 mV because the applied potential was close to the reduction potential of Reb A, and therefore the Reb A tends to accumulate on the electrode surface. Further increase (> -30mV vs. Ag/AgCl) in accumulation potential resulted in

the peak current gradually decreasing, hence -30mV was considered as the accumulation peak potential [Figure 6.16b].

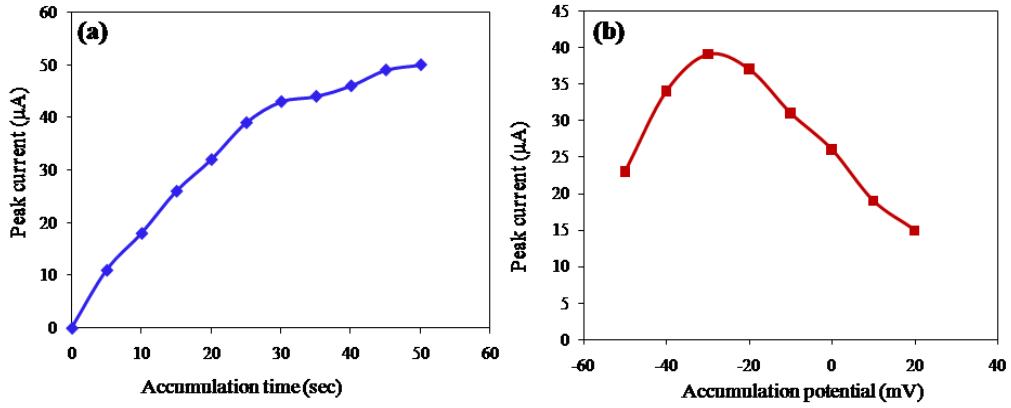

Figure 6.16: Plots for (a) The effect of accumulation time on peak current (b) effect of accumulation potential on peak current.

6.2.5 DPV method for quantitative determination of Reb A

Due to the higher current sensitivity and better peak separation, DPV method was used for the sensitive determination of Reb A at the Cyt c/AuNPs-GO/ MWCNTs/Pt. Under the optimum experimental conditions (pH 11.0, accumulation time: 30 s, accumulation potential: -30 mV, pulse amplitude: 50 mV, voltage step: 2 mV and voltage step time: 0.4 s) the DPV responses for various concentrations of Reb A at the modified electrode in 0.1 M borate buffer (pH 11.0) were measured. The results showed that a linear relationship between the concentration ranging from 0.001 to 1.5 mM of Reb A and are peak currents were observed are shown in Figure 6.17A. The peak current at potential -10mV increases sensitively with increase in the concentration of Reb A. The linear regression equation was I_{pa} (µA) = 11.90 C + 18.96 (R^2 = 0.9934) [Figure 6.17B]

with 0.26 µM of LOD and 0.75 µM of LOQ at signal to noise ratio of 3. Hence, this electrochemical biosensor is suitable and efficient for the determination of Reb A in food samples.

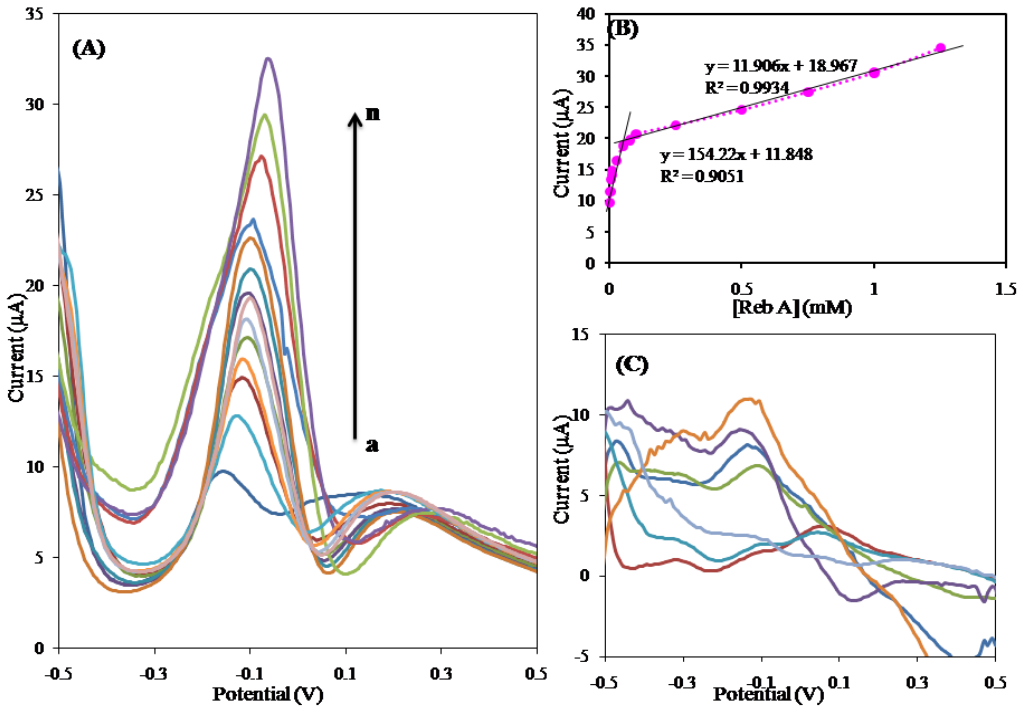

Figure 6.17: (A) Typical DPVs of (a) 0.001(b) 0.0025 (c) 0.005 (d) 0.0075 (e) 0.01 (f) 0.025 (g) 0.05 (h) 0.075 (i) 0.1 (j) 0.25 (k) 0.5 (l) 0.75 (m) 1 (n) 1.25 mM for Reb A in 0.1 M borate buffer (pH 11.0) (B) Calibration plot of Ip vs [Reb A] at low (0.001 to 0.05) and high (0.075 to 1.25) concentrations (C) DPVs for powder sample

6.2.6 Stability, recovery, accuracy and precision studies

The stability and repeatability of the developed biosensor were tested using CV, resulted in a decrease of 3.6 % current response after 50 cycles. The long term stability of the developed sensor was observed by measuring the response in 0.3 mM Reb A over a range of ten runs for three days using the same coating. The sensor maintained 89% of the original response on third day, demonstrating that the sensor retained its activity to a large extent. The analytical

parameters in terms of accuracy, precision and recovery were estimated by analyzing three different concentrations of Reb A standard solutions ranging from 0.1 to 0.7 mM in triplicate in a day. The relative error (bias) was observed as -0.13 to -0.0214 with a % RSD of 0.93 to 1.26, indicating a high accuracy and precision of the proposed method [Table 6.6]. The percentage recoveries of proposed sensor at same concentrations ranged from 87.0 to 98.0 %. The reproducibility of the sensor was studied by assaying cyclic voltammetric peak current using 0.3 mM Reb A at three prepared electrodes for three replicate measurements. The %RSD of 1.57% was obtained, suggesting an acceptable reproducibility of the proposed biosensor.

Table 6.6: Analytical parameters (Stability, accuracy, precision and recovery (n=3) obtained for Reb A at Cyt c/AuNPs-GO/ MWCNTs/Pt.

Stability		Analytical parameters				
Day	Peak responce[a](I_p)	Added (mM)	Found (mM)	Bias[a]	Recovery (%)	RSD[c] (%)
1	81	0.1	0.087	-0.13	87	1.32
2	76	0.4	0.391	-0.0225	97	0.93
3	72	0.7	0.685	-0.0214	98	1.26

[a]Average of three determinations,
[b]Bias= (found-added/added),
[c]Relative standard deviation for three individual determinations

6.2.7 Real sample analysis and Interference study

Finally, the developed biosensor was applied for the practical analysis of Reb A in three commercially available food samples described under section 4.1.3. For sample analysis each product was directly dissolved in deionized water, followed by serial dilution in 10 mL borate buffer (pH 11.0). Figure 6.15C shows DPV results for the analysis of the powdered sample and Table 6.7 shows the obtained analytical results with the developed biosensor.

Table 6.7: Detection of the Reb A in different food samples.

Sample	Available form	Reb A concentration found (g)/mL	RSD[d]
Green Canderel[a]	Tablet	0.0127	1.75
Stevia[b]	Powder	0.0106	1.36
Tantalize[c]	Liquid	0.0142	1.65

[a]Merisant Company 2, Sarl, Czech Republic,
[b]Dis-Chem Pty Ltd, South Africa,
[c]Delite Foods, South Africa
[d]Relative standard deviation for three individual determinations.

The selectivity of the proposed biosensor was studied by detecting 0.3 mM Reb A solution in the presence of several possible coexisting interferents such as aspartame, acesulfame K, hydrogen peroxide, nitrate, cocaine, nalidixic acid, fenofibrate and benzoylecgonine. Using the current ratio method the degree of substance interferences with Reb A was evaluated. The current ratio of 0.3 mM Reb A in presence of 1mM of different interfering substances (I_{R+S}) were calculated and compared with the peak current of 0.3 mM Reb A alone (I_R). The current ratios (I_{R+S}/ I_R) were 0.98, 1.01, 0.97, 0.89, 0.95, 0.93, 0.89 and 0.92 in the order of above mentioned coexisting interferents, respectively. From the results, the developed biosensor exhibited an excellent selectivity towards the determination of Reb A, since there were no significant changes in the current ratio with the interferences.

6.2.8 Docking analysis

Docking studies between Cyt c and Reb A were performed using the CDocker module [Wu et al., 2003] in Discovery Studio. The computed scoring function (CDocker interaction energy= -25.7) indicated that the Reb A fits tightly in the active site of the Cyt c. The computed binding energy around -106.7 kcal/mol further supported the stronger binding affinity of Reb A

for the Cyt c. The docked complexe of Cyt c and Reb A were then visualized to get a deeper understanding of their host-guest relationships and is pictorially shown in Figure 6.18.

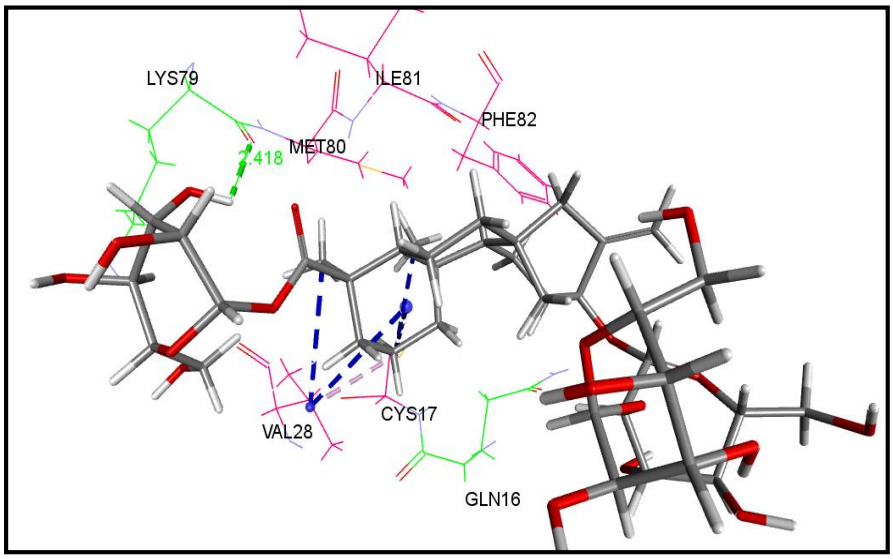

Figure 6.18: Conformation of Reb A (in sticks format) docked into the active site of Cyt c. Only interacting amino acid (AA) residues (in lines format) are shown. Hydrophobic and hydrophilic AA are shown in magenta and green colour lines. Hydrogen bond is shown as green dotted line, whereas hydrophobic interactions are depicted in blue dotted lines.

A closer inspection of Figure 6.18 revealed that Reb A interacted with the binding cavity of Cyt c through its glucose ring and tricyclic alkyl rings. Both hydrogen bonding and hydrophobic interactions were found to be important in the stabilization of their complex. Specifically, a single hydrogen bond (O…H = 2.418 Å) between the hydroxyl groups (-OH) of glucose ring (Reb A) and the carbonyl oxygen (-CO) groups of Lys 79, and hydrophobic interactions between the tricyclic ring carbons (Reb A) and the amino acids (Val 28 and Cys 17) were observed. The visualization of Cyt c in the surface format [Figures 6.19a-b] indicated the

presence of a groove in its structure, and was thought to be responsible for the comfortable penetration of Reb A into its active site with a stronger binding affinity.

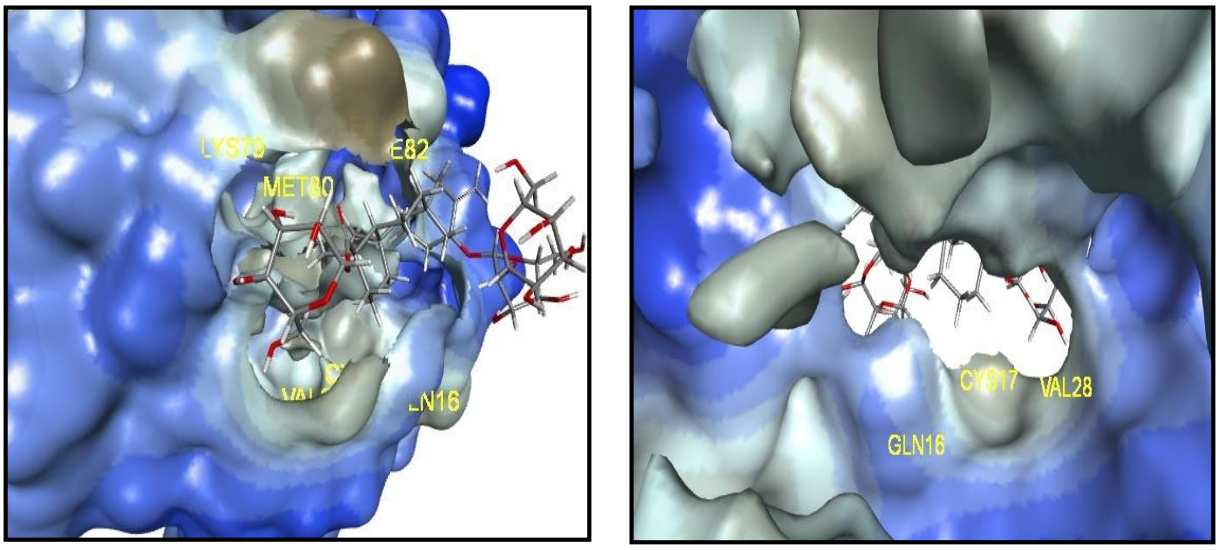

Side view **Inside view**

Figure 6.19: Surface representation of Cyt c showing the presence of a groove responsible for the penetration of Reb A (shown in sticks format) into its active site (a) side view (b) inside view

6.2.9 HOMO-LUMO calculations

The main objective of HOMO-LUMO calculations is to identify the exact positions of the oxidation or reduction reactions in a molecule with the help of electron density maps. Based on these arrangements, the frontier molecular orbitals in a molecule can easily determine the most appropriate functional groups or atoms undergo oxidation or reduction reaction. Hence, it is necessary to predict HOMO-LUMO band gaps of the molecule to explain the redox reactions in more accurate way. It is considered that, an electron transfers from its highest occupied molecular

orbital (HOMO) in a molecule, thus characterizing an oxidation process. Similarly, an electron flows from the metal electrode to the lowest unoccupied molecular orbitals (LUMO) in a reduction reaction.

For this reason, in order to get an accurate energy value of Reb A that agrees with the experimental accuracy, the geometries were optimized using B3LYP/6-31 g** basis set. According to Figure 6. 20, the less tightly held electrons are present in the highest occupied molecular orbitals (HOMO) situated at the oxygen atoms in three glucose rings. While the lowest unoccupied molecular orbital (LUMO) are located around the ester carbonyl groups. The results showed that the ester carbonyl groups will be the easiest route to the addition of electrons in the molecule. The proposed mechanism for the Reb A is a quasireverible reduction reaction between the ester carbonyl group and electrode surface with a one electron transfer. Therefore, the reduction of Reb A is expected to proceed in the same way and in good agreement with the both theoretical and experimental findings.

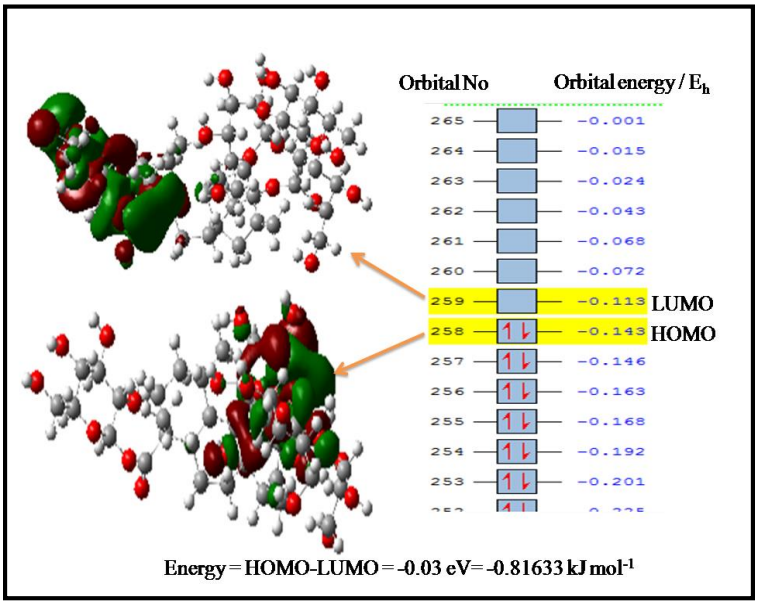

Figure 6.20: Predicted frontier molecular orbitals (HOMO-LUMO) for Reb A using DFT level 6-31 g basis set**

6.3 Analysis of sucralose using nanobiocomposite based on Lac/ZnO NPs-ATP-GO-GCE

p-aminothiophenol (ATP) has attracted a great deal of attention in making 2D/3D assembly of nanoparticles via covalent or electrostatic interactions [Gole et al., 2000]. The unique structure of ATP has been effectively used to design molecular assemblies via thiol and amine ends [Wang et al., 2003]. Graphene oxide (GO) can be considered as a ‘‘rising star’’ carbon material due to its unique properties and has been extensively used in different areas, especially in the field of biosensors [Yang et al., 2002; Ma et al., 2012]. Specifically, laccase in presence of mediator such as TEMPO [(2,2,6,6-Tetramethyl-piperidin-1-yl)oxyl] has been widely used for the oxidation of alcohols and convert them to carbonyl compounds [Baratto et al., 2006]. Accordingly, in this work ZnO NPs were functionalized with ATP and covalently attached to the GO to prepare the ZnO NPs-ATP-GO nanocomposite. Furthermore, this material was used to immobilize the laccase (Lac) to construct Lacccase/ZnO NPs-ATP-GO nanobiocomposite for the determination of sucralose.

6.3.1 Characterization of Lac/ZnO NPs-ATP-GO

Figure 6.21 (curve a-d) shows the FT-IR spectra of GO, ATP, ATP-ZnO NPs and GO-ATP-ZnO NPs composite. GO exhibited one characteristic peak at 3450 cm^{-1} which corresponds to the –OH stretching vibration. The sharp peaks at 1700 $cm^{-1}$and 1120 cm^{-1}were attributed to C=O and C-O-C stretch vibrations, respectively [Zeng et al., 2014]. ATP (curve b) exhibited three characteristic peaks at 1020, 1130 and 1580 cm^{-1}which corresponds to C-S, C-N and N-H stretching vibrations, respectively. ATP capped with ZnO NPs (curve c) showed shifts in C-S stretching vibrations about 34 cm^{-1}, indicating ZnO NPs were drastically capped by the thiol

groups than the amino groups. ATP capped with the ZnO NPs were covalently attached to GO (curve d) showed significant changes and the existence of the band at 3337 cm^{-1} for the N-H stretching vibrations confirmed the covalent functionalization of the carboxyl groups of the GO with ATP. In addition, the persistence of the amide bond (O=C-N) at 1682 cm^{-1} confirmed the covalent bond between carboxyl group of the GO with ATP [Silverstein and Webster, 1998].

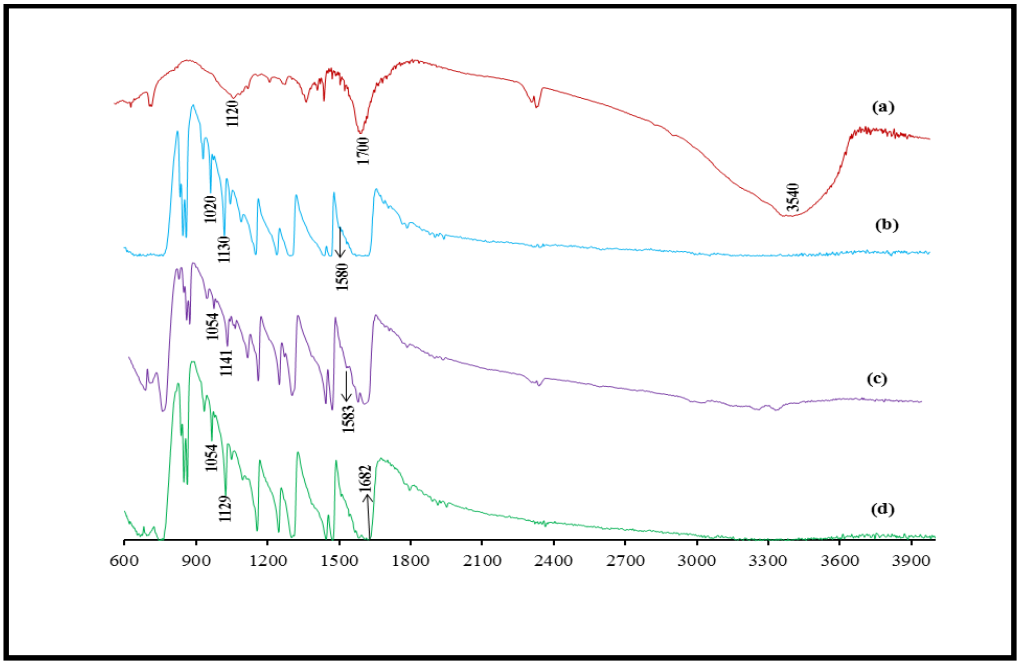

Figure 6.21: FT-IR spectras for (a) GO (b) ATP (c) ATP-ZnO NPs (d) GO-ATP-ZnO NPs composite

Crystalline structure and size of the ZnO NPS present in ZnO NPs-ATP-GO nanocomposites were examined by XRD analysis. Figure 6.22 shows XRD patterns of GO-ATP capped ZnO NPs observed over the range of angle shift values of 20 to 80^0. The diffraction angles at $2\theta = 31.14^0$, 37.65^0, $47.36^0$and 63.8^0 can be assigned to (110), (101), (102) and (200) planes of ZnO respectively. The peaks at 26.06^0 are attributed to the characteristic peaks of GO. The XRD peaks

of the studied nanocomposite corresponded well with the reported values of ZnO (JCPDS 36-1451) [Jiang and Gao, 2005; Sarma and Sarma, 2014].

The average crystalline sizes of ZnO NPs were calculated according to the Scherrer's formula [Martins et al., 2014]. The diffraction angles at $2\theta = 37.65^0$ (101) was obtained at 22.6 nm with a hexagonal phase.

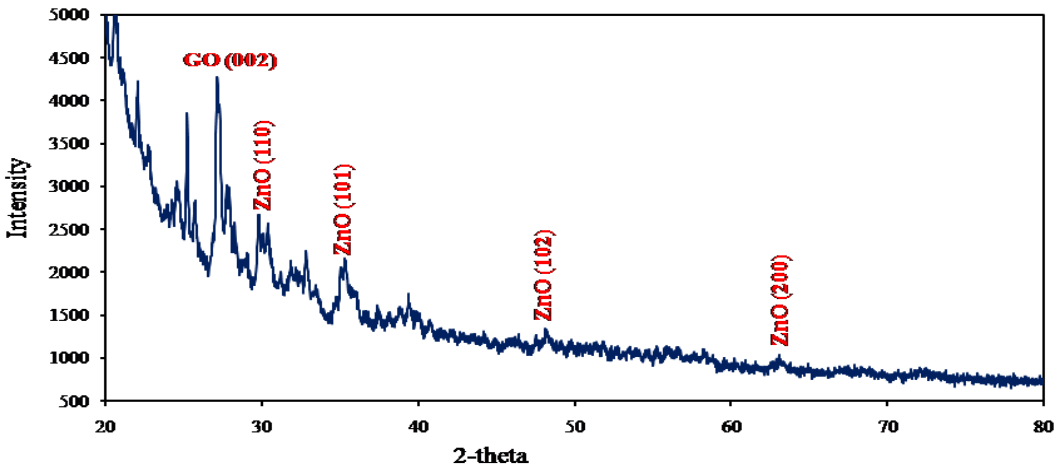

Figure 6.22: XRD pattern for GO-ATP-ZnO NPs nanocomposite

Thermogravimetric analysis (TGA) was conducted in order to investigate the thermal behaviour and stability of prepared nanocomposites. Figure 6.23 showed the TGA curves for GO (curve i), ATP (curve ii), ATP-ZnO NPs (curve iii) and GO-ATP-ZnO NPs (curve iv). Clearly, GO started to lose weight from 60 ^{0}C and the main weight loss occured around 90 ^{0}C with up to 98% of its total weight [Figure 6.23 curve i]. The weight loss is significant due to the pyrolysis of the labile oxygen containing functional groups such as -OH, -COOH to CO, CO_2 and steam [Stankovich et al., 2007; Pham et al., 2011]. The curve patterns of the GO-ATP-ZnO NPs nanocomposites were

similar to that of pure ATP and ATP-ZnO indicating that the features of the weigh-loss for the thermal decomposition mostly depends on the ATP matrix.

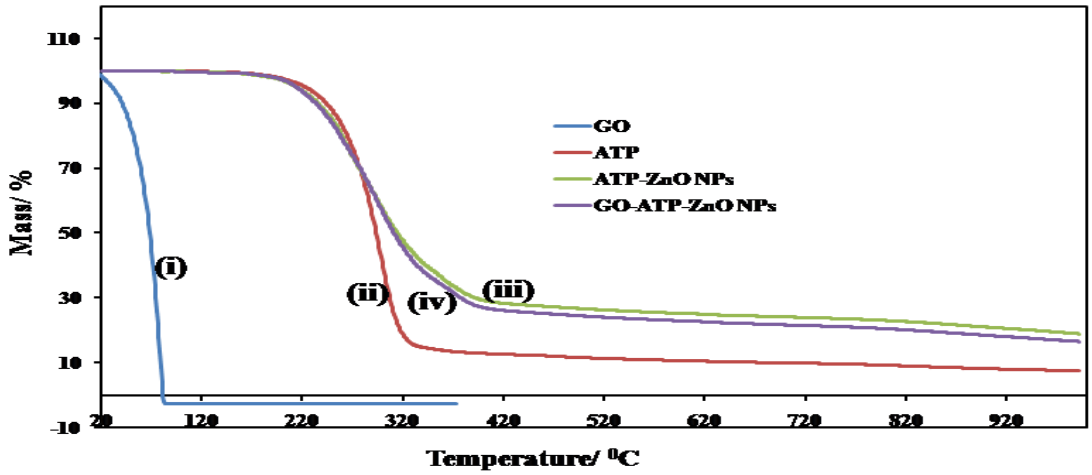

Figure 6.23: TGA curves for (i) GO (ii) ATP (iii) ATP-ZnO NPs (iv) GO-ATP-ZnO NP

The TGA curve [Figure 6.23 curve ii] revealed that the thermal transition of the ATP occurred at two temperature ranges: 50-120 and 240-350^0. In the first zone the weight loss was 2.2 %, due to desorption of water and the second weight loss of 84% corresponded to the ATP. Compared to ATP, ATP-ZnO NPs and GO-ATP-ZnO NPs materials showed higher thermal stability, clearly seen in Figure 6.23 curve ii. TGA traces of ATP-ZnO NPs and GO-ATP-ZnO NPs [curve iii and iv] showed weight losses in the temperature ranging from 60-180^0 and 210-480^0 with total weight loss of 55 and 67%, respectively. The results suggest that the thermal stability of the prepared materials were better improved due to the binding of ZnO NPs to the GO surface through covalent functionalization by ATP.

The morphological characterization of ZnO NPs was studied by TEM shown in Figure 6.24 a-c. Figure 6.24a shows the ultrathin sheet of pure GO with a diameter of nano to sub micro meter. While in Figure 6.24b, the agglomeration of ZnO NPs were well controlled by the functionalization with the ATP at 100 ^{0}C. It was observed that, the nano size ZnO particles were arranged over one another with a narrow size distribution. From the micrograph of GO-ATP-ZnO NPs composites [Figure 6.24c] it is clear that, the ATP capped ZnO NPs were well distributed on the surface of GO. The average size of the ATP capped ZnO NPs were found to be 30-50 nm with different shapes.

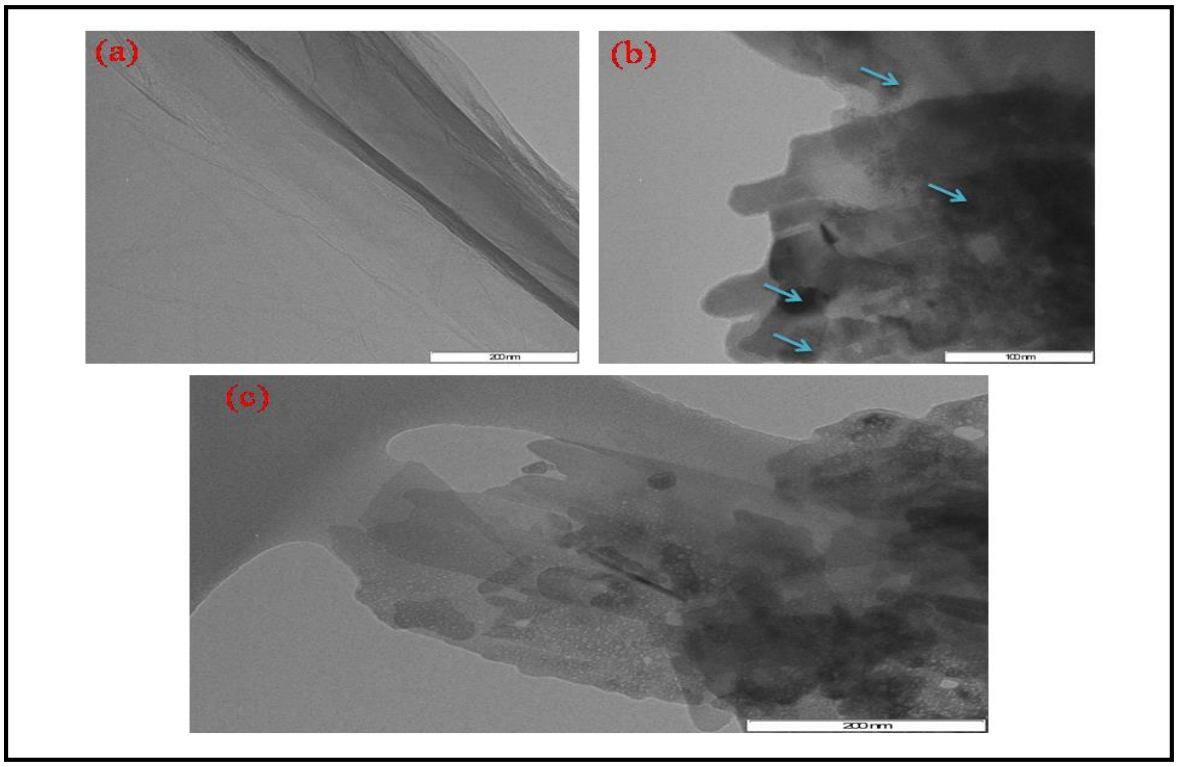

Figure 6.24: TEM images of (a) pure GO (b) ATP- ZnO NPs (c) GO-ATP-ZnO NPs

6.3.2 Electrochemical characterization of the developed sensor and electrochemical SUC behavior to Lac/ZnO NPs-ATP-GO/GCE

The electrochemical characterization of the developed sensor was studied using heterogeneous one electron transfer redox couple of $K_3Fe(CN)_6$ solution. Figure 6.25 illustrated the CV behavior of bare, GO, GO-ATP-ZnO NPs, Lac/GO-ATP-ZnO NPs-GCE's in 1M $[Fe(CN)_6^{3-/4-}]$. Bare GCE showed a couple of well–defined redox peaks at 0.22 and 0.16 V [Figure 6.25 i-a]. While, these redox peaks were observed around 0.13 and 0.04 V with an increased peak currents at GO coated GCE, due to the increase in surface area as well as increase in diffusion of $Fe(CN)_6^{3-/4-}$ions from solution to the electrode surface [Figure 6.25 i-b]. The addition of ZnO NPs-ATP significantly enhanced the redox peak currents at GO-ATP-ZnO NPs-GCE in contrast to GO-GCE, indicates that ATP can effectively increase the electron transfer rate of $Fe(CN)_6^{3-/4-}$ [Figure 6.25 i-c]. Moreover, the immobilization of the laccase on GO-ATP-ZnO NPs-GCE showed significantly higher redox peak currents [Figure 6.25 i-d], thus forming a bioelectrocatalytic cycle and thereby generating electrons which are passed to working electrode

Furthermore, the microscopic area of the developed biosensor was characterized using CV with $K_3Fe(CN)_6$ solution as a probe. The anodic and cathodic peak currents of $[Fe(CN)6]^{3-/4-}$reaction linearly increased, while peak potentials of the anodic and cathodic peaks towards shifted positive and negative potentials with increasing in the scan rates from 0.001 to 0.35 V/ s. The microscopic areas for bare and modified GCE was calculated using Randles–Sevcik equation [Kaur et al., 2013] [Eqn 6.3].

Where I_P refers to the peak current, A is the surface area of the electrode, C_0 is concentration of the $K_3Fe(CN)_6$, n is number of electrons transferred, D_R is the diffusion coefficient and v is the scan rate. The diffusion coefficient (D_R) of 6.7×10^{-6} cm^2 $s^{-1}$was calculated from the slope of the i_{pc}–$v^{1/2}$

graph. In case of bare GCE, the electrode surface area was calculated as 0.134 cm^2, while the Lac/GO-ATP-ZnO NPs-GCE were nearly eight times greater than the bare electrode.

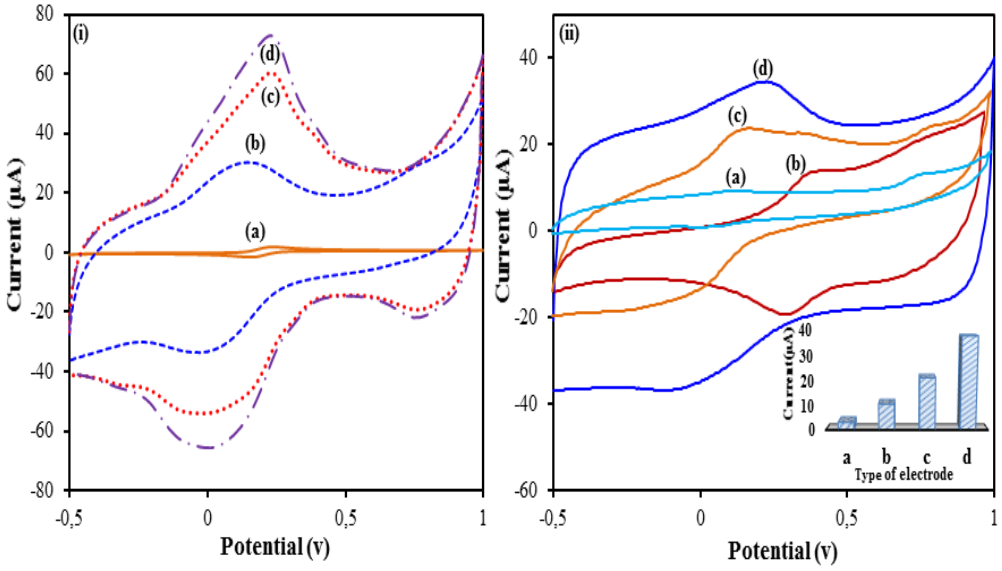

Figure 6.25: (i) Cyclic voltammograms of 1 M $K_3Fe(CN)_6$ at (a) bare GCE (b) GO-GCE (c) ZnO NPs-ATP-GO-GCE (d) Lac/ZnO NPs-ATP-GO-GCE (ii) Cyclic voltammograms of 0.5 mM SUC at (a) bare GCE (b) GO-GCE (c) ZnO NPs-ATP-GO-GCE (d) Lac/ ZnO NPs-ATP-GO-GCE, inset: current comparison among four electrodes

In order to investigate the electrochemical behaviour of SUC to the developed sensor, a comparative study was first conducted among different modified electrodes using CV in a 10 mL phosphate buffer (pH 5.0) at a scan rate of 0.1 V with 0.5 mM SUC. Figure 6.25 (ii) shows the electrochemical response of SUC with the bare GCE (curve a), GO-GCE (curve b), ZnO NPs-ATP-GO-GCE (curve c) and Lac/ZnO NPs-ATP-GO-GCE (curve d). At bare GCE, a broader and weaker intensity peak were observed due to the low electron transfer kinetics of oxidation process as shown in Figure 6.25 ii-a. In contrast to bare GCE, at GO-GCE a well-defined redox peaks with

increased peak currents were observed at 0.34 and 0.4 V [Figure 6.25 ii-b]. In the case of ZnO NPs-ATP-GO-GCE the redox peak potentials were shifted to -0.51 and 0.22 V with much increased peak currents observed, indicating the fast electron transfer by ATP [Figure 6.25 ii-c]. Finally, the immobilization of the laccase in the presence of TEMPO mediator showed a bioelectrocatalytic cycle thereby providing a rapid electron transfer to the electrode surface [Shervedani and Amini, 2012; Rawal et al., 2011; Wang et al., 2014] [Figure 6.25 ii-d]. The bar graph [inset Figure 6.25 ii] showed comparative current responses of the four electrodes. It was observed that the peak currents were directly proportional to the coating of electrode materials.

The mechanism for the oxidation of SUC by laccase involved a single-electron and proton reaction generating an oxidized product (an aldehyde), resulting in the appearance of redox peaks at 0.22 V [Scheme 6.3].

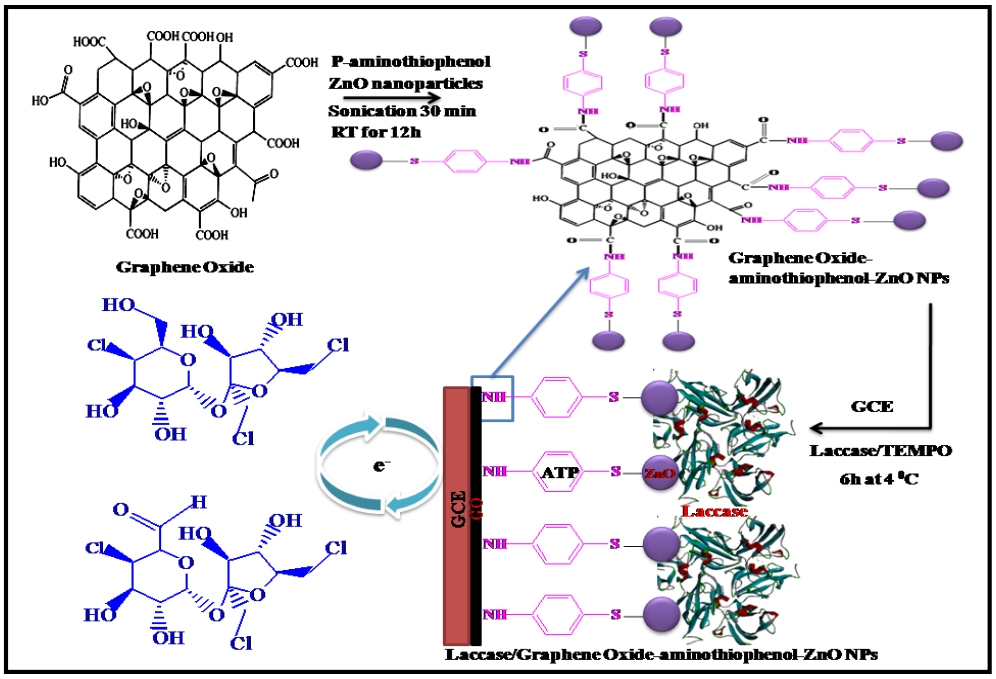

Scheme 6.3: A schematic representation of the typical electro-oxidation of SUC at Lac/ZnO NPs-ATP-GO-GCE

In this route, the actual oxidant is the oxoammonium ion which is easily generated from TEMPO on oxidation by laccase [Fabbrini et al., 2001]. Following this preliminary oxidation, a nucleophilic attackof the lone-pair of the SUC onto the TEMPO oxoammonium ion takes place to form an adduct. Deprotonation of the adduct at the C-H of ethanolic bond on the six membered ring resulted in the carbonylic product, a reduced form of TEMPO (i.e., N-OH). However, laccase oxidises the latter to regenerate TEMPO, and further oxidation led to the formation of an oxoammonium ion [Scheme 6.4] [Fabbrini et al., 2002]. The enzyme itself was finally oxidised by dioxygen, thereby completing the catalytic cycle. Laccase oxidized SUC by taking four electrons from the compound while the four Cu^{2+} of its active center are reduced to Cu^{+}. The reduced laccase returns to a rest status by transferring the electrons to produce water as shown in Scheme 6.4.

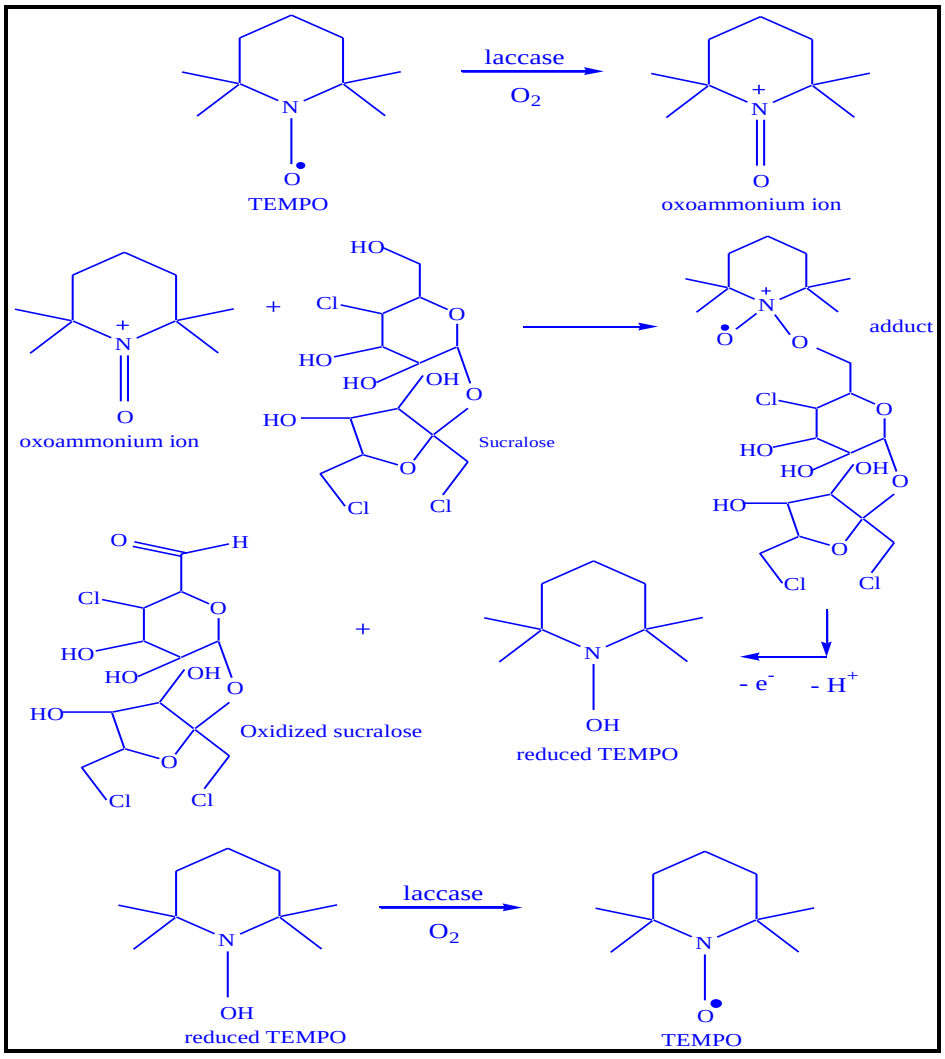

Scheme 6.4: The oxidation of SUC with laccase/TEMPO system

6.3.3 Effect of pH and scan rate on the peak potentials and peak current

The electrochemical redox behaviours of SUC with Lac/ZnO NPs-ATP-GO-GCE at different pH values ranging from 3.0 to 7.0 were investigated by DPV and the results are shown in Figure 6.26 (i). The oxidation peak potentials shifted negatively with an increase of pH value, indicating that protons involved in the electrode reaction. A good linear relationship between E_{pa} and pH was constructed with a linear regression equation as E_{pa} (V) = -0.0556 pH + 0.4568 (R^2 = 0.9841). The slope value of -55.6 mV/pH showed that the electron transfer in a redox reaction was

accompanied by an equal number of protons and electrons. At the same time, the effect of pH on peak currents were investigated in the same range and observed thatat pH 5.0 the electron transfer capacity of Lac/TEMPO system was superior [Fabbrini et al., 2002]. Hence, the oxidation peak current (I_{pa}) of SUC was higher at pH 5.0, therefore considering the sensitive determination for SUC the phosphate buffer of pH 5.0 was chosen as the optimal pH for further studies.

To investigate the reaction kinetics, the effect of scan rates on peak currents and peak potentials were investigated using CV at Lac/ZnO NPs-ATP-GO-GCE at different scan rates ranging from 0.001 to 0.35 V/s. Figure 6.26 (ii) shows the redox peak currents were simultaneously increases with increase in scan rate. The simultaneous increase in redox peak currents form scan rates 0.001 to 0.35 indicates that the redox reaction of SUC on Lac/ZnO NPs-ATP-GO-GCE was a typical diffusion controlled process. The linear relationship of scan rates with anodic and cathodic peak currents are showed in Figure 6.26C and the regression equations were:

Anodic: y= 186.12 pH – 2.5663; R^2 = 0.9984

Catodic: y= -191.5 pH + 1.6273; R^2 = 0.9993

In addition, at higher scan rates, the anode (E_{pa}) and cathode (E_{pc}) peak potentials have a linear relationship with the scan rates. The regression equations were E_{pa} (V) = 0.2993 v+ 0.1612 (R^2 = 0.956) and E_{pc} (V) = 0.2959 v- 0.0464 (R^2 = 0.8985), respectively. The relationship between the potential and scan rate could be described by Laviron's equations [Laviron, 1979] [Eqn 6.4].

Where α is the electron transfer coefficient, n is the number of transfer electrons, ks is the standard heterogeneous rate constant, R, T and F have their usual significance. The calculation results for α = 0.63, n = 1.35, ks= 0.58 s^{-1}, indicated that the electrochemical oxidation of SUC at

the Lac/ZnO NPs-ATP-GO-GCE were diffusion controlled process and not a surface controlled process as shown in Figure 6.26 B.

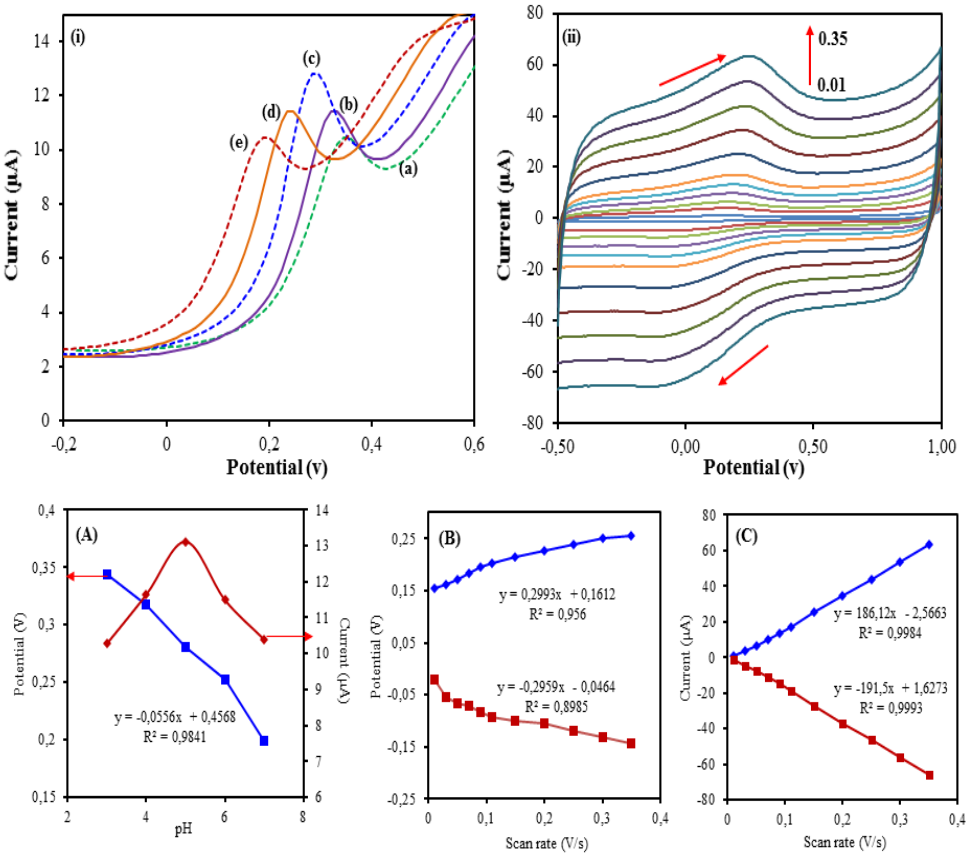

Figure 6.26: (i) Cyclic voltammograms recorded at different pHs (3.0 to 7.0) with 0.5 mM concentration of SUC and (A) shows the effect of pH on peak potentials and current (ii) Cyclic voltammograms recorded at different scan rates at Lac/ZnO NPs-ATP-GO-GCE. The scan rates from inner to outer are 0.01, 0.03, 0.05 0.07, 0.11, 0.15, 0.2, 0.25, 0.3, 0.35 V/s, showing the plots of peak potentials vs scan rate (B) and peak currents vs scan rate (c)

6.3.4 Effect of accumulation time and potential

The optimization of the accumulating conditions for the adsorption process of SUC on the modified electrode were studied using 0.5 mM of SUC by DPV method. The influence of the

accumulation time on the oxidation of SUC at Lac/ZnO NPs-ATP-GO-GCE were studied ranging from 0 to 50 s. The peak currents gradually increased with an increase in accumulation time ranging from 10 to 30 s. However with further increase in accumulation time no significant changes were observed in peak current, thus indicating that the electrode surfaces were in saturated. Hence, 30 sec was considered as the optimum accumulation time for further studies [Figure 6.27a].

The accumulation potential on the peak currents were studied ranging from -0.3 to 0.5 V vs. Ag/AgCl. The maximum peak current was observed at 0.2 V because the applied potential was closer to the oxidation potential of SUC and as, the SUC tends to accumulate on electrode surface. Further increase (> 0.2 V vs. Ag/AgCl) in accumulation potentials the peak currents gradually decreased, hence 0.2 V was considered as the accumulation peak potential [Figure 6.27b].

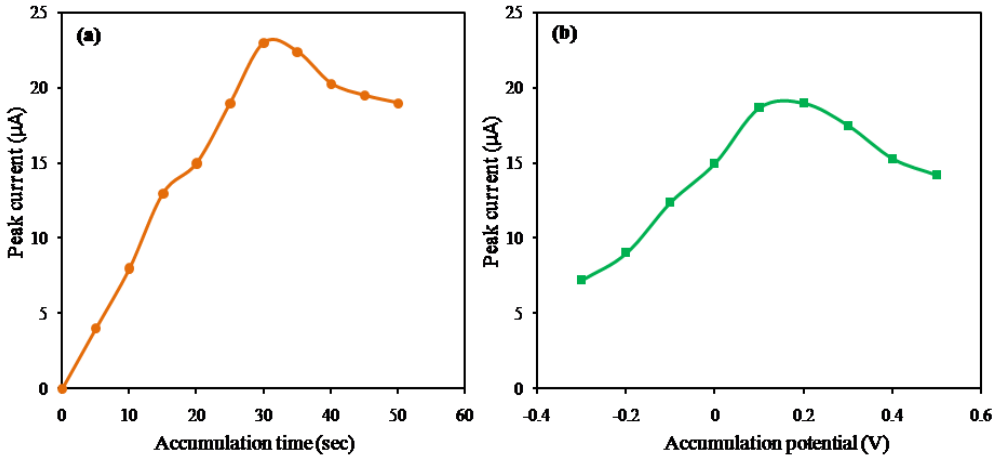

Figure 6.27: Plots for (a) effect of accumulation time on peak current (b) effect of accumulation potential on peak current

6.3.5 Effect of laccase concentration

The amount of enzyme loading on the electrode surface affects the sensitivity of the biosensor. The amount of the enzyme in the nanocomposite depends on the concentration of the enzyme solution used during the casting process. To investigate the effect of the enzyme and mediator concentration on the response currents, the enzyme electrodes were prepared with the laccase concentrations ranging from 0.25 and 4 mg/mL. The responses of the biosensor increased with an increase in the concentration of enzyme up to 1 mg/mL, and then no enhancement in the responses were observed indicating that the enzyme loading capacity of the electrode surfaces were saturated. The enzyme concentration of 1 mg/mLwas used for constructing the enzyme electrode with 1 mg/mL of TEMPO in all of measurements.

6.3.6 Effect of temperature

The activity of an enzyme depends on the temperature especially in the preparation of enzyme electrodes. The effect of temperature on the biosensor performance were studied at different temperatures ranging from 20 and 50^0C in 0.1 M PBS (pH 5.0) containing 0.5 mM SUC. The current response increased with an increase in temperature from 20 to 30 ^{0}C and the activity of Lac/ZnO NPs-ATP-GO-GCE reached a maximum value of 30 ^{0}C. Then, a gradual decrease in the current responses were observed due to the reduced activity of laccase at higher temperatures. The main reasons for change in current response at higher temperature were: (i) thermal deactivation of the enzyme [Pei and Li, 2000] and (ii) decreasing concentration of molecular oxygen in the solution [Turkmen et al., 2014]. The temperature effect on the current response of the biosensor can be described by the Arrhenius equation [Chen and Neeb, 1984] [Eqn 6.8],

$$i(T) = i_0 \exp\left(-E_a/RT\right) \quad \text{[Eqn 6.8]}$$

where *i* is the steady-state current, i_0 is a collection of currents, E_a is the activation energy, R is the universal gas constant and Tis the absolute temperature in Kelvin. The activation energy for the enzymatic reaction was determined by the analysis of slope of the plots (ln*i* vs. 1/T) in the range of 25-30 ^{0}C. The E_a value was calculated to be 55.10 kJ/ mol and also the effect of temperature on the response of Lac/ZnO NPs-ATP-GO-GCE was studied. The obtained E_a value for the oxidation of sucralose on modified electrode was found to be 41.59 kJ/ mol.

6.3.7 Quantitative determination of SUC using DPV method

Under the experimental conditions (accumulation time; 30 s, accumulation potential: 0.2 V, pulse amplitude: 0.5 V, voltage step: 0.2 V, voltage step time: 0.4 s, 0.1 M phosphate buffer and pH 5.0) DPV method was used for the sensitive determination of SUC. The obtained results shows that a linear relationship between the concentration of SUC and peak current. It was observed that the peak current at 0.25 V increases with increase in concentration of SUC by standard addition procedure ranging from 0.025 to 1 mM as shown in Figure 6.28. The calibration plots were constructed at two intervels: (i) first low concentrations (a→d) ranging from 0.025 to 0.1 mM and (ii) second high concentrations (e→h) ranging from 0.25 to 1 mM. The obtained regression equations were:

a→d: y= 49.6x + 9.1 R^2 = 0.9984

e→h: y= 3.24x + 14.4 R^2 = 0.9979

The LOD and LOQ values were calculated and noted as 0.32 μM and 1.15 μM of LOQ at signal to noise ratio of 3.

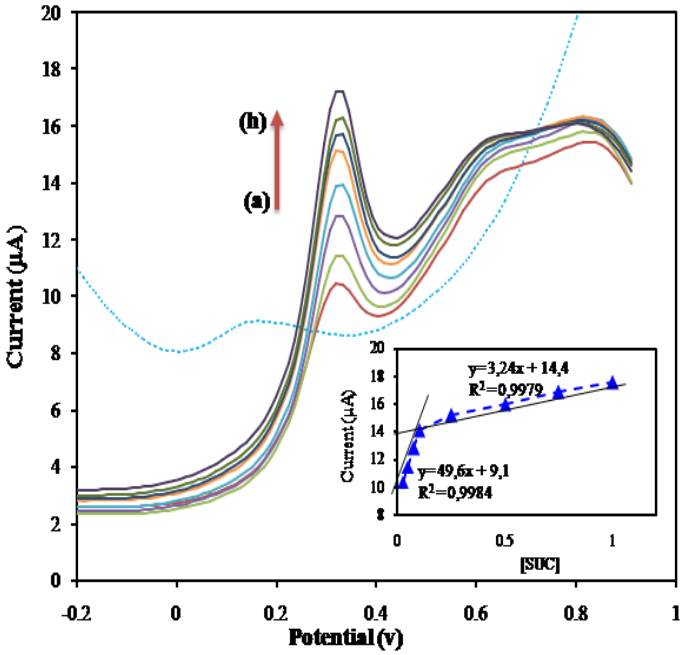

Figure 6.28: DPV response of SUC at different concentrations (a) 0.025 (b) 0.05 (c) 0.075 (d) 0.1 (e) 0.25 (f) 0.5 (g) 0.75 (h) 1 mM at Lac/ZnO NPs-ATP-GO-GCE and in inset calibration plot shows the linear dependence of i_{pa} vs [SUC]

6.3.8 Reproducibility, repeatability, stability and precision studies

The reproducibility and repeatability are vital parameters for the evaluation of the biosensor performance. The reproducibility of the developed sensor was estimated under the optimal conditions based on current response given by 0.5 mM SUC with five modified electrodes. The relative standard deviation was found to be 3.52% indicates the good reproducibility of the prepared biosensor. The repeatability of the biosensors was also examined by monitoring the current response to 0.5 mM SUC for six times and the observed RSD was 2.93%. The storage stability of the enzyme electrode was determined by measuring the current response of 0.5 mM SUC during a period of 10 days. The enzyme electrodes were kept in 0.1 M PBS (pH 5.0) at 4 ^{0}C

when not in use. The results obtained for the developed biosensor was shown in Figure 6.29, where i_0 is the current response of freshly fabricated biosensor, i is the current response at any storage time, i-i_0 is the change in the response current at any storage time. Lac/ZnO NPs-ATP-GO-GCE showed good stability during five days and the current response remained about 83% of its initial response. After that, an activity loss of 73% was observed after 10 days. The good stability of Lac/ZnO NPs-ATP-GO-GCE may be attributed to the aspect that ZnO NPs–ATP-GO matrix was stable.

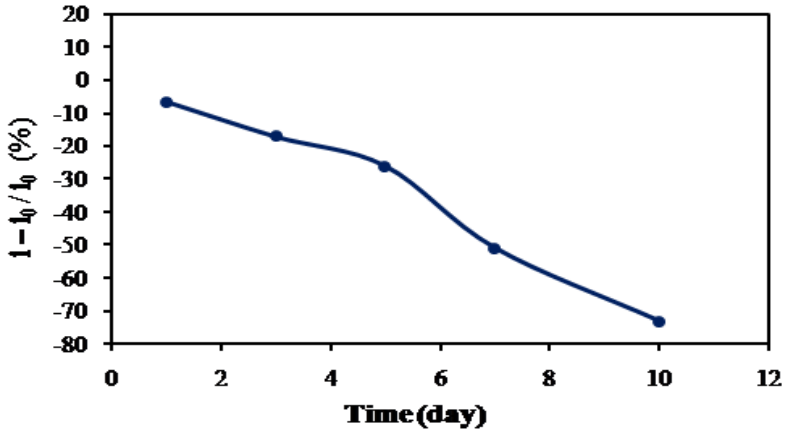

Figure 6.29: Stability of Lac/ZnO NPs-ATP-GO-GCE. Each data point of graph is based on measuring the DPV response of 0.5 mM of SUC in 0.1 M PBS at pH 5.0

The analytical parameters in terms of accuracy, precision and recovery was estimated by analyzing three different concentrations of SUC standard solutions ranging from 0.1 to 0.5 mM in triplicate in a day. The relative error (bias) was observed as -0.018 to -0.11 with a % RSD of 0.91 to 2.16 indicates high accuracy and precision of the proposed method [Table 6.8]. The recovery percentages of proposed sensor at same concentrations were found to be in the range from 93.0 to 99.0 %.

Table 6.8: Analytical parameters (precision and recovery) (n=3) obtained for SUC at Lac/ZnO NPs-ATP-GO-GCE.

Analyte	Analytical parameters				
	Added (mM)	Found (mM)	Bias[a]	Recovery (%)	RSD[b] (%)
SUC	0.1	0.089	-0.11	97	1.77
	0.3	0.285	-0.051	93	1.05
	0.5	0.419	-0.018	99	1.29

[a]Bias = (found-added/added)
[b]Relative standard deviation for three individual determinations

6.3.9 Real sample analysis

In order to evaluate the performance of the biosensor in practical analysis, Lac/ZnO NPs-ATP-GO-GCE was used to detect SUC in different food samples. Three SUC food samples mentioned in chapter 4.1.3 were purchased from local super market. The DPV method was used at applied potential of 0.2 V with the addition of 200 µL of sample into 10 mL of 0.1 M PBS (pH 5.0) to detect SUC. The SUC concentration in the samples was calculated from the calibration curves and the obtained results were shown in Table 6.9.

Table 6.9: Detection of SUC in different food samples.

Sample	Available form	SUC concentration found (g)/mL	RSD[d]
Canderelyellow[a,b]	Powder	0.0257	1.25
Canderelyellow	Tablet	0.0279	1.89
Hullets equisweet[c]	Tablet	0.0421	1.54

[a,b]Merisant Company 2, Sarl, 2000 Neuchatel-Switzerland
[c]Tongaat Hullet Sugar, Rossburgh, SA
[d]Relative standard deviation for three individual determination

One of the main challenges in SUC analysis is the elimination of interference response generated by some endogenous species. The selectivity of the proposed biosensor was studied by detecting 0.5 mM standard solution of SUC in the presence of several possible co-existing interferents such as glucose, sucrose, fructose, ascorbic acid and uric acid. The degree of substance interference with SUC was evaluated using current ratio method. The current ratio was calculated by measuring the peak current of 0.5 mM SUC (I_S) alone and compared this with the obtained peak current of 0.5 mM SUC in presence of 1mM of different interfering substances (I_{S+I}). The obtained current ratios (I_{S+I}/ I_S) were 0.89, 0.81, 0.92, 0.96 and 0.94 % in order of above mentioned co-existing interferents, respectively. The current ratios shows SUC significantly interfering with sucrose than other studied species. But, it was found that at low concentrations of glucose and sucrose (< 0.3 mM) the interference was very low with SUC. From the results the developed biosensor exhibits an excellent selectivity towards the determination of SUC in the presence of possible interferents.

6.3.10 Docking analysis

Docking studies between laccse and SUC were performed using the CDocker module [Wu et al., 2003] in Discovery Studio. The computed scoring function (CDocker interaction energy= -4.7) indicated that the SUC fits tightly in the active site of the laccase. The computed binding energy around -53.71 kcal/mol further supported the stronger binding affinity of SUC for the laccase. The docked complexe of laccase and SUC were then visualized to get a deeper understanding of their host-guest relationships and is pictorially depicted in Figure 6.30. A closer inspection of Figure 6.30 revealed that SUC interacted with the binding cavity of laccase through its fructose and galactose rings. Both inter and intra molecular hydrogen bonds, hydrophobic interactions were found to be important in the stabilization of their complex. Specifically, two intra

molecular hydrogen bonds (O…H) between amino acid ASP 242 (-CO and –OH) and galactose portion of SUC were observed. The fructose portion of SUC showed two intra molecular hydrogen bonds with amino acids LYS 261 and ASP 242. Furthermore two intermolecular hydrogen bonds were observed within the SUC molecule. Hydrophobic interactions between the chlorine atom in fructose ring and amino acid ARG 256 were observed and was thought to be responsible for the comfortable penetration of SUC into its active site with a stronger binding affinity.

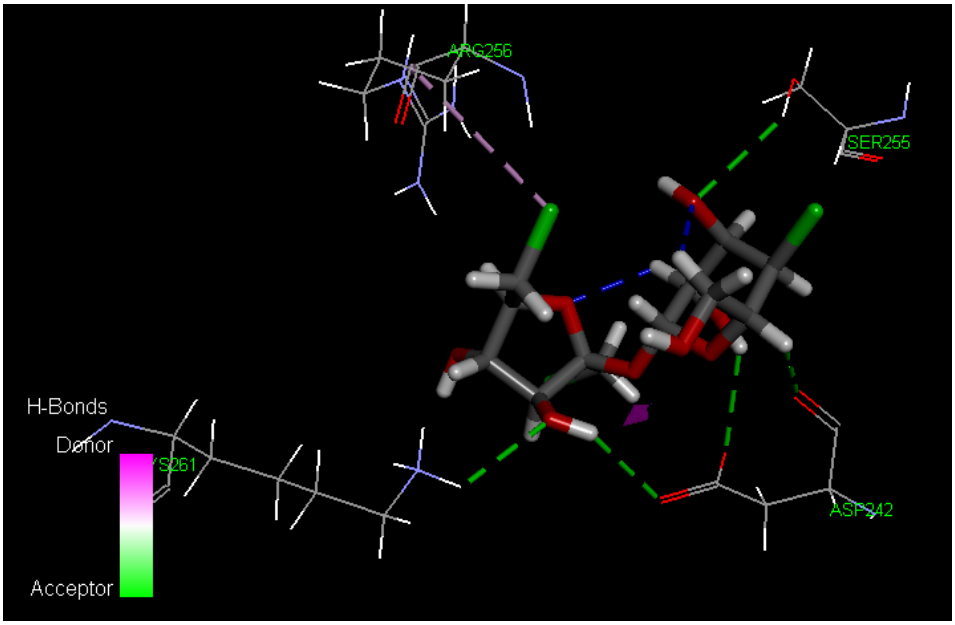

Figure 6.30: Conformation of SUC (in sticks format) docked into the active site of laccase. Only interacting amino acid (AA) residues (in lines format) are shown. Hydrophobic and hydrophilic AA are shown in magenta and green colour lines. Intra molecular hydrogen bonds are shown as green dotted line, whereas intermolecular hydrogen bonds and hydrophobic interactions are depicted in blue and pink dotted lines.

CHAPTER 7

SUMMARY AND CONCLUSIONS

The development of accurate, sensitive and specific methods for the quantitative determination of artificial sweeteners is a challenging task for researchers. The aim of this dissertation was to develop electrophoretic and biosensor methods for third generation artificial sweeteners such as steviol glycosides (rebaudioside A and stevioside), neotame and sucralose. Several analytical methodologies were developed and validated for their potential use in the analysis of high intensity sweeteners. Specifically, capillary electrophoresis (CE) as a complementary alternative to chromatographic techniques was found to offer greater opportunities for the determination of sweeteners. Accordingly in this work, two CE separation modes namely electro-kinetic chromatography and indirect UV-CZE were used for the analysis of artificial sweeteners. Additionally, nanomaterials in combination with electro analytical techniques resulted in high performance biosensors developed for the sensitive determination of sweeteners.

The first objective towards the overall goal of this project involved the separation and determination of sweeteners using CE. In this regard, the application of electro-kinetic chromatography (EKC-CE) was studied through the separation of steviol glycosides (rebaudioside A and stevioside) and neotame diastereomers (L,L and D,D) as discussed in Chapter 5.1 and 5.2. An indirect UV-CZE method was applied for the separation of sucralose as discussed in Chapter 5.3.

The simultaneous separation and determination of steviol glycosides with TM-β-CD were successfully implemented using the EKC–CE method and supported with molecular docking studies. The issue of poor resolution and longer migration times of the reported HPLC and MEKC-CE [Jaitak et al., 2008; Mauri et al., 1996] methods were resolved in the presence of TM-β-CD as

a separating agent. The optimum separation conditions were 50 mM phosphate buffer, pH 8.0, applied voltage 18 kV, cassette temperature of 30 ^{0}C with a 4 s sample injection time. The detection limits of 0.02017 and 0.07386 mM and relative standard deviation (n=5) of 1.10 and 1.17 were obtained with less than 7.5 min of separation time for rebaudioside A and stevioside respectively. Our results showed that the present method is a fast, efficient and facile method for the simultaneous separation and quantification of Reb A and Stv in real stevia samples. This study revealed that the good baseline resolution along with good reproducibility and repeatability, suggests that the inclusion of a separating agent, TM-β-CD greatly improved the separation efficiency of stevia glycosides. Moreover, the docking studies complimented the experimental results by highlighting the stability and the stronger interaction of Stv with TM-β-CD than with Reb A, thus supporting the order of elution obtained under experimental CE conditions (*Journal of the Iranian Chemical Society*, in 2015).

Further, a novel method has been reported for the chiral separation of neotame with EKC-CE in the presence of chiral separating agent TM-β-CD which resulted in good baseline resolution, reproducibility and accuracy with shorter migration times. The influence of buffer pH, buffer concentration, applied voltage, concentration of separating agent and capillary cassette temperature were studied on the retention and separation factors. Furthermore, the effect of temperature on the chiral separation was calculated in-terms of thermodynamic parameters (Gibbs free energy, entropy and enthalpy) according to the previously described van't Hoff equations and the results were in agreement with the experimental results, in terms of the elution order of two compounds. The optimum conditions were 50mM phosphate buffer, pH 5.5, applied voltage 20 kV,cassette temperature of 30 ^{0}C with a 4 s sample injection time. The calibration curve showed good linearity ($R^2 > 0.99$) with recoveries for both diastereomers ranging from 95.66–99.00% and

the limits of detection for L,L-neotame and D,D-neotame were 0.01857 and 0.08214 mM, respectively. The developed method showed analytical precision with relative standard deviations (n=5) of 1.20% and 1.17% with respect to migration times and peak areas, respectively. The obtained results suggest that the developed method is a reliable method to separate neotame in different food samples. The docking results supplied further evidence regarding the host-guest relationship between neotame diastereomers and TM-β-CD which supported the experimental results. However, large difference in the interaction energies observed between the diastereomers represents a significant differentiation. The results showed that both electrostatic and hydrophobic interactions played a significant role in stabilizing their inclusion complexes and consequently supported the elution order, based on their differential stabilities (*Analytical Letters,* in 2014).

The applicability of indirect UV-CZE method was investigated in the separation and determination of sucralose in different food samples. The separation of sucralose was achieved by nucleophilic substitution (S_N2) in the presence of amine buffers. Furthermore the FT-IR results were used to better understand the interaction of sucralose with amines. When compared to other amine buffers (ethyl amine, piperidine, triethylamine) morpholine showed good buffering capacity in terms of the migration time (< 8.0 min) and base line stability. The analytical applications of the proposed method showed by recovery percentages of sucralose in real sample analysis on an intra-day and inter-day basis at optimum experimental conditions 0.2 M buffer concentration, pH 12.0 and UV detection wavelength 230 nm. Recoveries ranged from 96.87 to 98.82 % for real samples and 94.45 to 98.06 % for the spiked samples respectively. Linearity was studied in the range of 2–10 mM and the regression equation and correlation coefficients are y = 167.27x + 0.3794 and 0.9942 respectively. The LOD and LOQ (signal to noise ratio *S/N*=3 and *S/N*=10) 0.3804 and 1.5215 mg/ L with %RSD (n = 5) ±1.27 and 1.19 % with respect to migration time and peak area. Furthermore

HOMO-LUMO calculations were employed to better understand the separation of sucralose with amine buffers. The results showed that, the HOMO-LUMO gap decreases in the presence of amine moiety irrespective of its nature.

The second objective of this project was to develop biosensors with good catalytic activity and conductivity using novel electrode materials for the determination of sweeteners. In this regard, different nanomaterials were used for the construction of biosensors and were used for the sensing of sweeteners. In Chapter 6.1, CuNPs loaded on to MWCNTs assimilated with β-CD modified GCE was presented for the determination of neotame. Cytochrome c and laccase based biosensors were developed for the analysis of rebaudioside A and sucralose as described in Chapters 6.2 and 6.3 respectively.

A novel high performance electrochemical sensor was fabricated for the electrochemical detection of neotame in different food samples. The physicochemical properties of the modified electrode were characterized by TEM, FT-IR, XRD and TGA techniques. The overall mass percentages of CuNPs, APDC and β-CD loaded on to MWCNTs were 62.83%. Overall, the TGA analysis supported the morphology studies are demonstrated that indeed the CuNPs were immobilized via the MWCNTs support paste. Furthermore, it was concluded that the functionalization improved the grafting of CuNPs on to MWCNTs also improved the thermal stability of the nanocomposites. Additionally, the electrochemical behavior of the developed sensor for neotame was further investigated using CV and DPV. Our results indicated that the CuNPs–APDC–MWCNTs-β-CD-GCE exhibited an efficient electro-catalytic oxidation for NTM with a relatively high sensitivity and stability. Under the optimized conditions, linear calibration DPV plots for the detection of NTM ranged from 0.03 to 2.0 mM with a detection limit of 0.013 mM. The applicability of the

developed electrochemical sensor was tested on NTM food samples and the results were in agreement with the CE method (*Biosensors and Bioelectronics,* in 2015).

A cytochrome c modified nanocomposite electrochemical biosensor was developed for the electrochemical determination of rebaudioside A in different food samples. The morphological characterization of the modified electrode was studied by UV, TEM, EDS, XRD and TGA techniques. The results from CV and DPV indicated that the Cyt c/AuNPs-GO/MWCNTs/Pt exhibited an efficient electrocatalytic reduction for Reb A at -0.1 V with a relatively high sensitivity and stability. Under the optimized conditions, linear calibration DPV plots for the detection of Reb A ranged from 0.001 to 1.25 mM (R^2 = 0.9936) with detection limits ranging from (*S/N = 3*) 0.264 μM to 0.75 μM. The applicability of the developed electrochemical sensor was tested on Reb A food samples and found that the concentrations ranged from 0.0106 to 0.0142 g/mL. Docking simulations further revealed that the Reb A has stronger tendencies to bind with the Cyt c *via* hydrogen bonding and hydrophobic interactions.

Further, Lacccase immobilized on ZnO NPs-ATP-GO nanocomposite based biosensor was constructed for the determination of sucralose in different food samples. The morphological characterization of the developed sensor was studied by FT-IR, TEM, XRD and TGA techniques. The developed biosensor showed fair responses in the presence of the mediator TEMPO to the oxidation of sucralose at +0.22 V. The effect of scan rate, pH, accumulation time and potential, laccase concentration and temperature were studied on the performance of sensor to sucralose oxidation. Under optimum conditions the results obtained from DPV showed a linear calibration plot (R^2 = 0.9984) was achieved in the concentrations ranging from 0.025 to 1 mM. The LODs and LOQs values were calculated and noted as 0.32 μM and 1.15 μM at signal to noise ratio of 3. The recovery percentages of the proposed sensor was found to range from 93.0 to 99.0 %. The

applicability of the developed biosensor was tested on SUC food samples with concentrations ranging from 0.0257 to 0.0421 g/mL.

Finally, even though different instrumentations, methodologies and materials were used in this work, a comparative study was conducted. Each method had their own merits and de-merits such as CE is a simple and highly selective method, but suffers poor reproducibility, detection limits and analysis time. However, in order to increase the simplicity and performance level of the determinations a highly sensitive, fast, selective and accurate methods were able to replace the classical methods such as HPLC, CE and this purpose and biosensor methods were developed in this study. The results obtained from both capillary electrophoresis and biosensor methods revealed that at optimum experimental conditions, with CE typical detection limits ranging from 0.02017 to 0.07386 mM for steviol glycosides, 0.01857 to 0.08214 mM for neotame diastereomers and for sucralose 0.2804 mM were achieved. In contrast to CE methods, biosensor methods attained very low detection limits of 0.264 µM, 0.013 mM and 0.325 µM for rebaudioside A, neotame and sucralose respectively. The unique properties of nanomaterials used in combination with electro chemical techniques provided best results in shorter analysis time in contrast to conventional separation methods.

References

Aboul-Enein, H. Y., High-performance liquid chromatographic enantioseparation of drugs containing multiple chiral centers on polysaccharide-type chiral stationary phases. *Journal of Chromatography A,* 906 **(2001)** 185–193.

Aboul-Enein, H. Y., and S. A. Bakr. Comparative study of the separation and determination of aspartame and its decomposition products in bulk material and diet soft drinks by HPLC and CE. *Journal of Liquid Chromatography and Related Technologies,* 20 (1997) 1437-1444.

Accelrys, Materials Studio Release Notes, Release 4.1; AccelrysSoftware, San Diego, CA (2006).

Achterberg, E. P., and C. Braungardt. Stripping voltammetry for the determination of trace metal speciation and in-situ measurements of trace metal distributions in marine waters. *AnalyticaChimicaActa,* 400 **(1999)** 381–397.

Alghamdi, A. H., A. F. Alghamdi, and A. A. Alwarthan. Determination of content levels of some food additives in beverages consumed in riyadh city. *Journal of the King Saud University,* 18 **(2005)** 99-109.

Altria, K. D., R. C. Harden, M. Hart, and J. Hevizi. Inter-company cross validation exercise on capillary electrophoresis-chiral analysis of clenbuterol. *Journal of Chromatography,* 641(**1993**) 147-153.

Amin, E. K., B. Larijani, and A. E. Habibi, Neohesperidin dihydrochalcone: Presentation of a small molecule activator of mammalian alpha-amylase as an allosteric effector. *FEBS Letters,* 587 **(2013)** 652–658.

Anastos, N.,N. W. Barnett, S. W. Lewis, J. R. Pearson and K. P. Kirkbride.Rapid determination of carbohydrates in heroin drug seizures using capillary electrophoresis with short-end injection. *Journal of Forensic Sciences,* 50 **(2005)**.

References

Anderson, R.L., Practical statistics for analytical chemists, Van Nostrand Reinhold, New York,1987.

Anderson, A. D. G., P. Poon, G. M. Greenway, and J. MacFie. A simple method for the analysis of urinary sucralose for use in tests of intestinal permiability. *Annals of Clinical Biochemistry: An international journal of biochemistry and laboratory medicine*, 42 **(2005)** 224-226.

Arai, T., M. Ichinose, H. Kuroda, N. Mimura, and T. Kinoshita. Chiral separation by capillary affinity zone electrophoresis using an albumin- containing support electrolyte. *Analytical Biochemistry,* 217 **(1994)** 7-11.

Arends, I. W. C. E., Y. X. Li, R. Ausan, and R. A. Sheldon. Comparison of TEMPO and its derivatives as mediators in laccase catalysed oxidation of alcohols. *Tetrahedron*, 62 **(2006)** 6659–6665.

Aturki, Z., and M. Sinibaldi. Separation of diastereomers of flavanone-7-Oglycosides by capillary electrophoresis using sulfobutyl ether-*β*-cyclodextrin as the selector. *Journal of Separation Sciences*, 26 **(2003)** 844–850.

Avula, B., R. B. Manyam, E. Bedir and I. A. Khan. Rapid separation and determination of four phenylpropanoid glycosides from T. chamaedrys by capillary electrophoresis method. *Chromatographia,* 58 **(2003)** 751-755.

Azzam, E. M. S., A. F. M. El-farargy, and A. A. Abd-Elaal. Enhancement the detection of Ni^{2+} and Zn^{2+} ions using nanostructure of synthesized dithiol surfactants with gold nanoparticles. *Journal of Industrial and Engineering Chemistry,* 20 **(2014)** 3905–3912.

Bahndorf, D., and U. Kienle. World market of sugar and sweeteners. International Association for Stevia Research, Hirschstraße 12, D- 70771 Leinfelden-Echterdingen, April 2004.

Bajpai, S. K., Y. M. Mohan, M. Bajpai, R. Tankhiwale, and V. Thomas. Synthesis of polymer stabilized silver and gold nanostructures. *Journal of Nanoscience and Nanotechnology,* 7 **(2007)** 2994–3010.

Ballester, P.J., and J.B. O. Mitchell. A machine learning approach to predicting protein-ligand binding affinity with applications to molecular docking. *Bioinformatics*, 26 **(2010)** 1169-1175.

Bannach, G., R. R. Almeida, L. G. Lacerda, E. Schnitzler and M. Ionashiro.Thermalstability and thermal decomposition of sucralose.*Ecletica Química São Paulo,*34 **(2009)** 21-26.

Banerjee, A., E. Mikhailova, S. Cheley, L.Q. Gu, M. Montoya, Y. Nagaoka, E. Gouaux, and H. Bayley. Molecular bases of cyclodextrin adapter interactions withengineered protein nanopores. *Proceedings of the National Academy of Sciences of the United States of America,* 107 **(2010)** 8165- 8170.

Barker, G. E., P. Russo, and R. A. Hartwick. Chiral separation of leucovorin with bovine serum albumin using affinity capillary electrophoresis. *Analytical Chemistry*, 64 **(1992)** 3024-3028.

Baratto, L., A. Candido, M. Marzorati, F. Sagui, S. Riva, and B. Danieli. Laccase-mediated oxidation of natural glycosides. *Journal of Molecular Catalysis B: Enzymatic*, 39 **(2006)** 3–8.

Baruwati, B., D. K. Kumar, and S. V. Manorama. Hydrothermal synthesis of highly crystalline ZnO nanoparticles: A competitive sensor for LPG and EtOH. *Sensors and Actuators B,* 119 **(2006)** 676–682.

Batchu, S. R., N. Quinete, V. R. Panditi, and P. R. Gardinali. Online solid phase extraction liquid chromatography tandem mass spectrometry (SPE-LC-MS/MS) method for the determination

of sucralose in reclaimed and drinking waters and its photo degradation in natural waters from South Florida. *Chemistry Central Journal*, 7 **(2013)** 1-16.

Bathinapatla, A., S. Kanchi, P. Singh, M. I. Sabela, M. Dovey, and K. Bisetty. Analytical evaluation of steviol glycosides by capillary electrophoresis supported with molecular docking studies. *Journal of the Iranian Chemical Society*, 12 **(2015)** 127-136.

Bathinapatla, A., S. Kanchi, P. Singh, M. I. Sabela, and K. Bisetty.Determination of neotame by high-performance capillary electrophoresisusing ß-cyclodextrin as a chiral selector. *Analytical Letters*, 47 (17) **(2014)** 2795-2812.

Bathinapatla, A., S. Kanchi, P. Singh, M. I. Sabela, and K. Bisetty. Fabrication of copper nanoparticles decorated multiwalled carbon nanotubes as a high performance electrochemical sensor for the detection of neotame. *Biosensors and Bioelectronics*, 67 **(2014)** 200-207**.**

Batra, B., S. Lata, M. Sharma, and C.S. Pundir. An acrylamide biosensor based on immobilization of hemoglobin onto multiwalled carbon nanotube/copper nanoparticles/polyaniline hybrid film. *Analytical Biochemistry*, 433 **(2013)** 210–217.

Bei, X. L., D. C. Bing, and H. Q. Qiong.Method for quantitative determination of sucralose in food. *Shanghai Journal of Preventive Medicine*, 4 **(2005)** 156-158.

Bergs, D., B. Burghoff, M. Joehnck, G. Martin, and G. Schembecker. Fast and isocratic HPLC-method for steviol glycosides analysis from Stevia rebaudiana leaves. *Journal für Verbraucherschutz und Lebensmittelsicherheit*,7 **(2012)** 147–154.

Berset, J. D., and N. Ochsenbein. Stability considerations of aspartame in the direct analysis of artificial sweeteners in water samples using high-performance liquid chromatography-tandem mass spectrometry (HPLC–MS/MS). *Chemosphere*, 88 **(2012)** 563–569.

References

Bird, R. B., W. E. Stewart, and E. N. Lightfoot. Transport Phenomena.John Wiley & Sons Inc., 2nd edition,2001.

Biswal, J., S. P. Ramnani, S. Shirolikar, and S. Sabharwal. Synthesis of rectangular plate like gold nanoparticles by in situ generation of seeds by combining both radiation and chemical methods.*Radiation Physics and Chemistry,* 80 **(2011)** 44–49.

Bopp, B. A., R. C. Sonders, and J. W. Kesterson. Toxicological aspects of cyclamate and cyclohexylamine. *Critical Reviews of Toxicology,* 16 **(1986)** 213–306.

Brizuela, A. B., A. B. Raschi, M. V. Castillo, P. Leyton, E. Romano, and S. A. Brandán.Theoretical structural and vibrational properties of the artificial sweetener sucralose. *Computational and Theoretical Chemistry,* 1008 **(2013)** 52–60

Buchgraber, M., and A. Wasik. Determination of nine intense sweeteners in foodstuffs by high-performance liquid chromatography and evaporative light-scattering detection: inter laboratory study. *Journal of AOAC International,* 92 **(2009)** 208–222.

Buzea, C., I. I. P. Blandino, and K. Robbie. Nanomaterials and nanoparticles: Sources and toxicity. *Biointerphases,* 2 (4) **(2007)** MR17 - MR172.

Cakir, S., E. Coskun, E. Bicer, and O. Cakir.Electrochemical study of the complexes of aspartame with Cu(II), Ni(II) and Zn(II) ions in the aqueous medium. *Carbohydrate Research,* 338, **(2003)** 1217–1222.

Calza, P., V. A. Sakkas, C. Medana, A. D. Vlachou, F. DalBello, and T. A. Albanis.Chromometric assesment and investigation of mechanism involved in photo-Fenton and Tio_2 photocatalytic degradation of the artificial sweetener sucralose in aqueous media. *Applied catalysis B: Environmental,* 129 **(2013)**71-79.

References

Campa, C., Ph. S. Kopplin, T.R.I. Cataldi, S.A. Bufo, D. Freitag, A. Kettrup.Analysis of cyanogenic glycosides by micellar capillary electrophoresis. *Journal of Chromatography B,* 739 **(2000)** 95–100.

Cao, Y., P. Hu, W. Pan, Y. Huang, and D. Jia.Methanal and xylene sensors based onZnO nanoparticles and nanorods prepared by room-temperature solid-statechemical reaction. *Sensors and Actuators B,* 134 **(2008)** 462–466.

Chankvetadze, B., and G. Blaschke. Enantioseparations in capillary electromigration techniques: recent developments and future trends. *Journal of Chromatography A,* 906 **(2001)** 309–363.

Chang, C. S., and T. S. Yeh. Detection of 10 sweeteners in various foods by liquid chromatography/ tandem mass spectrometry. *Journal of food and drug analysis,* **(2014)**, http://dx.doi.org/10.1016/j.jfda.2014. 01.024.

Charifson, P. S., J. J. Corkery, M. A. Murcko, and W. P. Walters.Consensus scoring: a method for obtaining improved hit rates from docking databases of three-dimensional structures into proteins. *Journal of Medicinal Chemistry,* 42 **(1999)** 5100–5109.

Chattopadhyay, S., U. Raychaudhuri, and R. Chakraborty. Artificial sweeteners–a review. *Journal of Food Science and Technology*, **(2011)** DOI 10.1007/s13197-011-0571-1.

Chauhan, N., J. Narang, R. Rawal, and C.S. Pundir. A highly sensitive non-enzymatic ascorbate sensor based on copper nanoparticles bound to multi walled carbon nanotubes and polyaniline composite. *Synthetic Metals,*161**(2011)** 2427– 2433.

Cheemalapati, S., S. Palanisamy, V. Mani, and S.M. Chen. Simultaneous electrochemical determination of dopamine andparacetamol on multiwalled carbon nanotubes/graphene oxidenanocomposite-modified glassy carbon electrode. *Talanta,* 117 **(2013)** 297-304.

Chekmeneva, E., J. M. D. Cruz, C. Arino, and M. Esteban. Binding of Hg^{2+} by Cys, Cys-Gly and reduced glutathione: Study by differential pulse voltammetry on rotating Au-disk electrode, electrospray ionization mass-spectrometry and isothermal titration calorimetry.*Journal of Electroanalytical Chemistry,* 644 **(2010)** 20–24.

Chen, W., D. Ghosh, J. Sun, M. C. Tong,F. Deng, and S. Chen. Dithiocarbamate-protected ruthenium nanoparticles: synthesis, spectroscopy, electrochemistry and STM studies. *Electrochimica Acta,* 53 **(2007)** 1150–1156.

Chen, G., J. Zhang, and J. Ye. Determination of puerarin, daidzein and rutin in Pueraria lobata (Wild.) Ohwi by capillary electrophoresis with electrochemical detection. *Journal of Chromatography A,* 923 **(2001)** 255-262.

Chen, H. Y., and R. Neeb. On the temperature dependence of polarographic currents.*Fresenius Journal of Analytical Chemistry,* 319 **(1984)** 240-247.

Chung, M. S., H. J. Suh, W. Yoo, S. H. Choi, Y. J. Cho, Y. H. Cho, and C. J. Kim. Daily intake assessment of saccharin, stevioside, D-sorbitol and aspartame from various processed foods in Korea. *Food Additives and Contaminants,* 22(11) **(2005)** 1087–1097.

Clark, L. C. Jr., and, C. Lions. Electrode systems for continuous monitoring in cardiovascular surgery. *Annals of the New York Academy of Sciences,* 102 (1962) 29-45.

Claub, K., and H. Jensen. Cycloadditionen von halogensulfonylisocyanatenan acetylene. *Tetrahedron Letters,* 11 **(1970)** 119–122.

Cohen, A. S., A. Paulus, and B. L. Karger. High-performance capillary electrophoresis using open tubes and gels. *Chromatographia,* 24 **(1987)** 15-24.

Conradi, S., C. Vogt and E. Rohde. Separation of enantiomeric barbiturates by capillary electrophoresis using a cyclodextrin containing run buffer. *Journal of Chemical Education,* 74 **(1997)** 1122-1125.

Cowan, J. A., Inorganic Biochemistry: An Introduction; VCH: New York, 1993.

Crow, D. R., Polarography of Metal Complexes; Academic Press: New York, 1969, p. 39.

Čučković, L., I. M. Hodžić and S. R. Niketić. Computational study of the chromatographic enantioseparation of tris(acetylacetonato)cobalt(III) complexes on an arginine complex of cobalt(III) acting as a chiral selector. *Journal of Serbanian Chemical Society*, 67 **(2002)** 735–744.

Daniel, M. C., and D. Astruc. Gold nanoparticles: assembly, supramolecular chemistry, quantum-size-related properties, and applications toward biology, catalysis, and nanotechnology.*Chemical Reviews*, 104 **(2004)** 293–346.

Demarse, N., and C. Quinn. Determination of a protein ligand interaction via continuous isothermal titration calorimetry. TA Instruments-Application note, MCAPN-2011-01.

Dharuman, V., J. H. Hahn, K. Jayakumar, and W. Teng. Electrochemically reduced graphene–gold nano particle composite onindium tin oxide for label free immuno sensing of estradiol. *Electrochimica Acta*, 114 **(2013)** 590–597.

Diamond, D., (Ed.), Chemical and Biological Sensors. Wiley, New York, 1998.

Dobashi, A., T. Ono, S. Hara, and J. Yamaguchi. Optical resolution of enantiomers with chiral mixed micelles by electrokinetic chromatography. *Analytical Chemistry,* 61 **(1989)** 1984-1986.

References

Duffy, V. B., and G. H. Anderson. Position of the American dietetic association: Use of nutritive and non-nutritive sweeteners. *Journal of the American Dietetic Association*, 98 (5) **(1998)** 580-587.

EC 2003 European parliament and council Directive 2003/115/EC: Amendment to European parliament and council Directive 94/35/EC on sweeteners for use in foodstuffs. Off JL114:15-17, L237:3-12.

Eggins, B., Chemical sensors and biosensors. Analytical Techniques in the Sciences. John Wiley & Sons, West Sussex, 2002.

Ellis, J. W., Overview of Sweeteners. *Journal of Chemical Education,* 72 (8) **(1995)** 671–675.

Erkucuk, A., I. H. Akgun, and O. Y. Celiktas. Supercritical CO2 extraction of glycosides from Stevia rebaudiana leaves: Identification and optimization. *Journal of Supercritical Fluids,* 51 **(2009)** 29–35.

Ewing, A. G., R. A. Wallingford, and T. M. Olefirowicz. Capillary Electrophoresis. *Analytical Chemistry,* 61 **(1989)** 292A–303A.

Fabbrini, M., C. Galli, P. Gentili, and D. Macchitella. An oxidation of alcohols by oxygen with the enzyme laccase and mediation by TEMPO. *Tetrahedron Letters*, 42 **(2001)** 7551-7553.

Fabbrini, M., C. Galli, and P. Gentili. Comparing the catalytic efficiency of some mediators of laccase.*Journal of Molecular Catalysis B: Enzymatic,* 16 (**2002**) 231-240.

Fabbrini, M., C. Galli, and P. Gentili. Radical or electron-transfer mechanism of oxidation with some laccase/mediator systems. *Journal of Molecular Catalysis B: Enzymatic,*18 **(2002)** 169-171.

Fanali, S., Enantioselective determination by capillary electrophoresis with cyclodextrins as chiral selectors.*Journal of Chromatography A,* 875 **(2000)** 89-122.

References

FDA statement on European aspartame study. CFSAN/ Office of Food Additive Safety. Available atwww.fda.gov/Food/FoodingredientsPackaging/FoodAdditives/ucm208580.

Ferrer I., and E. M. Thurman. Analysis of sucralose and other sweeteners in water and beverage samples by liquid chromatography/time-of-flight mass spectometry. *Journal of chromatography A*, 1217 **(2010)** 4127-4134.

Fernandez, C. L., Electro-catalytic reactions, The University of Hull, Doctoral Thesis 2009.

Fisher, R. S., Aspartame, neurotoxicity and seizures: A review. *Journal of Epilepsy*, 2(2) **(1989)** 55-64.

Fitch, C., and K. S. Keim. Position of the academy of nutrition and dietetics: Use of nutritive and nonnutritive sweeteners. *Journal of the Academic Nutrition Diet*, 112 **(2012)** 739-758.

Friesner, R. A., J. L. Banks, R. B. Murphy, T. A. Halgren, J. J. Klicic, D. T. Mainz, M. P. Repasky, E. H. Knoll, M. Shelley, J. K. Perry, D. E. Shaw, P. Francis, and P. S. Shenkin. Glide: A new approach for rapid, accurate docking and scoring. Method and assessment of docking accuracy. *Journal of Medicinal Chemistry*, 47 **(2004)** 1739-1749.

Frisch, M. J., G. W. Trucks, H. B. Schlegel, G. E. Scuseria, M. A. Robb, J. R. Cheeseman, G. Scalmani, V. Barone, B. Mennucci, G. A. Petersson, H. Nakatsuji, M. Caricato, X. Li, H. P. Hratchian, A. F. Izmaylov, J. Bloino, G. Zheng, J. L. Sonnenberg, M. Hada, M. Ehara, K. Toyota, R. Fukuda, J. Hasegawa, M. Ishida, T. Nakajima, Y. Honda, O. Kitao, H. Nakai, T. Vreven, J. A. Jr. Montgomery, J. E. Peralta, F. Ogliaro, M. Bearpark, J. J. Heyd, E. Brothers,K. N. Kudin, V. N. Staroverov, R. Kobayashi, J. Normand, K. Raghavachari, A. Rendell, J. C. Burant, S. S. Iyengar, J. Tomasi, M. Cossi, N. Rega, N. J. Millam, M. Klene, J. E. Knox, J. B. Cross, V. Bakken, C. Adamo, J. Jaramillo, R. Gomperts, R. E. Stratmann,O. Yazyev, A. J. Austin, R. Cammi, C. Pomelli, J. W. Ochterski, R. L. Martin, K. Morokuma,

V. G. Zakrzewski, G. A. Voth, P. Salvador,J. J. Dannenberg, S. Dapprich, A. D. Daniels, Ö. Farkas, J. B. Foresman, J. V. Ortiz, J. Cioslowski, and D. J. Fox, Gaussian 09, Revision D.01, Gaussian, Inc., Wallingford CT, 2009.

Gan, Z., H. Sun, R. Wang, and B. Feng. A novel solid-phase extraction for the concentration of sweeteners in water and analysis by ion-pair liquid chromatography–triple quadrupole masss pectrometry. *Journal of Chromatography A,*1274 **(2013)** 87– 96.

Gassmann, E, .J. E. Kuo, and R. N. Zare. Electrokinetic separation of chiral compounds. *Science,* 230 **(1985)** 813-814.

Geuns, J.M.C., Stevia and Steviol Glycosides (Euprint Ed., Heverlee, 2010).

Giuffrida, A., R. Caruso, M. Messina, G. Maccarrone, A. Contino, A. Cifuentes, and V. Cucinotta. Chiral separation of amino acids derivatised with fluorescein isothiocyanate by single isomer derivatives 3-monodeoxy-3-monoamino-β- and γ-cyclodextrins: the effect of the cavity size. *Journal of Chromatography A,*1269 **(2012)** 360–365.

Godel, H., and R. Weinberger. Chiral Recognition by Capillary Electrophoresis with Cyclodextrins. Application Note Hewlett-Packard Company, Publication Number 12-5963-5502E, 1995.

Gole, A., S. R. Sainkar, and M. Sastry. Electrostatically controlled organization of carboxylic acid derivatized colloidal silver particles on amine-terminated self-assembled monolayers. *Chemistry of Materials,* 12 **(2000)** 1234-1239.

Gooding, J. J., and D. B. Hibbert. The application of alkane thiol self-assembled monolayers to enzyme electrodes. *TrAC Trends in Analytical Chemistry,* 18 **(1999)** 525-533.

Goodsell, D. S.,and A. J. Olson. Automated docking of substrates to proteins by simulated annealing. *Proteins,* 8 **(1990)** 195-202.

References

Gopalan, A. I., K. P. Lee, K. M. Manesh, P. Santhosh, and J. H. Kim. Gold nanoparticles dispersed into poly(aminothiophenol) as a novel electro catalyst—Fabrication of modified electrode and evaluation of electrocatalytic activities for dioxygen reduction.*Journal of Molecular Catalysis A: Chemical,* 256 **(2006)** 335–345.

Gopalan, A. I., K. P. Lee, K. M. Manesh, P. Santhosh, J. H. Kim, and J. S. Kang. Electrochemical determination of dopamine and ascorbic acid at a novel gold nanoparticles distributed poly(4-aminothiophenol) modified electrode. *Talanta,* 71 **(2007)** 1774–1781.

Grant, J. A., B. T. Pickup, and A. Nicholls.A Smooth Permittivity Function for Poisson-Boltzmann Solvation Methods.*Journal of Computational Chemistry,* 22 **(2001)** 608–640.

Guijuan, L., F. Yongyu, and H. Yongguang.Investigation on the measurement of sucralose in food by HPLC-ELSD. *Liquor-Making Science and Technolgy,*5 **(2012)**104-109.

Gumede, N. J., Harmonization of internal quality tasks in analytical laboratories case studies: water analysis methods using polarographic and voltammetric techniques, Durban University of Technology, Master's Thesis 2008.

Harvey, A. E., and D. L. Manning. Spectrophotometric methods of establishing empirical formulas of colored complexes in solution. *Journal of the American Chemical Society,* 72 **(1950)** 4488-4493.

Hellsten, I., Implicit media frames: Automated analysis of public debate on artificialsweeteners. *Public Understanding of Science,*19 (5) **(2010)** 590-608.

He, Y. C., S. Fang, and X. J. Xu. Simultanious determination of acesulfame-K, aspartame and stevioside in sweetener blends by ultraviolet spectroscopy with variable selection by sipls algorithm. *Macedonian Journal of Chemistry and Chemical Engineering,* 31 **(2012)** 17–28.

Head, R. D., M. L. Smythe, T. I. Oprea, C. L. Waller, S. M. Green, and G. R. Marshall. Validate: A new method for the receptor-based prediction of binding affinities of novel ligands. *Journal of the American Chemical Society,* 118 **(1996)** 3959–3969.

Hearn, L. K., and P. P. Subedi.Determining levels of steviol glycosides in the leaves of Stevia rebaudiana by near infrared reflectance spectroscopy. *Journal of Food Composition and Analysis,* 22 **(2009)** 165–168.

Heiger, D., High performance capillary electrophoresis: An introduction, Agilent Technologies, Publication Number 5968-9963E, (2000).

Henze, G., Introduction to Polarography and Voltammetry, Metrohm Monograph: (3-52) (2007).

Henk, H. L., and P. R. Gerard. High performance capillary electrophoresis-agilent technologies. Publication number 5990-3777EN, (2010).

Hester, W.F., Rohm & Hass Co., 1953. Fungicidal composition, U.S.P.2, 317, 765 (1943). Re-issue no. 23,742.

Heyrovsky, J., The development of polarographic analysis. Analyst, 81 **(1956)** 189–192.

Hu, F., L. Xu, F. Luan, H. Liu, and Y. Gao.Determination of neotame in non-alcoholic beverage by capillary zone electrophoresis.*Journal of the Science of Food and Agriculture*, 93 **(2013)** 3334–3338.

Hua, N. W., and Z. Dan.Determination of sucralose in drink by LC-MS. *China Food Additives,* 2 **(2011)** 235-238.

Huang, N., C. Kalyanaraman, J. J. Irwin, and M. P. Jacobson.Physics based soring of protein-ligand complex: enrichment of known inhibitors in large scale virtual screening. *Chemical Information and Modeling,* 46 **(2006)** 243–253.

Huang, X., M.J. Gordon, and R.N. Zare. Bias in quantitative capillary zone electrophoresis caused by electrokinetic sample injection. *Analytical Chemistry,* 60 **(1988)** 375–377.

Hurum, D., and J. Rohrer. Steviol glycoside determination by HPLC with charged aerosol and UV detections using the acclaim trinity P1 column, Application Note: 293 (2011).

Hutapea, A. M., C. Toskulkao, P. Wilairat, and D. Buddhasukh. High-performance liquid chromatographic separation and quantification of stevioside and its metabolites. *Journal of Liquid Chromatography & Related Technologies,* 22 (8) **(1999)** 1161-1170.

Ibrahim, M.S., I. S. Shehatta, and M.R. Sultan. Cathodic adsorptive stripping voltammetric determination of nalidixic acid in pharmaceuticals, human urine and serum. *Talanta,* 56 **(2002)** 471-479.

Idris, M., J. V. Rao, D. Middha, S. K. Shukla, and T. R. Baggi. Determination of sucralose by controlled UV photodegradation followed by UV spectrophotometry. *Journal of AOAC International*, 96 **(2013)** 603-606.

Idris, M., S. Srivastava, T. R. Baggi, S. K. Shukla, and A. K.Ganjoo.Rhodamine-sulphuric acid-A new visualization reagent for thedetermination of sucralose by HPTLC. *E-Journal of Chemistry*, 7 **(2010)** 559-565.

Introduction to Capillary electrophoresis, Beckman Coulter, Hand book. Available at:https://www.google.co.in/?gws_rd=ssl#q=Introduction+to+Capillary+electrophoresis%2C+Beckman+Coulter%2C+Hand+book.

Jackson, A. U., A. Tata, C. Wu, R. H. Perry, G. Haas, L. West, and R. G. Cooks. Direct analysis of Stevia leaves for diterpene glycosides by desorption electrospray ionization mass spectrometry. *Analyst*, 134 **(2009)** 867–874.

References

Jadhao, D. B., S. D. Katekhaye, and B. N. Thorat. Improved RP-HPLC method for quantitative determination of stevioside in Stevia rebaudiana Bertoni Burm. *International Journal of Phytopharmacy,* 1 (2) **(2011)** 27-34.

Jaitak, V., A.P. Gupta, V.K. Kaul, and P.S. Ahuja.Validated high-performance thin- layer chromatography method for steviol glycosides in stevia rebaudiana. *Journal of Pharmaceutical and Biomedical Analysis,* 47 **(2008)** 790-794.

Jain, A. N.,Scoring noncovalent protein-ligand interactions: A continuous differentiable function tuned to compute binding affinities. *Journal of Computer-Aided Molecular Design,*10 **(1996)** 427–440.

Jain, A. N., Surflex: Fully automatic flexible molecular docking using a molecular similarity-based search engine. *Journal of Medicinal Chemistry,* 46 **(2003)** 499-511.

Japan FFCR, Standards for use, according to use categories. The Japan Food Chemical Research Foundation. Available at:http://www.ffcr.or.jp/zaidan/FFCRHOME.nsf/7bd44c20b0dc562649256502001b65e9/8a4352b95978b195492569990007fbaa/$FILE/Standards%20for%20Use%2013Dec04.pdf.

Jorgenson, J. W., and K. D. Lukacs. High-resolution separations based on electrophoresis and electroosmosis. *Journal of Chromatograophy A,* 218 **(1981)** 209-216.

Jenner, M. R., and A. Smithson. Physicochemical properties of the sweetener sucralose. *Journal of Food Science,* 54 **(1989)** 1646-1649.

Ji, C., Y. Sun, X. Li, X. Chu, and Z. Chen. Simultaneous determination of artificial sweeteners in beverage by ultra-performance liquid chromatography. *Chinese Journal of Chromatography,* 27 **(2009)** 111–113.

Jia, D., J. Dai, H. Yuan, L. Lei, and D. Xiao.Selective detection of dopamine in the presence of uric acid using a gold nanoparticles-poly(luminol) hybrid film and multi-walled carbon nanotubes with incorporated β-cyclodextrin modified glassy carbon electrode. *Talanta,* 85 **(2011)** 2344–2351.

Jia, Y., K. Yu, and K. Qian. Facile approach to prepare multi-walled carbonnanotubes/graphene nanoplatelets hybridmaterials. *Nanoscale Research Letters,* 8 **(2013)** 1-6.

Jiang, T. F., Y. H. Wang, Z. H.Lv and M. E. Yue. Determination of kava lactones and flavonoid glycoside in *Scorzonera austriaca* by capillary zone electrophoresis. *Journal of Pharmaceutical and Biomedical Analysis*, 43 **(2007)** 854–858.

Jiang, L., and L. Gao. Fabrication and characterization of ZnO-coated multi-walled carbon nanotubes with enhanced photocatalytic activity. *Materials Chemistry and Physics,* 91 **(2005)** 313–316

Jizhi, C., L. Jie, and L. Jinhua. Determination of neotame in food byhigh performance liquid chromatography. *Guangdong Chemical Industry,* 36 **(2009)** 176–188.

Johns, P., and L. Dowlati. Determination of acesulfame and sucralose in oral electrolyte maintenance solution by liquid chromatography. *Journal of AOAC International,* 86 **(2003)** 79-85.

Jones, G., P. Wilett, R. C. Glein, A. R. Leach, and R. Taylor. Development and validation of genetic algorithm and an empirical binding free energy function. *Journal of Molecular Biology,*267 **(1997)** 727-748.

Kakigi, Y., T. Suzuki, T. Icho, A. Uyama, and N. Mochizuki.Classification of stevia sweeteners in soft drinks using liquid chromatography and time-of-flight mass spectrometry. *Food Additives and Contaminants: A,* **(2013)** http://dx.doi.org/10.1080/19440049.2013.843101.

Kanchi, S., P. Singh, and K. Bisetty. Dithiocarbamates as hazardous remediation agent:A critical review on progress in environmental chemistryfor inorganic species studies of 20th century. *Arabian Journal of Chemistry,* 7 **(2014)** 11-25.

Kara, P., A. E. Muniz, M. M. Costa, M.M. Guix, M. Ozsoz, and M. A. Merkoci.Aptamers based electrochemical biosensor for protein detection using carbon nanotubes platforms. *Biosensors and Bioelectronics,* 26 **(2010)** 1715–1718.

Kaur, B., T. Pandiyan, B. Satpati, and R. Srivastava. Simultaneous and sensitive determination of ascorbic acid, dopamine, uric acid, and tryptophan with silver nanoparticles-decorated reduced graphene oxide modified electrode. *Colloids and Surfaces B: Biointerfaces,*111 **(2013)** 97– 106.

Kedik, S. A., S. V. Fedorov, N. A. Yanul, L. V. Prokhorova, E. V. Smirnova, and A. V. Panov. Chromatographic determination of stevioside in raw plant material. *Pharmaceutical Chemistry Journal*, 37 (10) **(2003)** 19–22.

Keilin, D., On cytochrome, a respiratory pigment, common to animals, yeast, and higher plants, *Proceedings of the Royal Society of London Series B,* 98 **(1925)** 312–339.

Knight, I.,The development and applications of sucralose, a new high-intensity sweetener. *Canadian Journal of Physiology and Pharmacology*,72 **(1994)** 435-439.

Kobayashi, C., M. Nakazato, Y. Yamajima, I. Ohno, M. Kawano, and K. Yasuda.Determination of sucralose by HPLC. *Shokuni Eiseigaku Zasshi*, 42 **(2001)** 139-143.

Kobayashi, Y., T.Shirochi, Y.Yasuda,and T.Morita.Synthesis of silver/copper nanoparticles and their metal-metal bonding property.*Journal of Mining and Metallurgy Section B: Metallurgy,* 49 **(2013)** 65-70.

Kok, W., Capillary electrophoresis: instrumentation and operation. *Chromatographia,* 4 **(2000)** Online ISBN 978-3-322-83133-0.

Kokotou, M. G., and n. S. Thomaidis. Determination of eight artificial sweeteners in wastewater by hydrophilic interaction liquid chromatography-tandem mass spectrometry. *Analytical Methods*,5 **(2013)** 3825-3833.

Kolb, N., J. L. Herrera, D. J. Ferreyra, and R. F. Uliana.Analysis of sweet diterpene glycosides from Stevia rebaudiana: Improved HPLC method. *Journal of Agricultural and Food Chemistry,*49 **(2001)** 4538-4541.

Koppenol, W.H., and J.Butler. The radiation chemistry of cytochrome c. *Israel Journal of the Chemistry,* 24 **(1984)** 11–16.

Koppensteiner, W. A., and M. J. Sippl. Knowledge-based potentials—back to the roots.*Biochemistry (Moscow),* 63 **(1998)** 247–252.

Kroger, M., K. Meister, and R. Kava. Low-calorie sweeteners and other sugar Substitutes: A review of the safety issues. *Comprehensive Reviews in Food science and Food safety,* 5 **(2006)** 35-47.

Kroemer, G., Cytochrome c. *Current Biology,* 9(13) **(1999)** R468-R468.

Kuhn, R., F. Stoecklin, and F. Erni. Chiral separations by host-guest complexation with cyclodextrin and crown ether in capillary zone electrophoresis. *Chromatographia,* 33 **(1992)** 32-36.

Kuntz, D., J. M. Blaney, S. J. Oatley, R. Langringe, and T. E. Ferrin. A geometric approach to macromolecule-ligand Interactions. *Journal of Molecular Biology,*161 **(1982)** 269-288.

Kuo, K. L., H. Y. Huang and Y.Z. Hsieh. High Performance Capillary ElectrophoreticAnalysis of Synthetic Food Colorants. *Chromatographia,* 47 **(1998)** 249-256.

Kuznesof, P.M.,The 68th JECFA Steviolglycosides (CTA) **(2007)** pp. 1–8

Larry, W., and D. C. Greenly. A doctor's guide to sweeteners. Clinical Tearout, 2 (2) 2003.

Lata, S., B. Batra, P. Kumar, and C.S. Pundir. Construction of an amperometric D-amino acid biosensor based on D-amino acid oxidase/carboxylated mutliwalled carbon nanotube/copper nanoparticles/polyalinine modified gold electrode. *Analytical Biochemistry,* 437 **(2013)** 1–9.

Lauer, H. H., and D. McManigill. Capillary zone electrophoresis of proteins in untreated fused silica tubing.*Analytical Chemistry,* 58 **(1986)** 166–170.

Laviron, E., General expression of the linear potential sweep voltammogramin the case of diffusion less electrochemical systems. *Journal of Electroanalytical Chemistry,* 101 **(1979)** 19-28.

Learn about cancer. Aspartame. Last Revised: 05/28/2014.Available at http://www.cancer.org/Cancer/CancerCauses/OtherCarcinogens/AtHome/aspartame,

Lee, C., W. Yang, and R.G. Parr, Development of the Colic-Salvetti correlation-energy formulainto a functional of the electron density. *Physical Review B,* 37 **(1988)** 785-789.

Li, B., and D. T. Haynie, Chiral Drug Separation. Encyclopedia of Chemical Processing Taylor & Francis, **(2006)** 449-458 DOI: 10.1081/E-ECHP-120039232.

Li, D., M. B. Muller, S. Gilje, R.B. Kaner, and G.G. Wallance. Processable aqueous dis-persions of graphene nanosheets. *Nature Nanotechnology,* 3 **(2008)** 101–105.

Li, J., T. Ehlers, J. Sutter, S. Varma-Obrien, and J. Kirchmair. CAESAR:a new conformer generation algorithm based on recursive buildup and local rotational symmetry consideration. *Journal of Chemical Information and Modeling,* 47 **(2007)** 1923-1932.

Li, X., X. Wang, L. Li, H. Duan, and C. Luo. Electrochemical sensor based on magnetic graphene oxide@gold nanoparticles-molecular imprinted polymers for determination of dibutyl phthalate. *Talanta,*131 **(2015)** 354–360.

Li, Y. F., Z. M. Liu, and Y. L. Liu. A mediator-free phenol biosensor based on immobilizing tyrosinase to ZnO nanoparticles. *Analytical Biochemestry*, 349 **(2006)** 33-40.

Li, Z. L., Y. Ying, L. Y. Ming, W. Jun, Z. Hui, and Z. J. Hua. Determination of sucralose in foodstuffs by ultraperformance liquid chromatography-electrospray negative ionization mass spectrometry. *Journal of Instrumental Analysis,* 10 **(2011).**

Li, Y., L. Zhang, M. Li, Z. Pan, and D. Li. A disposable biosensor based on immobilization of laccase with silica spheres on the MWCNTs-doped screen-printed electrode. *Chemistry Central Journal,* 6(103) **(2012)** 1-8.

Li, Y. L., C. X. Ding, H. L. Wang, Y. R. Suo, J. M. You and G. C. Chen. Separation and determination of flavone and xanthone glycosides in tibetan folk medicinal species Swertiamussotii and S. franchetiana by capillary electrophoresis. *Journal of Analytical Chemistry,* 63 **(2008)** 574–579.

Liau, A. S., J. T. Liu, L. C. Lin, Y. C. Chiu, Y. R. Shu, C. C. Tsai and C. H. Lin. Optimization of a simple method for the chiral separation of methamphetamine and related compounds in clandestine tablets and urine samples by β-cyclodextrin modified capillary electrophoresis: a complementary method to GC–MS. *Forensic Science International,* 134 **(2003)** 17–24.

Liebminger, S., M. Siebenhofer, and G. Guebitz. Oxidation of glycerol by 2,2,6,6 tetramethylpiperidine-N-oxyl (TEMPO) in the presence of laccase. *Bioresource Technology,* 100 **(2009)** 4541–4545.

Lim, H. S., S. K. Park, K. I. S. Kwak, H. Kim, J. H. Sung, S. J. Jang, M.Y. Byun, and S. H. Kim. HPLC-MS/MS analysis of 9 artificial sweeteners in imported foods. *Food Science Biotechnology,* 22 **(2013)** 233-240.

Lin, K. C., Y. C. Lin, and S. M. Chen. A highly sensitive nonenzymatic glucose sensor based on multi-walled carbonnanotubes decorated with nickel and copper nanoparticles. *Electrochimica Acta,* 96 **(2013)** 164–172.

Lina, B. A. R., H. C. Dreef-van der Meulen, and D. C. Leegwater. Subchronic (13-week) oral toxicity of neohesperidine dihydrochalcone in rats. *Food and Chemical Toxicology,* 28 (7) **(1990)** 507-513.

Lina, X., Y. Nia, and S. Kokot. Electrochemical mechanism of eugenol at a Cu doped goldnanoparticles modified glassy carbon electrodeand its analytical application in food samples. *Electrochimica Acta,* 133 **(2014)** 484–491.

Liu, F., Y. Wang, Y. Wang, J. Zhou, and C. Yan.Simultaneous determination of five synthetic sweeteners in food by solid phase extraction high performance liquid chromatography evaporative light scattering detection.*Chinese Journal of Chromatography,* 30 **(2012)** 292-297.

Liu, J., C.P. Ong, and S.F.Y. Li.Subcritical fluid extraction of stevia sweeteners from stevia rebaudiana.*Journal of Chromatographic Science,* 35 (9) **(1997)** 446-450.

Liu, J., and S. F. Y. Li.Separation and determination of stevia sweeteners by capillary electrophoresis and high performance liquid chromatography. *Journal of Liquid Chromatography,* 18 **(1995)** 1703-1719.

Liu, W. W., S. P. Chai, A. R. Mohamed, and U. Hashim. Synthesis and characterization of graphene and carbon nanotubes: A review on the past and recent developments. *Journal of Industrial and Engineering Chemistry*, 20 **(2014)** 1171–1185.

Loos, R., B. M. Gawlik, K. Boettcher, G. Locoro, S. Contini, and G. Bidoglio. Sucralose screening in European suface waters using a solid phase extraction-liquid chromatography –triple quadrapole mass spectrometry method. *Journal of chromatography A,* 1216 **(2009)** 1126-1131.

Lorenzo, C., J. Serrano-Diaz, M. Plaza, C. Quintanilla, and G. L. Alonso. Fast methodology of analysing major steviol glycosides from Stevia rebaudiana leaves. *Food Chemistry*, 157 **(2014)** 518–523.

Lovric, S.K.,I. Novak, and B. Novak, Measurementof steviosideby square-wave polarography. *Electroanalysis*, 22 **(2010)** 2211-2215.

Lukacs, K. D., and J. W. Jorgenson. Capillary zone electrophoresis: Effect of physical parameters on separation efficiency and quantitation. *Journal of High Resolution Chromatography,* 8 **(1985)** 407–411.

Lux, J. A., H. F. Yin, and G. Schomburg. A simple method for the production of gel-filled capillaries for capillary gel electrophoresis, *Journal of High Resolution Chromatography*, 13, **(1990)** 436-437.

Ma, X., H. Tao, K. Yang, L. Feng, L. Cheng, X. Shi, Y. Li, L. Guo, and Z. Liu. A functionalized graphene oxide–iron oxide nanocomposite for magnetically targeted drug delivery, photothermal therapy, and magnetic resonance imaging. *Nano Research,* 5 **(2012)** 199-212.

Martin, H., 1959. The Scientific Principles of Crop Protection. Edward Arnold Ltd., London.

Martins, C. A., P. S. Fernández, F. de Lima, H. E. Troiani, M. E. Martins, A. Arenillas, G. Maia, and G. A. Camara. Remarkable electrochemical stability of one-step synthesized Pd nanoparticles supported on graphene and multi-walled carbon nanotubes. *Nano Energy,* 9 **(2014)** 142–151.

Matsumoto, H., K. Hirata, N. Sakamaki, K. Hagino, and H. Ushiyama. Simultaneous determination of neotame, alitame and aspartame in foods by HPLC. *Shokuhin Eiseigaku Zasshi*, 49 **(2008)** 31–36.

Mauri, P., G. Catalano, C. Gardana, and P. Pietta.Analysis of Stevia glycosides by capillary electrophoresis. *Electrophoresis,* 17 **(1996)** 367-371.

Mayer. S., and V. Schurig. Enantiomer separation by electrochromatography on capillaries coated with chirasil-dex. *Journal of High Resolution Chromatography,* 15 **(1992)** 129-131.

Mayer, S., and V. Schurig. Enantiomer separation using mobile and immobile cyclodextrin derivatives with electromigration. *Electrophoresis*, 15 **(1994)** 835-841

Mayhew, D. A., C. P. Comer, and W. W. Stargel. Food consumption and body weight changes with neotame, a new sweetener with intense taste: differentiating effects of palatability from toxicity in dietary safety studies. *Regulation of Toxicology and Pharmacology,* 38 **(2003)** 124–143.

McCourt, J., J. Stroka, and E. Anklam. Experimental design-based development and single laboratory validation of a capillary zone electrophoresis method for the determination of the artificial sweetener sucralose in food matrices. *Analytical Bioanalytiocal Chemistry*, 382 **(2005)** 1269-1278.

McNeil, Strong clinical database that supports safety of splenda sweetener products. McNeil Nutritionals, LLC.Retrieved 2009-12-30 **(2009)**. http://www.splenda.com/

McLaughlin, G., R. Palmieri, and K. Anderson. Benefits of automation in the separation of biomolecules by high performance capillary electrophoresis, Techniques in Protein Chemistry II, Academic Press, **(1991)** 3-19.

Mead, R. N., J. B. Morgan, G. B. Jr. Avery, R. J. Kieber, A. M. Kirk, S. A. Skrabal, and J. D. Willey. Occurrence of the artificial sweetener sucralose in coastal and marine waters of the United States. *Marine Chemistry,* 116 **(2009)** 13–17.

Medeiros, R. A., A. E. de Carvalho, R. C. Rocha-Filho, and O. Fatibello-Filho. Square-wave voltammetry determination of aspartame in dietary products using a boron-doped diamond electrode. *Analytical Letters,* 40 **(2007)** 3195-3207.

Medeiros, R. A., A. E. de Carvalho, R. C. Rocha-Filho, and O. Fatibello-Filho. Simultaneous square-wave voltammetric determination of aspartame and cyclamate using a boron-doped diamond electrode. *Talanta,* 76 **(2008a)** 685–689.

Melis, M.S.,Renal excretion of stevioside in rats.*Journal of Natural Products,* 55 **(1992)** 688-690.

Melis, M.S.,Stevioside effect on renal function of normal and hypertensive rats.*Journal of Ethnopharmacology,* 36 **(1992)** 213-217.

Mello, L. C., A. Claudino, I. Rizatti, R. L. Bortoluzzi, and D. R. Zanette. Analysis of trace metals Cu^{2+}, Pb^{2+}, Zn^{2+} in coastal marine waste samples from Florianopolis, Santa Catarina state, Brazil. *Journal of Brazilian Chemical Society,* 16 **(2005)** 308-315.

Midmore, D. J., and A. H. Rank. A new rural industry–stevia–to replace imported chemical sweeteners. A report for Rural Industries Research and Development Corporation RIRDC Web, Publication No. W02/022 RIRDC Project No. UCQ-16A (2002).

Min, H., Z. Shulin, and C. Jie. Chiral separation of penicillamine enantiomers by capillary electrophoresis and its application. *Chinese Journal of Analytical Chemistry*,34 (5) **(2006)** 655-658.

Min, L. L., and P. J. Dong. Simultaneous determination of five sweeteners by reversed-phase high performance liquid chromatography. *Journal of Instrumental Analysis*, 27**(2008)** 549–552.

Minten, J., M. A. Erici, B. Bjorlenius, and T. Alsberg.A method for the analysis of sucralose with electrospray LC/MS in recipient waters and in sewage effluent subjected to tertiary treatment technologies. *International Journal of Environmental Analytical Chemistry*, 91 **(2011)** 357–366.

Moreto, N. G., R. Streich, and R. Galensa. Chiral separation of diastereomeric flavanone-7-O-glycosides in citrus by capillary electrophoresis. *Electrophoresis*, 24 **(2003)** 2716–2722.

Moreno, A., S. Leiva, J. Miralles, G. Ramis, J. M. Herrero and E. Simó. Improvement of analytical methods in post-market monitoring of food additives and testing of the improved methods (OC/EFSA/DCM/2012/04): Interim report on method development and in-house validation of the analysis method. External Scientific Report, EFSA supporting publication 2014:EN-706.

Motwani, H. V., S. Qiu, B. T. Golding, H. Kylin, and M. Tornqvist. Co(I)balamin reacts with sucralose to afford an alkylcobalamin: relevance to in vivo cobalamin and sucralose interaction. *Food and Chemical Toxicology*, 49 **(2011)** 750-757.

Mpanza, T., M. I. Sabela, S. S. Mathenjwa, S. Kanchi, and K. Bisetty. Electrochemical determination of capsaicin and silymarin using a glassy carbon electrode modified by gold nanoparticle decorated multiwalled carbon nanotubes.*Analytical letters*, 47 (17) **(2014)** 2813-2828.

References

Msagati, T. A. M., and J. C. Ngila. Voltammetric detection of sulfonamides at a poly(3-methylthiophene) electrode. *Talanta,* 58 **(2002)** 605-610.

Msangati, T. A. M., and J. C. Ngila, Voltammetric Determination of a benzimidazole anthelmintic mixture at a poly(3-methylthiophene)-modified glassy carbon electrode. *South African Journal of Chemistry,* 56 **(2003)** 5-9.

Murphy, C. J., A. M. Gole, S. E. Hunyadi, J. W. Stone, P. N. Sisco, and A. Alkilany. Chemical sensing and imaging with metallic nanorods. *Chemical Communications,* 5 **(2008)** 544–557.

Na, M. S., and D. Ken. Determination of sucralose contents in soy sauce and oyster sauce by HPLC. *Modern Food Science and Technology,* 25 **(2009)** 982-984.

Nabipour, H., Synthesis of a new dithiocarbamate cobalt complex and its nanoparticles with the study of their biological properties. *International Journal of Nano Dimension,* 1 **(2011)** 225–232.

National Standards of the People's Republic of China. Method forthe determination of neotame in foods by high-performance liquid chromatography. **(2009)** GB 23378–2009.

Nielsen, A. B.,and A. J. Holder. Gauss View 3.0, User's Reference, GAUSSIAN Inc., Pittsburgh, PA, 2000–2003.

Nishi, H., T. Fukuyama, M. Matsuo, and S. Terabe. Chiral separation of diltiazem, trimetoquinol and related compounds by micellar electrokinetic chromatography with bile salts. *Journal of Chromatography,* 515 **(1990)** 233-243.

Nofre, C., and J. M. Tinti. Neotame: discovery, properties, utility. *Food Chemistry,* 69 **(2000)** 245-257.

Nojiri, S., M. Nakazato, Y. Kasuya, I. Takano, M. Oishi, K. Yasuda, and S. Suzuki.Determination of sucralose in foods by HPLC using pre-column derivatization. *Journal of the Food Hygenic Society of Japan*, 43 **(2002)** 289-294.

Noviandri, I., and R. Rakhmana. Carbon paste electrode modified with carbon nanotubes and poly(3-Aminophenol) for voltammetric determination of paracetamol. *International Journal of Electrochemical Sciences,*7 **(2012)** 4479–4487.

Ohashi, M., T. Tanaka, H. Ohmae, K. Morii, K. Yasumura, and Y. Kitada. Analysis of sucralose in foods using LC/MS/MS. *Nara-ken Hoken Kankyo Kenkyu Senta Nenpo*, 38 **(2004)** 95-96.

Ordonez, E. Y., J. B. Quintana, R. Rodil, and R. Cela.Determination of artificial sweeteners in sewage sludge samples using pressurized liquid extraction and liquid chromatography–tandem mass spectrometry. *Journal of Chromatography A*, 1320 **(2013)** 10–16.

Ordonez, E. Y., J. B. Quintana, R. Rodil, and R. Cela. Determination of artificial sweeteners in water samples by solid-phase extraction and liquid chromatography–tandem mass spectrometry. *Journal of Chromatography A,* 1256 **(2012)** 197–205.

Otsuka, K., and S. Terabe. Effects of methanol and urea on optical resolution of phenylthio-hydantoin-DL amino acids by micellar electrokinetic chromatography with sodium-N-dodecanoyl- L-valinate. *Electrophoresis*, 11 **(1990)** 982-984.

Otsuka, K., J. Kawahara, K. Tatekawa, and S. Terabe. Chiral separations by micellar electrokinetic chromatography with sodium N-dodecanoyl- L-valinate. *Journal of Chromatography,* 559 **(1991)** 209-214.

Park, N. K., G. B. Han, S. H. Yoon, S. O. Ryu, and T. J. Lee. Preparation and absorption properties of ZnO nanostructures for cleanup of H_2S contained gas.*International Journal of Precision Engeneering and Manufacturing*, 11 **(2010)** 321–325.

Park, S., and R.S. Ruoff. Chemical methods for the production of graphenes, *Nature Nanotechnology*, 4 **(2009)** 217–224.

Patila, M., I. V. Pavlidis, E. K. Diamanti, P. Katapodis, D. Gournis, and H. Stamatis. Enhancement of cytochrome c catalytic behaviour by affecting the heme environment using functionalized carbon-based nanomaterials. *Process Biochemistry*, 48 **(2013)** 1010-1017.

Pavlova, V., V. Mirceski, Š.K. Lovric, S.P. Jovanovic, and B. Mitrevski. Studying electrode mechanism and analytical determination of cocaine and its metabolites at the mercury electrode using square-wave voltammetry. *Analytica Chimica Acta,* 512 **(2004)** 49-56.

Pei, J., and X.Y. Li. Xanthine and hypoxanthine sensors based on xanthine oxidaseimmobilized on a $CuPtCl_6$chemically modified electrode and liquid chromatography electrochemical detection.*Analytica Chimica Acta,* 414 **(2000)** 205-213.

Perkola, N., and P. Sainio. Quantification of four artificial sweeteners in Finnish surface waters with isotope-dilution mass spectrometry. *Environmental Pollution,* 184 **(2014)** 391-396.

Pesek, J. J., and M. T. Matyska. Determination of aspartame by high-performance capillary electrophoresis. *Journal of Chromatography A,* 781 **(1997)** 423-428.

Peng, Y.,J. Yuan, F. Liu, and J. Ye. Determination of active components in rosemary by capillaryelectrophoresis with electrochemical detection. *Journal of Pharmaceutical and Biomedical Analysis,* 39 **(2005)** 431–437.

Peng, Y.,and Q. Chen.Ultrasonic-assisted fabrication of highly dispersed copper/multi-walled carbon nanotube nanowires. *Colloids and Surfaces A: Physicochemical and Engineering Aspects*, 342 **(2009)** 132–135.

Peter, A., E. Vekes, and D. W. Armstrong. Effects of temperature on retention of chiralcompounds on a ristocetinA chiral stationary phase. *Journal of Chromatography A,* 958 **(2002)** 89–107.

Pham, T. A., B. C. Choi, K. T. Lim, and Y. T. Jeong. A simple approach for immobilization of gold nanoparticles on graphene oxidesheets by covalent bonding. *Applied Surface Science,*257 **(2011)** 3350–3357.

Pilehvar, S., J. A. Rather, F. Dardenne, J. Robbens, R. Blust, and K. D. Wael. Carbon nanotubes based electrochemical aptasensing platform for the detection of hydroxylated polychlorinated biphenyl in human blood serum. *Biosensors and Bioelectronics,* 54 **(2014)** 78–84.

Prabakaran, E.,and K. Pandian. Amperometric detection of Sudan I in red chili powder samples using Ag nanoparticles decorated graphene oxide modified glassy carbon electrode. *Food Chemistry,* 166 **(2015)** 198–205.

Prakash, I., I. Bishay, and S. Schroeder. Neotame: Synthesis, stereochemistry and sweetness. *Synthetic Communications,* 29 **(1999)** 4461-4467.

Pretorius, V., B. J. Hopkins and J. D. Schieke. Electro-osmosis: A new concept for high-speed liquid chromatography. *Journal of Chromatography A,* 99 **(1974)** 23-30.

Pruneanu, S., F. Pogacean, A. R. Biris, M. Coros, F. Watanabe, E. Dervishi, and A. S. Biris. Electro catalytic properties of graphene composites containing Au or silver nanoparticles *ElectrochimicaActa,* 89 **(2013)** 246– 252.

Pol, J., E. V. Ostra, P. Karasek, M. Roth, K. Benesova, P. Kotlarikova, and J. Caslavsky. Comparison of two different solvents employed for pressurised fluid extraction of stevioside from Stevia rebaudiana: methanol versus water. *Analytical Bioanalytical Chemistry,* 388 **(2007)** 1847–1857.

Qiu, W.Z. Wang, W. Nie, Y. Guo, and L. Huang. GC–MS Determination of Sucralose in Splenda. *Chromatographia,* 66 **(2007)** 935–939.

Qiu, D., P. S. Shenkin, F. P. Hollinger, and W. C. Still.The GB/SA Continuum Model for Solvation. A Fast Analytical Method for the Calculation of Approximate Born Radii. *The Journal of Physical chemistry A,* 101 **(1997)**3005–3014.

Raczi, C. P., R. D. Pascai, S. Szabolcs, I. Kacso, G. Tomoaia, A. Mocanu, O. Horovitzi and M. T. Cotisel. Inclusion Complex of β-Cyclodextrin and Quercetin, Thermodynamic Approach. *REV. CHIM. (Bucharest)* 62 **(2011)** 992-997.

Rajasekaran, T., A. Ramakrishna, K. U. Sankar, P. Giridhar, and G. A. Ravishankar. Analysis of predominant steviosides in Stevia rebaudiana Bertoni by Liquid Chromatography/ Electrospray Ionization-Mass spectrometry. *Food Biotechnology,* 22 **(2008)** 179–188.

Rajamani, R., and A. C. Good. Ranking poses in structure based lead discovery and optimization: current trends in scoring function development. *Current Opinion in Drug Discovery and Development,* 10 **(2007)** 308–315.

Rao, C. N.R., B.C.Sathish Kumar, M. Govindaraj, and M.Nath.Nanotubes. *Chemical Physics and Physical Chemistry,* 2 (2) **(2001)** 78-105.

Rashidian, M., and A. Fattahi. Comparison of thermochemistry of aspartame (artificial sweetener) and glucose. *Carbohydrate Research,* 344 **(2009)** 127–133.

Rawal, R., S. Chawla, and C. S. Pundir. Polyphenol biosensor based on laccase immobilized onto silver nanoparticles/multiwalled carbon nanotube/polyaniline goldelectrode. *Analytical Biochemistry,* 419 **(2011)** 196–204.

Rarey, M., B. Kramer, and T. Lengauer. Multiple automatic base selection: protein-ligand docking based on incremental construction without manual Intervention. *Journal of Computer-Aided Molecular Design,*11 **(1997)** 369-384.

Regulations relating to the use of sweeteners in foodstuffs. Foodstuffs, cosmetics and disinfectants act (1972), http://www. doh.gov.za/docs/foodcontrol/additives/2012/regr733

Rizelio, V. M., L. Tenfen, R. da Silveira, L. V. Gonzaga, A. C. O. Costa, R. Fett. Development of a fast capillary electrophoresis method for determination of carbohydrates in honey samples. *Talanta*, 93 **(2012)** 62–66.

Roberts, A., A. G. Renwick, J. Sims, and D. J. Snodin. Sucralose metabolism and pharmacokinetics in man. *Food and Chemical Toxicalogy*, 38 **(2000)** 31-41.

Rocchia, W., S. Sridharan, A. Nicholls, E. Alexov, A. Chiabrera, and B. Honig.Rapid grid-based construction of the molecular surface and the use of induced surface charge to calculate reaction field energies: applications to the molecular systems and geometric objects.*Journal of Computational Chemistry*,23 **(2002)** 128–137.

Rodero, A. B., L. D. Rodero, and R. Azoubel. Toxicity of sucralose in humans: A review. *International Journal of Morphology*, 27 **(2009)** 239-244.

Rudel, U., O. Geschke, and K. Cammann. Entrapment of enzymes in electropolymers for biosensors and graphite felt based flow-through enzyme reactors. *Electroanalysis*, 8 **(1996)** 1135-1139.

Samah, N.A., A.D.A. Hisham, and S.A. Rahim.Determination of stevioside and rebaudioside A in stevia rebaudiana leaves via preparative high performance liquid chromatography (prep-HPLC). *International Journal of Chemical and Environmental Engineering*, 332 **(2012)** 1-4.

Sarma, H., and K.C. Sarma. X-ray peak broadening analysis of ZnO nanoparticles derived by precipitation method. *International Journal of Scientific and Research Publications*, 4 **(2014)** 1-7.

Schiffman, S. S., and K. I. Rother. Sucralose, a synthetic organochlorine sweetener: Overview of biological issues. *Journal of Toxicology and Environmental Health B,* 16 **(2013)** 399–451.

Scheurer, M., H. J. Brauch, and F.T. Lange. Analysis and occurrence of seven artificial sweeteners in German waste water and surface water and in soil aquifer treatment (SAT). *Analytical Bioanalytical Chemistry,* 394 **(2009)** 1585–1594.

Schulz-Gasch, T., and M. Stahl. Binding site characteristics in structure-based virtual screening: evaluation of current docking tools. *Journal of Molecular Modeling,* 9 **(2003)** 47-57.

Scientific opinion of the Panel on Food Additives, Flavourings, Processing Aids and Materials in Contact with Food on a request from European Commission on neotame as a sweetener and flavor enhancer. EFSAJ 581:1–3 **(2007)**.

Seifert, M. H. J., J. Kraus, and B. Kramer. Virtual high-throughput screening of molecular databases. *Current Opinion in Drug Discovery and Development,*11 **(2007)** 298–307.

Sepaniak, M. J., R. O. Cole, and B. K. Clark. Use of native and chemically modified cyclodextrins for the capillary electrophoretic separation of enantiomers. *Journal of LiquidChromatography,* 15 **(1992)** 1023-1040.

Shafii, B., R. Vismeh, R. Beaudry, R. Warner, and A. D. Jones. Large-scale profiling of diterpenoid glycosides from Stevia rebaudiana using ultrahigh performance liquid chromatography/ tandem mass spectrometry. *Analytical Bioanalytical Chemistry,* 403 **(2012)** 2683–2690.

Shah, R., L. S. De Jager, and T. H. Begley.Simultaneous determination of steviol and steviol glycosides by liquid chromatography-mass spectrometry. *Food Additives & Contaminants: Part A,* 29 (12) **(2012)** 1861–1871.

Shankar, P., S. Ahuja, and K. Sriram. Non-nutritive sweeteners: Review and update. *Nutrition,* 29 **(2013)** 1293–1299.

Shimizu, T., T. Teranishi, S. Hasegawa, and M. Miyake. Size evolution of alkanethiol-protected gold nanoparticles by heat treatment in the solid state. *Journal of Physical Chemistry B,* 107 **(2003)** 2719-2724.

Sharma, D., S. Sharma, B.S. Kaith, J. Rajput and M. Kaur.Synthesis of ZnO nanoparticles using surfactant free in-air andmicrowave method. *Applied Surface Science,*257 **(2011)** 9661–9672.

Shervedani, R. K.,and A. Amini. Direct electrochemistry of dopamine on gold-agaricus bisporus laccase enzyme electrode: characterization and quantitative detection. *Bioelectrochemistry,* 84 **(2012)** 25–31.

Shoichet, B. K., S. L. McGovern, B. Wei, and J. J. Irwin.Lead discovery using molecular docking. *Current Opinion in Chemical Biology,* 6 **(2002)** 439-446.

Silverstein, R.M., and F. X. Webster. Spectroscopic identification of organic compounds, Wiley, New York, 1998.

Sippl, M. J.,Calculation of Conformational Ensembles from Potentials of Mean Force: an approach to the knowledge based prediction of local structures in globular proteins.*Journal of Molecular Biology,* 213 **(1990)** 859–883.

Soini, H., M. L. Riekkola, and M. V. Novotny. Chiral separation of basic drugs and quantitation of bupivacaine enantiomers in serum by capillary electrophoresis with modified cyclodextrin buffers. *Journal of Chromatography,* 608 **(1992)** 265-274.

Skálová, T., J. Dohnálek, L. H. Østergaard, P. R. Østergaard, P. Kolenko, J. Dušková, A. Štěpánková and J. Hašek.The structure of the small laccase from Streptomyces coelicolor

reveals a link between laccases and nitrite reductases. *Journal of Molecular Biology*, 385 **(2009)** 1165-1178

Spangenberg, B., J. Stroka, I. Arranz, and E. Anklam. A simple and reliable HPTLC method for the quantification of the intense sweetener sucralose. *Journal of Liquid Chromatography & Related Technologies,* 26 **(2003)** 2729-2739.

Stander, M. A., W. Kühna, and N. F. Hiten.Survey of South African fruit juices using a fast screening HILIC-MS method. *Food Additives & Contaminants: Part A,* 30 (9) **(2013)** 1473-1484.

Stankovich, S., D.A. Dikin, R.D. Piner, K.A. Kohlhaas, A. Kleinhamma, Y. Jia, Y. Wu,S. T. Nguyen, and R.S. Ruoff. Synthesis of graphene-based nanosheets via chemical reduction of exfoliated graphite oxide. *Carbon,* 45 **(2007)** 1558-1565.

Stroka, J., D. Ivanka, and B. Spangenberg. Determination of sucralose in soft drinks by high-performance thin-layer chromatography: Interlaboratory study. *Journal of AOAC International,* 92 **(2009)** 1153-1159.

Stroka, J., N. Dossi, and E. Anklam. Determination of the artificial sweetener sucralose by capillary electrophoresis. *Food Additives and Contaminents,* 20 **(2003)** 524-527.

Sturm, S., and H. Stuppner. Analysis of Iridoid Glycosides from *Picrorhizakurroa* by capillary electrophoresis and high performance liquid chromatography-mass spectrometry. *Chromatographia,* 53 **(2001)** 612-618.

Suomi, J., S. K. Wiedmer, M. Jussila, M. L. Riekkola. Analysis of eleven iridoid glycosides by micellar electrokineticcapillary chromatography (MECC) and screening of plant samples by partial filling (MECC)–electrospray ionisation mass spectrometry. *Journal of Chromatography A*, 970 **(2002)** 287–296.

Szejtli, J., Past, present and future of cyclodextrin research. *Pure Applied Chemistry,* 76 **(2004)** 1825-1845.

Tadhani, M. B., V. H. Patel, and R. Subhash.In vitro antioxidant activities of Stevia rebaudiana leaves and callus. *Journal of Food Composition and Analysis,* 20 **(2007)** 323-329.

Takano, T., and R.E. Dickerson. Redox conformation changes in refined tuna cytochrome c. *Proceedings of the National Academy of Sciences of the United States of America,* 77 **(1980)** 6371-6375.

Terabe, S., K. Otsuka, K. Ichikawa, A. Tsuchiya, and T. Ando. Electrokinetic separations with micellar solutions and open-tubular capillaries.*Analytical Chemistry,* 56 **(1984)** 111-116.

Terabe, S., Electrokinetic chromatography: an interface between electrophoresis and chromatography. *Trends in Analytical Chemistry,* 8 **(1989)** 129–134.

Thomas, P. D., and K. A. Dill. Statistical potentials extracted from protein structures: how accurate are they?.*Journal of Molecular Biology,* 257 **(1996)** 457–469.

Tobalina, F., F. Pariente, L. Hernandez, H. D. Abruna, and E. Lorenzo. Integrated ethanol biosensors based on carbon paste electrodes modified with [Re (phen-dione) $(CO)_3Cl$] and [Fe (phen-dione) $(PF_6)_2$]. *AnalyticaChimicaActa,* 395 **(1999)** 17-26.

Tomasik, P., Chemical and functional properties of food saccharides.CRC Press LLC 397, 2004.

Tran, N. H., J. Hu and S. L. Ong. Simultaneous determination of PPCPs, EDCs, and artificial sweeteners in environmental water samples using a single-step SPE coupled with HPLC–MS/MS and isotope dilution. *Talanta,* 113 **(2013)** 82–92.

Turkmen, E., S. Z. Bas, H. Gulce, and S. Yildiz. Glucose biosensor based on immobilization of glucose oxidase inelectropolymerized poly(o-phenylenediamine) film on

platinumnanoparticles-polyvinylferrocenium modified electrode. *Electrochimica Acta,* 123 **(2014)** 93–102.

Tung, V.C., M. J. Allen, Y. Yang, and R.B. Kaner. High-throughput solution processing of large-scale graphene.*Nature Nanotechnology*, 4 **(2009)** 25–29.

United States Food and Drug Administration. 2002a. Food additives permitted for direct addition to food for human consumption; neotame. Fed Reg 67:45300–10.

United States Food and Drug Administration. 2013. Department of Health and Human Services, Code of Federal Regulations Title 21 (21CFR172.829) Vol. 3, Revised as of April, 2013.

Vaher, M., M. Koel, J. Kazarjan and M. Kaljurand. Capillary electrophoretic analysis of neutral carbohydrates using ionic liquids as background electrolytes. *Electrophoresis,* 32 **(2011)** 1068–1073.

Vanek, T., A. Nepovim, and P. Valicek. Determination of stevioside in plant materials and fruit teas. *Journal of Food Composition and Analysis,* 14 **(2001)** 383-388.

Venkatachalam, C. M., X. Jiang, T. Oldfield, and M. Waldan. Ligand Fit: A novel method for the shape-directed rapid docking of ligands to protein active sites. *Journal of Molecular Graphics and Modelling,* 21 **(2003)** 289-307.

Vianna-Soares, C. D., and J. L. S. Martins. Saccharin analysis in pharmaceutical and cosmetic preparations by derivative ultraviolet spectrophotometry. *Brazilian Journal of Pharmaceutical Sciences*,38 **(2002)** 471-478.

Vindevogel, J., and P. Sandra, Introduction to Micellar Electrokinetic Chromatography. Hüthig Buch Verlag GmbH: Heidelberg, 1992, 100.

Voet, D., and J. G.Voet.*Biochemistry* (3rd ed.). Hoboken, NJ: John Wiley & Sons (2004).

Volkov, A. N., P. Nicholls, and J. A. R. Worrall. The complex of cytochrome c and cytochrome c peroxidase: The end of the road?.*Biochimica et Biophysica Acta*, 1807 **(2011)** 1482–1503.

Warren, C. R., and M. A. Adams. Capillary electrophoresis for the determination of major amino acids and sugars in foliage: application to the nitrogen nutrition of sclerophyllous species. *Journal of Experimental Botany*, 51 **(2000)** 1147-1157.

Wang, J., Carbon-Nanotube based electrochemical biosensors: A review. *Electroanalysis*, 17 (1) **(2005)** 7-14.

Wang, J. Analytical electrochemistry: VCH publishing, 2nd edition, 2000, 68-76.

Wang, K., P. Liu, Y. Ye, J. Li, W. Zhao, and X. Huang.Fabrication of a novel laccase biosensor based on silica nanoparticlesmodified with phytic acid for sensitive detection of dopamine. *Sensors and Actuators B*, 197 **(2014)** 292–299.

Wang, X., Y. Liu, and H. Wang. A structure-differential binding method for elucidating the interactions between flavonoids and cytochrome-c by ESI-MS and molecular docking. *Talanta*,116**(2013)**368–375.

Wang, Z., H. Zhang, L. Zhang, J. Yuan, S. Yan, and C. Wang. Low-temperature synthesis of ZnO nanoparticles by solid-state pyrolytic reaction.*Nanotechnology*, 14 **(2003)** 11–15.

Wang, P., and J. Ren. Separation of purine and pyrimidine bases by capillary electrophoresis using cyclodextrin as an additive. *Journal of Pharmaceutical and Biomedical Analysis*, 34 **(2004)** 277–283.

Wasik, A., J. McCourt, and M. Buchgraber. Simultaneous determination of nine intense sweeteners in foodstuffs by high performance liquid chromatography and evaporative light scattering detection-Development and single-laboratory validation. *Journal of Chromatography A*, 1157 **(2007)** 187–196.

References

Woelwer-Rieck, U., The leaves of Stevia rebaudiana (Bertoni), their constituents and the analyses thereof: A review. *Journal of Agricultural and Food Chemistry,* 60 **(2012)** 886-895.

Woelwer-Rieck, U., C. Lankes, A. Wawrzun, and M. Wust. Improved HPLC method for the evaluation of the major steviol glycosides in leaves of Stevia rebaudiana. *European Food Research Technology*, 231 **(2010)** 581–588.

Woelwer-Rieck, U., W. Tomberg and A. Wawrzun. Investigations on the stability of stevioside and rebaudioside A in soft drinks. *Journal of Agricultural and Food Chemistry,* 58 (**2010**) 12216–12220.

Wren, S. A. C., Theory of chiral separation in capillary electrophoresis. *Journal of Chromatography*, 636 **(1993)** 57–62.

Wren, S. A. C., R. C. Rowe, R. S. Payne. A theoretical approach to chiral capillary electrophoresis with some practical implications. *Electrophoresis,* 15**(1994)** 774–778.

Wu, F. Z., and P. Zhang. 2,3,6,30,40-Penta-O-acetyl-4,10,60-trichloro-4,10,60-trideoxysucrose,*Acta Crystallographica section E,*67**(2011)**02323-02329.

Wu, M., Y. Qian, J. M. Boyd, S. E. Hrudey, X. C. Le, and X. F. Li. Direct large volume injection ultra-high performance liquid chromatography-tandem mass spectrometry determination of artificial sweeteners sucralose and acesulfame K in well water. *Journal of Chromatography A,* **(2014)** http://dx.doi.org/10.1016/j.chroma.2014.07.035.

Wu, S. J., H. X. Wang, and G. J. Tao. Ultra-high pressure liquidchromatography–mass spectrometry method for simultaneous determination of six micro-sweeteners in distilled spirit. *Journal of Food Science and Biotechnology,* 29 **(2010)** 670–675.

References

Wu, G., D.H. Robertson, C.L. Brooks III, and M. Vieth.Detailed analysis of grid-based molecular docking: A case study of CDOCKER—A CHARMm-based MD docking algorithm. *Journal of Computational Chemistry,* 24 **(2003)**1549-1562.

Xu, X., P. Lu, Y. Zhou, Z. Zhao, and M. Guo. Laccase immobilized on methylene bluemodified mesoporous silica MCM-41/PVA. *Materials Science and Engineering C,* 29 (7) **(2009)** 2160–2164.

Xu, Y., Tutorial: Capillary electrophoresis. *The Chemical Educator,* 1**(1996)** 1-14.

Yang, D., and B. Chen. Determination of neotame in beverages, cakes and preserved fruits by column-switching high-performance liquid chromatography. *Food Additives and Contaminants Part A,* 27 **(2010)** 1221-1225.

Yang, D., and B. Chen. Simultaneous determination of non-nutritive sweeteners in foods by HPLC/ESI–MS. *Journal of Agricultural and Food Chemistry*, 57 **(2009)** 3022–3027.

Yang, Y., Y.M. Zhang, Y. Chen, D. Zhao, J. T. Chen, and Y. Liu. Construction of graphene oxide based noncovalent multiple nanosupramolecular assembly as a scaffold for drug delivery. *Chemistry-A European Journal,* 18 **(2012)** 4208-4215.

Yi, Z. W., and D. X. Juan.Determination of sucralose by High Performance Liquid Chromatography. *Food Science,* 7 **(2007).**

Yola, M. L., and N. Atar. A novel voltammetric sensor based on gold nanoparticles involved in p-aminothiophenol functionalized multi-walled carbon nanotubes: Application to the simultaneous determination of quercetin and rutin. *Electrochimica Acta,*119 **(2014)** 24– 31.

Yola, M. L., N. Atar, Z. Ustundag, and A. O. Solak. A novel voltammetric sensor based on p aminothiophenol functionalized graphene oxide/gold nanoparticles for determiningquercetin in the presence of ascorbic acid. *Journal of Electroanalytical Chemistry,* 698 **(2013)** 9–16.

References

Yoshikawa, K., S. Saito and A. Sakuragawa.Simultaneous analysis of acidulants and preservatives in food samplesby using capillary zone electrophoresis with indirect UV detection. *Food Chemistry,*127 **(2011)**1385-1390.

You, J. M., D. Kim, S. K. Kim, M. S. Kim, H. S. Han, and S. Jeon. Novel determination of hydrogen peroxide by electrochemically reduced graphene oxide grafted with aminothiophenol–Pd nanoparticles. *Sensors and Actuators B,*178 **(2013)** 450– 457.

Youssef, R. M., M. A. Korany, E. F. Khamis, H. Mahgoub, and M. F. Kamal. Kinetic spectrophotometric methods for the determination of artificial sweetener (Sucralose) in tablets. *Drug Testing and Analysis,* 3 **(2011)** 214-220.

Zeng, Y., Y, Zhou, T. Zhou, and G. Shi.A novel composite of reduced graphene oxide and molecularlyimprinted polymer for electrochemical sensing 4-nitrophenol. *ElectrochimicaActa,* 130 **(2014)** 504–511.

Zhang, L., H. Zhang, R. Zhou, Z. Chen, Q. Li, S. Fan, G. Ge, R. Liu, and K. Jiang. A graphene oxide–carbon nanotube grid for high-resolution transmission electron microscopy of nanomaterials.*Nanotechnology,* 22 **(2011)** 5704-5711.

Zhang, Q., S. Yang, J. Zhang, L. Zhang, P. Kang, J. Li, J. Xu, H. Zhou, and X.M. Song. Fabrication of an electrochemical platform based on the self-assembly of graphene oxide–multiwall carbon nanotube nanocomposite and horseradish peroxidase: direct electrochemistry and electrocatalysis. *Nanotechnology,* 22 **(2011)** 4010-4017.

Zhao, Y., X. Chen, X. Li, S. Yao, and M. Jin. Influences of ion-suppressors on retention behaviours of nine food additives in reversed-phase high performance liquid chromatographic separation. *Chinese Journal of Chromatography,* 29 **(2011)** 988–994.

References

Zhao, Y. G., X. H. Chen, S. S. Yao, S. D. Pan, X. P. Li, and M. C. Jin. Analysis of nine food additives in red wine by ion-suppression reversed phase high-performance liquid chromatography using trifluoroaceticacid and ammonium acetate as ion-suppressors. *Analytical Sciences,* 28 **(2012)** 967-971.

Zhao, Y. G., M. Q. Cai, X. H. Chen, S. D. Pan, S. S. Yao, and M. C. Jin. Analysis of nine food additives in wine by dispersive solid-phase extraction and reversed-phase high performance liquid chromatography. *Food Research International,* 52 **(2013)** 350–358.

Zhao, R. R., and B. P. Johnson. Capillary Electrochromatography: Analysis of sucralose and related carbohydrate compounds. *Journal of Liquid chromatography&Related Technologies,* 23 **(2000)** 1851-1857.

Zhou, Y., H. Zhang, J. Zhang, T. Liu, and W. Tang. Electrochemically sensitive determination of dopamine and uric acid based on poly (beryllon II)/nanowires-LaPO4 modified carbon paste electrode. *Sensors and Actuators B,* 182 **(2013)** 610– 617.

Zhoua, X., Z. Hea, Q. Liana, Z. Lia, H. Jiang, and X. Lu. Simultaneous determination of dihydroxybenzene isomers basedon graphene-graphene oxide nanocomposite modified glassycarbon electrode. *Sensors and Actuators B,* 193 **(2014)** 198– 204.

Zimmermann, B. F., U. Woelwer-Rieck, and M. Papagiannopoulos.Separation of steviol glycosides by hydrophilic liquid interaction chromatography. *Food Analytical Methods,* 5 **(2011)** 266-271.

Zygler, A., A. Wasik, and J. Namiesnik. Analytical methodologies for determination of artificial sweeteners in foodstuffs. *Trends in Analytical Chemistry*, 28 (9) **(2009)** 1082-1102.

Zygler, A., A. Wasik, A. Kot-Wasik, and J. Namiesnik. Determination of nine high-intensity sweeteners in various foods by high-performance liquid chromatography with mass spectrometric detection. *Analytical Bioanalytical Chemistry,* 400 **(2011)** 2159–2172.

Zyglar, A., A. Wasik, A. Kot-Wasik, and J. Namiesnik.The content of high-intensity sweeteners in different categories of foods available on the Polish market. *Food Additives & Contaminants: Part A,* 29 **(2012)**1391–1401.

Definitions

Accuracy:

The closeness of agreement between a test result and the accepted reference value.

Bias:

The difference between the expectation of the test results and an accepted reference value.

Calibration curve:

The graphical representation of measuring signal a function of quantity of analyte.

Chiral

Handed‘‘, having the characteristic of ―handedness‖, which is having the potential to exist as two non-superimposable structures that are mirror images; not synonymous with the terms enantiomerically pure or optically active.

Enantiomers

Two stereoisomers whose molecules are non-superimposable mirror images of one another.

Diastereoisomerism

Stereoisomerism other than enantiomerism and *cis-trans* isomerism. Diastereoisomers (or diastereomers) are stereoisomers not related as mirror images. Diastereoisomers are characterized by differences in physical properties, and by differences in chemical behaviour towards achiral as well as chiral reagents.

Interference:

An interference is a substance, other than the assayed material, that can be measured by the chosen analytical method or that can prevent the assayed material from being measured.

Limit of detection:

The lowest content that can be measured with reasonable statistical certainty.

Appendix 1: Definitions

Limit of quantitation:

The content equal to or greater than the lowest concentration point on the calibration curve.

Measurement:

Set of operations having the object of determining a value of a quantity.

Precision:

The closeness of agreement between independent test results obtained under stipulated conditions.

Sensitivity:

The change in the response of a measuring instrument divided by the corresponding change the stimulus.

Specificity or selectivity:

The ability of a method to measure only what it is intended to measure.

Stability:

Ability of a material to persist unchanged a period of time under the expected conditions of storage and use.

Recovery:

Yield of a preconcentration or extraction for an analyte divided by the amount of analyteinitially present in the original sample.

Repeatability:

Precision under repeatability conditions, i.e. conditions where independent test results are obtained with the same method on identical test items in the same laboratory by the same operator using the same equipment within short intervals of time.

Appendix 1: Definitions

Repeatability (of results of measurements):

Closeness of the agreement between the results of successive measurement of the same measure and carried out in the same condition of measurement.

Reproducibility:

Precision under reproducibility conditions, i.e. conditions where test results are obtained with the same method on identical test items in different laboratories with different operators using different equipment.

Relative standard deviation:

Relative standard deviation is a measure of precision in data analysis. Relative standard deviation is calculated by dividing the standard deviation of a series of values by the average of the values.

Reproducibility standard deviation:

The standard deviation of test results obtained under reproducibility conditions

Robustness:

The robustness of an analytical procedure is a measure of its capacity to remain unaffected by small, but deliberate variations in method parameters and provides an indication of its reliability during normal usage.

Validation:

Confirmation by examination and provision of objective evidence that the particular requirements for a specified intended use are fulfilled

Table 2.1: Molecular dimensions and physical properties of α-, β-, and γ- cyclodextrins [CDs]

Type of cyclodextrin	No. of glucose units	Molecular weight	Molecular dimensions (Å)			Solubility at 25 °C (g/100 mL H_2O	[α] D,25
			Inside diameter	Outside diameter	Height		
α	6	973	5.7	13.7	7.0	14.50	150
β	7	1135	7.8	15.3	7.0	1.85	162
γ	8	1297	9.5	16.9	7.0	23.20	177

Table 2.2: Regulatory status for the ten sweeteners in the present study by different countries.

Compound	EU	US FDA	Japan	FSANZ	China	Taiwan
SAC	Yes[a]	Yes	Yes	Yes	Yes	Yes
CYC	Yes	No	No	Yes	Yes	Yes
ASP	Yes	Yes	Yes	Yes	Yes	Yes
ACS-K	Yes	Yes	Yes	Yes	Yes	Yes
ATM	Yes	No	Yes	Yes	Yes	Yes
NHDC	Yes	No	No	No	No	No
NTM	Yes	Yes	No	Yes	Yes	Yes
SCL	Yes	Yes	Yes	Yes	Yes	Yes
STV	Yes	No	No	Yes	Yes	Yes
DUC	No[b]	No	No	No	No	No

ACS-K = acesulfame potassium; ATM = alitame; ASP = aspartame; CYC = cyclamate; DUL = dulcin; EU = European Union; FSANZ = Food Standards Australia New Zealand; NTM = neotame; NHDC = neohesperidindihydrochalcone; SAC = saccharin; SCL = sucralose; STV = steviol glycosides; US FDA = US Food and Drug Administration.
[a]Yes: permitted food additives.
[b]No: nonpermitted food additives.

Table 2.3: Properties and structures of sweeteners

Sweetener	Properties of sweeteners	Structure[a]
Saccharine E-No: E-954 [a]CAS NO: 81-07-2	Formulae $C_7H_5NO_3S$ [a]Molecular weight 183.18 [a]pKa1.60 Log Kow0.910 [b]W.S (g L^{-1}) 4 [d]M.U.D (mg L^{-1}) 80[e] Sweeteness300-500	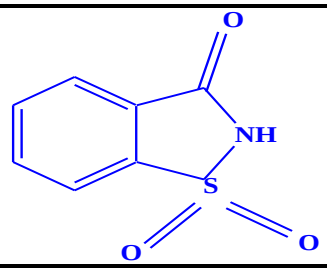
Cyclamate E-No: E-952 [a]CAS NO: 139-05-9	Formulae $C_6H_{12}NO_3SNa$ [a]Molecular weight 201.22 [a]pKa-8.66[c] Log Kow-2.63 [b]W.S (g L^{-1})1000 [d]M.U.D (mg L^{-1})250 Sweeteness30	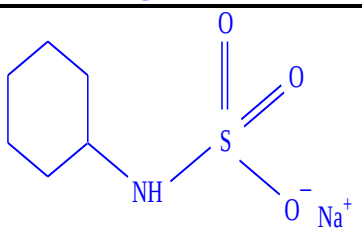
Acesulfame- K E-No: E-950 [a]CAS NO: 55589-62-3	Formulae $C_4H_4KNO_4S$ [a]Molecular weight 201.24 [a]pKa~2 Log Kow-0.31 [b]W.S (g L^{-1}) 270 [d]M.U.D (mg L^{-1}) 350 Sweeteness200	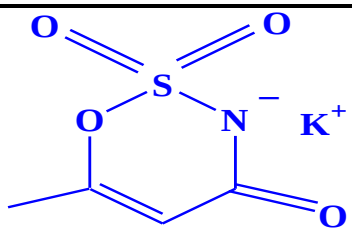
Neohesperidinedi hydrochalcone E-No: E-959 [a]CAS NO: 20702-77-6	Formulae $C_{26}H_{36}O_{15}$ [a]Molecular weight 612.58 [a]pKa6.85 Log Kow0.205 [b]W.S (g L^{-1}) 0.4-0.5 [d]M.U.D (mg L^{-1}) 30 Sweeteness 1900	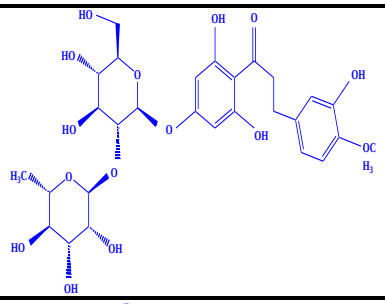
Aspartame E-No: E-951 [a]CAS NO: 22839-47-0	Formulae $C_{14}H_{18}N_2O_5$ [a]Molecular weight 294.30 [a]pKa[c]3.21, 5.0, 7.7 Log Kow0.542 [b]W.S (g L^{-1}) 10 [d]M.U.D (mg L^{-1}) 600 Sweeteness180-200	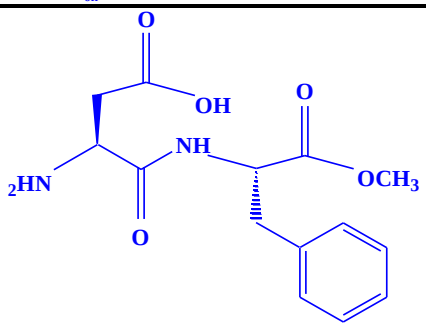
Alitame E-No: E-956 [a]CAS NO: 80863-62-3	Formulae $C_{14}H_{25}N_3O_4S$ [a]Molecular weight 331.431 [a]pKa[c]3.44, 8.23 Log Kow ---- [b]W.S (g L^{-1})0.18 [d]M.U.D (mg L^{-1}) ---- Sweeteness 2000	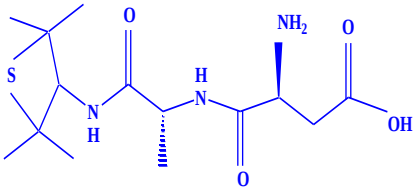

Appendix 2: Tables

Rebaudioside A E-No: E-960 [a]CAS NO:58543-16-1	Formulae C44H70O23 [a]Molecular weight 967.01 [a]pKa 8.0 Log Kow ----- [b]W.S (g L-1) 80 [d]M.U.D (mg L -1) ---- Sweeteness 250-400	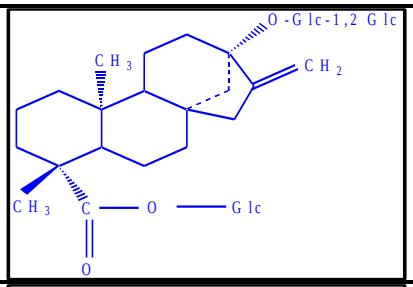
Stevioside E-No: E-960 [a]CAS NO: 57817-89-7	Formulae C38H60O18 [a]Molecular weight 804.87 [a]pKa 8.4 Log Kow --- [b]W.S (g L-1) 13 [d]M.U.D (mg L -1) --- Sweeteness 200-250	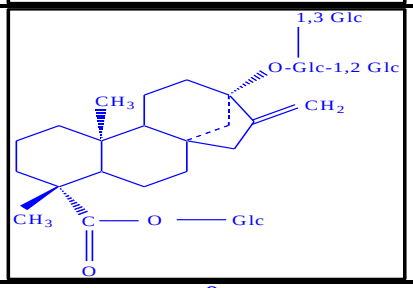
Neotame E-No: E-961 [a]CAS NO: 165450-17-9	FormulaeC20H30N2O5 [a]Molecular weight 378.46 [a]pKa[c]3.68, 5.5, 8.1 Log Kow3.834 [b]W.S (g L-1)12.6 [d]M.U.D (mg L -1)20 Sweeteness10000	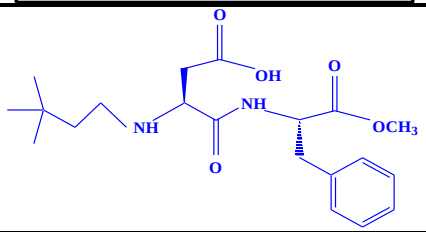
Sucralose E-No: E-955 [a]CAS NO: 56038-13-2	FormulaeC12H19Cl3O8 [a]Molecular weight 397.63 [a]pKa11.8 Log Kow-0.49, -0.51, -1.0 [b]W.S (g L-1)282 [d]M.U.D (mg L -1)300 Sweeteness600	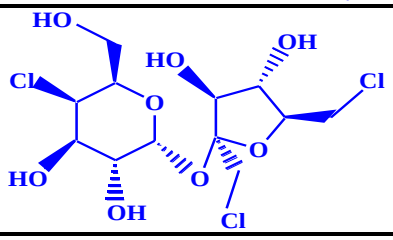

W. S = Water solubility
M. U. D = Maximum usable dosase
[a]Data from SciFinder Scholar Database (Calculated using Advanced Chemistry Development (ACD/Labs) Software VII. 02 (©1994–2011 ACD/Labs)): http://www.cas.org/products/sfacad/
[b] Experimental values, from database of physicochemical properties. Syracuse Research Corporation: http://www.syrres.com/esc/physdemo.htm
[c] Protonated form.
[d]Maximun usable dose (MUD) authorized in EU legislation for use in non-alcoholic drinks. European Commission, Directive 94/35, 1994; European Commission, Directive 96/83, 1996; European Commission, Directive 2003/115, 2003; European Commission, Directive 2006/52, 2006 and European Commission, Directive 2009/163, 2009)
[e] 'Gaseosa': non-alcoholic water based drink with added carbon dioxide, sweeteners and flavorings, 100 mg L^{-1}

J IRAN CHEM SOC (2015) 12:127–136
DOI 10.1007/s13738-014-0465-z

ORIGINAL PAPER

Analytical evaluation of steviol glycosides by capillary electrophoresis supported with molecular docking studies

Bathinapatla Ayyappa · Suvardhan Kanchi · Parvesh Singh · Myalowenkosi I. Sabela · Martin Dovey · Krishna Bisetty

Received: 17 December 2013 / Accepted: 5 May 2014 / Published online: 27 May 2014

Abstract This paper reports on a newly developed electrokinetic chromatographic method for the simultaneous separation and determination of steviol glycosides in real stevia samples by capillary electrophoresis and supported by molecular docking studies. Our results obtained using 30-mM heptakis-(2,3,6-tri-*o*-methyl betacyclodextrin) as a separating agent, suggest that at optimum experimental conditions the detection limits of 2.017×10^{-5} and 7.386×10^{-5} M and relative standard deviations ($n = 5$) of 1.10 and 1.17 were obtained for rebaudioside-A and stevioside, respectively. In addition, the molecular docking studies explained to a certain extent why the separation was successful. The calculated binding free energy results for the rebaudioside-A and stevioside complexes formed with the separating agent showed that although both ligands penetrated deeply into the hydrophobic cavity of the separating agent, the presence of additional hydrogen bonding in the case of stevioside is probably responsible for its stronger binding affinity than that of rebaudioside-A.

B. Ayyappa · S. Kanchi (✉) · M. I. Sabela · K. Bisetty (✉)
Department of Chemistry, Durban University of Technology, P.O. Box 1334, Durban 4000, South Africa
e-mail: ksuvardhan@gmail.com

K. Bisetty
e-mail: bisettyk@dut.ac.za

P. Singh
School of Chemistry and Physics, University of KwaZulu Natal, P/Bag X54001, Westville, Durban 4000, South Africa

M. Dovey
Kerry Ingredients and Flavours, Hillcrest 3610, KZN, South Africa

Keywords Steviol glycosides (rebaudioside-A, stevioside) · Heptakis 2,3,6-tri-*o*-methyl betacyclodextrin (TM-β-CD) · Capillary electrophoresis (CE) · Molecular docking (MD)

Introduction

Stevia rebaudiana Bertoni, an herbaceous perennial shrub, belonging to the *Asteraceae* family also known as "Sweet-Leaf" has attracted economic and scientific interest due to the non-nutritive sweetness and the therapeutic properties of its leaf [1]. Japan and Korea, are the largest consumers of stevia extract consuming about 200 and 115 tons respectively, on an annual basis. In Japan, stevia replaces the artificial sweeteners like aspartame which were around since the 1970s. The stevia sweeteners are approximately 300 times sweeter than sugar [2, 3]. Lately, the use of stevia has been approved by the Food and Drug Association in South Africa with the recent promulgation (Foodstuffs, Cosmetics and Disinfectants Act, 1972, 10th September 2012) of the new sweetener regulations [4].

Stevia leaves contain diterpene glycosides, the most abundant of which are stevioside (Stv) and rebaudioside-A (Reb A) [5] as shown in Table 1. Traditionally, the dry weight percentages of glycosides present in the leaves were reported as Stv ranging from 5 to 10 %, Reb A from 2 to 4 % and with a lower percentage reported for rebaudioside-C (Reb C). On the other hand, the relative sweetness of the Stv ranges from 60 to 70 % and between 110 to 270 times sweeter than sugar, while Reb A ranges from 30 to 40 % and between 180 to 400 times sweeter than sugar, resulting in these two compounds being the sweetest compounds amongst the remaining glycosides [1]. Apart from these sweetening properties, other health benefits of steviol

Table 1 Structure of major steviol glycosides

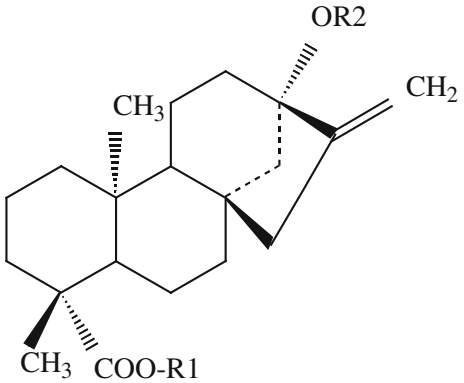

Compound	Abbreviation	R1	R2
Stevioside	Stv	Glu	Glu–1,2–Glu
Rebaudioside-A	Reb A	Glu	Glu—1,2—Glu | 1,3—Glu
Rebaudioside-C	Reb C	Glu	Glu—1,2—Rham | 1,3—Glu
Dulcoside-A	Dul	Glu	Glu–1,2–Rham

Glu Glucose, *Rham* rhamnose

glycosides includes antihypertensive, antihyperglycemic and anti-human rotavirus activities [6]. On the other hand, the reported drawbacks for the impure stevia glycosides include hypotension, diuresis, natriuresis and kaliuresis [7–9].

The composition of the stevia components in the leaves is highly dependent on the nature of the soil, climate and the methods used for extraction and purification [10]. A survey of the reported literature for the separation and determination of steviol glycosides in different food samples revealed that most of the analytical work was done with high-performance liquid chromatography (HPLC) [11–23], liquid chromatography coupled with tandem mass spectrometry (LC–MS) [26–28, 30] and liquid chromatography coupled with electrospray ionization mass spectrometry (LC–ESI–MS) [25, 29] but with only a few capillary electrophoretic (CE) methods [2, 7, 24]. Moreover, the above-reported chromatographic techniques require expensive experimental setup [11, 23, 25, 30] for the simultaneous separation and determination of steviol glycosides. A CE method using the micellar electrokinetic chromatography (MEKC) mode previously reported by Mauri et al. [7] used sodium dodecyl sulfate (SDS) as a charged micelle in methanol for separation of steviol glycosides. Liu and Li [2] developed subcritical fluid extraction (SubFE) method for the extraction of steviol glycosides from *Stevia rebaudiana*, suggested that CE is a valuable alternative to HPLC, but with longer migration times and poor resolution between the two peaks.

In modern years, a growing interest in the use of stevia in the natural food market has prompted the development of a fast, reliable, cost effective and reproducible analytical method to determine the sweetening components in *Stevia rebaudiana*. Accordingly, in this paper, we present a modern eco-friendly method for the separation of steviol glycosides using electrokinetic chromatography–capillary electrophoresis (EKC–CE) in the presence of TM-β-CD as a separating agent. However, a detailed mechanism for the separation of steviol glycosides by TM-β-CD remains unclear. Fortunately, molecular modeling methods have recently been proposed as powerful tools to obtain information about the interactions involving CD complexes [31]. For this purpose, and to the best of our knowledge, the molecular docking (MD) studies were utilized in this study for the first time, to better understand the mechanism of the separation between steviol glycosides and TM-β-CD.

Experimental

Apparatus

All analytical experiments were performed using Agilent Technologies 7100 CE system equipped with a diode array detector (DAD), an auto-sampler and a temperature controller (15–60 ± 0.1 °C). Instrument control and data analysis were carried out by Agilent Chemstation software installed on a personal computer. A fused silica capillary with 50 µm inner diameter and 363 µm outer diameter with total and effective lengths of 64.5 and 56 cm, respectively, was employed (Agilent Technologies, SA). For pH measurements, a pH meter (CRISON micro pH 2000) calibrated with a precision of 0.1 pH units was used. All samples were sonicated before analysis using an Ultra sonic (Labcon 5019 U model) supplied by Lasec (Durban, SA).

Materials

Individual standards of Reb A and Stv with 98 % analytical quality were obtained from (Ganzhou Julong High Tech Industrial Co., Ltd, China). Deionized water was generated from an aqua MAX^{TM}—basic 360 series water purification system from TRILAB SUPPORT (Durban, SA). Sodium dihydrogen orthophosphate, heptakis 2,3,6-tri-*o*-methyl betacyclodextrin (TM-β-CD), Sodium hydroxide, Hydrochloric acid and methanol were purchased from Capital Lab Supplies CC (KwaZulu-Natal, SA). All solutions and samples were prepared in deionized water filled in vials with disposable syringes filtering through a 0.45-µm pore

size and 25-mm diameter syringe filters containing cellulose acetate as filter medium supplied from Anatech Instruments (Pty) Ltd. (Durban, SA) before analysis.

Reagents

3-mM stevia standard solutions, each containing 98 % of Reb A and Stv were prepared quantitatively by weighing an equivalent amount in a 5-mL volumetric flask and diluting with deionized water. 30-mM TM-β-CD was prepared by dissolving 0.4288 g in 50-mM phosphate buffer in a 10-mL volumetric flask at 60 °C. 50-mM phosphate buffer was prepared by dissolving 0.780 g of sodium dihydrogen orthophosphate with adequate amount of deionized water in a 100-mL volumetric flask, and then adjusted to pH 8.0 with 1.0 M NaOH.

Capillary electrophoresis procedure

The new capillaries were first conditioned by flushing for 15 min with 1 M NaOH and then rinsed for 5 min with deionized water and 15 min with phosphate buffer at 30 °C. At the beginning of each working day, the capillary was cleaned and conditioned as follows: (i) 2 min rinse with deionized water (ii) 2 min rinse with 0.1 M NaOH (iii) 2 min rinse with deionized water and (iv) 2 min with phosphate buffer at 1,000 mbar. The samples were injected at a pressure of 50 mbar for 4 s; between runs the capillary was flushed with 1 M NaOH for 2 min and with water for 2 min; and finally with the separation buffer for 3 min to generate a stable electro-osmotic flow (EOF) in the capillary. The detection wavelength was set ranging from 200 to 240 nm.

The resolution (R_s) between Reb A and Stv was calculated using the expression:

$$R_s = \frac{2(t_2 - t_1)}{w_1 + w_2}$$

where t_1 is the migration time of first elution compound (Reb A), t_2 is the migration time of second elution compound (Stv), w_1 is the peak width of first elution compound at the base (Reb A), w_2 is the peak width of second elution compound at the base (Stv).

Procedure for real sample analysis

Real stevia samples used in this study were purchased from a local supermarket in different forms containing steviol glycosides, tablet samples (Green Canderel, Merisant Company 2, Czech Republic), powder samples (Stevia, Dis-Chem Pty Ltd, SA) and liquid samples (Tantalize, Delite Foods, SA). All standard solutions were kept at 4 °C in a refrigerator for stability. All the samples were used without any further purification. Specifically, in the preparation of a tablet sample, one tablet was ground into fine powder and dissolved in the equivalent of 5-mL deionized water. Powdered samples were prepared by dissolving the equivalent amount in a 5-mL volumetric flask with deionized water. Liquid samples were prepared directly by dissolving the equivalent amount in deionized water. Before the analysis, all the samples were diluted up to optimized dilution level (100-fold) to avoid possible interferences from the other substances.

Molecular docking methodology

Due to the absence of the X-ray structure for heptakis 2,3,6-tri-*o*-methyl betacyclodextrin (TM-β-CD) the atomic coordinates of β-cyclodextrin_hemolysin complex crystal (pdb id: 3M3R) were retrieved from the protein data bank [32] and were used as a reference to construct the 3D structure of TM-β-CD. The molecular mechanics force field (MMFF) was considered for the development of partial atomic charges. The unreasonable bond distances and angles of both ligands (Stv and Reb A) were adjusted by optimization using the Forcite module in Materials Studio (MS) [33]. The initial structure of TM-β-CD was energetically minimized using the Builder module in Discovery Studio (DS) 3.1 [34]. Docking studies were performed using the CDOCKER module of DS. CDOCKER is a grid-based molecular docking method where the receptor is held rigid while the ligands are allowed to flex during the refinement process. The ionic states of both ligands were determined at pH 8.0 followed by a conformational search using the Prepare Ligands and Conformations modules in DS [34], resulting in 40 and 22 conformations generated for Stv and Reb A, respectively. The lowest energy conformation for each ligand was further used for docking simulations. Prior to docking, a binding sphere of dimensions 30.4, 32.5 and 21.0 Å covering the whole TM-β-CD was created using the Define and Edit binding site modules in DS. Different ligand conformations were generated using molecular dynamics method and were refined further by grid-based (GRID 1) simulated annealing and a final grid-based minimization. The pose showing the highest docking score (CDOCKER energy) was considered for the binding energy (BE) calculations. The higher negative value of BE indicates a stronger binding and therefore a more favorable binding of the steviol glycoside to TM-β-CD.

Results and discussion

Electrokinetic studies of the host–guest complexation

The interaction of the analytes (Reb A and Stv) with the separating agent (TM-β-CD) depends on the complex

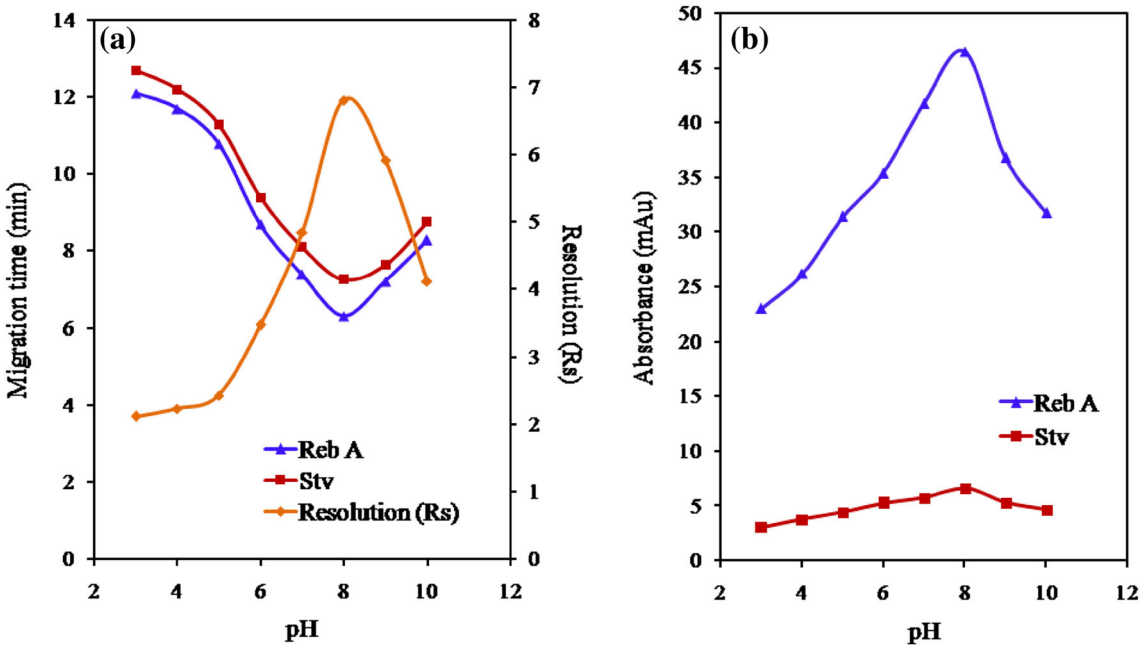

Fig. 1 Effect of buffer pH on **a** migration time and resolution **b** absorbance (conditions: 50-mM phosphate buffer, 30 mM TM-β-CD, 18 kV applied voltage, 30 °C temperature, 200 nm wavelength)

formation inside the capillary along with the EOF of the buffer. If the separating agent was directly bound to the capillary surface as a modifier, then the net velocity of the complex would be zero, but if the separating agent was directly added to the buffer, then the net velocity of the complex would not be zero. Accordingly, three different injection methods were employed for a better understanding of the interaction between the analytes and TM-β-CD. In first method, the analytes were injected followed by the separating agent. While in the second method, the separating agent was injected before the analytes. Finally, in the third method, the analytes were sandwiched by the separating agents.

Results from this study revealed that no separation was achieved in the first method, due to the higher mobilities of the analytes; hence there was an insufficient interaction between the analytes and the separating agent. However, in the second method, the EOF of the analytes was blocked by the slow moving TM-β-CD leading to some interaction and separation being observed. The weaker hydrophobic interactions between Reb A and TM-β-CD resulted in a less stable complex, whereas Stv formed a more stable complex with TM-β-CD, due to the stronger hydrophobic interactions with two more hydrogen bonds as confirmed by the molecular docking calculations. On the other hand, the less stable Reb A-(TM-β-CD) complex having a higher EOF and a higher velocity was eluted first. While in the third method, the hydrophobic interactions between the analytes and the hydrophobic cavity of TM-β-CD were very high due to the presence of TM-β-CD on either side of the analyte (sandwich). Therefore, the resulting complexes were more stable, with longer migration times than the corresponding complexes formed in the second method but

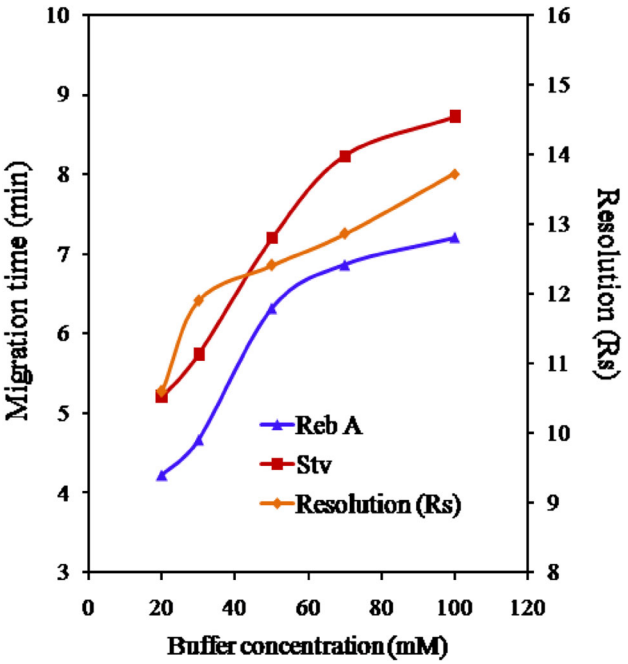

Fig. 2 Effect of buffer concentration on migration time and resolution (conditions: 30 mM TM-β-CD with pH 8.0, 18 kV applied voltage, 30 °C temperature, 200 nm wavelength)

with a similar elution order observed. For this purpose, the second method was selected, but with the corresponding parameters re-optimized in accordance with the host–guest molecular docking studies undertaken to evaluate the separation mechanism.

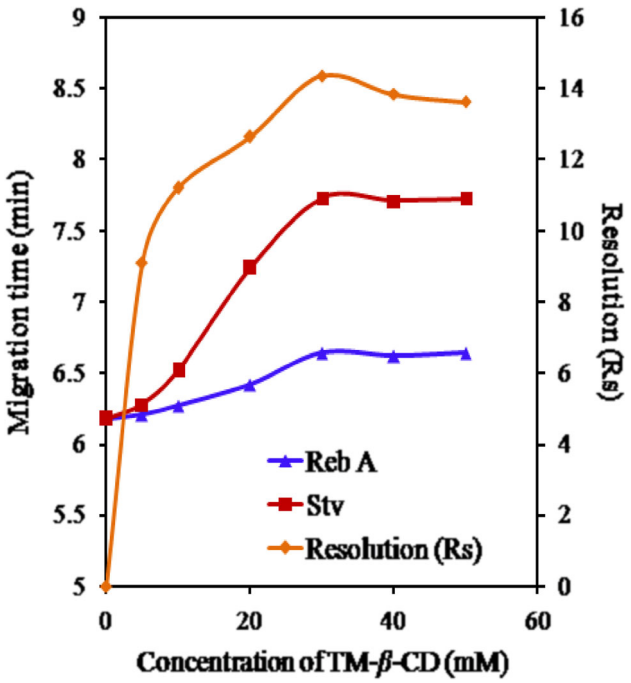

Fig. 3 Effect of concentration of TM-β-CD on migration time and resolution of compounds (conditions: 50-mM phosphate buffer with pH 8.0,18 kV applied voltage, 30 °C temperature, 200 nm wavelength)

Optimization of separation conditions

Effect of pH on resolution and absorbance

The pH of the running buffer plays a pivotal role in the separation mechanism because it affects the EOF, zeta (ζ) potential and the overall charge of the analytes [35]. Accordingly, in this study, the influence of pH ranging from 3.0 to 10.0 using a 50-mM phosphate buffer on the migration times and resolution of Reb A and Stv were investigated. Poor resolution and longer migration times with noisy baseline were observed at pH values ranging from 3.0 to 3.9, whereas good resolutions on the peaks were observed at pH 4.0. A further increase in pH from 4.0 to 8.0 resulted in shorter migration times, greater absorbances and good resolution between Reb A and Stv. At higher pH values, the deprotonation of the hydroxyl groups was favored [36, 37], as it promotes the complex formation between the negatively charged oxygen atoms in steviol glycosides with the hydrogen atoms in TM-β-CD, resulting in a better resolution and absorbances as shown in Fig. 1a, b. However, at pH >8.0, no significant differences in resolution capacities and migration times were observed. Consequently, 50-mM phosphate buffer at pH 8.0 was selected as the running buffer in this study.

Effect of buffer concentration

The viscosity coefficient of the solution, diffusion coefficient of the analytes and the zeta (ζ) potential of the inner

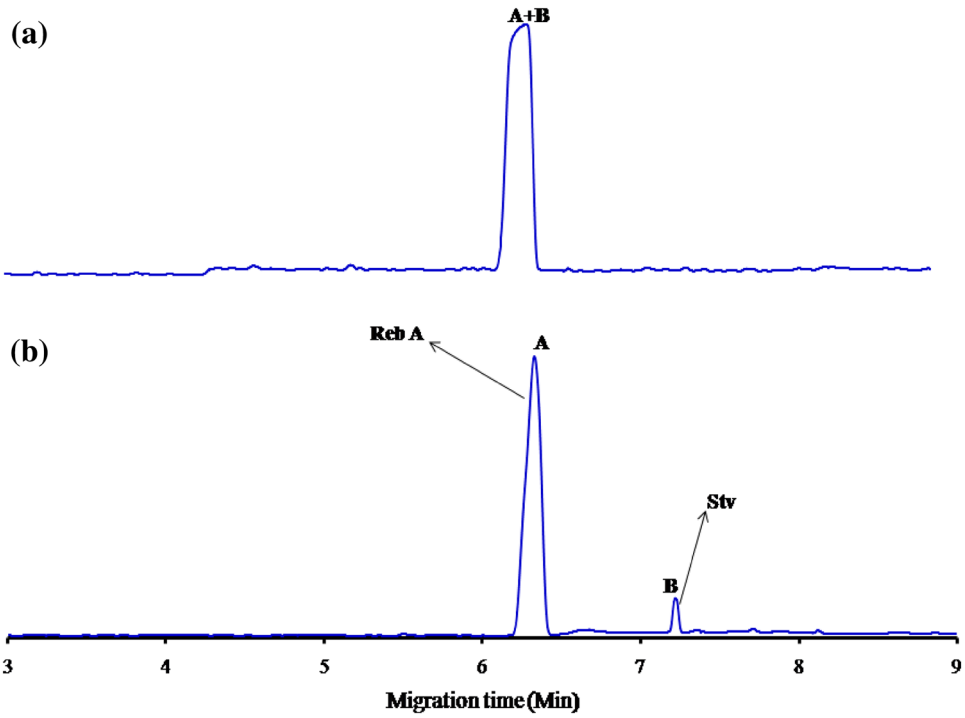

Fig. 4 Electropherograms showing the effect of TM-β-CD on the resolution of steviol glycosides **a** without TM-β-CD and **b** with TM-β-CD of *A* Reb A and *B* Stv (conditions: 50-mM phosphate buffer, 30 mM TM-β-CD with pH 8.0, 18 kV applied voltage, 30 °C temperature, 200 nm wavelength)

Table 2 Analytical figures of merit for the separation of Reb A and Stv

Sample	$y = a + bx$	Correlation coefficient	LOD (M)	LOQ (M)
Rebaudioside-A	$y = 12{,}669x + 27.05$	0.9935	2.017×10^{-5}	6.114×10^{-5}
Stevioside	$y = 4{,}079.6x - 16.46$	0.9850	7.386×10^{-5}	2.2881×10^{-4}

Regression equation ($y = a + bx$), where y is the peak areas of Reb A and Stv, x is the concentration (mM) of Reb A and Stv, r is the correlation coefficient, LOD's & LOQ's is calculated according to signal-to-noise ratio $S/N = 3$ and $S/N = 10$ respectively

Table 3 Analytical data for the determination of steviol glycosides from the spiked samples

Sample	Concentration added (mM)					
	1 mM		2 mM		3 mM	
	Found	Recovery ± RSD[a]	Found	Recovery ± RSD[a]	Found	Recovery ± RSD[a]
Rebaudioside-A	0.00392	97.51 ± 1.10	0.00746	92.78 ± 1.32	0.01195	99.08 ± 1.28
Stevioside	0.00384	95.52 ± 1.25	0.00789	98.13 ± 1.68	0.0102	84.57 ± 1.17

[a] Relative standard deviation for five individual determinations

surface of the capillary are mainly dependent on the concentration of running buffer which in turn affects the peak resolution, migration time and the absorbance of the analytes. Accordingly, in this experiment, different concentrations of the buffer ranging from 20 to 100 mM were examined on the resolution of Reb A and Stv. Figure 2 shows the influence of the buffer concentration on the resolution and migration time of Reb A and Stv. At low concentrations (<50 mM of phosphate buffer), low instrumental current was observed at an applied voltage of approximately 18 kV. However, at higher concentrations of phosphate buffer (>50 mM), joule heating becomes more pronounced resulting in a negative effect on the LOD values. The maximum resolution values were obtained with a 50-mM phosphate buffer at pH 8.0 and therefore chosen as the running buffer for further investigation in this work.

Effect of applied voltage

The applied voltage mainly affects the resolution, migration time and the peak shapes of the analytes. Shorter migration times with a good resolution between analytes were possible with higher voltages applied, as the EOF increases with increasing voltage. However, higher voltages are not preferred due to the increased joule heating generated from the capillary walls. In this investigation, the effect of the applied voltages ranging from 12 to 20 kV was examined. Application of a higher voltage 20 kV resulted in a noisy baseline with a maximum peak resolution and poor detection limits. However, the use of a lower voltage (12 kV) resulted in good baseline resolved peaks, but with longer migration times. Consequently the optimum voltage for this analysis was chosen at approximately 18 kV.

Table 4 Determination of Reb A and Stv in food samples

Sample	Available form	Active ingredients	Stevia glycoside concentration (g) Found	RSD[d]
Green Canderel[a]	Tablet	Rebaudioside-A stevioside	0.0119	1.15
			0.0112	1.53
Stevia[b]	Powder	Rebaudioside-A stevioside	0.0118	1.46
			0.0102	1.57
Tantalize[c]	Liquid	Rebaudioside-A stevioside	0.0125	1.55
			0.0114	1.87

[a] Merisant Company 2, Sarl, Czech Republic

[b] Dis-Chem Pty Ltd, South Africa

[c] Delite Foods, South Africa

[d] Relative standard deviation for five individual determinations

Effect of cassette temperature

In this study, the effect of cassette temperature ranging from 20 to 40 °C on baseline resolution was examined. As the capillary temperature increases the viscosity of the buffer decreases and the EOF of the buffer increases, resulting in shorter migration times but with good resolutions achieved. As a consequence of this, the optimum temperature of 30 °C was selected to sustain a baseline resolution with a shorter migration time and good peak shapes for both Reb A and Stv.

Effect of sample injection time

The effect of sample volume on the separation of Reb A and Stv was studied by changing the injection times ranging from 2 to 10 s. It was observed that the resolution between the two peaks decreased while the migration times

of the two analytes increased with an increase in injection times of the samples. Increasing the injection time beyond 4 s resulted in a peak broadening, hence lowering of the resolution between the two peaks. Therefore, 4 s was selected as an optimum injection time to enhance the separation of Reb A and Stv.

Effect of concentration of TM-β-CD

Figure 3 shows the influence of the concentration of TM-β-CD ranging from 5 to 50 mM. The separations of steviol glycosides with and without TM-β-CD are depicted in Fig. 4a, b respectively. Clearly, the migration times and the resolution between Reb A and Stv reached a maximum value at a concentration of 30 mM, and for this reason 30 mM of TM-β-CD was chosen as the optimum concentration.

Repeatability and reproducibility

Repeatability and reproducibility in terms of relative standard deviation of this method were studied on three types of stevia real samples described above. The reproducibility mainly depends on the dissociation of the silanol groups present on the inner walls of the capillary. To achieve a good reproducibility between the consecutive runs, the capillary has to be equilibrated. For this purpose, the capillary was flushed sequentially with deionized water for 2 min, 1 M NaOH for 2 min to refresh the silanol groups, and finally with the separation buffer for 2 min. Repeatability was evaluated by performing five replicates with the pH 8 buffer solution resulting in the percentage relative standard deviations (%RSD $n = 5$) of ±1.13 and ±1.43 % for migration time and 0.94 and 1.38 % for peak area.

Calibration curve and detection limit

For calibration studies, 98 % of Reb A and Stv standards was used with different concentrations ranging from 1 to 5 mM. The detection limits were calculated using individual standards at the following optimum conditions: 50-mM phosphate buffer, 30-mM TM-β-CD with pH 8.0, 18 kV applied voltage, 30 °C cassette temperature and 4 s of sample injection. From the calibration plots, the analytical figures of merit for the separation of Reb A and Stv are represented in Table 2.

Interference study

To test the selectivity of the developed method, the effect of foreign species was performed in this study. According

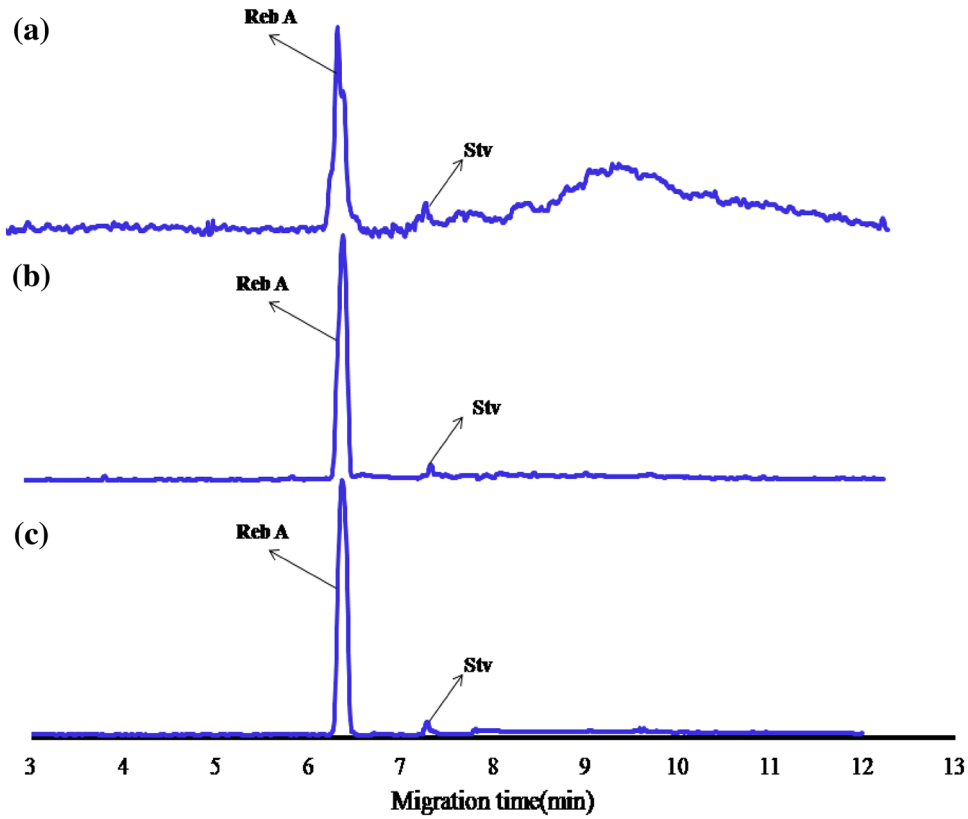

Fig. 5 Electropherograms for Reb A and Stv in real samples **a** tablet **b** powder **c** liquid samples (conditions: 50-mM phosphate buffer, 30 mM TM-β-CD with pH 8.0, 18 kV applied voltage, 30 °C temperature, 200 nm wavelength)

to the manufacturer's label, the tablet, liquid and powder samples contain lactose, fructose, citric acid, sorbic acid, natural flavors, colorants, wheat and gluten along with steviol glycosides. To discriminate the interferences from other foreign species, the dilution method was adopted to determine the optimum dilution level that would minimize the amount of fructose, lactose, citric acid, sorbic acid in the capillary while maintaining a measurable amount of steviol glycosides. The following dilutions: 2-, 10-, 50-, 100-, 500- and 1,000-fold were tested. A 100-fold dilution was optimized to measure steviol glycosides for all the studied real samples without any interference.

Performance evaluation of present method with reported methods

The performance of the developed method was assessed by comparing with those reported in the literature [2, 7, 16–18, 20]. From the data presented in Tables 3, 4 it is clear that the present method is fast, reliable and reproducible with shorter migration times and better resolution capacity in contrast to the reported methods [2, 7]. The selectivity pattern was superior to most of the cited references; however, it offers a better limit of detection than some of the previous reports [2, 7].

Analytical applications

The developed method worked well under laboratory conditions and was successfully applied to Reb A and Stv with no significant separation observed in the absence of the separating agent (TM-β-CD) (Fig. 4). To evaluate the accuracy of the developed method, real stevia samples in tablet, powder and liquid forms as described in the reagents section were purchased and analyzed. The obtained electropherograms for the real samples are shown in Fig. 5. The percentages of Reb A and Stv ranged from 92.78 to 99.08 % and 84.57 to 98.13 % while their % RSD was 1.10 and 1.17 %, respectively, are depicted in Tables 3, 4.

Computational discussion

To get a deeper understanding of the host–guest interactions of Reb A and Stv with TM-β-CD, molecular docking simulations were performed using the CDOCKER module of Discovery Studio 3.1 [34]. The docked complexes of Reb A and Stv with TM-β-CD are diagrammatically depicted in Fig. 6a, b, respectively. In contrast, a closer inspection of Fig. 5 reveals that both ligands (Reb A and Stv) penetrated the cavity of the TM-β-CD, thereby stabilizing their geometries, probably due to the hydrophobic interactions between their aliphatic functional groups and the hydrophobic cavity of the TM-β-CD ring. Apart from these hydrophobic interactions, two additional hydrogen bonds between the hydroxyl (–OH) groups and the oxygen atoms of the glucopyranose rings were observed in the case of Stv (Fig. 6b; Table 5), which accounts for their stronger interaction with the TM-β-CD than the Reb A (Fig. 6a) as evidenced by its lower CDOCKER energy (CDE score = −278.4). Moreover, it is believed that the more folded docked conformation of Stv (Fig. 6b) brought the hydroxyl groups (−OH) in the vicinity of the side chains of the TM-β-CD and facilitated the hydrogen-bonded interactions between them. The conformation of Reb A (Fig. 6a) on the other hand, was comparatively extended and simply penetrated through the cavity of the TM-β-CD. Thus, the proton acceptor/donor sites of Reb A were not close enough to form hydrogen bonds with the cyclodextrin. Finally, the computed binding energy (energy of complex-energy of ligand-energy of TM-β-CD) of Stv was found to be lower than Reb A, thus confirming the stronger interaction of the former with TM-β-CD than the later (Table 5). Moreover, the lower migration times of Stv

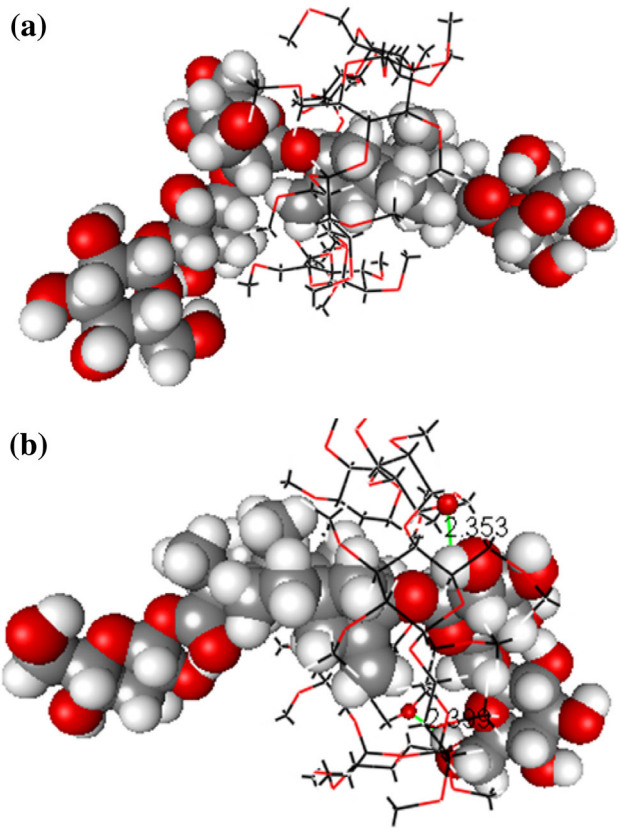

Fig. 6 Docked conformation of **a** Reb A and **b** Stv with TM-β-CD. Both ligands are shown in CPK format, while the TM-β-CD is shown in line format. Oxygen atoms of TM-β-CD participating in hydrogen bonding are shown in ball format and the hydrogen bonds are presented in *green*

Table 5 Docking results of Reb A and Stv with TM-β-CD using docking studies

Compound	CDocker energy (CDE) score	Binding energy (kcal mol^{-1})	Migration time (min) in CE	Number of H-bonds	H-bond distance (Å)
Stevioside	−278.4	−34.9	7.21	2	2.39, 2.35
Rebaudioside-A	−175.4	−25.4	6.32	0	–

observed in our CE experiments can also be explained on the basis of its stronger interaction with TM-β-CD (Table 5), resulting in its slower movement toward the anodic end of CE system compared to the Reb A–TM-β-CD complex, under the influence of EOF.

Conclusions

In this study, the simultaneous separation and determination of stevia glycosides with TM-β-CD were successfully implemented using the EKC–CE method, supported with molecular docking (MD) studies. Our results showed that the present method is a fast, efficient and facile method for the simultaneous separation and quantification of Reb A and Stv in real stevia samples. This study revealed that the good baseline resolution along with the reproducibility and repeatability renders this method to be more superior to those reported by HPLC methods, suggesting that the inclusion of a separating agent, TM-β-CD greatly improved the separation efficiency of stevia glycosides. Moreover, the MD studies complimented the experimental results by highlighting the stability and the stronger interaction of Stv with TM-β-CD than with Reb A, thus supporting the order of elution obtained under experimental CE conditions. To the best of our knowledge, this is the first attempt at using the CE-MD approach for the simultaneous separation and determination of stevia glycosides in real samples, which could have a special significance to the food flavoring industry.

Acknowledgments KB is grateful for the financial support provided by the Durban University of Technology and National Research Foundation of South Africa for this work. The authors would like to express their acknowledgement to the Centre for High Performance Computing, an initiative supported by the Department of Science and Technology of South Africa.

References

1. D.J. Midmore, A.H. Rank, A new rural industry—stevia—to replace imported chemical sweeteners. A report for Rural Industries Research and Development Corporation RIRDC Web, Publication No. W02/022 RIRDC Project No. UCQ-16A (2002)
2. J. Liu, C.P. Ong, S.F.Y. Li, J. Chromatogr. Sci. **35**, 446 (1997)
3. J.M.C. Geuns, *Stevia and Steviol Glycosides* (Euprint Ed., Heverlee, 2010)
4. Regulations relating to the use of sweeteners in foodstuffs. Foodstuffs, cosmetics and disinfectants act (1972), http://www.doh.gov.za/docs/foodcontrol/additives/2012/regr733
5. U. Woelwer-Rieck, J. Agric. Food Chem. **60**, 886 (2012)
6. M.B. Tadhani, V.H. Patel, R. Subhash, J. Food Compos. Anal. **20**, 323 (2007)
7. P. Mauri, G. Catalano, C. Gardana, P. Pietta, Electrophoresis **17**, 367 (1996)
8. M.S. Melis, J. Nat. Prod. **55**, 688 (1992)
9. M.S. Melis, J. Ethnopharmacol. **36**, 213 (1992)
10. P.M. Kuznesof, The 68th JECFA Steviolglycosides (CTA) (2007), pp. 1–8
11. H.C. Makapugay, N.P.D. Nanayakkara, A.D. Kinghorn, J. Chromatogr. **283**, 390 (1984)
12. J.M.C. Geuns, Analysis of steviol glycosides: validation of the methods, in *Proceedings of the 2nd Stevia Symposium*, ed. by J.M.C. Geuns (Euprint ed., Leuven, 2008), pp. 59–78
13. J.M.C. Geuns, T. Struyf, EUSTAS round robin testing of steviol glycosides, in *Proceedings of the 3rd Stevia Symposium*, ed. by J.M.C. Geuns (Euprint, Leuven, 2009), pp. 35–48
14. B. Hoekstra, J. Traub, K. Chamberlain, S. Baugh, S.K. Venkataraman, Planta Med. **75**, 1003 (2009)
15. N. Kolb, J.L. Herrera, D.J. Ferreyra, R.F. Uliana, J. Agric. Food Chem. **49**, 4538 (2001)
16. N.A. Samah, A.D.A. Hisham, S.A. Rahim, Int. J. Chem. Environ. Eng. **332**, 1 (2012)
17. C. Tianhong, Z. Yang, L. Xiaohang, S. Zuoqing, S. Juntan, H. Binglin, Sci. China **42**, 277 (1999)
18. V. Jaitak, A.P. Gupta, V.K. Kaul, P.S. Ahuja, J. Pharm. Biomed. Anal. **47**, 790 (2008)
19. U. Woelwer-Rieck, C. Lankes, A. Wawrzun, M. Wust, Eur. Food Res. Tech. **231**, 581 (2010)
20. B.F. Zimmermann, U. Woelwer-Rieck, M. Papagiannopoulos, Food Anal. Methods **5**, 266 (2011)
21. D. Hurum, J. Rohrer, Steviol glycoside determination by HPLC with charged aerosol and UV detections using the acclaim trinity P1 column, Application Note: 293 (2011)
22. D. Bergs, B. Burghoff, M. Joehnck, G. Martin, G. Schembecker, J. Verbr. Lebensm. **7**, 147 (2012)
23. M. Puri, D. Sharma, C.J. Barrow, A.K. Tiwary, Food Chem. **132**, 1113 (2012)
24. J. Liu, S.F.Y. Li, J. Liq. Chromatogr. **18**, 1703 (1995)
25. T. Rajasekaran, A. Ramakrishna, K. Udaya Sankar, P. Giridhar, G.A. Ravishankar, Food Biotechnol. **22**, 179 (2008)
26. J.I. Zhang, X. Li, Z. Ouyang, R.G. Cooks, Analyst **137**, 3091 (2012)
27. B. Shafii, R. Vismeh, R. Beaudry, R. Warner, A.D. Jones, Anal. Bioanal. Chem. **403**, 2683 (2012)
28. R. Shah, L.S.D. Jager, T.H. Begley, Food Addit. Contam. A **29**, 1861 (2012)
29. P. Montoro, I. Molfetta, M. Maldini, L. Ceccarini, S. Piacente, C. Pizza, M. Macchia, Food Chem. **141**, 745 (2013)
30. Y. Kakigi, T. Suzuki, T. Icho, A. Uyama, N. Mochizuki, Food Addit. Contam. A (2013), http://dx.doi.org/10.1080/19440049.2013.843101
31. L. Wuhong, L. Changhai, T. Guangguo, Z. Xinrong, Z. Zhenyu, Y.F. Chai, Int. J. Mol. Sci. **13**, 710 (2012)

32. A. Banerjee, E. Mikhailova, S. Cheley, L.Q. Gu, M. Montoya, Y. Nagaoka, E. Gouaux, H. Bayley, Proc. Natl. Acad. Sci. USA **107**, 8165 (2010)
33. Accelrys, Materials Studio Release Notes, Release 4.1; Accelrys Software, San Diego, CA (2006)
34. G. Wu, D.H. Robertson, C.L. Brooks III, M. Vieth, J. Comp. Chem. **24**, 1549 (2003)
35. G. Chen, J. Zhang, J. Ye, J. Chromatogr. A **923**, 255 (2001)
36. G. Chen, H.W. Zhang, J.N. Ye, Anal. Chim. Acta **423**, 69 (2000)
37. P. Youyuan, Y. Jianjun, L. Fanghua, Y. Jiannong, J. Pharm. Biomed. Anal. **39**, 431 (2005)

Analytical Letters
Publication details, including instructions for authors and subscription information:
http://www.tandfonline.com/loi/lanl20

Determination of Neotame by High-Performance Capillary Electrophoresis Using ß-cyclodextrin as a Chiral Selector

Ayyappa Bathinapatla [a], Suvardhan Kanchi [a], Parvesh Singh [b], Myalowenkosi I. Sabela [a] & Krishna Bisetty [a]

[a] Department of Chemistry, Durban University of Technology, Durban, South Africa

[b] School of Chemistry and Physics, University of KwaZulu Natal, Westville, Durban, South Africa

Accepted author version posted online: 23 Jun 2014.Published online: 02 Sep 2014.

To cite this article: Ayyappa Bathinapatla, Suvardhan Kanchi, Parvesh Singh, Myalowenkosi I. Sabela & Krishna Bisetty (2014) Determination of Neotame by High-Performance Capillary Electrophoresis Using ß-cyclodextrin as a Chiral Selector, Analytical Letters, 47:17, 2795-2812, DOI: 10.1080/00032719.2014.924008

To link to this article: http://dx.doi.org/10.1080/00032719.2014.924008

Analytical Letters, 47: 2795–2812, 2014

ISSN: 0003-2719 print/1532-236X online
DOI: 10.1080/00032719.2014.924008

Taylor & Francis
Taylor & Francis Group

Electrophoresis

DETERMINATION OF NEOTAME BY HIGH-PERFORMANCE CAPILLARY ELECTROPHORESIS USING ß-CYCLODEXTRIN AS A CHIRAL SELECTOR

Ayyappa Bathinapatla,[1] Suvardhan Kanchi,[1] Parvesh Singh,[2] Myalowenkosi I. Sabela,[1] and Krishna Bisetty[1]

[1]*Department of Chemistry, Durban University of Technology, Durban, South Africa*

[2]*School of Chemistry and Physics, University of KwaZulu Natal, Westville, Durban, South Africa*

An electrokinetic chromatographic method was developed for the chiral separation of neotame, a new high intensity artificial sweetener, using a chiral separating agent heptakis 2,3,6-tri-o-methylbetacyclodextrin. The purpose of this study was to better understand diastereomer-resolution interactions between neotame and the chiral separating agent. Molecular docking studies were performed to elucidate the mechanism of the separation. The optimum conditions were 50 mM phosphate buffer, pH 5.5, applied voltage 20 kV, cassette temperature of 30°C, and a 4 s sample injection time. The calibration curve showed good linearity ($r^2 > 0.99$) with recoveries for both diastereomers, ranging from 95.66–99.00% and the limits of detection for L,L-neotame and D,D-neotame were 0.01857 and 0.08214 mM, respectively. The developed method showed analytical precision with relative standard deviations ($n = 5$) of 1.20% and 1.17% with respect to migration time and peak area, respectively. A large difference in the interaction energies observed between the diastereomers represents a significant differentiation. The results showed that both electrostatic and hydrophobic interactions played a significant role in stabilizing their inclusion complexes and consequently supported the elution order based on their differential stabilities.

Keywords: Diastereomers; Electrokinetic chromatography (EKC); Food samples; Heptakis 2,3,6 tri-*o*-methylbetacyclodextrin; Molecular docking; Neotame

INTRODUCTION

In 2000, Nofri and Tinti reported neotame as a non-nutritive artificial sweetener with an *N*-substituted aspartame derivative, (*N*-[*N*-(3,3-dimethylbutyl)-L-α-aspartyl]-L-phenylalanine-1-methyl ester) and with a dipeptide bond as shown in Figure 1. In 2013,

Received 22 January 2014; accepted 27 April 2014.

Address correspondence to K. Bisetty and S. Kanchi, Department of Chemistry, Durban University of Technology, P.O. Box 1334, Durban 4000, South Africa. E-mail: bisettyk@dut.ac.za or ksuvardhan@gmail.com

Color versions of one or more of the figures in the article can be found online at www.tandfonline.com/lanl.

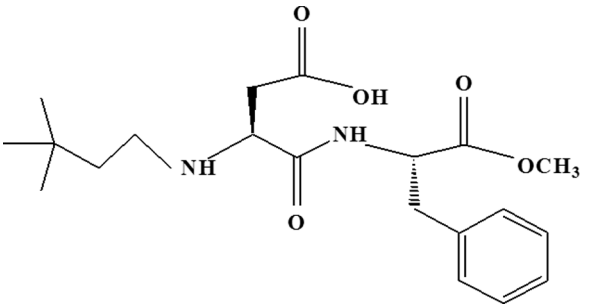

Figure 1. Structure of neotame.

neotame was approved by the United States Food and Drug Administration as a new artificial sweetener (U.S. Food and Drug Administration, news releases, May 19, 2013). On an industrial scale, neotame, which contains all the elements of aspartame, is prepared by the reductive alkylation of aspartame with a 3,3-dimethylbutyl group. In contrast to aspartame, neotame has fewer side effects and the mechanism of neotame safety compared to aspartame is generally due to the enzymes "peptidases," which are used to break the peptide bonds (Fisher 1989). In neotame, the bond between the aspartic acid and the phenylalanine groups are effectively blocked by the presence of the 3,3-dimethylbutyl moiety, thus reducing the availability of phenylalanine and eliminating concerns for those who suffer from phenylketonuria (Nofre and Tinti 2000). The safety of neotame has been investigated and the results indicate that neotame is not carcinogenic, genotoxic, teratogenic, or associated with any reproductive toxicity (Scientific Opinion 2007). However, 3,3-dimethylbutyraldehyde, a highly flammable component used in the synthesis of neotame, may cause minor side effects such as irritation to the skin, eyes, respiratory, and reproductive systems after prolonged consumption (Mayhew, Comer, and Stargel 2003; Tomasik 2004).

Due to the presence of amino acids and organic groups, neotame exhibits high sweeteness nearly 10,000 times sweeter than sugar and 40 times more sweeter than aspartame (Prakash, Bishay, and Schroeder 1999). Neotame has two chiral centers at the C_3 and C_5 positions; hence, it can form four diastereomers, namely L,L; L,D; D,D; and D,L neotame, and their sweetness is attributed to the presence of well-oriented hydrophobic groups in the L,L-diastereomer (Prakash et al. 1999).

Neotame has been approved in more than 35 countries around the world. The acceptable daily intake for neotame has been set at 0–2 mg kg^{-1} body weight by the Joint Expert Committee for Food Additives in 2003 as well as by the European Food Safety Authority in 2007. The Center for Science in the Public Interest indicates that neotame is not being used as a sweetener throughout the world, yet it has a wide potential application as a second-generation dipeptide sweetener (Hu et al. 2013; Tomasik 2004). Owing to its low cost, safety, and high sweetness, the demand and importance of neotame as a sweetener has gained widespread recognition by the food industry. Accordingly, the growing interest of the use of neotame in food and beverages has prompted the need to develop a simple, accurate, and reliable method for the determination of neotame. However, some natural food components in complicated food matrices will interfere with the determination of the analyte

(Alghamdi, Alghamdi, and Alwarthan 2005; He, Fang, and Xu 2012; Vianna-Soares and Martins 2002). Therefore, the highly sensitive and specific determination of the sweetener in foods is an analytical challenge.

A literature survey revealed that high-performance liquid chromatography (HPLC) methods are the most widely used methods for the determination of neotame in various foodstuffs (Jizhi, Jie, and Jinhua 2009; Ji et al. 2009; Min and Dong 2008; Matsumoto et al. 2008; National Standard Method of China 2009; Yang and Chen 2010; Zhao et al. 2011, 2012, 2013). Hyphenated techniques with HPLC included evaporative light scattering detection (HPLC–ELSD) (Buchgraber and Wasik 2009; Wasik, McCourt, and Buchgraber 2007) and mass spectrometry (HPLC–MS) (Gan et al. 2013; Lim et al. 2013; Berset and Ochsenbein 2012; Hui et al. 2009; Scheurer, Brauch, and Lange 2009; S. J. Wu, Wang, and Tao 2010; Yang and Chen 2009; Zygler et al. 2011). However, these analytical methods are more expensive than capillary electrophoresis (CE) a powerful alternative to HPLC, due to its high separation efficiency, high versatility, speed of analysis, and low consumption of samples and reagents resulting in a lower environmental impact (Chankvetadze and Blaschke 2001). Several papers have demonstrated applications of CE for the separation and quantification of many artificial sweeteners. However, there is only one reported study on the separation of neotame in food by CE (Hu et al. 2013). To the best of our knowledge, the present work is the first attempt for the chiral separation of neotame by CE using electrokinetic chromatography (EKC).

In a racemic mixture of neotame, the L,L-diastereomer is present as the sweetener, while the D,D-diastereomer is not sweet. However, the detailed mechanism for the separation of neotame diastereomers using a separating agent such as heptakis 2,3,6 tri-*o*-methylbetacyclodextrin remains unclear. Accordingly, this work is targeted at developing a simple and reliable method to establish appropriate conditions for the determination of neotame diastereomers in food. Previous studies undertaken in our laboratory revealed that molecular modeling methods served as powerful complimentary tools to obtain information about the (±) catechin interactions involving betacyclodextrin complexes (Sabela et al. 2012). For this purpose, molecular docking studies were utilized in this study to better understand the mechanism of separation between neotame diastereomers and heptakis 2,3,6 tri-*o*-methylbetacyclodextrin. The molecular docking results not only supported the elution order observed under experimental conditions, but also suggested a stronger interaction of the D,D-neotame with heptakis 2,3,6 tri-*o*-methylbetacyclodextrin than with L,L-neotame.

EXPERIMENTAL

Apparatus

All CE experiments were performed using an Agilent Technologies 7100 instrument equipped with a photodiode array detector, an autosampler, and a temperature controller (15–60 ± 0.1°C). Instrument control and data analysis were performed using Agilent Chemstation software on a personal computer. A pH meter (Crison micro pH 2000) calibrated with a precision of 0.1 pH units was used for all measurements. All samples were treated before analysis using an ultrasonic mixer (Labcon 5019 U model).

Chemicals

L,L and D,D-neotame standards of 97% analytical quality were obtained from Hullets, South Africa. Sodium dihydrogenorthophosphate, heptakis 2,3,6-tri-*o*-methylbetacyclodextrin, sodium hydroxide, hydrochloric acid, and methanol were analytical grade purchased from Capital Lab Supplies CC (Durban, SA). All solutions and samples were prepared with deionized water from an aqua MAX – Basic 360 series water purification system supplied by Trilab Support (Durban, SA). All samples were filtered prior to analysis with disposable syringes fitted with a 0.45-μm pore size and 25-mm diameter syringe filters made of cellulose acetate, supplied by Anatech Instruments (Durban, SA).

All samples were used without any further purification, and a stock solution of neotame (5.0 mM) was prepared by weighing an appropriate amount in a 5-mL volumetric flask and dilution with 20% methanol. Spiked neotame samples (3.0, 5.0, and 7.0 mM) were prepared using mango juice, a cola soft drink, and orange soft drink purchased from a local supermarket. The spiked samples were prepared by direct dissolution of neotame in 5-mL volumetric flasks with the aforementioned beverages. A phosphate buffer (50 mM) was prepared by dissolving an appropriate amount of sodium dihydrogenorthophosphate in 100-mL volumetric flasks and diluted to mark with ultra-pure water and the solution was adjusted to pH 5.5 with 1.0 M NaOH or HCl. 30 mM Heptakis 2,3,6 tri-*o*-methylbetacyclodextrin solution was prepared by dissolving an appropriate amount in 50-mM phosphate buffer in a 10-mL volumetric flask at 60°C. All standards were stored at 4°C.

Electrophoresis

All separations were performed with a 75 μm inner diameter and 363 μm outer diameter, fused silica capillary with total and effective lengths of 64.5 and 56.0 cm, respectively (Agilent Technologies, Germany). New capillaries were conditioned at 60°C using the following sequence: 7 min rinse with 20% methanol, 20 min rinse with 1.0 M NaOH, 5 min rinse with deionized water, and with a 20 min rinse with the running buffer. At the beginning of each working day, the capillaries were conditioned by flushing for 10 min with 1.0 M NaOH, 5 min with deionized water, and thereafter treated for 10 min with 50 mM, pH 5.5 phosphate buffer solution as the background electrolyte, and 30 mM heptakis 2,3,6 tri-*o*-methylbetacyclodextrin as a chiral selector. The solutions were flushed through the capillary by applying a pressure of 100 mbar for 5 s. Separation was performed by applying 20 kV, and the capillary was thermostated at 30°C with the ultraviolet detector wavelength set to 200 nm.

Docking Methodology

The atomic coordinates of beta-cyclodextrin_hemolysin complex crystal (pdb id: 3M3 R) were retrieved from the protein data bank (Banerjee et al. 2010) and used as a reference to construct the three-dimensional structure of heptakis 2,3,6 tri-*o*-methylbetacyclodextrin. All starting structures were energetically minimized using the Builder module in Discovery Studio 3.1 (G. Wu et al. 2003). The partial charges of ligands were generated using molecular mechanics molecular force field (MMFF)

embedded in DS. Three different ionic states (zwitterion, anion, and cation) of both neotame isomers (L,L and D,D) were predicted at experimental pH conditions (3.01, 5.5, 8.02) using the "Prepare Ligand" module in DS (G. Wu et al. 2003). The conformational analysis for each structure was subsequently performed and the lowest energy structures were used as starting structures for the docking procedure. A binding sphere of dimensions 30.4, 32.5, 21.0 Å covering heptakis 2,3,6 tri-*o*-methylbetacyclodextrin were created using the "Define and Edit Binding" site modules in Discovery Studio. Docking simulations were performed using the Cdocker module of Discovery Studio. The best poses showing efficient host-guest interactions were identified on the basis of the Cdocker energy (CDE) and Cdocker interaction energy scoring functions.

RESULTS AND DISCUSSION

Optimization of Separation Conditions

The electroosmotic flow (EOF), the zeta potential (ζ), and the charge of the analytes depend on the pH of the running buffer. The separation capacity and changes in migration time and the resolution of analytes also depend on the pH of the running buffer. In this work, the effect of pH on the migration times and the resolution of analytes were investigated using 50 mM phosphate buffer at pH values between 3.0 and 8.5, and the results are depicted in Figure 2. Based on the *pKa* values (pK_1 3.01 and pK_2 8.02; isoelectric point 5.5), neotame exhibits a cationic form due to the protonation of the amino groups below pH 3.01(Nofre and Tinti 2000). At this pH, the D,D-cationic form elutes later due to the higher stability complex (D,D-cationic-heptakis 2,3,6 tri-*o*-methylbetacyclodextrin) compared to the corresponding L,L-cationic form. When the pH increases from 3.01 to 5.5, a gradual decrease in migration times were observed. At the isoelectric point (5.5), neotame exhibits a zwitterionic form with a (+ve) charge at the amino group and

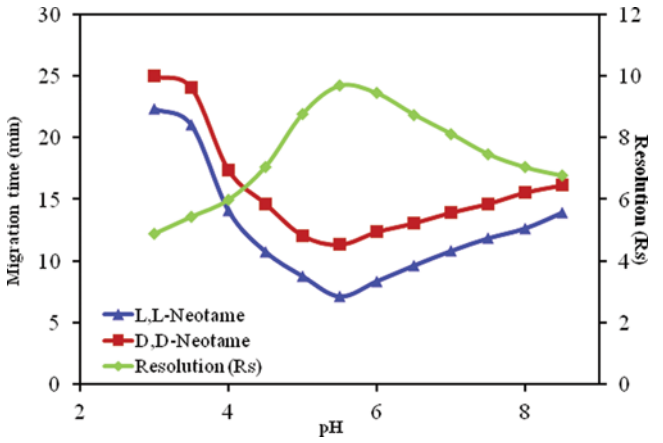

Figure 2. Effect of buffer pH on migration time and resolution. Conditions: 50 mM phosphate buffer, 30 mM heptakis 2,3,6 tri-o-methylbetacyclodextrin, 20 kV applied voltage, 30°C temperature, 200 nm detection wavelength.

a (–ve) charge at the carboxyl group. The charged groups present in the L,L-zwitterionic form, results in weak hydrophobic interactions or hydrogen bonds with the hydrophobic cavity of heptakis 2,3,6 tri-*o*-methylbetacyclodextrin; hence, it elutes first in contrast to the D,D-zwitterionic form. At this pH, a baseline separation was achieved with shorter migration times with respect to the cationic and anionic forms. However, a further increase in pH from 5.5 to 8.5 resulted in the conversion of the zwitterionic form to the anionic form, due to deprotonation of the amino group. Furthermore, a gradual increase in migration times were observed with an increase in pH due to an increase in the stability of the anionic neotame-heptakis 2,3,6 tri-*o*-methylbetacyclodextrin complex. Similar elution patterns were observed in the two ionic forms. The L,L-anionic form eluting first was attributed to the presence of weaker hydrogen bonds present in L,L-anionic-heptakis 2,3,6 tri-*o*-methylbetacyclodextrin complex than the corresponding D,D-anionic complex. The effect of pH on the separation, resolution, and the retention factors were also explored in this work. The separation and resolution factor values at pH 3, 5.5, and 8.5 were 1.15, 2.43, 1.39, and 4.88, 9.67, and 8.12, respectively. These results suggest a maximum separation, resolution, and peak absorbance were obtained at pH 5.5.

The viscosity coefficient of the solution, diffusion coefficient of analytes, and the ζ-potential of the inner surface of the capillary tube were dependent on the concentration of the running buffer. In this work, the buffer concentrations ranging from 30 to 100 mM were examined in relation to the migration times and the resolution of analytes. The migration times and resolution of the analytes increased with a higher concentration of the running buffer. Low concentrations of the phosphate buffer (30 mM) resulted in low instrumental current (15–20 mA) at an applied voltage of 20 kV. However, at higher concentrations (>50 mM), the joule heating effect is more pronounced and thus decreases the peak area, resulting in negative effects on the limits of detection. The retention factors (k_1' and k_2') gradually increased from 0.533 to 1.999 with a corresponding decrease in separation factors from 2.729 to 1.999. The resolution factors also increased from 3.97 to 5.87 with a corresponding increase in buffer concentrations. At low concentrations, good resolution was observed between two peaks with shorter migration times. Hence, 50 mM phosphate buffer at pH 5.5 was chosen as the running buffer for further studies.

In this work, the effect of the applied voltage from 14 to 22 kV was investigated on the resolution, migration times, and separation factors. At higher voltages, the EOF of the mobile phase increased, and thus shorter migration times were obtained as shown in Figure 3. To achieve stable baselines and appropriate peak shapes, the applied voltages were reduced from 22 to 14 kV. At lower voltages, longer migration times were observed with satisfactory baseline separations. However, careful consideration of migration times, resolution, and peak shapes suggested that low voltages were not desirable; therefore, 20 kV was selected as the optimum voltage. Retention factors for L,L-neotame and D,D-neotame were significantly decreased from 1.287 to 0.545 and from 2.282 to 1.365, respectively. The resulting separation factors increased from 1.773 to 2.504 and the resolution factors also increased from 4.16 to 6.78 with an increase in voltage, suggesting that the resolution between two peaks were good at higher voltages.

The viscosity and EOF of the running buffer depend on the cassette temperature. At higher temperatures, the viscosity decreased and the EOF increased resulting in

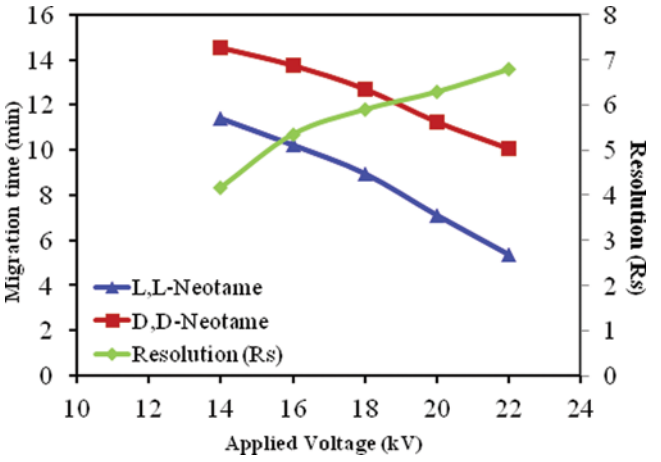

Figure 3. Effect of applied voltage on migration time and resolution. Conditions: 50 mM phosphate buffer, 30 mM heptakis 2,3,6 tri-o-methylbetacyclodextrin, 20 kV applied voltage, 30°C temperature, 200 nm wavelength.

shorter migration times. As the kinetic effect influences the viscosity and diffusion coefficient of the solute, the thermodynamic effect (enthalpy and entropic contributions) influences the transfer of the Gibbs free energy change (ΔG) between buffer systems including chiral selector and analyte (Peter, Vekes, and Armstrong 2002).

Kinetic effects of the cassette temperature on the migration times and resolution were evaluated from 15°C to 40°C. Clearly above 30°C, the excess joule heating generated from the inside of the capillary resulted in a noisy baseline with peak splitting, while longer migration times and broader peaks were observed below 30°C. The retention factors for both L,L and D,D diastereomers were increased from 0.4169 to 2.2444 and from 1.001 to 3.755, respectively, with a corresponding increase in temperature from 15°C to 40°C. However, with an increase in temperature, the separation and resolution factors gradually decreased from 2.4010 to 1.6733 and 8.23 to 5.24, respectively. These results suggest that the gaps between the two peaks (resolution) and the migration time decreases with an increasing temperature, as depicted in Table 1. Accordingly, the cassette temperature for baseline separation was selected at 30°C.

A mathematical model describing the thermodynamic effects based on the enthalpy and entropy contributions is derived from the van't Hoff equations:

$$\ln k = \frac{-\Delta H}{RT} + \frac{\Delta S}{R} + \ln \phi \tag{1}$$

and

$$\ln \alpha = -\frac{\Delta_{R,S}\Delta H^{\circ}}{RT} + \frac{\Delta_{R,S}\Delta S^{\circ}}{R} \tag{2}$$

where ΔH and ΔS are the standard enthalpy and entropy of transfer of the solute from the mobile phase to the stationary phase and $\Delta_{R,S}\Delta H^{\circ}$ and $\Delta_{R,S}\Delta S^{\circ}$ are the

Table 1. Effect of temperature on retention, separation, and resolution factors (K′, α, RS)

Temperature °C	Migration time (min)		Retention factor (K′)		Separation factor (α)	Resolution factor (R_s)	van't Hoff equation R^2	$\Delta H/\Delta_{R,S}\Delta H^0$ kJ mol^{-1}	$\Delta S/\Delta_{R,S}\Delta S^0$ kJ mol^{-1}
	L,L	D,D	K_1'	K_2'					
15	9.21	13.01	0.416	1.001	2.401	8.23	$\ln k_1 = 23.902/T - 1.1892$ (0.92)	−21.7464	−1.1892
20	9.03	12.32	0.556	1.124	2.018	7.89	$\ln k_2 = 15.373/T - 0.1529$ (0.93)	−23.0431	−0.1529
25	7.42	10.67	0.725	1.481	2.041	7.12	$\ln\alpha = 7.413/T - 4.3952$ (0.94)	−19.0502	−4.3952
30	7.13	11.24	1.376	2.746	1.995	6.65			
35	6.42	9.44	1.918	3.290	1.715	5.91			
40	5.84	8.56	2.244	3.755	1.673	5.22			

Note: L,L and D,D = neotame diastereomers; K_1' and K_2' = retention factors for first and second eluted analytes (L,L-neotame and D,D-neotame); ΔH = standard enthalpy for the transfer of energy from mobile phase to stationary phase; $\Delta_{R,S}\Delta H^0$ = difference in the enthalpy for the first (L,L-neotame) and second (D,D-neotame) analytes.

differences of $\Delta H_2 - \Delta H_1$ and $\Delta S_2 - \Delta S_1$, respectively. From the aforementioned expressions, linear graphs were obtained by plotting ln k vs. 1/T and ln α vs. 1/T with slopes of $-\Delta H/R$, $-\Delta_{R,S}\Delta H^o/R$ and intercepts of $\Delta S/R + \ln \phi$, $\Delta_{R,S}\Delta S^o/R$, respectively. Plots of ln α vs. 1/T were constructed between 15°C and 40°C for L,L-neotame and D,D-neotame. Thermodynamic parameters for the compounds were calculated and van't Hoff isotherms were found to be linear ($r^2 > 0.93$). At low temperatures, the resolution factors were high because the transfer of the Gibbs free energy (ΔG) between buffer systems to the analyte was low. The resolution and separation factors decreased with increasing temperature. At the optimum temperature, the transfer of energies were −21.7464 and −23.0431 for L,L-neotame and D,D-neotame, respectively. These results suggested that the resolution and elution order of the analytes controlled by the enthalpy were due to weaker interactions of the L,L-neotame with the stationary phase (heptakis 2,3,6 tri-*o*-methylbetacyclodextrin) in contrast to D,D-neotame. Consequently, L,L-neotame eluted prior to D,D-neotame, and 30°C was considered as the optimum working temperature.

The effect of injection time on the migration and resolution were investigated by changing the injection times of the analyte from 2 s to 8 s. An increase in injection time of the sample resulted in peak broadening and a slight shift in the peaks toward the right hand side resulted in longer migration times. On the other hand, an increase in migration time resulted in a decrease in the resolution between the peaks from 4.54 to 3.70. Injection times beyond 4 s affected the peak broadening and ultimately resulted in lower resolutions. For this purpose, 4 s was chosen as the optimum injection time of the sample into the capillary.

The electrophoretic mobility depends on the concentration of the chiral selector. In CE, the process responsible for the separation is the formation of complexes between the neotame diastereomers and the chiral selector. The presence of additives

such as cyclodextrins in the electrophoresis buffer changes the viscosity of the media, which in turn affects the effective electrophoretic mobilities. The corrected electrophoretic mobility ($\mu_{\text{corrected}}$) of neotame diastereomers in the presence of heptakis 2,3,6 tri-*o*-methylbetacyclodextrin at different concentrations are reported in Table 2. The observed electrophoretic mobility is provided by the following equation:

$$\mu(\text{obs}) = \mu(\text{EOF}) + [\mu(f) \times x(f)] + [\mu(c) \times x(c)] \tag{3}$$

where μ(obs) is the observed mobility, μ(EOF) is the electroosmotic mobility, x is the molar fractions, and f and c represent the free and the complexed (by the chiral selector) analyte, respectively. In general, μ(EOF) is equal for both the diastereomers to be separated in the same electrophoretic run and, dealing with chiral separations, μ(f) must be equal for the two diastereomers (Giuffrida et al. 2012). Thus, the resulting equations are:

$$\Delta(\mu(\text{obs})) = \Delta[(\mu(\text{c})) - \mu(f) \times x(\text{c})] \tag{4}$$

$$\mu_{\text{corr}} = \mu_{\text{obs}} - \mu_{\text{EOF}} \tag{5}$$

This equation shows that two different factors, i.e., the difference in the electrophoretic mobility between the free and the complexed analyte, and the difference in their degrees of formation are responsible for the separation. At optimum pH 5.5, neotame forms complexes with heptakis 2,3,6 tri-*o*-methylbetacyclodextrin in the zwitterionic state and thus forms a less stable anionic complex as shown by the mobility values. However, the mobility value increases with an increasing concentration of the chiral selector. Furthermore, the complexes are significantly more bulky than the free analytes, resulting in an increase of the selector concentration.

The chiral selector therefore plays an important role in the separation of diastereomers. It is widely believed that a combination of interactions such as hydrogen bonding, hydrophobic interactions, dipole–dipole interactions, and charge transfer

Table 2. Effect of concentration of heptakis 2,3,6 tri-o-methylbetacyclodextrin on retention, separation, and resolution factors (K′, α, RS)

Concentration of heptakis 2,3,6 tri-*o*-methylbetacyclodextrin	Migration time (min)		Retention factor (K′)		Separation factor (α)	Resolution factor (R_s)	$\mu_{\text{corrected}}$ (10^{-9} m^2 V^{-1} s^{-1})	
	L,L	D,D	K'_1	K'_2			L,L	D,D
0	6.85	6.85	0.662	0	1	0	−4.05	
5	6.93	7.72	0.682	0.80	1.281	0.80	−3.52	−3.84
10	7.08	8.26	0.718	1.71	1.398	1.71	−3.33	−3.48
20	7.19	9.95	0.745	2.52	1.902	2.52	−2.95	−3.24
30	7.12	11.35	0.728	3.79	2.409	3.79	−2.61	−2.87
40	7.16	11.31	0.737	3.98	2.367	3.98	−2.53	−2.75
50	7.15	11.33	0.735	4.06	2.380	4.06	−2.41	−2.64

Note: L,L and D,D = neotame diastereomers; K'_1 and K'_2 = retention factor for first and second eluted analytes (L,L-neotame and D,D-neotame).

complexes (π-π) may influence chiral recognition (Hassan 2001), where the main chiral absorbing sites are the methoxy groups for heptakis 2,3,6 tri-*o*-methylbetacyclodextrin. The results revealed that at an optimum pH 5.5, the concentration of heptakis 2,3,6 tri-*o*-methylbetacyclodextrin affected the resolution of the peaks, whereas at concentrations less than 20 mM of heptakis 2,3,6 tri-*o*-methylbetacyclodextrin, the separation factor was 1.281 and resolution factor was 0.80, indicating that the capacity of separation was low. When the concentration increased from 20 to 30 mM, the separation factors increased to 2.409 and the resolution factor increased to 3.79. Thus, the capacity of separation increased up to 30 mM and a further increase in the concentration of heptakis 2,3,6 tri-*o*-methylbetacyclodextrin showed no specific changes either on the separation or the resolution factors. Higher concentrations of heptakis 2,3,6 tri-*o*-methylbetacyclodextrin affected peak shapes and baseline separations, as depicted in Table 2. Figure 4 shows the effect of concentration of heptakis 2,3,6 tri-*o*-methylbetacyclodextrin on the resolution. Based on the separation and resolution factors, 30 mM was considered the optimum concentration for heptakis 2,3,6 tri-*o*-methylbetacyclodextrin.

Interaction Mechanism of Heptakis 2,3,6 tri-*o*-Methylbetacyclodextrin with Neotame

The chiral separation of neotame diastereomers (L,L and D,D) with heptakis 2,3,6 tri-*o*-methylbetacyclodextrin is governed by the relative mobilities of the isomers in the applied electric field, which are related to their charge, mass, and shape. Despite the absence of the electrophoretic mobility of heptakis 2,3,6 tri-*o*-methylbetacyclodextrin, the complex formation and the elution of the analyte-heptakis 2,3,6 tri-*o*-methylbetacyclodextrin complex varies with the pH of the running buffer. Accordingly, the separation of neotame diastereomers was studied

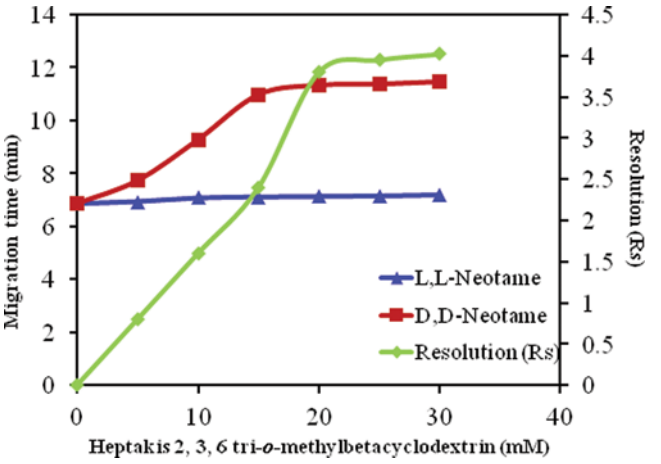

Figure 4. Effect of heptakis 2,3,6 tri-o-methylbetacyclodextrin concentration on migration time and resolution of compounds. Conditions: 50 mM phosphate buffer, 30 mM heptakis 2,3,6 tri-o-methylbetacyclodextrin, 20 kV applied voltage, 30°C temperature, 200 nm detection wavelength.

at different pH ranges. Due to the injection of heptakis 2,3,6 tri-*o*-methylbetacyclodextrin into the capillary followed by neotame isomers, the EOF of the isomers were hindered by the slow moving heptakis 2,3,6 tri-*o*-methylbetacyclodextrin, leading to some interactions with the isomers. Therefore, the cationic and anionic isomers showed strong interactions with the heptakis 2,3,6 tri-*o*-methylbetacyclodextrin and eluted at longer migration times. In the case of the zwitterionic form at pH 5.5, the shorter migration time was observed due to weaker interactions with heptakis 2,3,6 tri-*o*-methylbetacyclodextrin than the corresponding cationic and anionic forms. Moreover, the computed hydrogen bond lengths for the complexes of heptakis 2,3,6 tri-*o*-methylbetacyclodextrin with cationic, anionic, and zwitterionic forms also supported the observed experimental elution orders. In the case of the cationic and anionic complexes, shorter hydrogen bond lengths were observed than the zwitterionic form, suggesting their stronger interaction with the heptakis 2,3,6 tri-*o*-methyl betacyclodextrin in terms of longer migration times.

Precision

In order to achieve good reproducibility between consecutive runs, the capillaries were flushed with deionized water for 2 min and thereafter with NaOH for 2 min to replenish the silanol groups, and the separation buffer was used to equilibrate the capillaries. To obtain good reproducibility for the developed method in terms of migration time and peak absorbances, five successive runs with heptakis 2,3,6 tri-*o*-methylbetacyclodextrin/phosphate buffer of pH 5.5 were performed with the same solutions. The repeatability was evaluated by performing five determinations with the same solution resulting in the percentage relative standard deviations (RSD, $n = 5$) of 1.20% and 1.45% with respect to migration time and the 1.17% and 1.28% for peak area for L,L and D,D-neotames, respectively.

Analytical Figures of Merit

L,L and D,D-neotame were determined using EKC-CE under the following optimum conditions: 50 mM phosphate buffer/30 mM heptakis 2,3,6 tri-*o*-methylbetacyclodextrin with pH 5.5, 20 kV applied voltage, 30°C cassette temperature, and a 4 s sample injection. The regression equations and the correlation coefficients were $y = 44837x + 70.214$, $y = 11511x - 3.8789$ and 0.9977, 0.9887 for L,L-neotame and D,D-neotame, respectively. The LOD and LOQ (signal to noise ratios of 3 and of 10) were 0.01857 and 0.08214 mM and 0.07428 and 0.24891 mM for L,L-neotame and D,D-neotame, respectively.

Performance of the Present Method with Reported Methods

The performance of the developed method was compared with previously reported methods (Matsumoto et al. 2008; Prakash et al. 1999; Yang and Chen 2010). The present method is rapid, sensitive, and reproducible with shorter migration times (Prakash et al. 1999; Yang and Chen 2010). Lower detection limits were achieved in this method in contrast to previously reported methods (Hu et al.

2013; Matsumoto et al. 2008; National Standard Method of China 2009; Yang and Chen 2010), as shown in Table 3.

Analytical Applications

The chiral separation and determination of neotame in standard samples were performed according to the aforementioned procedures and good separation with satisfactory resolution was observed as shown in Figure 5. The accuracy of this method was tested using three neotame spiked samples under the same optimum conditions and the resulting electropherograms are illustrated in Figure 6. Intra- and inter-day precision and accuracy were evaluated by analyzing three sets of spiked food samples at three concentration levels (3.0, 5.0, and 7.0 mM) on three separate days. The overall intra- and inter-day variations (%RSDs) of the two analytes in the samples were found to be 1.20% and 1.50%, respectively, with recoveries between 95.66% and 99.00%, as shown in Table 4.

Docking Discussion

The geometric aspects and the binding interactions of neotame diastereomers with heptakis 2,3,6 tri-*o*-methylbetacyclodextrin were studied using docking simulations. Accordingly, three different ionic states (cation, anion, and zwitterion) of D,D-neotame and L,L-neotame were based on the experimental pH. For expediency, the ionic states of D,D-neotame are labeled as $DD_{zwitterion}$, DD_{cation} and DD_{anion}, whereas $LL_{zwitterion}$, LL_{cation} and LL_{anion} represents the ionic states of the L,L-neotame. The inclusion complexes of neotame with heptakis 2,3,6 tri-*o*-methylbetacyclodextrin showed important host-guest interactions and the detailed docking results are summarized in Table 5. Close inspection of the results revealed that the electrostatic and hydrophobic interactions are important in locking the geometries of the ligands in the cavity of the ring. For instance, both zwitterions ($DD_{zwitterions}$ and $LL_{zwitterion}$), in addition to hydrophobic interactions, formed intermolecular hydrogen bonds with the heptakis 2,3,6 tri-*o*-methylbetacyclodextrin atoms. The structure in the case of $DD_{zwitterion}$ was more folded due to an additional intramolecular hydrogen bond formed between its carbonyl oxygen and amine hydrogen. Moreover, the hydrogen bond distances in the case of $DD_{zwitterions}$ were comparatively shorter, suggesting stronger interactions with the heptakis 2,3,6 tri-*o*-methylbetacyclodextrin than the $LL_{zwitterions}$ variant (see Table 5). The cationic forms, DD_{cation} and LL_{cation}, of both neotame isomers also interacted comfortably with the heptakis 2,3,6 tri-*o*-methylbetacyclodextrin through two hydrogen bonds formed between their nitrogen atoms and the oxygen atoms of the heptakis 2,3,6 tri-*o*-methylbetacyclodextrin ring. Although the complexes of DD_{cation} and LL_{cation} with heptakis 2,3,6 tri-*o*-methylbetacyclodextrin exhibited equal number of hydrogen bonds, the computed hydrogen bond lengths were shorter in the former than the latter, suggesting stronger interaction with the heptakis 2,3,6 tri-*o*-methylbetacyclodextrin. Similarly, the DD_{anion} compared to its structural isomer LL_{anion} also exhibited stronger interactions with the heptakis 2,3,6 tri-*o*-methylbetacyclodextrin ring through two stronger hydrogen bonds as evidenced by their shorter distances.

Table 3. Comparison of reported methods with the present method

Analyte	Technique	Limit of Detection	Limit of Quantification	Migration time (min)	Reference
NTM, ASP, ATM	HPLC	0.01 g Kg^{-1}	0.1 g Kg^{-1}	8.70	Matsumoto et al. 2008
NTM	HPLC	0.2 mg Kg^{-1}	0.5 mg Kg^{-1}	7.40	Yang and Chen 2010
NTM, ASP, ACS, SAC, CA, BA, SOR, DAA, STE	RP-HPLC	0.19 mg L^{-1}	0.63 mg L^{-1}	22.00	Zhao et al. 2012
NTM, ASP, ACS, SAC, CA, BA, SOR, DAA, STE	RP-HPLC	0.15 mg L^{-1}	0.46 mg L^{-1}	20.50	Zhao et al. 2013
NTM, ASP, ACS, SAC, CYC, ATM, DUL, NHDC, SUC	HPLC-ELSD	13 μg g^{-1}	26 μg g^{-1}	22.80	Wasik et al. 2007
NTM, ASP, ACS, SAC, CYC, ATM, DUL, NHDC, SUC	SPE/HPLC-MS	0.005 μg mL^{-1}	0.02 μg mL^{-1}	23.80	Zygler et al. 2011
NTM, ASP, ACS, SAC, CYC, ATM, SUC, STE, WFS	HPLC-ESI-MS	0.02 μg mL^{-1}	0.05 μg mL^{-1}	22.02	Yang and Chen 2009
NTM, ASP, ACS, SAC, CYC, NHDC, SUC	HPLC-MS/MS	ND	ND	–	Scheurer et al. 2009
NTM, ASP, ACS, SAC, CYC, NHDC, SUC, DKP	HPLC-MS/MS	ND	10 ng L^{-1}	10.80	Berset and Ochsenbein 2012
NTM, ASP, ACS, SAC, CYC, NHDC, SUC, ATM, DUC	HPLC-MS/MS	0.001 μg mL^{-1}	0.003 μg mL^{-1}	25.19	Lim et al. 2013
NTM, ASP, ACS, SAC, CYC, NHDC, SUC	LC- MS/MS	9.5 ng L^{-1}	31.6 ng L^{-1}	12.30	Gan et al. 2013
NTM	CZE-CE	0.118 μg mL^{-1}	0.395 μg mL^{-1}	4.30	Hu et al. 2012
NTM	EKC-CE	0.0185 (L,L), 0.0821(D,D) mM	0.0742(L,L), 0.248(D,D) mM	7.1 (L,L), 11.3(D,D) min	Present work

Note: NTM: Neotame, ASP: Aspartame, ACS: Acesulfame-K, SAC: Saccharine, CYC: Sodium cyclamate, CA: Caffien, BA: Benzoic acid, SOR: Sorbic acid, DAA: Dehydroacetic acid, STE: Stevioside, NHDC: Neohesperidinedihydrochalcone, ATM: Alitame, SUC: Sucralose, DUC: Dulcine, DKP: Diketopiperigine, WFS: Warfarine sodium, HPLC: High performance liquid chromatography, RP-HPLC: Reversed phase-High performance liquid chromatography, HPLC–ELSD: High performance liquid chromatography–Evaporative light scattering detector, SPE/HPLC–MS: Solid phase extraction/High performance liquid chromatography–Mass spectrometry, HPLC–ESI-MS: High performance liquid chromatography–Electrospray ionization-Mass spectrometry, LC–MS/MS: Liquid chromatography–Mass spectrometry/Mass spectrometry, CZE-CE: Capillary zone electrophoresis, EKC: Electrokinetic chromatography; ND = Not detectable.

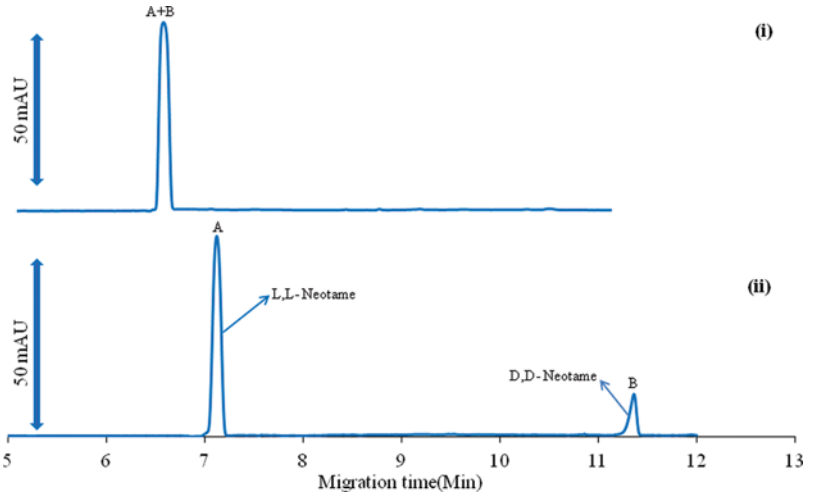

Figure 5. Electropherogram of standards (i) without heptakis 2,3,6 tri-o-methyl betacyclodextrin and (ii) with heptakis 2,3,6 tri-o-methylbetacyclodextrin of (A) L,L-neotame and (B) D,D-neotame. Conditions: 50 mM phosphate buffer, 30 mM heptakis 2,3,6 tri-o-methylbetacyclodextrin, pH 5.5, 20 kV applied voltage, 30°C temperature, 200 nm detection wavelength.

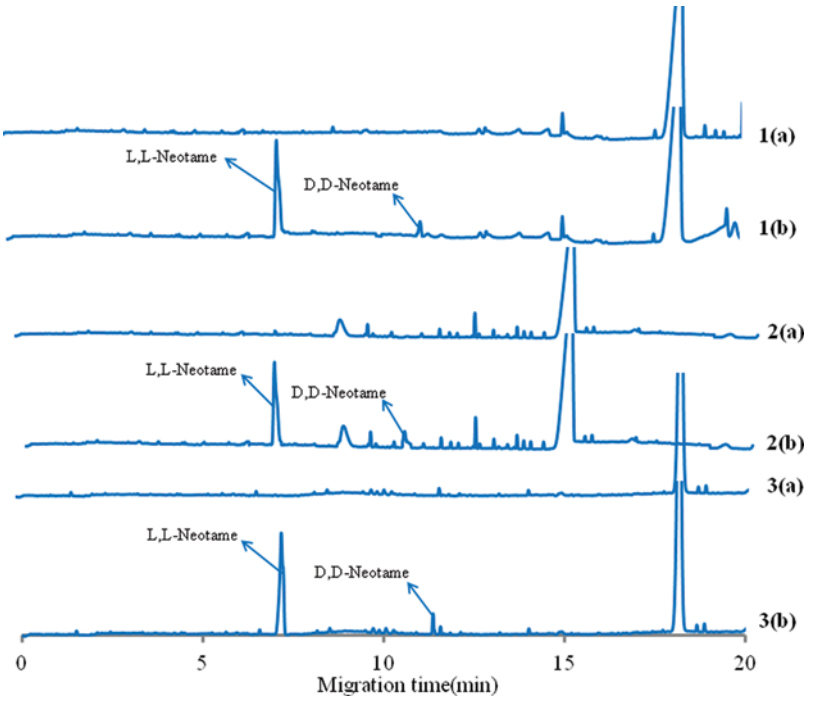

Figure 6. Electropherograms (1a) blank mango juice; (1b) spiked mango juice; (2a) blank orange drink; (2b) spiked orange drink; (3a) blank soft drink; (3b) spiked sof drink for L,L-neotame and D,D-neotame. Conditions: 50 mM phosphate buffer, 30 mM heptakis 2,3,6 tri-o-methylbetacyclodextrin, pH 5.5, 20 kV applied voltage, 30°C temperature, 200 nm detection wavelength.

Table 4. Intra-day and inter-day precision and accuracy for the determination of neotame ($n = 5$)

			Intra-day ($n = 5$)		Inter-day ($n = 3$)	
Sample	Active components	Neotame conc. added (g)	Relative standard deviation (%)[a]	Recovery (%)[a]	Relative standard deviation (%)[a]	Recovery (%)[a]
SS-1	L,L-Neotame	0.00378	1.9	96.67	1.2	97.33
	D,D-Neotame		2.3	97.66	1.8	95.66
SS-2	L,L-Neotame	0.00567	2.1	98.21	1.3	97.26
	D,D-Neotame		1.5	97.40	2.0	98.41
SS-3	L,L-Neotame	0.00756	1.7	99.00	2.2	98.39
	D,D-Neotame		2.0	97.71	1.9	98.87

Note: SS=Spiked sample.

[a]Relative standard deviation for five individual determinations, SS-1 (mango juice), SS-2 (orange soft drink), SS-3 (cola soft drink).

Table 5. Docking results of neotame diastereomers with the heptakis 2,3,6 tri-*o*-methylbetacyclodextrin

Neotame ionic form	Migration time (min)	CDocker energy	CDocker interaction energy	Number of H-bonds	H-bond distance (in Å)
L,L-Cationic	20.5	−13.9488	−20.1	2	1.959, 2.139
L,L-Anionic	16.4	−7.3080	−22.4	2	2.079, 2.406
L,L-Zwitterionic	7.1	−16.5620	−19.5	2	1.978, 2.146
D,D-Cationic	23.1	−14.7310	−23.2	2	1.80, 2.082
D,D-Anionic	18.7	−9.40130	−23.3	2	1.959, 1.865
D,D-Zwitterionic	11.3	−19.0030	−22.7	3	2.108, 1.786, 1.967

The results were further substantiated on the basis of two scoring functions, C-Docker energy (CDE) and C-Docker interaction energy (CDIE), as shown in Table 5. Clearly, the computed CDE and CDIE of D,D-neotame were comparatively lower than L,L-neotame, irrespective of their ionic states, supporting the better fitting of the former in the heptakis 2,3,6 tri-*o*-methylbetacyclodextrin cavity. Moreover, a good relationship between the scoring functions (CDE and CDIE) and migration times in CE was observed (Table 5). For instance, all ionic states of D,D-neotame exhibited lower values of CDE and CDIE compared to their structural isomers. Heptakis 2,3,6 tri-*o*-methylbetacyclodextrin, owing to its large size migrates slowly in the capillary under CE conditions. It is believed that the stronger bonding of D,D-neotame with the heptakis 2,3,6 tri-*o*-methylbetacyclodextrin restricted its movement toward the anodic electrode, and is probably responsible for its greater migration time in CE than its structural diastereomer.

CONCLUSIONS

A novel method has been reported for the chiral separation of neotame with EKC-CE. The chiral separating agent, heptakis 2,3,6 tri-*o*-methylbetacyclodextrin, resulted in good baseline resolution, reproducibility, and accuracy with short migration times. This method is inexpensive and easy to handle with minimal sample volumes.

The influence of buffer pH, buffer concentration, applied voltage, concentration of separating agent, and capillary cassette temperature were studied on the retention and separation factors. Furthermore, thermodynamic parameters were also calculated according to the previously described van't Hoff equations and the results were in agreement with the experimental results in terms of the elution order of two compounds. Our results suggest that the developed method is a reliable method to separate neotame in different food samples. The docking results supplied further evidence regarding the host-guest relationship between neotame diastereomers and heptakis 2,3,6 tri-*o*-methylbetacyclodextrin and supported the experimental results.

ACKNOWLEDGMENTS

The authors would like to express their acknowledgement to the Center for High Performance Computing, an initiative supported by the Department of Science and Technology of South Africa.

FUNDING

K. Bisetty is grateful for the financial support provided by the Durban University of Technology and National Research Foundation of South Africa for this work.

REFERENCES

Alghamdi, A. H., A. F. Alghamdi, and A. A. Alwarthan. 2005. Determination of content levels of some food additives in beverages consumed in Riyadh city. *J. King Saud Univ.* 18: 99–109.

Banerjee, A., E. Mikhailova, S. Cheley, L. Q. Gu, M. Montoya, Y. Nagaoka, E. Gouaux., and H. Bayley. 2010. Molecular bases of cyclodextrin adapter interactions with engineered protein nanopores. *Proc. Natl. Acad. Sci. USA.* 107: 8165–8170.

Berset, J. D., and N. Ochsenbein. 2012. Stability considerations of aspartame in the direct analysis of artificial sweeteners in water samples using high-performance liquid chromatography–tandem mass spectrometry (HPLC–MS/MS). *Chemosphere.* 88: 563–569.

Buchgraber, M., and A. Wasik. 2009. Determination of nine intense sweeteners in foodstuffs by high-performance liquid chromatography and evaporative light-scattering detection: Interlaboratory study. *J. Assoc. Off. Anal. Chem. Int.* 92: 208–222.

Chankvetadze, B., and G. Blaschke. 2001. Enantio separations in capillary electromigration techniques: Recent developments and future trends. *J. Chromatogr. A.* 906: 309–363.

Fisher, R. S. 1989. Aspartame, neurotoxicity and seizures: A review. *J. Epilepsy.* 2(2): 55–64.

Gan, Z., H. Sun, R. Wang, and B. Feng. 2013. A novel solid-phase extraction for the concentration of sweeteners in water and analysis by ion-pair liquid chromatography–triple quadrupole mass spectrometry. *J. Chromatogr. A.* 1274: 87– 96.

Giuffrida, A., R. Caruso, M. Messina, G. Maccarrone, A. Contino, A. Cifuentes, and V. Cucinotta. 2012. Chiral separation of amino acids derivatized with fluorescein isothiocyanate by single isomer derivatives 3-monodeoxy-3-monoamino-β- and γ-cyclodextrins: The effect of the cavity size. *J. Chromatogr. A.* 1269: 360–365.

Hassan, Y. A. E. 2001. High-performance liquid chromatographic enantioseparation of drugs containing multiple chiral centers on polysaccharide-type chiral stationary phases. *J. Chromatogr. A.* 906: 185–193.

He, Y. C., S. Fang, and X. J. Xu. 2013. Simultanious determination of acesulfame-K, aspartame and stevioside in sweetener blends by ultraviolet spectroscopy with variable selection by sipls algorithm. *Maced. J. Chem. Chem. Eng.* 31: 17–28.

Hu, F., L. Xu, F. Luan, H. Liu, and Y. Gao. 2013. Determination of neotame in non-alcoholic beverage by capillary zone electrophoresis. *J. Sci. Food Agric.* 93: 3334–3338.

Hui, L. C., L. S. Juan, A. Juan, and L. J. Zhong. 2009. Simultaneous determination of various kinds of synthetic sweeteners in foods by RPLC/MS/MS. *Sci. Technol. Food Ind.* 30: 319–320.

Ji, C., Y. Sun, X. Li, X. Chu, and Z. Chen. 2009. Simultaneous determination of artificial sweeteners in beverage by ultra-performance liquid chromatography. *Chin. J. Chromatogr.* 27: 111–113.

Jizhi, C., L. Jie, and L. Jinhua. 2009. Determination of neotame in food by high performance liquid chromatography. *Guangdong Chem. Ind.* 36: 176–188.

Lim, H. S., S. K. Park, K. I. S. Kwak, H. Kim, J. H. Sung, S. J. Jang, M. Y. Byun, and S. H. Kim. 2013. HPLC-MS/MS analysis of 9 artificial sweeteners in imported foods. *Food Sci. Biotechnol.* 22: 233–240.

Matsumoto, H., K. Hirata, N. Sakamaki, K. Hagino, and H. Ushiyama. 2008. Simultaneous determination of neotame, alitame and aspartame in foods by HPLC. *Shokuhin Eiseigaku Zasshi* 49: 31–36.

Mayhew, D. A., C. P. Comer, and W. W. Stargel. 2003. Food consumption and body weight changes with neotame, a new sweetener with intense taste: Differentiating effects of palatability from toxicity in dietary safety studies. *Regul. Toxicol. Pharm.* 38: 124–143.

Min, L. L., and P. J. Dong. 2008. Simultaneous determination of five sweeteners by reversed-phase high performance liquid chromatography. *J. Instrum. Anal.* 27: 549–552.

National Standard Method of China. 2009. Method for the determination of neotame in foods – high-performance liquid chromatography. GB 23378–2009.

Nofre, C., and J. M. Tinti. 2000. Neotame: Discovery, properties, utility. *Food Chem.* 69: 245–257.

Peter, A., E. Vekes, and D. W. Armstrong. 2002. Effects of temperature on retention of chiral compounds on a ristocetinA chiral stationary phase. *J. Chromatogr. A* 958: 89–107.

Prakash, I., I. Bishay, and S. Schroeder. 1999. Neotame: Synthesis, stereochemistry and sweetness. *Synth. Commun.* 29: 4461–4467.

Sabela, M. I., P. Singh, N. J. Gumede, K. Bisetty, and S. Sagrado. 2012. Evaluation of enantiomer resolution of (±)-catechin using electrokinetic chromatography and molecular docking. *J. Sci. Res. Pharm.* 1(2): 1–4.

Scientific opinion of the Panel on Food Additives, Flavorings, Processing Aids, and Materials in Contact with Food on a request from European Commission on neotame as a sweetener, and flavor enhancer. 2007. EFSAJ. 581: 1–3.

Scheurer, M., H. J. Brauch, and F. T. Lange. 2009. Analysis and occurrence of seven artificial sweeteners in German waste water and surface water and in soil aquifer treatment (SAT). *Anal. Bioanal. Chem.* 394: 1585–1594.

Tomasik, P. 2004. *Chemical and functional properties of food saccharides*. CRC Press LLC, 397 p.

United States Food and Drug Administration. 2013. Department of Health and Human Services, Code of Federal Regulations Title 21 (21CFR172.829) Vol. 3, Revised as of April, 2013.

Vianna-Soares, C. D., and J. L. S. Martins. 2002. Saccharin analysis in pharmaceutical and cosmetic preparations by derivative ultraviolet spectrophotometry. *Braz. J. Pharm. Sci.* 38: 471–478.

Wasik, A., J. McCourt, and M. Buchgraber. 2007. Simultaneous determination of nine intense sweeteners in foodstuffs by high performance liquid chromatography and evaporative light scattering detection-Development and single-laboratory validation. *J. Chromatogr. A.* 1157: 187–196.

Wu, G., D. H. Robertson, C. L. Brooks III, and M. Vieth. 2003. Detailed analysis of grid-based molecular docking: A case study of CDOCKER-A CHARMm-based MD docking algorithm. *J. Comp. Chem.* 24: 1549–1562.

Wu, S. J., H. X. Wang, and G. J. Tao. 2010. Ultra-high pressure liquid chromatography–mass spectrometry method for simultaneous determination of six micro-sweeteners in distilled spirit. *J. Food Sci. Biotechnol.* 29: 670–675.

Yang, D., and B. Chen. 2009. Simultaneous determination of non-nutritive sweeteners in foods by HPLC/ESI–MS. *J. Agric. Food. Chem.* 57: 3022–3027.

Yang, D., and B. Chen. 2010. Determination of neotame in beverages, cakes and preserved fruits by column-switching high-performance liquid chromatography. *Food Addit. Contam. Part A* 27: 1221–1225.

Zhao, Y. G., M. Q. Cai, X. H. Chen, S. D. Pan, S. S. Yao, and M. C. Jin. 2013. Analysis of nine food additives in wine by dispersive solid-phase extraction and reversed-phase high performance liquid chromatography. *Food Res. Int.* 52: 350–358.

Zhao, Y., X. Chen, X. Li, S. Yao, and M. Jin. 2011. Influences of ion-suppressors on retention behaviors of nine food additives in reversed-phase high performance liquid chromatographic separation. *Chin. J. Chromatogr.* 29: 988–994.

Zhao, Y. G., X. H. Chen, S. S. Yao, S. D. Pan, X. P. Li, and M. C. Jin. 2012. Analysis of nine food additives in red wine by ion-suppression reversed phase high-performance liquid chromatography using trifluoroaceticacid and ammonium acetate as ion-suppressors. *Anal. Sci.* 28: 967–971.

Zygler, A., A. Wasik, A. Kot-Wasik, and J. Namiésnik. 2011. Determination of nine high-intensity sweeteners in various foods by high-performance liquid chromatography with mass spectrometric detection. *Anal. Bioanal. Chem.* 400: 2159–2172.

Biosensors and Bioelectronics 67 (2015) 200–207

Contents lists available at ScienceDirect

Biosensors and Bioelectronics

journal homepage: www.elsevier.com/locate/bios

Fabrication of copper nanoparticles decorated multiwalled carbon nanotubes as a high performance electrochemical sensor for the detection of neotame

Ayyappa Bathinapatla [a], Suvardhan Kanchi [a,*], Parvesh Singh [b], Myalowenkosi I. Sabela [a], Krishna Bisetty [a,*]

[a] Department of Chemistry, Durban University of Technology, P.O. Box 1334, Durban 4000, South Africa
[b] School of Chemistry and Physics, University of KwaZulu Natal, Westville, Private Bag X54001, Durban 4000, South Africa

ARTICLE INFO

Article history:
Received 19 May 2014
Received in revised form
25 July 2014
Accepted 4 August 2014
Available online 19 August 2014

Keywords:
Neotame
Electrochemical sensor
Cyclic voltammetry
Differential pulse voltammetry

ABSTRACT

A highly sensitive and novel electrochemical sensor for the detection of neotame using differential pulse voltammetry with a modified glassy carbon electrode is presented. The method was further customized by the fabrication of the electrode surface with copper nanoparticles–ammonium piperidine dithiocarbamate–mutiwalled carbon nanotubes assimilated with β-cyclodextrin. The multiwalled carbon nanotubes assimilated with β-cyclodextrin/glassy carbon electrode exhibited catalytic activity towards the oxidation of neotame at a potential of 1.3 V at pH 3.0. The transmission electron microscopy, thermogravimetric analysis, frontier transform infrared spectroscopy and cyclic voltammetry were employed to characterize the electrochemical sensor. The sensitivity and detection limits of the electrode increased two-fold in contrast to the β-CD-MWCNTs/GCE sensor. The developed method was successfully applied for the determination of neotame in food samples, with results similar to those achieved by our modified capillary electrophoresis method with a 96% confidence level.

1. Introduction

Neotame (NTM), a high intensity artificial sweetener is nearly 40 and 10,000 times sweeter than aspartame and sugar respectively. It is a dipeptide methyl ester derivative, (*N*-[*N*-(3.3-dimethylbutyl)-L-α-aspartyl]-L-phenylalanine-1-methyl ester), which can be synthesized by aspartame and 3.3-dimethyl butyraldehyde at an industrial scale. According to the studies undertaken by the European Food Safety Authority (EFSA) neotame is not carcinogenic, genotoxic, teratogenic or associated with any reproductive toxicity (Scientific Opinion, EFSA, 2007). However, it has been approved in more than 35 countries around the world and the Acceptable Daily Intake (ADI) has been set at 0–2 mg/kg body weight by the Joint Expert Committe for Food Additives (JECFA) in 2003 as well as by the EFSA in 2007. The Center for Science in the Public Interest (CSPI) indicates that NTM worldwide is still not being used as a sweetener yet, it has a wide potential application as a second-generation sweetener (Tomasik, 2004). Owing to its low cost, high intensity sweetness, safety, good stability and solubility it can be used as a substitute for chemical sweeteners (Hu et al., 2013). Literature reports for the determination of NTM revealed that various techniques have been employed, including HPLC (Jizhi et al., 2009; Matsumoto et al., 2008; National Standard Method of China, 2009; Yang and Chen, 2010; Zhao et al., 2011, 2012, 2013) and hyphenated techniques with HPLC like HPLC-ELSD (Buchgraber and Wasik, 2009; Wasik et al., 2007), HPLC–MS (Gan et al., 2013; Lim et al., 2013; Berset and Ochsenbein, 2012; Hui et al., 2009; Scheurer et al., 2009; Wu et al., 2010; Yang and Chen, 2009; Zygler et al., 2011; Chang and Yeh, 2014) and CE (Hu et al., 2013; Ayyappa et al., 2014).

Although, the selectivity and the detection limits are relatively satisfactory for the above mentioned chromatographic methods; these methods are rather time consuming in terms of analysis, instrumentally expensive and require a large number of standard operating procedures (SOPs). In comparison with other methods, electrochemical methods showed some distinct advantages, including the absence of matrix effects, rapid response, high sensitivity, easy operation and lower cost. A literature survey revealed that there are no available electrochemical studies reported for the determination of NTM. Accordingly, the broader goals of this study were to develop a simple and accurate method for the analysis of NTM in food samples. Since the last two decades, carbon alltropes such as multiwalled carbon nano tubes (MWCNTs) have been

* Corresponding authors. Tel.: +27 31 3736008x2311; fax: +27 866740243.
E-mail addresses: ksuvardhan@gmail.com (S. Kanchi), bisettyk@dut.ac.za (K. Bisetty).

http://dx.doi.org/10.1016/j.bios.2014.08.017
0956-5663/

widely investigated in the fabrication of electrodes. The exceptional features of MWCNTs make them extremely attractive for a wider range of sensing applications (Wang, 2005).

Copper nanoparticles (CuNPs) demonstrated good performances propelled by large effective surface area, which enhances mass transport and catalysis. Futhermore, their good biocompatibility has led to the development of various electrochemical sensors based on CuNPs (Pedrosa et al., 2009). The most common strategy to overcome aggregation or precipitation is to use stabilizers or protective capping agents, which does not only prevent their aggregation, but also results in functionalized nanoparticles (Bicer and Sisman, 2010; Yan et al., 2010). Specifically β-cyclodextrins (β-CD), a cyclic oligosaccharides which consist of seven glucose molecules in a ring with hydrophilic outer sides and hydrophobic inner cavities (Chen et al., 2011) shows large surface area and high conductivity in combination with nanoparticles and carbon allotropes. β-CDs will act as a platform material to assemble the thiol capped CuNPs and MWCNTs on the surface by the formation of hydrogen bonds and weak hydrophobic interactions, thereby increasing the stability and reproducibility of the coated electrodes.

Accordingly, in this work β-CD was utilized in the modification of the GCE using CuNPs anchored with ammonium piperidine dithiocarbamate (APDC) on the MWCNTs. The purpose of the MWCNTs was to facilitate electron transfer between the electroactive species and the electrode, while β-CD was used as a dispersing reagent for the CNTs (Jia et al., 2011). Moreover, APDC capped CuNPs were added onto the CNTs to generate additional electrocatalytic sites and to increase the sensitivity and detection limits of the electrodes. To the best of our knowledge, this is the first electroanalytical attempt at using CuNPs–APDC–MWCNTs-β-CD for the detection of NTM.

2. Experimental section

2.1. Chemicals and reagents

A stock standard solution of neotame with analytical quality of 97.0% purity was obtained from Hullets, South Africa (SA). The 20–30% MWCNTs basis with O.D. $\times L$ 7–12 nm $\times$ 0.5–10 μm (cas no. 308068-56-6) were purchased from Aldrich (Durban, SA). Analytical grades of sodium dihydrogen orthophosphate, betacyclodextrin, copper sulfate, ascorbic acid, piperidine, carbon disulfide, ammonium hydroxide, sodium hydroxide, hydrochloric acid and sulfuric acid were purchased from Capital Lab Supplies CC (Durban, SA). Nitrogen of 99.9% purity was obtained from AFROX (Durban, SA). Alumina powder $\leq$3.0 μm was supplied by Metrohm (Durban, SA). All solutions and samples were prepared with deionized water from an aqua MAX™-Basic 360 series water purification system supplied by TRILAB SUPPORT (Durban, SA). All standard solutions were kept in a refrigerator at 4 °C for stability.

2.2. Apparatus

All electrochemical measurements were performed using a 797 VA computrace from Metrohm (Herisau, Switzerland) equipped with the Computrace 1.3.1 software. Voltammograms were recorded at room temperature using a three electrode system consisting of a glassy carbon electrode (GCE) with 3.0 mm diameter as a working electrode, Ag/AgCl (3 M KCl) as a reference electrode and the platinum wire as a counter electrode. Capillary electrophoresis (CE) experiments were performed using the Agilent Technologies 7100 CE system equipped with a photo diode array detector, and the Chemstation software. All electrochemical solutions examined were initially purged for 10 min with purified nitrogen gas. pH measurements were made on a CRISON micro pH 2000 digital meter. FT-IR spectra of CuNPs capped with APDC decorated on MWCNTs were characterized using a Varian 800 FT-IR Scimitar Series supplied by SMM Instruments (Durban, SA) respectively. Morphology studies of MWCNTs, MWCNTs–CuNPs, MWCNTs–CuNPs–APDC and MWCNTs–CuNPs–APDC-β-CD were carried out using transmission electron microscope model JEM 2100 equipped with a LaB_6 emitter (MAX OXFORD instruments). All solutions were sonicated using an Labcon 5019 U ultrasonic bath. The STAR^e system of TGA/DCS 1 SF/1346 model was supplied with a STAR^e software version 9.20 by METTLER TOLODO (Johannesberg, South Africa). The sample was placed in a 10 μL alumina sample holder for thermal analysis at 10 °C min^{-1} heating rate for all the studies.

2.3. Preparation of standard, supporting electrolyte and spiked samples

0.5 mM NTM standard solutions were prepared quantitatively by weighing equivalent amount in a 5.0 mL volumetric flask and diluted using 20% methanol. 0.1 M phosphate buffer was prepared by dissolving an equivalent amount of sodium dihydrogen orthophosphate in 100 mL distilled water. The optimum pH 3.0 was achieved by quantitatively adding NaOH/HCl and thereafter stored at 4 °C. Spiked neotame samples (0.05, 0.10, 0.15 mM) were prepared with Mango juice (Checkout Manufacturers Pty Ltd, Quilbert-4078, SA), Tab cool drink (SAB Miller House, England) and Busta orange soft drink (SMJ Beverages SA Pty Ltd., New Germany 3610, SA) were purchased from a local supermarket. The spiked samples were prepared by direct dissolution of NTM in 5.0 mL volumetric flasks with the real samples mentioned above. All samples were filtered through a disposable syringes fitted with a 0.45 μm pore size and 25 mm diameter syringe filters made of cellulose acetate as a filter (Anatech Instruments (Pty) Ltd.) before voltammetric and electrophoretic measurements.

2.4. Preparation and fabrication of CuNPs–APDC–MWCNTs-β-CD nanocomposite

Synthesis of ammonium piperidine dithiocarbamate (APDC) was carried out as previously reported (Kanchi et al., 2011a, 2011b, 2012, 2013, 2014). CuNPs were prepared from the previously reported methods (Kobayashi et al., 2013), briefly 0.5 mM of hydrazine was added to the aqeous solution of 0.5 mM of copper sulfate followed by drop by drop addition of ascorbic acid under vigorous stirring at room temperature under nitrogen gas bubbling about 30 min. Then this solution was left 3 h under continueous stirring results in the dark red color solution, indicates formation of CuNPs. The preparation of functionalized CuNPs were prepared as follows: to the prepared CuNPs solution, aqueous NaOH was used to control the pH and this solution was heated for 30 min at 85 °C. Then 20 mL of 0.5 M APDC was introduced slowly into the solution with rapid stirring; the solution was further boiled for 30 min and then cooled to room temperature. In this process, the brick red colloidal solution finally changes to a pale yellow color. The APDC capped CuNPs [Fig. 1B (inset ii)] were separated by filtration and washed with deionised water followed by vacuum drying. Finally, a paste of MWCNTs was prepared by adding 0.3 g of MWCNTs to 3.0 mL of 0.1 mM β-CD solution followed by the addition of 0.1 g of APDC capped CuNPs powder. The resulting mixture was ultrasonicated for 30 min at 60 °C until a black dispersion of CuNPs–APDC–MWCNTs-β-CD was obtained (Noviandri and Rakhmana, 2012).

A bare GCE was manually polished carefully to a mirror like finish with $\leq$3 μm alumina slurry and then rinsed with distilled

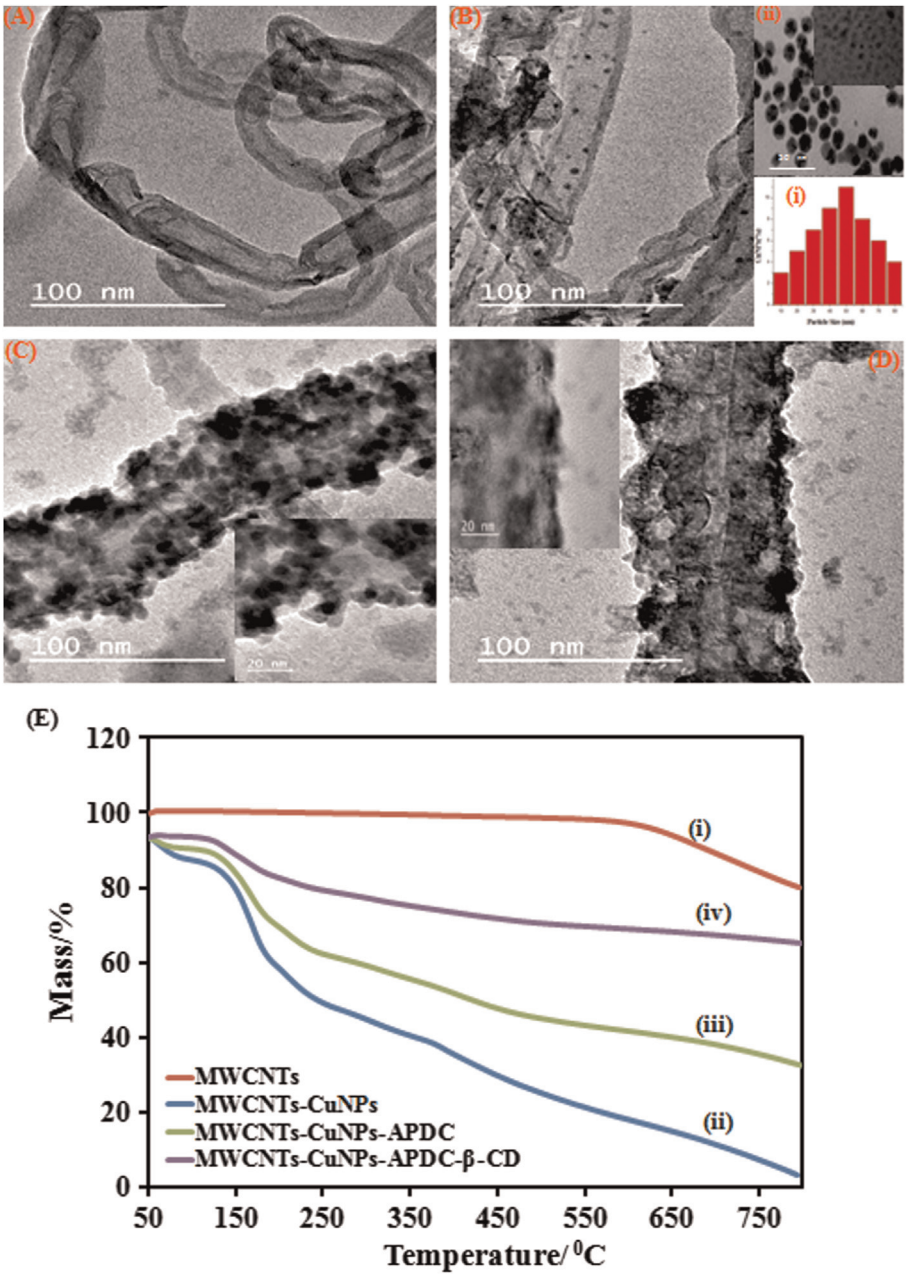

Fig.1. TEM images of (A) pure MWCNTs, (B) MWCNTs–CuNPs, (C) CuNPs–APDC–MWCNTs, (D) CuNPs–APDC–MWCNTs-β-CD. (E) TGA curves (i) MWCNTs (ii) CuNPs–MWCNTs (iii) CuNPs–APDC–MWCNTs (iv) CuNPs–APDC–MWCNTs-β-CD.

water followed by electrochemical cleaning by cycling at a potential range of −1.0 to +0.20 V for 30 cycles in acidified distilled water. This process enabled the removal of any physisorbed or chemisorbed materials from the electrode surface. Thereafter, the GCE was coated by careful addition of 6.0 μL of nanocomposite paste and oven dried at 50 °C for 15 min. After cooling to room temperature, the modified electrode was ready for use.

2.5. Electrochemical measurements with CuNPs–APDC–MWCNTs-β-CD-GCE

Approximately 10 mL of the phosphate buffer (pH 3.0) was introduced into the electrochemical cell in which either the bare or the fabricated GCE was immersed prior to electrochemical measurements. Several cyclic sweeps were applied until a low background current was achieved. An aliquot of the analyte solution was then introduced into the electrochemical cell, and a pre-concentration potential was applied to the working electrode while the solution was stirred at 400 rpm. At the end of the pre-concentration stage, stirring was stopped and the solution was allowed 5 s to equilibrate. The voltammograms were then recorded by scanning the potential towards the positive direction using differential pulse or linear sweep potential at a scanning rate of 0.1 V s^{-1}.

3. Results and discussion

3.1. Characterization of CuNPs–APDC–MWCNTs-GCE

Fig. 1A–D shows the typical TEM image of pure MWCNTs, MWCNTs-CuNPs, MWCNTs–CuNPs–APDC and MWCNTs–CuNPs–

APDC-β-CD respectively. Fig. 1 A shows the morphological structure of MWCNTs where the crystalline tubular structure of nanotubes are observed. It is observed that the nanotubes have clear inner channels. Fig. 1B displays the TEM images of MWCNTs decorated with CuNPs. It shows the morphology and the size distribution of CuNPs. It can be seen that the size of nanoparticles is distributed from 10.5 to 80 nm, and the mean particle size is about ~50 nm. The CuNPs were covalently bonded to the APDC through the strong chelating undefined atoms, resulting in a uniform size of the nanoparticles on the outer surface of the MWCNTs (Fig. 1C and D). Furthermore, FT-IR studies helped in understanding the role of the APDC in the formation of the homogeneous nanoparticles. The FT-IR spectra for APDC capped CuNPs showed a strong intensity band in the range 1025–1009 cm^{-1}, which may be attributed to the (C–S) vibrations with a stronger intensity band observed around 1438–1497 cm^{-1}, corresponding to the thiuride (C–N) vibrations. On the other hand, the free APDC (without CuNPs) showed a positive shift of around 10–35 cm^{-1} for the (C–S) bands and with no significant changes observed for the (C–N) bands. This suggests that the CuNPs were capped with APDC through an exohedral conjugation with their thiol (–SH) groups instead of the nitrogen atoms.

The amount of CuNPs, APDC and β-CD grafted on the MWCNTs is estimated by thermal analysis. Since, the approach that is adopted in this work for mass loaded on the surface of MWCNTs involves three stages. Therefore, samples are analyzed in successive stages starting with the pure MWCNTs. The thermogravimetric analysis (TGA) curve for MWCNTs shown in Fig. 1E (i) exhibits a well defined step at 630 °C can be associated to the carbon oxidation. On the other hand, CuNPs decorated MWCNTs show different TGA profile, with two drop downs at 173 °C and 440 °C as shown in Fig. 1E(ii). The mass percentage of CuNPs on the MWCNTs can be calculated as about 36.07%, which might be due to the strong electrostatic effect between CuNPs and MWCNTs. In addition, the mass percentage of APDC and β-CD loaded on the MWCNTs was estimated to be 12.98% and 13.84% respectively as depicted in Fig. 1E(iii and iv). The high mass loss in CuNPs–MWCNTs is probably due to the oxidation of Cu to CuO in the absence of the APDC and β-CD. Certainly, the TGA analysis also confirmed the presence of the CuNPs on the MWCNTs, however, there is another interesting discovery that is observed on the improvement of the thermal stability of the CuNPs–MWCNTs with the addition of APDC and β-CD.

3.2. Electrochemical behavior of NTM on CuNPs–APDC–MWCNTs-β-CD-GCE

The developed electrochemical sensor was further characterized by cyclic voltammetry (CV), using $K_3Fe(CN)_6$ as a probe in a 1 M solution. The microscopic areas of the CuNPs–APDC–MWCNTs-β-CD modified and the bare GCE were obtained at different scan rates (Kaur et al., 2013) according to the following Randles–Sevcik equation:

$$i_{pa} = 2.69 \times 10^5 A C_0 n^{3/2} D_R^{1/2} v^{1/2}$$

where i_{pa} is the anodic peak current, A is the surface area of the electrode, C_0 is the concentration of the $K_3Fe(CN)_6$, n is the number of electron transferred, D_R is the diffusion coefficient, and v is the scan rate. The diffusion coefficient (D_R) of 6.9×10^{-6} cm^2 s^{-1} was calculated from the slope of the i_{pa}–$v^{1/2}$ graph. In the case of CuNPs–APDC–MWNTs-β-CD modified GCE, the electrode surface area was 0.674 cm^2, while the bare GCE was nearly five times smaller than the modified electrode.

The electrochemical performance of the CuNPs–APDC–MWCNTs-β-CD-GCE towards the detection of NTM was evaluated by measuring the current–potential responses. First, a comparative study on the behavior of the bare GCE and the MWCNTs-β-CD-GCE was investigated using CV in a 10 mL phosphate buffer (pH 3.0) at a scan rate of 0.11 V s^{-1}. The mechanism for the oxidation of NTM involved a single proton and electron to produce hydroxylamine and an aldehyde, resulting in the appearance of an irreversible oxidation peak at 1.30 V (versus Ag/AgCl) in the potential ranging from −0.2 to 2.0 V (Scheme 1) as reported in the literature (Medeiros et al., 2007, 2008; Elmer et al., 1978).

Fig. 2A shows the responses of NTM with the GCE (curve a), MWCNTs-β-CD-GCE (curve b) and CuNPs–APDC–MWCNTs-β-CD (curve c). However, curve d in Fig. 2A represents the response of a CuNPs–APDC–MWCNTs-β-CD electrode in a blank solution. The

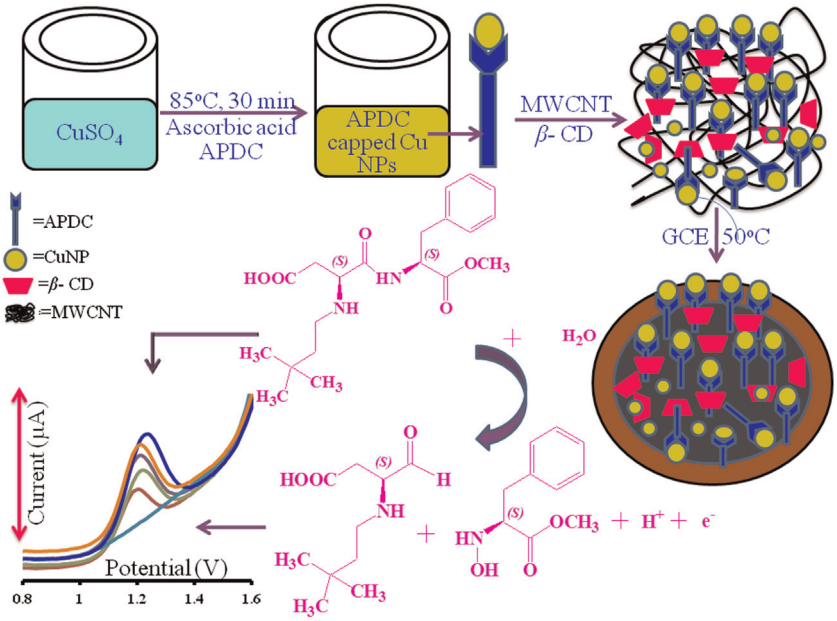

Scheme 1. A schematic representation of the typical electro-oxidation of NTM at CuNPs–APDC–MWCNTs-β-CD modified GCE.

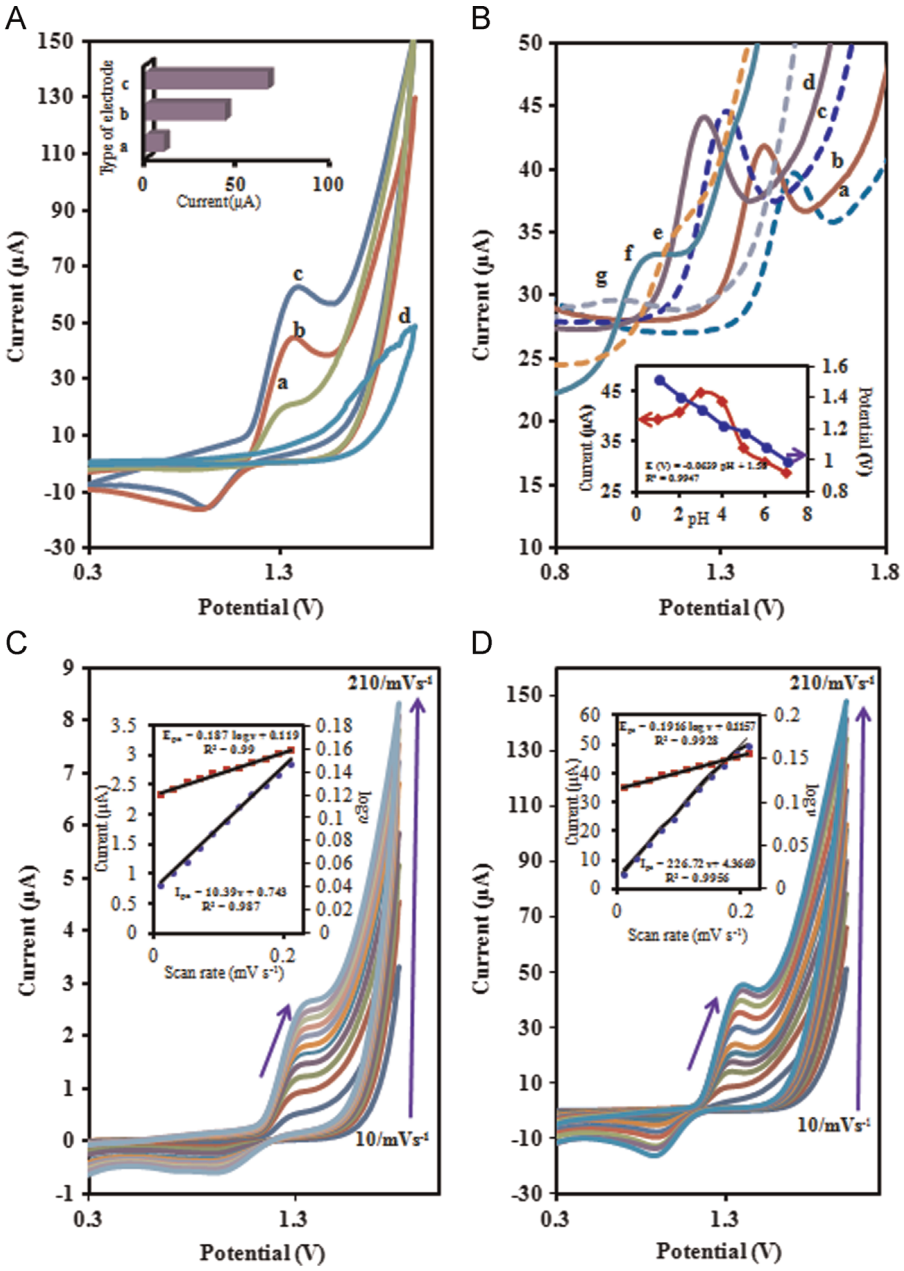

Fig. 2. (A) Cyclic voltammograms of 0.5 mM NTM at (a) bare GCE, (b) β-CD-MWCNTs-GCE and (c) CuNPs–APDC–MWCNTs–β-CD-GCE, inset: current comparison among three electrodes. (B) DPV responses of 0.5 mM NTM at CuNPs–APDC–MWCNTs-β-CD-GCE at different pHs: (a) 1, (b) 2, (c) 3, (d) 4, (e) 5, (f) 6, (g) 7, inset: the plot of pH verses peak current and peak potential in phosphate buffer (pH 3.0), scan rate: 0.11 V s^{-1}. Cyclic voltammograms of (C) bare GCE and (D) CuNPs–APDC–MWCNTs-β-CD-GCE at different scan rates. The scan rates from inner to outer are 0.01, 0.03, 0.05, 0.07, 0.09, 0.11, 0.13, 0.15, 0.17, 0.19, 0.21 V s^{-1}, respectively. Inset is the plot of scan rates versus anodic peak currents and log v.

oxidation peak for the bare GCE was sluggish, broad and much smaller. In contrast to the well defined peaks observed with good responses for the MWCNTs-β-CD-GCE and CuNPs–APDC–MWCNTs-β-CD electrodes. The bar-graph (inset of Fig. 2A) shows a comparative current responses for the three electrodes, with the peak currents of NTM recorded at the bare GCE (curve a) and the MWCNTs-β-CD-GCE (curve b). Clearly, the peak currents recorded for CuNPs–APDC–MWCNTs-β-CD (curve c) were higher than the currents obtained for a bare electrode and the MWCNTs-β-CD-GCE (curves a and b). On this basis, the nanometer dimensions and the topological effects of the MWCNTs, CuNPs–MWCNTs surfaces (Kara et al., 2010; Pilehvar et al., 2014) resulted in a significant catalytic effect for the electrochemical oxidation of NTM in terms of peak currents.

3.3. *Effect of pH and scan rate on the peak potentials and peak current*

In this study the effect of pH ranging from 1.0 to 7.0 was investigated on the anodic peak potentials and peak currents of NTM using the DPV method in a solution containing 0.5 mM NTM. Fig. 2B shows the electrochemical behavior of NTM on the CuNPs–APDC–MWCNTs-β-CD electrodes at different pHs. Clearly, the peak potentials linearly decreased with the increase in pH with a slope (inset Fig. 2B) of 63.9 mV/pH. Our results are similar to those reported in the literature (Medeiros et al., 2007, 2008), suggesting that equal number of protons and electrons were involved in the overall oxidation process. In this study the electrochemical responses (i_{pa}) for the detection of NTM due to the CuNPs–APDC–MWCNTs-β-CD electrodes are pH

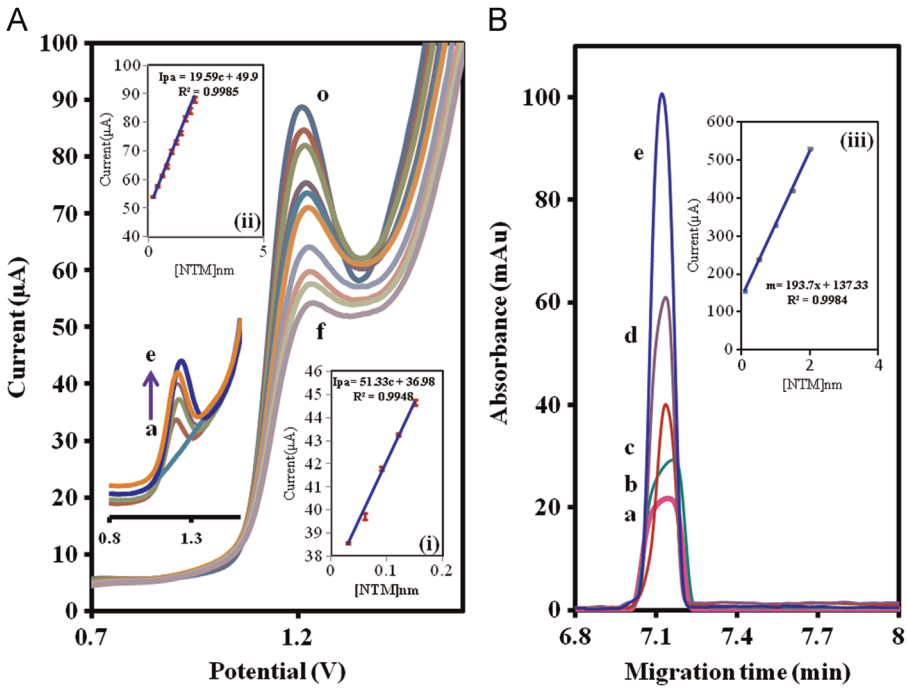

Fig. 3. (A) DPV recorded at CuNPs–APDC–MWCNTs-β-CD-GCE at different concentrations of NTM a→e (0.03–0.15 mM) and f→o (0.2–2 mM), inset: plots (i) and (ii) show for linear dependence of *ipa* versus [NTM]. (B) Electropherograms obtained using the CE method at different concentrations of NTM a→e (0.05–2 mM), inset shows the calibration curve for [NTM] versus peak area [conditions for DPV=pH: 3.0, accumulation time: 30 s, accumulation potential: 0.11 V s^{-1}, pulse amplitude: 50 mV, voltage step: 2 mV and voltage step time: 0.4 s].

dependent. The maximum peak current was observed at pH 3.0 (Fig. 2B inset), due to the dissociation of the amide bond into two molecules, resulting in higher current signals. Consiquently, the phosphate buffer at pH 3.0 was selected as the optimum for the determination of NTM.

The effect of the scan rates on peak current/potentials were investigated using 0.5 mM NTM ranging from 0.01 to 0.21 V s^{-1}. The CVs of NTM at pH 3.0 on the bare GCE and the CuNPs–APDC–MWCNTs-β-CD electrodes at different scan rates were depicted in Fig. 2C and D. The oxidation peak current gradually increases with an increase in scan rates on the bare and the modified electrodes. In the case of both bare and modified GCEs, a maximum scan rate of 0.21 V s^{-1} resulted in peak currents of 2.6 and 48 μA respectively, indicating a linear relationship with scan rate between NTM and the modified electrode surface (inset Fig. 2C and D). The peak potential of NTM shifted linearly towards the more positive values with increasing scan rates, hence the optimum scan rate of 0.11 V s^{-1} was selected in this study. At this scan rate the electron transfer rate constant, K_s for CuNPs–APDC–MWCNTs-β-CD/GCE electrode surface were calculated based on the Laviron theory (Zhou et al., 2013). The average K_s values for the bare and modified GCE were 1.14 s^{-1} and 5.78 s^{-1} respectively.

3.4. DPV technique for quantitative detection of NTM

Based on the higher current sensitivity and better peak separations, DPV was used for the sensitive detection of NTM using CuNPs–APDC–MWCNTs-β-CD/GCE (Zhou et al., 2013), and the optimized parameters were tabulated (see Table S1 in supplementary information). Fig. 3A shows the DPV responses for the various concentrations of NTM in two intervals for the modified electrode in 0.1 M phosphate buffer (pH 3.0). The results illustrates a linear relationship between the concentration of NTM and anodic peak currents observed in the concentration ranging from 0.03 to 2.0 mM. The anodic peak currents at 1.2 V increased with an increasing concentration of NTM, the first (a→e) and second (f→o)

Table 1
Analytical parameters (stability, accuracy, precision and recovery) obtained for NTM at CuNPs–APDC–MWCNTs-β-CD-GCE.

Stability		Analytical parameters				
Day	Peak response[a] (I_{pa})	Added (mM)	Found (mM)	Bias[b]	Recovery (%)	RSD[c] (%)
1	55	0.1	0.089	−0.109	89	0.71
2	51	0.2	0.192	−0.038	96	1.24
3	46	0.3	0.276	−0.078	92	1.36

[a] Average of three determinations.
[b] Bias=(found−added/added) × 100.
[c] Relative standard deviation for three individual determinations.

interval calibration curves (insets i and ii) were obtained at low concentrations ranging from 0.03 to 0.15 mM and from 0.2 to 2.0 mM with a detection limit of 0.013 mM. The results were compared with CE in terms of detection limits at different concentrations ranging from 0.05 to 2 mM as shown in Fig. 3B. From the obtained analytical outputs, it is clear that the proposed electrochemical method showed lower limits of detection than the CE method, similar to the previously reported methods (Hu et al., 2013; Matsumoto et al., 2008; National Standard Method of China, 2009; Yang and Chen, 2010). These results suggest that the developed electrochemical sensor is suitable and efficient for the detection of NTM in food samples.

3.5. Stability, recovery, accuracy and precision studies

The stability of the sensor was tested using CV in a phosphate buffer at pH 3.0, resulting in a 4.1% decrease of the current response after 50 cycles. The long term stability of the sensor was observed by measuring the responses in 0.5 mM NTM over a range of ten runs for three days using the same coating. The sensor maintained 83.0% of the original response on the third day, clearly

Table 2
Results obtained for the determination of NTM in spiked food samples analyzed by CuNPs–APDC–MWCNTs-β-CD-GCE (DPV) and CE method.

Sample	NTM added (mM)	Method				*t*-Test	*f*-Test
		DPV[a]		CE[a]			
		Recovery ± RSD[b]	Relative error (%)[c]	Recovery	Relative error (%)[d]		
SS-1	0.05	98.97 ± 1.3	−2.0	96.23 ± 1.9	1.87	2.58	0.99
SS-2	0.10	94.33 ± 2.1	−5.7	95.66 ± 1.5	−1.35	2.73	0.75
SS-3	0.15	95.24 ± 1.7	−4.8	98.14 ± 1.1	−2.98	2.16	0.41

SS = spiked sample.

[a] Average of three measurements.
[b] Relative standard deviation for three individual determinations.
[c] Relative error 1 (%) = 100 × (DPV value − added value)/added value.
[d] Relative error 2 (%) = 100 × (DPV value − CE value)/CE value.

suggesting that the sensor retained its activity to a large extent. The analytical parameters in-terms of accuracy, precision and recovery were estimated by analyzing three different concentrations of standard NTM in triplicate on one day ranging from 0.05 to 0.15 mM. The range of values for the relative error (bias) and % RSD were −0.109 to −0.038 and 0.71 to 1.36 respectively, indicating a higher accuracy and precision of the developed method (Table 1). The percentage recoveries of NTM from the fabricated sensor ranged from 89.0% to 96.0%. On the other hand, the reproducibility of the sensor was studied by assaying the CV peak currents using 0.5 mM NTM on three different modified GCE for three replicate measurements. A % RSD of 1.89 suggests an acceptable reproducibility of the developed sensor.

3.6. Real sample analysis

The applicability of the developed sensor was tested using three different NTM spiked samples described in the above mentioned procedure. Furthermore, the DPV results were validated with the CE results in terms of detection limits as shown in Table 2. The validation of the present method was compared with the CE method by applying the paired student *t*-test and the variance ratio *f*-test (Anderson, 1987) at a 96% confidence level. Results in Table 2 revealed that there were no significant differences between the amount of NTM obtained by both methods, thus confirming the validity of the developed method.

3.7. Effect of potential interferents

The selectivity of the developed sensor was studied by the simultaneous addition of possible interferents such as acesulfame-K, saccharine, aspartame, cyclamate, tryptophan, tyrosine, sodium benzoate, silicon dioxide, sunset yellow, tartrazine and brilliant blue to 0.05 mM NTM standard solution. The anodic peak potentials of the intereferents aspartame (0.9 V), tartrazine (1.6 V), cyclamate (1.9 V) and acesulfame-K (2.2 V) were observed on CuNPs–APDC–MWCNTs-β-CD-GCE using DPV. The applied tolerance limit for the interfering species at the maximum concentration resulted in a relative error of ±5%. However, 50-fold tryptophan, tyrosine, sodium benzoate, silicon dioxide, sunset yellow, tartrazine and brilliant blue and 10-fold acesulfame-K, saccharine, aspartame, cyclamate solutions had no effect on the determination of NTM. These results clearly indicated that the determination of NTM in food samples should not be significantly affected by the potential common interferents mentioned above.

4. Conclusion

A novel high performance electrochemical sensor was fabricated for the electrochemical detection of NTM in different food samples. The physicochemical properties of the modified electrode were characterized by TEM and FT-IR techniques. The overall mass percentages of CuNPs, APDC and β-CD loaded on MCNTs were calculated to be 62.83%. Overall, the TGA analysis supported by the morphology studies demonstrated that indeed the CuNPs were immobilized via the MWCNTs support paste. Furthermore, it was concluded that the functionalization improve the grafting of CuNPs on MWCNTs also improving the thermal stability of the paste. Additionally, the electrochemical behavior of the developed sensor for NTM was further investigated using CV and DPV. Our results indicated that the CuNPs–APDC–MWCNTs-β-CD-GCE exhibited an efficient electrocatalytic oxidation for NTM with a relatively high sensitivity and stability. Under the optimized conditions, linear calibration DPV plots for the detection of NTM ranged from 0.05 to 2.0 mM. The applicability of the developed electrochemical sensor was tested on NTM food samples, and the results were in agreement with the CE method. The good performance of the CuNPs–APDC–MWCNTs-β-CD-GCE provided a promising alternative in routine sensing applications in the food industry.

Acknowledgements

KB is grateful for the financial support provided by the Durban University of Technology and National Research Foundation of South Africa for this work. The authors would like to express their acknowledgement to the Centre for High Performance Computing, an initiative supported by the Department of Science and Technology of South Africa.

Appendix. Supporting information

Supplementary data associated with this article can be found in the online version at http://dx.doi.org/10.1016/j.bios.2014.08.017.

References

Anderson, R.L., 1987. Practical Statistics for Analytical Chemists. Van Nostrand Reinhold, New York.
Ayyappa, B., Kanchi, S., Singh, P., Sabela, M.I., Bisetty, K., 2014. Anal. Lett. http://dx.doi.org/10.1080/00032719.2014.924008.
Berset, J.D., Ochsenbein, N., 2012. Chemosphere 88, 563–569.
Bicer, M., Sisman, I., 2010. Powder Technol. 198, 279–284.
Buchgraber, M., Wasik, A., 2009. J. Assoc. Off. Anal. Chem. Int. 92, 208–222.
Chang, C.S., Yeh, T.S., 2014. J. Food Drug Anal. http://dx.doi.org/10.1016/j.jfda.2014.01.024.
Chen, Q.S., Zhou, Z.Y., Vidal-Iglesias, F.J., Solla-Gullon, J., Feliu, J.M., Sun, S.G., 2011. J. Am. Chem. Soc. 133, 12930–12933.
Elmer, J.R., Rosen, G.M., Barbara, B.K., 1978. Mol. Pharmacol. 15, 131–137.

Gan, Z., Sun, H., Wang, R., Feng, B., 2013. J. Chromatogr. A 1274, 87–96.
Hu, F., Xu, L., Luan, F., Liu, H., Gao, Y., 2013. J. Sci. Food Agric. 93, 3334–3338.
Hui, L.C., Juan, L.S., Juan, A., Zhong, L.J., 2009. Sci. Technol. Food Ind. 30, 319–320.
Jia, D., Dai, J., Yuan, H., Lei, L., Xiao, D., 2011. Talanta 85, 2344–2351.
Jizhi, C., Jie, L., Jinhua, L., 2009. Guangdong Chem. Ind. 36, 176–188.
Kanchi, S., Saraswathi, K., Venkatasubba Naidu, N., 2011a. Environ. Monit. Assess. 183 (1), 531–543.
Kanchi, S., Sulochana, M., Babu Naidu, K., Saraswathi, K., Venkatasubba Naidu, N., 2011b. Food Anal. Method 4 (4), 453–464.
Kanchi, S., Saraswathi, K., Venkatasubba Naidu, N., 2012. Food Anal. Method 5 (1), 69–81.
Kanchi, S., Singh, P., Sabela, M.I., Bisetty, K., Venkatasubba Naidu, N., 2013. Int. J. Electrochem. Sci. 8, 4260–4282.
Kanchi, S., Singh, P., Bisetty, K., 2014. Arabian J. Chem. 7, 11–25.
Kara, P., Escosura–Muniz, A., Costa, M.M., Guix, M., Ozsoz, M., Merkoci, A., 2010. Biosens. Bioelectron. 26, 1715–1718.
Kaur, B., Pandiyan, T., Satpati, B., Srivastava, R., 2013. Colloids Surf. B 111, 97–106.
Kobayashi, Y., Shirochi, T., Yasuda, Y., Morita, T., 2013. J. Min. Metall. Sect. B—Metall. 49 (1), 65–70.
Lim, H.S., Park, S.K., Kwak, K.I.S., Kim, H., Sung, J.H., Jang, S.J., Byun, M.Y., Kim, S.H., 2013. Food Sci. Biotechnol. 22, 233–240.
Matsumoto, H., Hirata, K., Sakamaki, N., Hagino, K., Ushiyama, H., 2008. Shokuhin Eiseigaku Zasshi 49, 31–36.
Medeiros, R.A., Carvalho, A.E., Rocha-Filho, R.C., Fatibello-Filho, O., 2007. Anal. Lett. 40, 3195–3207.
Medeiros, R.A., Carvalho, A.E., Rocha-Filho, R.C., Fatibello-Filho, O., 2008. Talanta 76, 685–689.
National Standards of the People's Republic of China, 2009. Method for the determination of neotame in foods – high-performance liquid chromatography. GB 23378-2009.
Noviandri, I., Rakhmana, R., 2012. Int. J. Electrochem. Sci. 7, 4479–4487.
Pedrosa, V.A., Epur, R., Benton, J., Overfelt, R.A., Simonian, A.L., 2009. Sens. Actuators B 140, 92–97.
Pilehvar, S., Rather, J.A., Dardenne, F., Robbens, J., Blust, R., Wael, K.D., 2014. Biosens. Bioelectron. 54, 78–84.
Scientific Opinion of the Panel on Food Additives, Flavourings, Processing Aids and Materials in Contact with Food on a Request from European Commission on Neotame as a Sweetener and Flavor Enhancer, 2007. EFSA J. 581, 1–3.
Scheurer, M., Brauch, H.J., Lange, F.T., 2009. Anal. Bioanal. Chem. 394, 1585–1594.
Tomasik, P., 2004. Chemical and Functional Properties of Food Saccharides. CRC Press LLC, USA p. 397.
Wang, J., 2005. Electoanalysis 17, 7–14.
Wasik, A., McCourt, J., Buchgraber, M., 2007. J. Chromatogr. A 1157, 187–196.
Wu, S.J., Wang, H.X., Tao, G.J., 2010. J. Food Sci. Biotechnol. 29, 670–675.
Yang, D., Chen, B., 2009. J. Agric. Food Chem. 57, 3022–3027.
Yang, D., Chen, B., 2010. Food Addit. Contam. A 27, 1221–1225.
Yan, Z., Bao, R., Dinu, C.Z., Huang, Y., Caruso, A.N., Chrisey, D.B., 2010. J. Optoelectron. Adv. Mater. 12, 437–439.
Zhao, Y., Chen, X., Li, X., Yao, S., Jin, M., 2011. Chin. J. Chromatogr. 29, 988–994.
Zhao, Y.G., Chen, X.H., Yao, S.S., Pan, S.D., Li, X.P., Jin, M.C., 2012. Anal. Sci. 28, 967–971.
Zhao, Y.G., Cai, M.Q., Chen, X.H., Pan, S.D., Yao, S.S., Jin, M.C., 2013. Food Res. Int. 52, 350–358.
Zhou, Y., Zhang, H., Zhang, J., Liu, T., Tang, W., 2013. Sens. Actuators B 182, 610–617.
Zygler, A., Wasik, A., Kot-Wasik, A., Namie´sn, J., 2011. Anal. Bioanal. Chem. 400, 2159–2172.

DUT DURBAN UNIVERSITY OF TECHNOLOGY WRITING CENTRE

CONSULTATION REPORT

Date: 21-11-14 Student / Staff Name: AYYAPPA SATHINAPALA Student / Staff No: 21243352

Email Address: [redacted] Home Language: Telugu

Programme: D. Tech Level: _____

Course: _____ Lecturer: Prof. K. Bisetty

Is this session required by your lecturer? Y / N Do you have an appointment? Y / N Have you consulted on this assignment before? _____ Tutor: _____ Duration of session: _____

Assignment Topic: _____

What are you hoping to achieve from this session? To improve writing skills and plagerism checking in Thesis for submission

Stage of Process:

Planning	First Draft	Second Draft...	Revising / Rewriting	Final write up ✓

What we worked on in this session...

Development	**Style**	**Grammar & Mechanics**
Understanding topic	Audience Analysis	Grammar
Developing ideas	Tone and word choice	Spelling and punctuation
Planning	Flow	Proofreading
Formulating argument	Clarity and conciseness	In-text and list of references
Refining main ideas	Passive to active voice	
Organising	Linking words	**Techniques**
Streamlining	Integrating sources/quotes	Brainstorm/Free write
Introduction	Visual presentation	Discussed w/o Reading
Supporting evidence	Format	Read aloud
Analysis		Academic Reading - strategies (4N's)
Conclusion		Discussed paper / sentence - level issues

DUT DURBAN UNIVERSITY OF TECHNOLOGY WRITING CENTRE P O Box 1334, Durban, 4000, South Africa
2014 -11- 21
Name Ajaite Signature [redacted]

Resources

Turn-it-in ☑ WhiteSmoke ☐ Webpage ☐ FaceBook ☐

Tutor's Comments: (progress, recommendations)

16% similarity